Cloud Feedbacks in the Climate System

Submitted by **Mark Jonathan Webb**, to the University of Exeter as a thesis for the degree of Doctor of Philosophy by Publication in Mathematics, December 2020.

I certify that all material in this thesis which is not my own work has been identified and that any material that has previously been submitted and approved for the award of a degree by this or any other University has been acknowledged.

(Signature)

UNIVERSITY OF EXETER

Abstract

It is well established that inter-model differences in cloud feedbacks are the leading cause of differences in equilibrium climate sensitivity, the change in global mean near-surface temperature that eventually follows an instantaneous doubling in carbon dioxide concentrations. This thesis presents the contribution from four peer reviewed publications which seek to understand cloud feedback mechanisms.

Webb et al. (2015a) investigated the diurnal cycle of marine cloud feedbacks in seven climate models using high frequency outputs at selected locations, and found that reductions in marine low-cloud fraction in the warmer climate are in almost all cases largest in the mornings when more cloud is present in the control simulations.

Webb et al. (2015b) assessed the impact of convective parametrization on cloud feedback by analysing SST forced climate change experiments performed with ten climate models with convective parametrizations deactivated. This reduced the range of longwave cloud feedback but not shortwave or net cloud feedback, indicating that differences in convective parametrizations are not primarily responsible for the overall range in cloud feedback.

Webb et al. (2018) perturbed surface evaporation and radiative cooling independently in a climate model, quantifying their individual contributions to changes in stability and low-cloud responses with climate warming, as well as to those in the near-surface atmospheric properties which regulate the hydrological sensitivity. Enhancing evaporation at the surface increased atmospheric stability and low-cloud fraction, while enhancing atmospheric radiative cooling destabilised the atmosphere and reduced low cloud.

Webb and Lock (2020) investigated the finding of Tian (2015) that CMIP3 and CMIP5 climate models with larger double-ITCZ biases have lower climate sensitivities. It was hypothesized that deep convection encroaching into subtropical low-level cloud regions disrupts the formation of low clouds and inhibits positive low-cloud feedback. Results from sensitivity tests with a single model were consistent with this, but not all of the predicted regional correlations were statistically significant in the multi-model ensemble.

Contents

i Acknowledgements and Dedication

I would like to thank my supervisors Prof. Geoffrey Vallis and Prof. Matthew Collins for encouraging me to pursue this PhD by publication, and supporting me during the process. I would also like to thank the Met Office for allowing me to complete this in work time and for paying my fees.

I would like to give special thanks to my wife Ann for her support, encouragement and patience, and not just over the last two years.

This thesis is dedicated to my father, John Webb BEM (1935-2017).

"If you're not failing every now and again, it's a sign you're not doing anything very innovative."

— Woody Allen

ii List of Tables and Illustrations

iii List of Accompanying Material

The four publications submitted for this PhD by publication are included at the end of this document. They are, in order of publication date, Webb et al. (2015a), Webb et al. (2015b) and Webb et al. (2018), Webb and Lock (2020).

iv Author's declaration

This extended introductory chapter is entirely my own work, although minor comments and suggestions by my supervisors Prof. Geoffrey Vallis and Prof. Matthew Collins were taken into account. The vast majority of the work published in the four submitted publications is my own. I led the development of the ideas for the work in all cases, discussing with my colleague Dr. Adrian Lock and other co-authors and making modifications as I saw fit based on their suggestions. I ran all of the sensitivity experiments with HadGEM2-A, making use of code modifications provided by Dr. Adrian Lock for Webb et al. (2018) and Webb and Lock (2020). I

wrote all of the text, performed all of the analysis of the model outputs and produced all of the figures. Notable contributions from other authors included the production and/or supply of the CFMIP-2 experiments with high frequency model outputs from models other than HadGEM2-A for Webb et al. (2015a) and the production of the convection-off experiments from models other than HadGEM2-A for Webb et al. (2015b). Also, Dr. F. Hugo Lambert suggested the addition of a radiative cooling perturbation experiment for Webb et al. (2018), while Dr. Alejandro Bodas-Salcedo provided observational data sub-sampled over locations of interest for Webb et al. (2015a).

v Abbreviations and Definitions

ALPI Angular LTS/Precipitation Index (Webb et al., 2015b). A hybrid index of surface precipitation rate and LTS, diagnosed as the angle of declination of a line connecting each point in LTS/precipitation space with an 'anchor point' close to the locations of the maximum LTS and precipitation values.
AMIP Atmospheric Model Intercomparison Project (Gates et al., 1999). AMIP experiments are performed using atmosphere and land model components only, forced with observed SSTs and sea ice fractions.
AMIP+4K experiment An AMIP experiment where SSTs are uniformly increased by 4K.
APE Aqua-Planet Experiment (Neale and Hoskins, 2000). Experiment where an atmosphere model is run without land or ocean components, forced with zonally symmetric SSTs and no seasonal cycle.
AR5 Fifth Assessment Report of the Intergovernmental Panel on Climate Change (Stocker et al., 2013).
CFMIP-2 The Second Phase of the Cloud Feedback Model Intercomparison Project (Bony et al., 2008).
CFMIP-3 The Third Phase of the Cloud Feedback Model Intercomparison Project (Webb et al., 2017).
CMIP3 The Third Phase of the Coupled Model Intercomparison Project (Meehl et al., 2007).
CMIP5 The Fifth Phase of the Coupled Model Intercomparison Project (Taylor et al., 2012).
CMIP6 The Sixth Phase of the Coupled Model Intercomparison Project (Eyring et al., 2016).
CO_2 Carbon dioxide.
CRE Cloud Radiative Effect, an alternative term for Cloud Radiative Forcing.
CRF Cloud Radiative Forcing, the net downward all-sky radiative flux at the top of the atmosphere minus the net downward clear-sky flux. Examples include the shortwave (SW) CRF, the longwave (LW) CRF and the net (LW+SW) CRF (Coak-

ley Jr and Baldwin, 1984).

ECS Equilibrium climate sensitivity. This quantity is commonly defined as the equilibrium change in global mean near-surface temperature following an instantaneous doubling of CO_2 concentration, assuming that ice sheets, vegetation and other minor and trace gases remain unchanged.

EIS Estimated Inversion Strength (Wood and Bretherton, 2006). A measure of low-level inversion strength similar to LTS, but which assumes a moist adiabatic lapse rate between the inversion and the 700 hPa level.

ESM Earth System Model, a climate model containing representations of chemical and biological processes, for example representing the cycling of carbon through the Earth system.

FAR First Assessment Report of the IPCC (Houghton et al., 1990).

GCM General Circulation Model or Global Climate Model.

GEWEX The Global energy and water cycle experiment (Chahine, 1992).

GPCP Global Precipitation Climatology Project (Adler et al., 2003).

HadGEM2-A Version 2-A of the Hadley Centre Global Environment Model (Martin et al., 2011).

Hydrological sensitivity The rate of change in global precipitation and evaporation per degree warming, excluding the effects of rapid precipitation adjustments to radiative forcing.

IPCC The Intergovernmental Panel on Climate Change (Houghton et al., 1990).

ISCCP The International Satellite Cloud Climatology Project (Schiffer and Rossow, 1983).

ITCZ Intertropical Convergence Zone, a zonally elongated band of low-level convergence in the tropics associated with deep convection and heavy rainfall.

LTS Lower-Tropospheric Stability, a measure of lower-tropospheric stability usually defined as the difference between the potential temperature of air at the 700 hPa level and near the surface. In the presence of low-level inversions this is often used as a measure of inversion strength.

Moist static energy A thermodynamic quantity which measures the total energy in a parcel of air, including sensible heat from temperature, latent heat from water vapour and potential energy from height.

NASA The National Aeronautics and Space Administration, an agency of the U.S. federal government responsible for the civilian space programme.

PRP Partial Radiative Perturbation, a feedback analysis technique which separates radiative feedbacks into components by perturbing inputs to a radiation code one at a time. (Wetherald and Manabe (1980), Soden et al. (2004)).

QObs An experiment from the APE project with zonal mean SSTs designed to be close to the observed zonal mean climatology (Neale and Hoskins, 2000).

RCE Radiative-Convective Equilibrium, an equilibrium state of the atmosphere where radiative cooling is balanced by latent heat release and sensible heat fluxes from the surface.

RCE Model Radiative-Convective Equilibrium Model. Can refer to a single column model that assumes Radiative-Convective Equilibrium (e.g. Manabe and Strickler (1964)), or a general circulation model or cloud resolving model subject to horizontally uniform forcing conditions, often without rotation (e.g. Wing et al. (2018)).

S The effective equilibrium climate sensitivity to doubling CO_2, estimated from climate models subject to an instantaneous CO_2 doubling or quadrupling by linearly regressing global net downward top-of-atmosphere radiation against global mean near-surface air temperature and extrapolating to radiative equilibrium (Gregory et al., 2004).

SPOOKIE Selected Process On/Off Klima Experiment. A model intercomparison of climate models with convective parametrizations deactivated (Webb et al., 2015b).

SST Sea surface temperature.

WCRP World Climate Research Programme.

1 Introduction

Continuing uncertainty in the magnitude of the climate change expected in response to anthropogenic emissions of greenhouse gases confounds decision making in the arena of climate policy. The amount of CO_2 that can be emitted while limiting long-term changes in global mean temperature to a given level varies approximately inversely with the equilibrium climate sensitivity (ECS). This quantity is commonly defined as the equilibrium change in global mean near-surface temperature following an instantaneous doubling of CO_2 concentration, assuming that ice sheets, vegetation and other minor and trace gases remain unchanged. The earliest climate models that resolved the global atmospheric circulation employed simple 'swamp' ocean models, or mixed-layer ocean models which reached equilibrium much more quickly than contemporary models with full dynamical oceans, which are only rarely run for the thousands of years that are required for them to reach equilibrium. ECS is commonly estimated in modern climate models using the effective equilibrium climate sensitivity (hereafter S), which is diagnosed from experiments subject to an instantaneous CO_2 doubling or quadrupling by linearly regressing global net downward top-of-atmosphere radiation against global mean near-surface air temperature and extrapolating to radiative equilibrium (Gregory et al., 2004). While other metrics of climate sensitivity are used for a range of purposes elsewhere, here I focus on S and the ECS. Where I use the term 'climate sensitivity' as below, I am referring to S unless otherwise stated.

The first coordinated assessment of evidence on equilibrium climate sensitivity (Charney et al., 1979) estimated a most likely value to be approximately 3K with a probable error of +/- 1.5K, indicating a 50% probability of the ECS lying in the range 1.5-4.5K. This was based on a combination of physical arguments and results from early global circulation models. More recently, the fifth Assessment Report (AR5) of the Intergovernmental Panel on Climate Change (Stocker et al., 2013) assessed multiple lines of evidence on climate sensitivity, including estimates from comprehensive climate models and based on fitting simple models to historical warming. Their assessment was that S was likely (>66% probability) in the range 1.5-4.5K.

Progress on narrowing uncertainties in climate sensitivity in IPCC assessments has clearly been slow in recent decades. This is not only a problem for predicting changes in global mean temperatures; many aspects of regional climate change scale strongly with S (Murphy et al. (2004),Grose et al. (2018)). Some promising progress has however been made since the AR5, with methods to formally combine constraints from multiple lines of evidence using Bayesian Statistics (Annan and Hargreaves, 2006) being revisited (Stevens et al. (2016), Sherwood et al. (2020)). In a climate sensitivity assessment coordinated independently of the IPCC by the World Climate Research Programme, Sherwood et al. (2020) combined evidence on climate feedbacks and climate sensitivity from phys-

ical theory and contemporary observations, the observed post-industrial warming record, and paleoclimate records. The resulting Bayesian calculations yielded a 66% range for the effective climate sensitivity of 2.6-3.9K, which remained within the bounds 2.3-4.5K under plausible robustness tests, resulting in a significant increase in the lower bound compared to previous IPCC assessments.

It is clearly desirable to understand the underlying causes of uncertainty in S, and there has been considerable progress in this area in recent years. It is now well established that inter-model differences in the responses of clouds to increasing temperature (cloud feedbacks) are the leading cause of differences in climates and S (Cess et al. (1990), Cess et al. (1996), Webb et al. (2006), Webb et al. (2013), Vial et al. (2013), Zelinka et al. (2020)). Furthermore, inter-model differences in low cloud feedbacks are a leading cause of uncertainty in cloud feedback (Bony and Dufresne (2005), Webb et al. (2006), Webb et al. (2013), Vial et al. (2013), Zelinka et al. (2012), Zelinka et al. (2020)). This has led sections of the cloud feedback community to focus attention on understanding the physical mechanisms underlying low cloud feedbacks. Developments in the last decade in this area have included using high resolution process models to estimate the magnitude of low cloud feedbacks (Blossey et al. (2013), Bretherton et al. (2013), Zhang et al. (2013)), assessing the impact of parametrizations such as convection on low cloud feedbacks (Zhao (2014),Webb et al. (2015b)), and constraining low cloud feedbacks by assessing the sensitivity of low clouds to environmental controlling factors in observations (Qu et al. (2014), Qu et al. (2015), Klein et al. (2017)). These approaches point towards low-level subtropical cloud feedbacks being positive, ruling out the negative low-cloud feedbacks seen in some climate models. A parallel development in the last decade has been the increasing application of the 'emergent constraint' approach to estimating cloud feedbacks and climate sensitivity (Qu et al. (2014), Qu et al. (2015), Sherwood et al. (2014), Tian (2015), Cox et al. (2018)). Many, but not all of these point to higher values of S. However, the physical mechanisms underlying such constraints are opaque in many cases, and it is not possible to exclude the possibility of model bias in such constraints (Caldwell et al. (2018), Hall et al. (2019)).

This introductory chapter is organised into two further sections. Section 2 provides a literature review of key developments in understanding cloud feedbacks and climate sensitivity from the advent climate modelling up to and including the first IPCC Assessment Report in 1990. This includes the use of simple models and physical arguments for prediction, including the single column global radiative convective equilibrium (RCE) models in use before the advent of three dimensional atmospheric circulation models, and the first studies which used models to explore the impact of increasingly sophisticated cloud processes on cloud feedbacks and climate sensitivity. The final section provides an integrative discussion of my papers submitted as part of this PhD by publication, demonstrating how they form a coherent whole, and how they meet the doctoral assessment criteria.

2 Key developments in clouds and climate sensitivity from the advent climate modelling to the first IPCC Assessment Report

Edwards (2011) reviews the history of climate modelling, from the earliest conceptual models through physical analogue models, radiative transfer and simple energy balance models, radiative-convective models to Global Circulation Models (GCMs) and eventually Earth System Models (ESMs). Here I will review key developments with a particular emphasis on cloud feedbacks and climate sensitivity, up to and including the First Assessment Report (FAR) of the Intergovernmental Panel on Climate Change (Houghton et al., 1990). A comprehensive review of the literature on clouds and climate sensitivity was not possible within the word limit for this introductory chapter. I chose this period because, while many review papers cover more recent developments (e.g. Bretherton (2015), Vial et al. (2017), Ceppi et al. (2017), Zelinka et al. (2017), Webb et al. (2017) and Sherwood et al. (2020)), few delve into this 'golden era' of climate modelling from the perspective of cloud feedbacks.

Arrhenius (1896) estimated that doubling CO_2 would raise the global average temperature by 5–6K. This was the first study to estimate the climate sensitivity of the Earth to doubling CO_2, and was based on radiative equilibrium calculations of surface warming in response to increasing CO_2 in different locations and seasons, assuming radiative equilibrium between a single-layer atmosphere and the local surface (Figure 1). Although clouds were assumed not to change with the warming climate, they were included in the calculations of the energy balance of the current climate. Observations of 'nebulosity' (cloud fraction) were specified as a function of latitude and cloud albedo was assumed similar to that observed for 'freshly fallen snow'. Relative humidity was assumed not to change with warming, and the dynamics of the ocean and atmosphere were neglected. A number of other studies around that time argued for the role of carbon dioxide in determining past climates (e.g. Chamberlin (1899)).

The idea that CO_2 is major driver of climate fell out of favour in the first half of the 20th century, when it was often argued that water vapour absorption limited the radiative effects of CO_2 (Plass, 1956). However estimates of the effect of CO_2 on climate were still made (e.g. Callendar (1938), Callendar (1949)), and new measurements in the mid-50s stimulated a revival in investigations of the role of CO_2 in climate change (Plass, 1956). A number of estimates of climate sensitivity were subsequently made between the mid 1950s and mid 1970s, initially using radiative equilibrium models (e.g. Plass (1956), Kaplan (1960), Möller (1963)), and later radiative-convective equilibrium models (e.g. Manabe and Strickler (1964), Manabe and Wetherald (1967)) - see Schneider (1975) for a review. These all had fixed clouds and hence no cloud feedback, but had increasingly sophisticated

Figure 1: Image of Table VII from Arrhenius (1896) showing warming in response to increasing carbon dioxide as a function of latitude and season. Reproduced with permission of Taylor and Francis (http://www.tandfonline.com).

TABLE VII.—*Variation of Temperature caused by a given Variation of Carbonic Acid.*

Latitude.	Carbonic Acid = 0·67.					Carbonic Acid = 1·5.					Carbonic Acid = 2·0.					Carbonic Acid = 2·5.					Carbonic Acid = 3·0.				
	Dec.–Feb.	March–May.	June–Aug.	Sept.–Nov.	Mean of the year.	Dec.–Feb.	March–May.	June–Aug.	Sept.–Nov.	Mean of the year.	Dec.–Feb.	March–May.	June–Aug.	Sept.–Nov.	Mean of the year.	Dec.–Feb.	March–May.	June–Aug.	Sept.–Nov.	Mean of the year.	Dec.–Feb.	March–May.	June–Aug.	Sept.–Nov.	Mean of the year.
70	−2·9	−3·0	−3·4	−3·1	−3·1	3·3	3·4	3·8	3·6	3·52	6·0	6·1	6·0	6·1	6·05	7·9	8·0	7·9	8·0	7·95	9·1	9·3	9·4	9·4	9·3
60	−3·0	−3·2	−3·4	−3·3	−3·22	3·4	3·7	3·6	3·8	3·62	6·1	6·1	5·8	6·1	6·02	8·0	8·0	7·6	7·9	7·87	9·3	9·5	8·9	9·5	9·3
50	−3·2	−3·3	−3·3	−3·4	−3·3	3·7	3·8	3·4	3·7	3·65	6·1	6·1	5·5	6·0	5·92	8·0	7·9	7·0	7·9	7·7	9·5	9·4	8·6	9·2	9·17
40	−3·4	−3·4	−3·2	−3·3	−3·32	3·7	3·6	3·3	3·5	3·52	6·0	5·8	5·4	5·6	5·7	7·9	7·6	6·9	7·3	7·42	9·3	9·0	8·2	8·8	8·82
30	−3·3	−3·2	−3·1	−3·1	−3·17	3·5	3·3	3·2	3·5	3·47	5·6	5·4	5·0	5·2	5·3	7·2	7·0	6·6	6·7	6·87	8·7	8·3	7·5	7·9	8·1
20	−3·1	−3·1	−3·0	−3·1	−3·07	3·5	3·2	3·1	3·2	3·25	5·2	5·0	4·9	5·0	5·02	6·7	6·6	6·3	6·6	6·52	7·9	7·5	7·2	7·5	7·52
10	−3·1	−3·0	−3·0	−3·0	−3·02	3·2	3·2	3·1	3·1	3·15	5·0	5·0	4·9	4·9	4·95	6·6	6·4	6·3	6·4	6·42	7·4	7·3	7·2	7·3	7·3
0	−3·0	−3·0	−3·1	−3·0	−3·02	3·1	3·1	3·2	3·2	3·15	4·9	4·9	5·0	5·0	4·95	6·4	6·4	6·6	6·6	6·5	7·3	7·3	7·4	7·4	7·35
−10	−3·1	−3·1	−3·2	−3·1	−3·12	3·2	3·2	3·2	3·2	3·2	5·0	5·0	5·2	5·1	5·07	6·6	6·6	6·7	6·7	6·65	7·4	7·5	8·0	7·6	7·62
−20	−3·1	−3·2	−3·3	−3·2	−3·2	3·2	3·2	3·4	3·3	3·27	5·2	5·3	5·5	5·4	5·35	6·7	6·8	7·0	7·0	6·87	7·9	8·1	8·6	8·3	8·22
−30	−3·3	−3·3	−3·4	−3·4	−3·35	3·4	3·5	3·7	3·5	3·52	5·5	5·6	5·8	5·6	5·62	7·0	7·2	7·7	7·4	7·32	8·6	8·7	9·1	8·8	8·8
−40	−3·4	−3·4	−3·3	−3·4	−3·37	3·6	3·7	3·8	3·7	3·7	5·8	6·0	6·0	6·0	5·95	7·7	7·9	7·9	7·9	7·86	9·1	9·2	9·4	9·3	9·25
−50	−3·2	−3·3	—	—	—	3·8	3·7	—	—	—	6·0	6·1	—	—	—	7·9	8·0	—	—	—	9·4	9·5	—	—	—
−60																									

treatments of physical processes relevant to other climate feedbacks, such as the introduction of convection to support a limited representation of atmospheric motions on the near-surface energy balance (Manabe and Wetherald, 1967), and representation of amplifying feedbacks due to reductions in snow and ice albedo with warming (e.g. Sellers (1969), Budyko (1972)).

Paltridge (1974) was one of the first to model cloud feedback in an energy balance model, assuming that the energy balance of the cloud layer depended on the surface latent heat flux, which was assumed to increase with surface warming. This resulted in an increase in cloud cover with warming, and a negative cloud feedback. Weare and Snell (1974) took a different approach, representing clouds as a diffuse cloud of water droplets with a concentration related to the difference between the atmospheric temperature and its dew point, allowing for a certain amount of condensate to be rained out by convection. This formulation resulted in an increase of cloud condensate with a warming climate, resulting again in a negative cloud feedback. Estimates of climate sensitivity from energy balance and radiative-convective models during this period ranged from 0.7K (Weare and Snell, 1974) to 9.6K (Möller, 1963). Schneider (1975) however challenged the assumptions made in various of these studies, and argued that 'state of the art' energy balance and radiative-convective models predicted climate sensitivities in the range 1.5-3K. That study stressed however that this range might be high or low by "several-fold" due to feedback mechanisms not properly accounted for thus far, in particular due to clouds.

Radiative-convective models continued to be developed with increasing levels of sophistication. For example, Charlock (1982) introduced interactive cloud radiative properties and liquid water contents which were proportional to the water vapour mixing ratio. This produced a strong negative shortwave cloud feedback on climate change, accompanied by a positive longwave cloud feedback from thin cirrus. Somerville and Remer (1984) thereafter pointed out that cumulus clouds are observed to have larger water contents at higher temperatures, and argued that this might also mean that cloud optical depths increase with a warming climate. They ran a radiative-convective model with this effect included and showed that this could reduce its climate sensitivity from 1.7K to 0.8K or lower. Again a small positive longwave cloud feedback from increased optical depths in thin cirrus clouds was more than compensated for by a negative shortwave cloud feedback from low and mid-level clouds. Such models were used for several years subsequently to interpret results from more complex models (e.g. Hansen et al. (1984)).

General circulation models (GCMs) started to appear in the 1950s, representing atmospheric variables such as temperature, humidity and resolved vertical and horizontal motions in three dimensions. Vertical resolution increased over the next decade from the two-level model of Phillips (1956) to the nine level model of Smagorinsky et al. (1965). The first study to use a GCM to predict climate sensitiv-

ity was Manabe and Wetherald (1975), using the model of Manabe (1969), which specified fixed clouds and a single idealised continent, simulated nine levels in the atmosphere and assumed no heat capacity or heat transport in the ocean. This study noted a strengthening hydrological cycle with warming, and estimated the climate sensitivity to be 2.9K. This larger sensitivity compared to the authors' previous estimate of 2.4K using a radiative-convective model was attributed to enhanced warming at high latitudes, caused by surface albedo feedback and a tendency for warming to be trapped near the surface by locally stable conditions.

Charney et al. (1979) was the first study to estimate an uncertainty range for climate sensitivity based on predictions from multiple GCMs. They combined unpublished results from three variants of the nine-layer model of Manabe and Wetherald (1975), one with interactive cloud feedback, and two variants of the seven-layer model from the NASA Goddard Institute for Space Studies, both with cloud feedback, later described by Hansen et al. (1983). Some of these models had 'swamp' oceans which had zero heat capacity but allowed surface evaporation, while others had 'mixed-layer' oceans with small heat capacities commensurate with an oceanic mixed layer of fixed depth (Figure 2). All models neglected ocean heat transport. The versions of these models that were considered the most realistic predicted climate sensitivities of 2-3.5K. This study also discussed cloud feedbacks, arguing that increases in low and mid-level clouds would be expected to give a negative feedback, while increases in high clouds would be expected to give a positive feedback. An additional margin for error of 0.5K was added to the lower bound for climate sensitivity to account for potential negative feedbacks from low and mid-level clouds, while 1.0K was added to the upper bound due to potential positive feedbacks from upper level clouds, resulting in an overall range of 1.5-4.5K. This range was quite similar to estimates based on radiative-convective models (1.6-4.5K).

Manabe and Wetherald (1980) was the first study to present estimates of climate sensitivity in response to CO_2 doubling using a documented GCM with interactive clouds, and so including the effects of cloud feedback. The model used was similar to that of Manabe and Wetherald (1975), with a single idealised continent covering half of the domain and nine vertical levels. Clouds were placed wherever condensation of water vapour was predicted, and were represented as black bodies at terrestrial wavelengths with zonally specified reflectivity and absorption coefficients at solar wavelengths. Cloudiness decreased in the mid-upper troposphere with increasing CO_2, but increased at lower levels. The cloud feedbacks in the longwave and shortwave approximately cancelled each other in this experiment, resulting in a climate sensitivity of 3.0K, very similar to that of Manabe and Wetherald (1975).

Hansen et al. (1984) was the first study to estimate climate sensitivity in response to CO_2 using a documented GCM with interactive cloud feedbacks and a realistic land/sea distribution (Model II, Hansen et al. (1983)). Convective cloud

Figure 2: Image of Table 1 from Charney et al. (1979) describing the climate models used.

TABLE 1 Characteristics of General-Circulation Models Examined (λ, Longitude; ϕ, Latitude; T, Temperature)

Model	Model Predictions				
Characteristics	M1[a]	M2[a]	M3[a]	H1[b]	H2[b]
Domain	$0° < \lambda < 120°$[c] $0° < \phi < 81.7°$	$0° < \lambda < 120°$[c] $0° < \phi < 90°$	Global	Global	Global
Land–ocean distribution	Ocean for $60° < \lambda < 120°$ $0° < \phi < 66.5°$	Ocean for $60° < \lambda < 120°$ $0° < \phi < 90°$	Realistic	Realistic	Realistic
Ocean	Swamp	Swamp	Mixed layer	Mixed layer	Swamp
Seasonal change	No	No	Yes	Yes	No
Cloud feedbacks	No	Yes	No	Yes	Yes
Snow and ice albedo	When $T < -25°C$ 0.7 When $T > -25°C$ 0.45 for snow 0.35 for ice	When $T < -10°C$ 0.7 When $T > -10°C$ 0.45 for snow 0.35 for ice	Depends on depth and underlying surface albedo For deep snow, 0.8 For thick ice, 0.7	For snow, depends on snow age, snow depth, underlying surface albedo, etc. For ice, 0.45	Same as H1
Horizontal resolution	About 500 km on a mercator projection	5° in longitude 4.5° in latitude	Spectral model with the maximum zonal wave number 15	10° in longitude 8° in latitude	Same as H1
Vertical resolution	9 layers	9 layers	9 layers	7 layers	7 layers

[a] Models developed by S. Manabe and colleagues at the NOAA Geophysical Fluid Dynamics Laboratory, Princeton, N.J.
[b] Models developed by J. Hansen and colleagues at the NASA Goddard Institute for Space Studies, New York, N.Y.
[c] Cyclic continuity assumed at boundaries.

fraction was diagnosed to be proportional to the mass of saturated air rising through the lower boundary of each layer, while large-scale cloud cover was taken as the saturated fraction of the grid-box, assuming a uniform sub-grid specific humidity and a Gaussian sub-grid temperature. This model also represented condensation relative to ice saturation humidity rather than water below -40^{o}C, in unseeded conditions where ice was not falling into a layer from above. Convective clouds had fixed optical thicknesses specified over a given vertical pressure interval, while

large-scale clouds had optical thicknesses which reduced with increasing height. This atmosphere model was coupled to a mixed layer ocean model with seasonally varying mixed layer depths and ocean heat transports, with a simple thermodynamic sea ice scheme. The model predicted a climate sensitivity of 4K, and the authors estimated the magnitude of the cloud feedback by running a radiative-convective model with changes in clouds specified according to the cloud changes in the GCM. Cloud feedbacks were found to amplify the climate sensitivity, due to an increase in cloud amount and altitude for high clouds, and a reduction in cloud cover for mid-low level clouds (Figure 3).

Until the late 1980s, most climate models had fixed clouds, or cloud amounts which were a function of relative humidity with fixed cloud radiative properties. Roeckner et al. (1987) was the first study to quantify the impact of introducing interactive cloud water contents and radiative properties into a full GCM. Their eight-level GCM incorporated a novel cloud scheme based on the cloud liquid-water continuity equation with parametrizations for cloud micro-physical processes such as condensation of water vapour, evaporation of cloud droplets and rain drops and conversion of small droplets to large rain drops by coalescence. In a solar-forced climate warming experiment they found increases in cloud water content which became larger with increasing altitude, with high-level water contents increasing more than twice as much per degree warming as in the case of Somerville and Remer (1984). This was found to result in a net positive cloud feedback (Schlesinger, 1988), due to a longwave positive feedback from increased emissivity of optically thin cirrus which overwhelmed the negative shortwave optical depth feedback from optically thick clouds (Roeckner, 1988).

Mitchell et al. (1989) was the first study to quantify the impact of changes in cloud phase on cloud feedbacks and climate sensitivity in a GCM. They ran climate change experiments with an eleven-layer model in which the relative humidity based scheme was replaced with one that calculated cloud fraction and cloud liquid water contents from a joint probability density function of two 'cloud-conserved variables', liquid-frozen water temperature and total water content (Smith, 1990). This reduced the climate sensitivity of the model from 5.2K to 2.7K, in the main by replacing substantial reductions in mid-latitude cloud fractions near the freezing level with small increases. Introducing interactive cloud radiative properties for liquid and ice clouds reduced the climate sensitivity further to 1.9K; this resulted in a more negative cloud feedback at midlatitudes as ice clouds were replaced by more reflective liquid water clouds in the warmer climate.

Following these pioneering studies, many modelling groups started to add interactive cloud processes to their models and to estimate climate sensitivity. The First Assessment Report (FAR) of the IPCC (Houghton et al., 1990) quoted a range of climate sensitivity of 1.9 to 5.2K from 21 climate model versions from ten modelling groups, and acknowledged that the incomplete understanding of clouds was a cause of uncertainty in the predicted magnitude of climate change. They

Figure 3: Figure 6(b) from Hansen et al. (1984). Contributions to the global-mean temperature rise in a CO_2 doubling experiment as estimated by inserting changes obtained in the 3-D experiments into 1-D radiative convective model. Reproduced with permission of the American Geophysical Union.

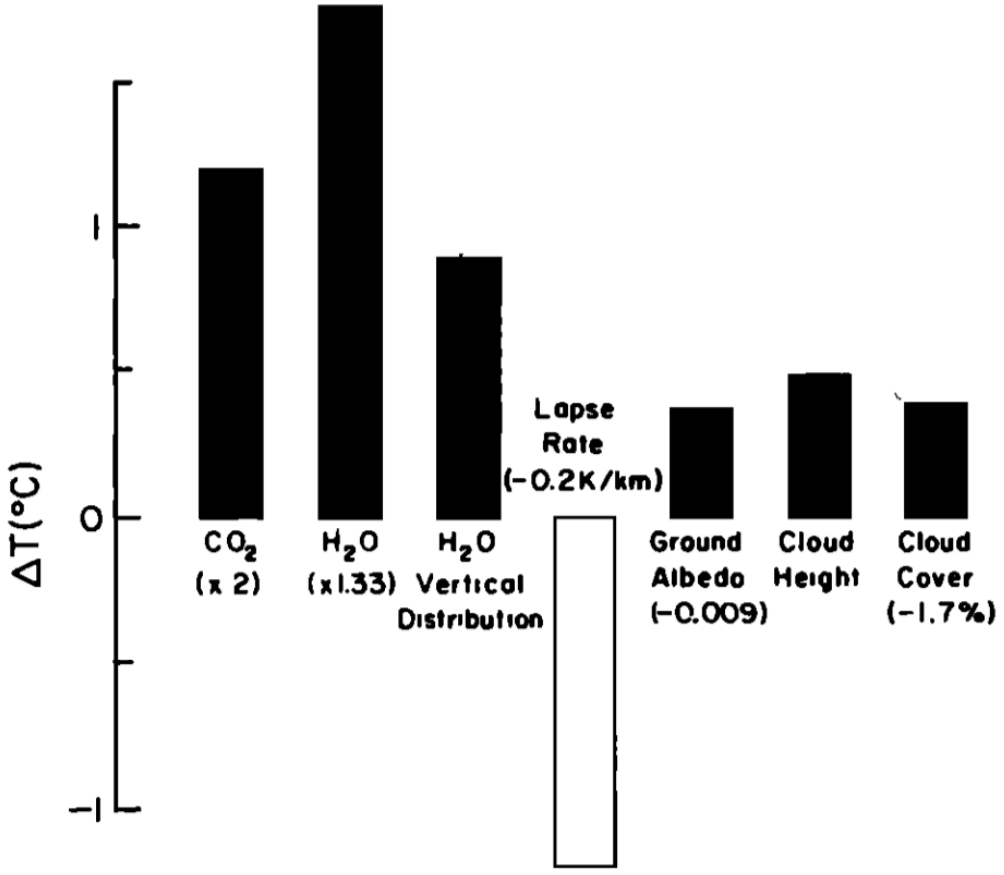

concluded: ”Most results are close to 4.0°C but recent studies using a more detailed but not necessarily more accurate representation of cloud processes give results in the lower half of this range. Hence the models results do not justify altering the previously accepted range of 1.5 to 4.5^{o}C.”

Although climate models have increased in complexity and resolution over the last thirty years, the range of climate sensitivities that they produce has not changed substantially until recently, and the IPCC’s Fifth assessment report (Stocker et al., 2013) concluded that climate sensitivity was ”likely in the range 1.5 to 4.5^{o}C”.

3 Discussion of papers submitted towards PhD by Publication

The four lead-author papers submitted as part of this PhD by publication are Webb et al. (2015a), Webb et al. (2015b), Webb et al. (2018) and Webb and Lock (2020). The first three were published within the five years prior to my application in August

2018, while the last was accepted and published online in 2020. All are primarily my own work on the topic of understanding cloud feedbacks in climate models. In 2017 I also published a multi-author paper (Webb et al., 2017) which provided a review of published studies associated with Phase 2 of the Cloud Feedback Model Intercomparison Project (CFMIP-2), and documented the experimental protocol for CFMIP-3/CMIP6. This paper is not included in this thesis because it is not primarily based on my own personal research. From 2016 to 2020 I also co-led the World Climate Research Programme (WCRP) assessment on climate sensitivity (Sherwood et al., 2020). This publication is not included for the same reason as above, but also because it would result in the word limit of 100,000 words being exceeded. Below I discuss each of the submitted publications in turn, describing the aims, objectives and results of my research, as well as the contribution made in the context of understanding cloud feedbacks in the climate system. I then conclude by explaining how the papers submitted as part of the PhD form a coherent whole, and how they meet the doctoral assessment criteria.

3.1 The diurnal cycle of marine cloud feedback in climate models

The main aim of Webb et al. (2015a) was to understand the diurnal cycle of marine cloud feedback in climate models better, and to assess its relevance to inter-model spread in overall cloud feedback. We approached this by diagnosing the diurnal cycle of marine cloud feedbacks using high-frequency (15-30 minute) outputs at selected locations, produced from seven climate models as part of phase 2 of the Cloud Feedback Model Intercomparison Project (CFMIP-2, Bony et al. (2008)). These high frequency outputs were saved in atmosphere-only 'AMIP' experiments forced with observed sea surface temperatures (SSTs) and sea ice concentrations, and in 'AMIP+4K' experiments subject to a uniform increase in SSTs.

The models were shown to reproduce the observed phase and amplitude in the diurnal cycle of present-day marine low cloud properties well, with the maxima in low-level cloud fraction and liquid water path occurring in the early morning, and with the amplitudes of the diurnal cycle of liquid water paths consistent with observations. All of the models examined exhibited positive cloud feedbacks associated with reductions in low-level cloud amounts over the oceans in the warmer climate. In most cases the largest reductions in low-cloud fraction occurred in the mornings which was the time of day when there was the most cloud in the present climate. This meant that the low-level cloud feedback was strongest at this time of day. Additionally we found that the largest inter-model spread in the cloud feedback was also at this time of day. Models with more high-level cloud in the control simulation had larger diurnal variations in the response of high-level cloud to climate warming.

We also assessed the extent to which the diurnal cycle of the cloud feedback contributed to inter-model spread in the overall cloud feedback. The variation in the strength of the marine low-cloud feedback at different times of day in individual models was found to be considerably smaller than the inter-model spread in the overall (diurnally-averaged) low-cloud feedback, which suggested that the diurnal cycle in the cloud feedback did not contribute greatly to the overall uncertainty in cloud feedback in the climate models examined.

In this paper we also highlighted a number of unusual features of the cloud feedbacks in individual models. Outlier behaviour may be due to a given model representing a particular process unusually poorly or unusually well - in either case we argued that this information is valuable for the model development process.

3.2 The impact of parametrized convection on cloud feedback

For Webb et al. (2015b) the main aim was to assess the extent to which convective parametrizations contribute to inter-model spread in cloud feedbacks in climate models. I achieved this by organising the first phase of the Selected Process On/Off Klima Intercomparison Experiment (SPOOKIE), in which AMIP and AMIP+4K experiments were performed with ten climate models with convective parametrizations deactivated. Previous studies had suggested that different convective parametrizations were a major contributor to inter-model spread in cloud feedback and climate sensitivity (e.g. Sherwood et al. (2014), Zhao (2014)). Webb et al. (2015b) however found that the range in cloud feedbacks in the ten models examined did not change substantially when convective parametrizations were deactivated. The cloud feedbacks in some models in the middle of the range did change substantially, but it was found that this impact was greatly reduced if a simple scaling was applied to the cloud feedbacks to allow for the fact that the 'convection off' simulations were not retuned to have similar present day radiative balances to their standard versions. The main contribution of this work was to provide evidence that, while parametrized convection clearly did affect the cloud feedbacks in some of the models, other processes determined the range of cloud feedbacks across the full set of models examined.

We went on to examine the impact of deactivating the convective parametrizations on clouds and cloud feedbacks in various cloud regimes over the tropical oceans. For this purpose we developed a composite index based on the lower-tropospheric stability (LTS) and surface precipitation rate (the angular LTS/precipitation index, ALPI) to separate regimes dominated by deep convective clouds, shallow convective clouds and stratocumulus.

In the strong LTS/weak precipitation regime over the tropical oceans where shallow stratocumulus clouds are prevalent in nature, the 'ConvOff' versions of the models without parametrized convection tended to have larger low-level cloud fractions and liquid water paths than the standard model versions. Consequently

the ConvOff models had more negative shortwave and net cloud radiative effects (CREs) in this regime, and larger biases compared to observed shortwave and net CRE. Nonetheless the positive cloud feedbacks in this regime remained positive without convective parametrization and had similar inter-model spread, indicating that convective parametrizations were not responsible for either of these features of the standard model ensemble. Inter-model spread in longwave cloud feedback in strongly precipitating regions of the tropics was however reduced in the ConvOff experiments compared to the standard experiments, indicating that part of the spread in the longwave cloud feedback in the standard ensemble was due the differences in convective parametrizations.

Finally, we identified statistically significant relationships between cloud feedbacks and two aspects of the present day simulations which were present in both the standard and ConvOff ensembles. These showed that models with less mid-level cloud and less moist static energy near the top of the boundary layer tended to have more positive cloud feedbacks. We suggested that these relationships could be explained using a large-scale precipitation efficiency argument.

3.3 Interactions between hydrological sensitivity, radiative cooling, stability, and low-level cloud amount feedback

The hydrological sensitivity (the rate of global mean surface evaporation and precipitation increase in response to climate warming) is typically around 3%/K in climate models, considerably less than the 7%/K increase that would be expected in the absence of changes in near-surface relative humidity, air-sea temperature difference and near-surface winds (Richter and Xie, 2008). The first aim of Webb et al. (2018) was to explore the impact of hydrological sensitivity on low-cloud feedback, to establish whether or not muted (sub-7%/K) hydrological sensitivities contribute substantially to the low-cloud fraction reductions seen in climate models with warming.

We approached this by performing uniform +4K SST perturbation experiments with the aqua-planet configuration of HadGEM2-A (Martin et al., 2011) in which the surface evaporation was specified at the surface to yield a range of hydrological sensitivities between 0-7%/K. Together with the standard model version which had a hydrological sensitivity of 3%/K, these showed an approximately linear relationship between the hydrological sensitivity and the global mean low-level cloud response to warming, with larger hydrological sensitivities being associated with progressively weaker low-cloud reductions and eventually a low-cloud increase for a hydrological sensitivity of 7%/K. We also forced the surface evaporation to increase at 7%/K by increasing the radiative cooling within the atmosphere, which resulted in a low-cloud reduction slightly larger than in the standard experiment, in contrast to the increase in the surface-forced 7%/K experiment. This showed that hydrological sensitivity was not on its own a good predictor of the low cloud

response, and that muted hydrological sensitivity did not result in a stronger low-cloud decrease compared to all 7%/K scenarios. Also the fact that the low-cloud reduction was present in the absence of a surface evaporation change in the 0%/K experiment showed that factors other than surface evaporation contributed to the low-cloud reductions in HadGEM2-A.

The surface-forced experiments showed larger free-tropospheric warming across the tropics with stronger surface evaporation, resulting in larger increases in static stability. We argued that this was the cause of the progressively weaker reductions and eventual increases in low-cloud fraction with increasing hydrological sensitivity in these experiments, due to the well-known dependence of low-cloud fraction on lower-tropospheric stability and Estimated Inversion Strength (EIS, Wood and Bretherton (2006)). The stability responses across all experiments showed that the expected relationship between EIS and low-cloud fraction was maintained and that the difference in the low-cloud response between the surface-forced and radiatively cooled 7%/K experiments was due to very different stability responses. The surface-forced 7%/K experiments showed substantial increases in stability, while the radiatively cooled 7%/K experiments showed relatively little. We argued that enhanced surface-forced evaporation resulted in more latent heat release in the atmosphere and increased stability and EIS via increases in upper tropospheric temperatures. Conversely, enhancing radiative cooling directly destabilised the atmosphere initially, which tended to reduce the EIS. However this also stimulated deep convection and latent heat release which tended to stabilise the atmosphere and increase the EIS. A balance was reached with a smaller change in stability and low-cloud fraction than is seen in the surface-forced 7%/K experiment, for the same global mean surface evaporation increase.

Our experiments also contributed some insights into the mechanisms underlying hydrological sensitivity in models. It is well established that changes in atmospheric radiative cooling can result in changes in the global hydrological cycle, for example in the case of rapid changes in global precipitation in response to CO_2 doubling. We showed however that in the somewhat different case of climate warming, increases in surface evaporation modify the atmospheric temperature and humidity structure in such a way as to increase the atmospheric longwave radiative cooling. We also showed that while changes in near-surface wind speeds were well predicted by changes in atmospheric radiative cooling, changes in near-surface relative humidity and air-sea temperature difference could only be understood in terms of differing responses to perturbations in surface evaporation and radiative cooling.

By perturbing surface evaporation and radiative cooling independently in a climate model, this study was for the first time able to quantify their individual contributions to the changes in stability and low cloud responses with climate warming, as well as to those in the near-surface atmospheric properties which regulate the hydrological sensitivity.

3.4 Testing a physical hypothesis for the relationship between climate sensitivity and double-ITCZ bias in climate models

For Webb and Lock (2020) the main aim was to develop and test a physical hypothesis to explain the finding by Tian (2015) that climate models with more pronounced double-ITCZ biases tend to have lower climate sensitivities. Tian (2015) used a well established index of the double-ITCZ bias, the annual mean model error in the surface precipitation rate averaged over the Tropical Eastern Pacific region (150-100^{o}W, 0-30^{o}S) relative to observations from the Global Precipitation Climatology Project (GPCP, Adler et al. (2003)). They found a statistically significant anticorrelation between this precipitation bias and the effective climate sensitivity S in the CMIP3 and CMIP5 models and noted that models with higher climate sensitivities tended to have smaller precipitation biases. They argued that this could be used as an ”emergent constraint” (Caldwell et al., 2018) suggesting that S might be in the upper end of the model range, with the majority of climate models underestimating S. It is generally considered desirable for emergent constraints to be based on relationships which have a plausible physical explanation (e.g. Hall et al. (2019)). However Tian (2015) provided no physical explanation for the above relationship.

Webb and Lock (2020) discussed a number of potential physical explanations for this relationship, and hypothesized that deep convection encroaching into regions that should be dominated by low clouds might make it harder to form low clouds in the present climate, thus reducing the magnitude of positive low-level cloud feedbacks and giving smaller values of climate sensitivity.

Harrop and Hartmann (2016) showed that aqua-planet experiments with clouds made transparent to radiation tended to show a more split ITCZ with more deep convection encroaching into the subtropics, while Dixit et al. (2018) showed that the width of the ITCZ in aqua-planet simulations with a single model could be varied by modifying the amount of longwave radiative heating in the equatorial boundary layer from high clouds. We exploited these findings to design variants of the HadGEM2-A aqua-planet experiment with different amounts of longwave cloud heating in the atmosphere that resulted in varying amounts of deep convection encroaching into the subtropics. We found that model versions with more precipitation encroaching into the subtropics had weaker subtropical cloud radiative effects, less positive subtropical cloud feedbacks and less positive global cloud feedbacks, which supported our hypothesis and suggested that this was a plausible physical explanation for the Tian (2015) relationship.

We tested our hypothesis in a second way by testing each of its elements in the AMIP/AMIP+4K experiments from CFMIP-2/CMIP5 and SPOOKIE (Webb et al., 2015b). SST forced experiments were chosen because our hypothesis did not rely on changes in ocean heat transport. A statistically significant anticorrelation (r=-0.69) was found between the Tian (2015) precipitation index and

the global cloud feedback in these experiments, consistent with the idea that the relationship between the precipitation index and the climate sensitivity in these experiments was mediated by the cloud feedback. We also found a statistically significant relationship between the precipitation index and the present day cloud radiative effects averaged over the Peruvian marine stratus region of Klein and Hartmann (1993) (r=0.56), and with other low cloud regions, which supported the first element of our hypothesis, that deep convection encroaching into the subtropics weakens low-cloud radiative effects. The cloud feedback in the Peruvian stratus region was also found to be correlated significantly with the global cloud feedback (r=0.58), which was necessary to support the argument that the global cloud feedback is strongly affected by low cloud feedbacks.

However we did not find statistically significant correlations to support all elements of our hypothesis in the CMIP5/SPOOKIE models. The net cloud feedbacks and the present-day CRE values in the Peruvian stratus region were anticorrelated as predicted by our hypothesis, but the correlation coefficient (r=-0.44) was not statistically distinguishable from zero at the 5% confidence level, as the 5% significance threshold for an anticorrelation in this case was -0.5. Also an end-to-end test which correlated the precipitation index with local cloud feedbacks in all locations found that the most statistically significant correlations appeared in regions not typically associated with low-level clouds, and that correlations in the subtropics were small. These correlations in other regions (e.g. the midlatitudes) were not predicted by our hypothesis, which suggests that other explanations may be required to explain the full relationship between the precipitation index and the global cloud feedback in these models. Furthermore, examination of the AMIP/AMIP+4K experiments newly provided by CMIP6 and CFMIP-3 showed only a weak correlation (r=0.22) between the precipitation index and the global cloud feedback.

We concluded by arguing that although our results did not provide a compelling physical explanation for the Tian (2015) result, our contribution was to have demonstrated how a combination of idealised modelling, targeted sensitivity tests and multi-model analysis could be used to provide a stringent test for hypothesized mechanisms for emergent constraints.

3.5 Doctoral Assessment Criteria

These papers form a coherent whole in the sense that they all develop novel experimental techniques to apply them to understand cloud feedbacks in climate models, as described in sections 3.1-3.4.

The papers have all been published in peer-reviewed journals and so are clearly of a quality to satisfy peer review and merit publication. All provide evidence of the creation and interpretation of new knowledge through original research, extending the forefront of the discipline, as detailed above. For example,

Webb et al. (2015a) showed for the first time that reductions in marine low-cloud fraction in the warmer climate are in almost all cases largest in the mornings when more cloud is present in the control simulations. Meanwhile Webb et al. (2015b) was the first study to have demonstrated that deactivating convective parametrizations reduced the range of longwave cloud feedback but not in shortwave or net cloud feedback across a diverse set of climate models. Webb et al. (2018) showed for the first time that varying the hydrological sensitivity in a climate model had a substantial impact on the stability of the atmosphere and via that the low-level cloud feedback, while Webb and Lock (2020) found evidence to support relationships between tropical precipitation and subtropical low-cloud radiative effects, and between local low-cloud radiative effects and local cloud feedbacks.

My papers demonstrate that I have systematically acquired and understood a substantial body of knowledge which is at the forefront of research on the understanding of cloud-climate feedbacks. All four papers provide reviews of the relevant background literature in their introductory sections, and where appropriate interpret their results in the light of other relevant studies. This extended introductory chapter also includes a literature review of key developments in cloud feedbacks and climate sensitivity from the advent of climate modelling up until the first IPCC Assessment Report in 1990, which provides further evidence of my understanding of this area of climate science (see section 2).

My general ability to conceptualise, design and implement a project for the generation of new knowledge and understanding is demonstrated by all four of the papers submitted. For example, I recognised some years ago that the high-frequency model outputs saved at selected locations by a small number of modelling groups involved in the Climate Process Team on low-latitude cloud feedbacks on climate sensitivity (Bretherton (2006),Mapes et al. (2009)) could be usefully applied to understanding cloud feedbacks and their diurnal variations in climate models if they were included in climate change experiments. I organised the inclusion of these outputs in CFMIP-2/CMIP5 present-day and climate-change experiments, and Webb et al. (2015a) documented the choices of the locations as well as providing the first published results using these data. Similarly I recognised that experiments with convective parametrizations deactivated, which had hitherto been documented in individual models only, could be used to assess the impact of convective parametrizations on the cloud feedback range across models. This motivated me to organise the Selected Process On/Off Klima Intercomparison Experiment (SPOOKIE, Webb et al. (2015b)). I approached representatives of various modelling groups and encouraged them to run AMIP/AMIP+4K experiments without convective parametrizations, and subsequently analysed the results and published the findings. The study of Webb et al. (2018) was motivated by what I perceived to be a lack of clarity in the literature over how elements of the tropospheric energy budget reach a new balance as the global hydrological cycle changes with increasing global temperatures, and what implications if any such

changes have for low-cloud feedbacks. My approach was to design experiments in which both surface evaporation and radiative cooling are perturbed to explore the interactions between these elements of the tropospheric energy budget and other characteristics such as stability and low-cloud fraction. Specifying plausible surface evaporation and radiative cooling rates in a realistic configuration such as AMIP/AMIP+4K was found to be technically over-ambitious and so I decided to specify a zonal mean climatology in an idealised aqua-planet configuration. This was justified given that aqua-planet experiments have been shown to reproduce global cloud feedbacks in realistic configurations remarkably well (Ringer et al., 2014). The work leading to Webb and Lock (2020) was organised in a slightly different way in that it was motivated by my desire to develop and test a physical hypothesis to explain the correlation between double-ITCZ bias and climate sensitivity found by Tian (2015). This started with a systematic review of potential hypotheses, and selection of the one which seemed most physically plausible for further testing. I then developed radiative cooling perturbation experiments designed to manipulate the tropical convection in an aqua-planet experiment to test the hypothesis. The results from these experiments were encouraging, but I wanted to be sure that they were relevant to the multi-model ensemble as well, so I performed a multi-model regional correlation analysis to check each element of the argument in the CFMIP-2 and CFMIP-3 experiments. This two-pronged approach turned out to provide a very stringent test which we argued would be useful to apply to other hypothesized emergent constraints.

In some cases it was necessary to make adjustments to the projects' designs to allow for to unforeseen problems. One issue that arose with the convection-off experiments was that some of the models failed to run due to numerical instabilities that developed. We modified the experimental protocol to allow models to be run with shorter timesteps where necessary. Another example of overcoming an issue with the experimental design emerged when I ran the initial aqua-planet experiments for Webb et al. (2018). The 'QObs' aqua-planet configuration can be prone to flipping into an asymmetric state in response to certain perturbations, a behaviour which is not present in more realistic model configurations. Our initial experiments perturbing the hydrological cycle with this configuration of HadGEM2-A ran into this problem, which we resolved by using the APE "Control" dataset, which has more peaked SSTs in the tropics (Neale and Hoskins, 2000). The final example to note is that my initial idea for Webb and Lock (2020) was to focus exclusively on the aqua-planet perturbation experiments for the paper. These experiments were run and the results written up in a draft manuscript when I started to become concerned about the possibility that, although the experiments showed our mechanism to be physically credible, we had not excluded the possibility that some other mechanism could be operating in the multi-model ensemble. Unfortunately the subsequent regional correlation analysis in the CFMIP AMIP/AMIP+4K experiments did not provide strong support for the hypothesis. This was discour-

aging, but I decided that it was still worthwhile to publish these results for two reasons. Firstly, I hoped that they might be of interest to some in the scientific community. Secondly, doing so would reduce the likelihood that others would spend time repeating similar investigations.

The papers submitted demonstrate a detailed understanding of applicable techniques and advanced academic enquiry. I conducted the research for these papers independently without supervision, and the process of academic enquiry that I followed is described above. Here I discuss some of the techniques used. All of the papers included employ feedback analysis techniques to define and diagnose cloud radiative feedbacks. The convention that I tend to use for defining feedback parameters in my papers is based on that of Wetherald and Manabe (1988), where feedbacks are additive and expressed in units of $W/m^2/K$. I generally decompose cloud and non-cloud feedbacks using the change in the Cloud Radiative Forcing, which is the difference between the net downward all-sky and clear-sky radiative flux at the top of the atmosphere (Coakley Jr and Baldwin, 1984), now more commonly referred to as the cloud radiative effect (CRE). This feedback decomposition was first proposed by Cess et al. (1989), and is one of the most commonly used methods for diagnosing cloud feedbacks in climate models. Another approach, now generally known as the Partial Radiative Perturbation (PRP) method (Soden et al., 2004), was introduced in its earliest form by Manabe and Wetherald (1980). As applied in most contemporary studies, this requires instantaneous values of all inputs to the model's radiation scheme (clouds, water vapour, temperature etc.) to be saved from control and climate change experiments. These are then run through offline radiation calculations in which one variable is perturbed at a time to estimate its associated feedback term. PRP remains the "gold standard" for feedback analysis, but is technically demanding and suffers from budget closure issues due to the decorrelation between variables that occurs when variables are changed one at a time (Colman and McAvaney, 1997). Soden and Held (2006) introduced a radiative kernel method which allowed PRP-like feedbacks to be approximated using radiative kernels produced by running offline radiative calculations with small perturbations made to the non-cloud input variables. These are then multiplied by time mean changes temperature and water vapour etc. to give approximate values for the non-cloud feedbacks. Cloud feedbacks are then estimated as a residual term. The Cess et al. (1989) method is now understood to decompose feedbacks differently to the PRP method in the sense that it includes "cloud masking" effects (Soden et al., 2004). Note however that "cloud masking" has recently been shown to be a misleading term in some situations, and that these effects are perhaps better described in more general terms as the climatological effects of clouds on the non-cloud feedbacks or "cloud climatology effects" (Yoshimori et al., 2020). Kernel methods were subsequently refined to estimate the "cloud masking" term and combine this with the change in the CRE to estimate the PRP cloud feedback (e.g. Soden et al. (2008)) and to decom-

pose cloud feedbacks into contributions from different cloud types (e.g. Zelinka et al. (2012)). The CRE feedback decomposition method remains a convenient tool for comparing cloud feedbacks between models however because it is based on commonly available model outputs and side-steps issues with decomposition residuals which are common with kernel methods (e.g. Vial et al. (2013)).

Another technique employed in Webb et al. (2015b) is the mechanism denial experiment, where a process in climate model is suppressed, and the impact of this change relative to the original experiment is used to assess the importance of that process (e.g. Kim et al. (2011)). Although the term mechanism denial was first coined in 2011, such experiments have been performed for many years (e.g. Chao and Chen (2001)) and in particular applied to convective parametrization (e.g. Frierson (2007), Lin et al. (2008)). Other examples include studies which have determined the impact of clouds and cloud feedbacks on the large-scale circulation by removing cloud radiative effects (e.g. Slingo and Slingo (1988), Fermepin and Bony (2014), Li et al. (2015)) or by holding clouds seen by radiation fixed using ”cloud locking” experiments (e.g. Vavrus (2004), Mauritsen et al. (2013)). Mechanism denial experiments may be seen as a complement to many studies from the ”golden age” of climate modelling in the 1970s and 1980s where the impacts of many climate feedback processes were understood by introducing them into climate models for the first time. For example, Manabe and Wetherald (1980) was the first published study to implement interactive cloud feedbacks into a climate model with a three-dimensional atmosphere, Roeckner et al. (1987) was the first to introduce interactive cloud water contents and Mitchell et al. (1989) the first to introduce the effects of cloud phase changes. The interpretation of mechanism denial experiments may however be difficult in complex interacting systems. Suppression of one process may inhibit an emergent property of the system which depends on multiple interacting processes. To make an analogy, a concussion which makes a person lose consciousness may prevent them from walking even though their legs are unharmed (Geoffrey Vallis, pers comm). One would not learn everything one might want to know about the mechanism of walking from observing this case. To make another analogy, someone with a leg injury may still be able to move around by other means than walking. Disrupting a key process may not have the expected impact if another process takes over when it is suppressed. For example, our results in Webb et al. (2015b) still showed evidence of vertical mixing in the atmosphere even with convective parametrizations deactivated, presumably because instabilities were removed by resolved vertical motions and turbulent mixing processes rather than parametrized convection. Nonetheless we argue that such experiments may yield useful insights, even if care must be taken in their interpretation.

The last group of techniques that I have drawn on in my work are those used to decompose cloud feedbacks into contributions from different cloud types or regimes. Early studies that focused on different cloud types tended to examine

area averages over fixed regions where a given cloud type was commonly observed. For example, Klein and Hartmann (1993) identified a number of marine stratus regions which are still used today (e.g. Webb and Lock (2020)). Subsequent studies examined cloud feedbacks stratified as a function of sea surface temperature (e.g. Tselioudis et al. (1992)), 500 hPa vertical pressure velocity (e.g. Bony et al. (2004) Bony and Dufresne (2005)), lower-tropospheric stability (e.g. Wyant et al. (2009)), and subsequently joint distributions of such variables (e.g. Medeiros and Stevens (2011)) and hybrid indices (e.g. Webb et al. (2015b)), with an increasing focus on feedbacks from tropical marine low-cloud regimes in recent years (e.g. Bony and Dufresne (2005), Webb et al. (2006), Webb et al. (2013), Vial et al. (2013)). Decomposition of cloud feedbacks into contributions different cloud types has also become increasingly common with climate models participating in CFMIP producing outputs using the ISCCP simulator (Klein and Jakob (1999), Webb et al. (2001), Bodas-Salcedo et al. (2011)). This is a piece of code that can be built into a climate model to simulate cloud retrievals consistent with those from the International Satellite Cloud Climatology Project (ISCCP, Schiffer and Rossow (1983)). Two commonly employed approaches for this include firstly the use of daily ISCCP simulator outputs to decompose cloud feedbacks into contributions from known observed cloud types using a clustering algorithm (e.g. Williams and Webb (2009)) and secondly the use of cloud radiative kernels to decompose cloud feedbacks into contributions from changes in cloud fraction, cloud optical depth and cloud height using monthly-mean ISCCP simulator outputs (e.g. Zelinka et al. (2012), Zelinka et al. (2016)).

Finally, I believe that my work maintains a satisfactory level of literary presentation. My personal view is that the purpose of academic writing is to communicate the key elements of a study as clearly as possible while including all of the relevant details. I like to keep figures as simple as possible to convey the necessary information. Many scientists are not native English speakers and for this reason I try to write in plain English. I prefer to explain important concepts, supporting them with references where necessary, rather than requiring the reader to refer to other papers. My writing style is informal and accessible, but for the reasons described above, not particularly concise. For this reason I have written few short papers.

References

Adler, R. F., Huffman, G. J., Chang, A., Ferraro, R., Xie, P.-P., Janowiak, J., Rudolf, B., Schneider, U., Curtis, S., Bolvin, D., et al. (2003). The version-2 global precipitation climatology project (GPCP) monthly precipitation analysis (1979–present). *Journal of hydrometeorology*, 4(6):1147–1167.

Annan, J. D. and Hargreaves, J. C. (2006). Using multiple observationally-based constraints to estimate climate sensitivity. *Geophysical Research Letters*, 33(6).

Arrhenius, S. (1896). On the influence of carbonic acid in the air upon the temperature of the ground. *The London, Edinburgh, and Dublin Philosophical Magazine and Journal of Science*, 41(251):237–276.

Blossey, P. N., Bretherton, C. S., Zhang, M., Cheng, A., Endo, S., Heus, T., Liu, Y., Lock, A. P., de Roode, S. R., and Xu, K.-M. (2013). Marine low cloud sensitivity to an idealized climate change: The CGILS LES intercomparison. *Journal of Advances in Modeling Earth Systems*, 5(2):234–258.

Bodas-Salcedo, A., Webb, M., Bony, S., Chepfer, H., Dufresne, J.-L., Klein, S., Zhang, Y., Marchand, R., Haynes, J., Pincus, R., et al. (2011). COSP: Satellite simulation software for model assessment. *Bulletin of the American Meteorological Society*, 92(8):1023–1043.

Bony, S. and Dufresne, J.-L. (2005). Marine boundary layer clouds at the heart of tropical cloud feedback uncertainties in climate models. *Geophysical Research Letters*, 32(20).

Bony, S., Dufresne, J.-L., Le Treut, H., Morcrette, J.-J., and Senior, C. (2004). On dynamic and thermodynamic components of cloud changes. *Climate Dynamics*, 22(2-3):71–86.

Bony, S., Webb, M., Stevens, B., Bretherton, C., Klein, S., and Tselioudis, G. (2008). CFMIP-GCSS plans for advancing assessments of cloud-climate feedbacks. *GEWEX News*, 18(4):10–12.

Bretherton, C. (2006). The climate process team on low-latitude cloud feedbacks on climate sensitivity. *US Clivar Variations*, (4):7–12.

Bretherton, C. S. (2015). Insights into low-latitude cloud feedbacks from high-resolution models. *Philosophical Transactions of the Royal Society A: Mathematical, Physical and Engineering Sciences*, 373(2054).

Bretherton, C. S., Blossey, P. N., and Jones, C. R. (2013). Mechanisms of marine low cloud sensitivity to idealized climate perturbations: A single-LES exploration extending the CGILS cases. *Journal of Advances in Modeling Earth Systems*, 5(2):316–337.

Budyko, M. I. (1972). The future climate. *Eos, Transactions American Geophysical Union*, 53(10):868–874.

Caldwell, P. M., Zelinka, M. D., and Klein, S. A. (2018). Evaluating emergent constraints on equilibrium climate sensitivity. *Journal of Climate*, 31(10):3921–3942.

Callendar, G. S. (1938). The artificial production of carbon dioxide and its influence on temperature. *Quarterly Journal of the Royal Meteorological Society*, 64(275):223–240.

Callendar, G. S. (1949). Can carbon dioxide influence climate? *Weather*, 4(10):310–314.

Ceppi, P., Brient, F., Zelinka, M. D., and Hartmann, D. L. (2017). Cloud feedback mechanisms and their representation in global climate models. *Wiley Interdisciplinary Reviews: Climate Change*, 8(4).

Cess, R., Zhang, M., Ingram, W., Potter, G., Alekseev, V., Barker, H., Cohen-Solal, E., Colman, R., Dazlich, D., Del Genio, A., et al. (1996). Cloud feedback in atmospheric general circulation models: An update. *Journal of Geophysical Research: Atmospheres*, 101(D8):12791–12794.

Cess, R. D., Potter, G., Blanchet, J., Boer, G., Del Genio, A., Deque, M., Dymnikov, V., Galin, V., Gates, W., Ghan, S., et al. (1990). Intercomparison and interpretation of climate feedback processes in 19 atmospheric general circulation models. *Journal of Geophysical Research: Atmospheres*, 95(D10):16601–16615.

Cess, R. D., Potter, G., Blanchet, J., Boer, G., Ghan, S., Kiehl, J., Le Treut, H., Li, Z.-X., Liang, X.-Z., Mitchell, J., et al. (1989). Interpretation of cloud-climate feedback as produced by 14 atmospheric general circulation models. *Science*, 245(4917):513–516.

Chahine, M. T. (1992). GEWEX: The global energy and water cycle experiment. *Eos, Transactions American Geophysical Union*, 73(2):9–14.

Chamberlin, T. C. (1899). An attempt to frame a working hypothesis of the cause of glacial periods on an atmospheric basis. *The Journal of Geology*, 7(6):545–584.

Chao, W. C. and Chen, B. (2001). The role of surface friction in tropical intraseasonal oscillation. *Monthly Weather Review*, 129(4):896–904.

Charlock, T. P. (1982). Cloud optical feedback and climate stability in a radiative-convective model. *Tellus*, 34(3):245–254.

Charney, J. G., Arakawa, A., Baker, D. J., Bolin, B., Dickinson, R. E., Goody, R. M., Leith, C. E., Stommel, H. M., and Wunsch, C. I. (1979). *Carbon dioxide and climate: a scientific assessment*. National Academy of Sciences, Washington, DC.

Coakley Jr, J. and Baldwin, D. (1984). Towards the objective analysis of clouds from satellite imagery data. *Journal of Climate and Applied Meteorology*, 23(7):1065–1099.

Colman, R. and McAvaney, B. (1997). A study of general circulation model climate feedbacks determined from perturbed sea surface temperature experiments. *Journal of Geophysical Research: Atmospheres*, 102(D16):19383–19402.

Cox, P. M., Huntingford, C., and Williamson, M. S. (2018). Emergent constraint on equilibrium climate sensitivity from global temperature variability. *Nature*, 553(7688):319.

Dixit, V., Geoffroy, O., and Sherwood, S. C. (2018). Control of ITCZ width by low-level radiative heating from upper-level clouds in aquaplanet simulations. *Geophysical Research Letters*, 45(11):5788–5797.

Edwards, P. N. (2011). History of climate modeling. *Wiley Interdisciplinary Reviews: Climate Change*, 2(1):128–139.

Eyring, V., Bony, S., Meehl, G. A., Senior, C. A., Stevens, B., Stouffer, R. J., and Taylor, K. E. (2016). Overview of the Coupled Model Intercomparison Project Phase 6 (CMIP6) experimental design and organization. *Geoscientific Model Development*, 9(5):1937–1958.

Fermepin, S. and Bony, S. (2014). Influence of low-cloud radiative effects on tropical circulation and precipitation. *Journal of Advances in Modeling Earth Systems*, 6(3):513–526.

Frierson, D. M. (2007). The dynamics of idealized convection schemes and their effect on the zonally averaged tropical circulation. *Journal of the Atmospheric Sciences*, 64(6):1959–1976.

Gates, W. L., Boyle, J. S., Covey, C., Dease, C. G., Doutriaux, C. M., Drach, R. S., Fiorino, M., Gleckler, P. J., Hnilo, J. J., Marlais, S. M., et al. (1999). An overview of the results of the Atmospheric Model Intercomparison Project (AMIP I). *Bulletin of the American Meteorological Society*, 80(1):29–56.

Gregory, J., Ingram, W., Palmer, M., Jones, G., Stott, P., Thorpe, R., Lowe, J., Johns, T., and Williams, K. (2004). A new method for diagnosing radiative forcing and climate sensitivity. *Geophysical Research Letters*, 31(3).

Grose, M. R., Gregory, J., Colman, R., and Andrews, T. (2018). What climate sensitivity index is most useful for projections? *Geophysical Research Letters*, 45(3):1559–1566.

Hall, A., Cox, P., Huntingford, C., and Klein, S. (2019). Progressing emergent constraints on future climate change. *Nature Climate Change*, 9:269–278.

Hansen, J., Lacis, A., Rind, D., Russell, G., Stone, P., Fung, I., Ruedy, R., and Lerner, J. (1984). Climate sensitivity: Analysis of feedback mechanisms. *Climate Processes in Climate Sensitivity, Geophysical Monograph 29, Maurice Ewing, American Geophysical Union.*, 5:130–163.

Hansen, J., Russell, G., Rind, D., Stone, P., Lacis, A., Lebedeff, S., Ruedy, R., and Travis, L. (1983). Efficient three-dimensional global models for climate studies: Models i and ii. *Monthly Weather Review*, 111(4):609–662.

Harrop, B. E. and Hartmann, D. L. (2016). The role of cloud radiative heating in determining the location of the ITCZ in aquaplanet simulations. *Journal of Climate*, 29(8):2741–2763.

Houghton, J., Jenkins, G., and Ephraums, J. (1990). *Climate change: The IPCC scientific assessment (Contribution of Working Group I to the first assessment report of the Intergovernmental Panel on Climate Change)*. Cambridge University Press.

Kaplan, L. D. (1960). The influence of carbon dioxide variations on the atmospheric heat balance. *Tellus*, 12(2):204–208.

Kim, D., Sobel, A. H., and Kang, I.-S. (2011). A mechanism denial study on the Madden-Julian Oscillation. *Journal of Advances in Modeling Earth Systems*, 3(4).

Klein, S. A., Hall, A., Norris, J. R., and Pincus, R. (2017). Low-cloud feedbacks from cloud-controlling factors: a review. In *Shallow Clouds, Water Vapor, Circulation, and Climate Sensitivity*, pages 135–157. Springer.

Klein, S. A. and Hartmann, D. L. (1993). The seasonal cycle of low stratiform clouds. *Journal of Climate*, 6(8):1587–1606.

Klein, S. A. and Jakob, C. (1999). Validation and sensitivities of frontal clouds simulated by the ECMWF model. *Monthly Weather Review*, 127(10):2514–2531.

Li, Y., Thompson, D. W., and Bony, S. (2015). The influence of atmospheric cloud radiative effects on the large-scale atmospheric circulation. *Journal of Climate*, 28(18):7263–7278.

Lin, J.-L., Lee, M.-I., Kim, D., Kang, I.-S., and Frierson, D. M. (2008). The impacts of convective parameterization and moisture triggering on AGCM-simulated convectively coupled equatorial waves. *Journal of Climate*, 21(5):883–909.

Manabe, S. (1969). Climate and the ocean circulation: I. The atmospheric circulation and the hydrology of the Earth's surface. *Monthly Weather Review*, 97(11):739–774.

Manabe, S. and Strickler, R. F. (1964). Thermal equilibrium of the atmosphere with a convective adjustment. *Journal of the Atmospheric Sciences*, 21(4):361–385.

Manabe, S. and Wetherald, R. T. (1967). Thermal equilibrium of the atmosphere with a given distribution of relative humidity. *Journal of the Atmospheric Sciences*, 24(3):241–259.

Manabe, S. and Wetherald, R. T. (1975). The effects of doubling the CO_2 concentration on the climate of a general circulation model. *Journal of the Atmospheric Sciences*, 32(1):3–15.

Manabe, S. and Wetherald, R. T. (1980). On the distribution of climate change resulting from an increase in CO_2 content of the atmosphere. *Journal of the Atmospheric Sciences*, 37(1):99–118.

Mapes, B., Bacmeister, J., Khairoutdinov, M., Hannay, C., and Zhao, M. (2009). Virtual field campaigns on deep tropical convection in climate models. *Journal of Climate*, 22(2):244–257.

Martin, G., Bellouin, N., Collins, W., Culverwell, I., Halloran, P., Hardiman, S., Hinton, T., Jones, C., McDonald, R., McLaren, A., O'Connor, F., et al. (2011). The HadGEM2 family of Met Office Unified Model climate configurations. *Geoscientific Model Development*, 4(3):723–757.

Mauritsen, T., Graversen, R. G., Klocke, D., Langen, P. L., Stevens, B., and Tomassini, L. (2013). Climate feedback efficiency and synergy. *Climate Dynamics*, 41(9-10):2539–2554.

Medeiros, B. and Stevens, B. (2011). Revealing differences in GCM representations of low clouds. *Climate Dynamics*, 36(1-2):385–399.

Meehl, G. A., Covey, C., Delworth, T., Latif, M., McAvaney, B., Mitchell, J. F., Stouffer, R. J., and Taylor, K. E. (2007). The WCRP CMIP3 multimodel dataset: A new era in climate change research. *Bulletin of the American Meteorological Society*, 88(9):1383–1394.

Mitchell, J. F., Senior, C., and Ingram, W. (1989). CO_2 and climate: a missing feedback? *Nature*, 341(6238):132–134.

Möller, F. (1963). On the influence of changes in the CO_2 concentration in air on the radiation balance of the Earth's surface and on the climate. *Journal of Geophysical Research*, 68(13):3877–3886.

Murphy, J. M., Sexton, D. M., Barnett, D. N., Jones, G. S., Webb, M. J., Collins, M., and Stainforth, D. A. (2004). Quantification of modelling uncertainties in a large ensemble of climate change simulations. *Nature*, 430(7001):768.

Neale, R. B. and Hoskins, B. J. (2000). A standard test for AGCMs including their physical parametrizations: I: The proposal. *Atmospheric Science Letters*, 1(2):101–107.

Paltridge, G. (1974). Global cloud cover and earth surface temperature. *Journal of the Atmospheric Sciences*, 31(6):1571–1576.

Phillips, N. A. (1956). The general circulation of the atmosphere: A numerical experiment. *Quarterly Journal of the Royal Meteorological Society*, 82(352):123–164.

Plass, G. N. (1956). The carbon dioxide theory of climatic change. *Tellus*, 8(2):140–154.

Qu, X., Hall, A., Klein, S. A., and Caldwell, P. M. (2014). On the spread of changes in marine low cloud cover in climate model simulations of the 21st century. *Climate dynamics*, 42(9-10):2603–2626.

Qu, X., Hall, A., Klein, S. A., and DeAngelis, A. M. (2015). Positive tropical marine low-cloud cover feedback inferred from cloud-controlling factors. *Geophysical Research Letters*, 42(18):7767–7775.

Richter, I. and Xie, S.-P. (2008). Muted precipitation increase in global warming simulations: A surface evaporation perspective. *Journal of Geophysical Research: Atmospheres*, 113(D24).

Ringer, M. A., Andrews, T., and Webb, M. J. (2014). Global-mean radiative feedbacks and forcing in atmosphere-only and coupled atmosphere-ocean climate change experiments. *Geophysical Research Letters*, 41(11):4035–4042.

Roeckner, E. (1988). Negative or positive cloud optical depth feedback? *Nature*, 335(6188):304–304.

Roeckner, E., Schlese, U., Biercamp, J., and Loewe, P. (1987). Cloud optical depth feedbacks and climate modelling. *Nature*, 329(6135):138–140.

Schiffer, R. A. and Rossow, W. B. (1983). The International Satellite Cloud Climatology Project (ISCCP): The first project of the world climate research programme. *Bulletin of the American Meteorological Society*, 64(7):779–784.

Schlesinger, M. (1988). Comment on cloud optical depth feedback and climate modeling. *Nature*, 335:303–304.

Schneider, S. H. (1975). On the carbon dioxide–climate confusion. *Journal of the Atmospheric Sciences*, 32(11):2060–2066.

Sellers, W. D. (1969). A global climatic model based on the energy balance of the earth-atmosphere system. *Journal of Applied Meteorology*, 8(3):392–400.

Sherwood, S., Webb, M. J., Annan, J. D., Armour, K. C., Forster, P. M., Hargreaves, J. C., Hegerl, G., A, S., Marvel, K. D., Rohling, E. J., Watanabe, M., Andrews, T., Braconnot, P., Bretherton, C. S., Foster, G. L., Hausfather, Z., von der Heydt, A. S., Knutti, R., Mauritsen, T., Norris, J. R., Proistosescu, C., Rugenstein, M., Schmidt, G. A., Tokarska, K. B., and Zelinka, M. (2020). An assessment of Earth's climate sensitivity using multiple lines of evidence. *Reviews of Geophysics*, 58(4).

Sherwood, S. C., Bony, S., and Dufresne, J.-L. (2014). Spread in model climate sensitivity traced to atmospheric convective mixing. *Nature*, 505(7481):37.

Slingo, A. and Slingo, J. (1988). The response of a general circulation model to cloud longwave radiative forcing. i: Introduction and initial experiments. *Quarterly Journal of the Royal Meteorological Society*, 114(482):1027–1062.

Smagorinsky, J., Manabe, S., Holloway, J. L., et al. (1965). Numerical results from a nine-level general circulation model of the atmosphere. *Mon. Wea. Rev*, 93(12):727–768.

Smith, R. (1990). A scheme for predicting layer clouds and their water content in a general circulation model. *Quarterly Journal of the Royal Meteorological Society*, 116(492):435–460.

Soden, B. J., Broccoli, A. J., and Hemler, R. S. (2004). On the use of cloud forcing to estimate cloud feedback. *Journal of Climate*, 17(19):3661–3665.

Soden, B. J. and Held, I. M. (2006). An assessment of climate feedbacks in coupled ocean–atmosphere models. *Journal of Climate*, 19(14):3354–3360.

Soden, B. J., Held, I. M., Colman, R., Shell, K. M., Kiehl, J. T., and Shields, C. A. (2008). Quantifying climate feedbacks using radiative kernels. *Journal of Climate*, 21(14):3504–3520.

Somerville, R. C. and Remer, L. A. (1984). Cloud optical thickness feedbacks in the CO_2 climate problem. *Journal of Geophysical Research: Atmospheres*, 89(D6):9668–9672.

Stevens, B., Sherwood, S. C., Bony, S., and Webb, M. J. (2016). Prospects for narrowing bounds on Earth's equilibrium climate sensitivity. *Earth's Future*, 4(11):512–522.

Stocker, T. F., Qin, D., Plattner, G., Tignor, M., Allen, S., Boschung, J., Nauels, A., Xia, Y., Bex, V., and Midgley, P. (2013). *Climate Change 2013: The physical science basis. Intergovernmental panel on climate change, working group I contribution to the IPCC fifth assessment report (AR5)*. Cambridge University Press, Cambridge, UK and New York.

Taylor, K. E., Stouffer, R. J., and Meehl, G. A. (2012). An overview of CMIP5 and the experiment design. *Bulletin of the American Meteorological Society*, 93(4):485–498.

Tian, B. (2015). Spread of model climate sensitivity linked to double-intertropical convergence zone bias. *Geophysical Research Letters*, 42(10):4133–4141.

Tselioudis, G., Rossow, W. B., and Rind, D. (1992). Global patterns of cloud optical thickness variation with temperature. *Journal of Climate*, 5(12):1484–1495.

Vavrus, S. (2004). The impact of cloud feedbacks on arctic climate under greenhouse forcing. *Journal of Climate*, 17(3):603–615.

Vial, J., Bony, S., Stevens, B., and Vogel, R. (2017). Mechanisms and model diversity of trade-wind shallow cumulus cloud feedbacks: a review. In *Shallow Clouds, Water Vapor, Circulation, and Climate Sensitivity*, pages 159–181. Springer.

Vial, J., Dufresne, J.-L., and Bony, S. (2013). On the interpretation of inter-model spread in CMIP5 climate sensitivity estimates. *Climate Dynamics*, 41(11-12):3339–3362.

Weare, B. C. and Snell, F. M. (1974). A diffuse thin cloud atmospheric structure as a feedback mechanism in global climatic modeling. *Journal of the Atmospheric Sciences*, 31(7):1725–1734.

Webb, M., Senior, C., Bony, S., and Morcrette, J.-J. (2001). Combining ERBE and ISCCP data to assess clouds in the Hadley Centre, ECMWF and LMD atmospheric climate models. *Climate Dynamics*, 17(12):905–922.

Webb, M. J., Andrews, T., Bodas-Salcedo, A., Bony, S., Bretherton, C. S., Chadwick, R., Chepfer, H., Douville, H., Good, P., Kay, J. E., et al. (2017). The Cloud Feedback Model Intercomparison Project (CFMIP) contribution to CMIP6. *Geoscientific Model Development*, 2017:359–384.

Webb, M. J., Lambert, F. H., and Gregory, J. M. (2013). Origins of differences in climate sensitivity, forcing and feedback in climate models. *Climate Dynamics*, 40(3-4):677–707.

Webb, M. J. and Lock, A. P. (2020). Testing a physical hypothesis for the relationship between climate sensitivity and double-ITCZ bias in climate models. *Journal of Advances in Modeling Earth Systems*.

Webb, M. J., Lock, A. P., Bodas-Salcedo, A., Bony, S., Cole, J. N., Koshiro, T., Kawai, H., Lacagnina, C., Selten, F. M., Roehrig, R., et al. (2015a). The diurnal cycle of marine cloud feedback in climate models. *Climate Dynamics*, 44(5-6):1419–1436.

Webb, M. J., Lock, A. P., Bretherton, C. S., Bony, S., Cole, J. N., Idelkadi, A., Kang, S. M., Koshiro, T., Kawai, H., Ogura, T., et al. (2015b). The impact of parametrized convection on cloud feedback. *Philosophical Transactions of the Royal Society A: Mathematical, Physical and Engineering Sciences*, 373(2054).

Webb, M. J., Lock, A. P., and Lambert, F. H. (2018). Interactions between hydrological sensitivity, radiative cooling, stability, and low-level cloud amount feedback. *Journal of Climate*, 31(5):1833–1850.

Webb, M. J., Senior, C., Sexton, D., Ingram, W., Williams, K., Ringer, M., McAvaney, B., Colman, R., Soden, B. J., Gudgel, R., et al. (2006). On the contribution of local feedback mechanisms to the range of climate sensitivity in two GCM ensembles. *Climate Dynamics*, 27(1):17–38.

Wetherald, R. and Manabe, S. (1988). Cloud feedback processes in a general circulation model. *Journal of the Atmospheric Sciences*, 45(8):1397–1416.

Wetherald, R. T. and Manabe, S. (1980). Cloud cover and climate sensitivity. *Journal of the Atmospheric Sciences*, 37(7):1485–1510.

Williams, K. and Webb, M. (2009). A quantitative performance assessment of cloud regimes in climate models. *Climate dynamics*, 33(1):141–157.

Wing, A. A., Reed, K. A., Satoh, M., Stevens, B., Bony, S., and Ohno, T. (2018). Radiative–convective equilibrium model intercomparison project. *Geoscientific Model Development*, 11(2):793–813.

Wood, R. and Bretherton, C. S. (2006). On the relationship between stratiform low cloud cover and lower-tropospheric stability. *Journal of Climate*, 19(24):6425–6432.

Wyant, M. C., Bretherton, C. S., and Blossey, P. N. (2009). Subtropical low cloud response to a warmer climate in a superparameterized climate model. Part I: Regime sorting and physical mechanisms. *Journal of Advances in Modeling Earth Systems*, 1(3).

Yoshimori, M., Lambert, F. H., Webb, M. J., and Andrews, T. (2020). Fixed anvil temperature feedback: Positive, zero, or negative? *Journal of Climate*, 33(7):2719–2739.

Zelinka, M. D., Klein, S. A., and Hartmann, D. L. (2012). Computing and partitioning cloud feedbacks using cloud property histograms. Part I: Cloud radiative kernels. *Journal of Climate*, 25(11):3715–3735.

Zelinka, M. D., Myers, T. A., McCoy, D. T., Po-Chedley, S., Caldwell, P. M., Ceppi, P., Klein, S. A., and Taylor, K. E. (2020). Causes of higher climate sensitivity in CMIP6 models. *Geophysical Research Letters*, 47(1).

Zelinka, M. D., Randall, D. A., Webb, M. J., and Klein, S. A. (2017). Clearing clouds of uncertainty. *Nature Climate Change*, 7(10):674–678.

Zelinka, M. D., Zhou, C., and Klein, S. A. (2016). Insights from a refined decomposition of cloud feedbacks. *Geophysical Research Letters*, 43(17):9259–9269.

Zhang, M., Bretherton, C. S., Blossey, P. N., Austin, P. H., Bacmeister, J. T., Bony, S., Brient, F., Cheedela, S. K., Cheng, A., Del Genio, A. D., et al. (2013). CGILS: Results from the first phase of an international project to understand the physical mechanisms of low cloud feedbacks in single column models. *Journal of Advances in Modeling Earth Systems*, 5(4):826–842.

Zhao, M. (2014). An investigation of the connections among convection, clouds, and climate sensitivity in a global climate model. *Journal of Climate*, 27(5):1845–1862.

Clim Dyn (2015) 44:1419–1436
DOI 10.1007/s00382-014-2234-1

The diurnal cycle of marine cloud feedback in climate models

Mark J. Webb · Adrian P. Lock · Alejandro Bodas-Salcedo · Sandrine Bony · Jason N. S. Cole · Tsuyoshi Koshiro · Hideaki Kawai · Carlo Lacagnina · Frank M. Selten · Romain Roehrig · Bjorn Stevens

Received: 17 October 2013 / Accepted: 29 June 2014 / Published online: 24 July 2014

Abstract We examine the diurnal cycle of marine cloud feedback using high frequency outputs in CFMIP-2 idealised uniform +4 K SST perturbation experiments from seven CMIP5 models. Most of the inter-model spread in the diurnal mean marine shortwave cloud feedback can be explained by low cloud responses, although these do not explain the model responses at the neutral/weakly negative end of the feedback range, where changes in mid and high level cloud properties are more important. All of the models show reductions in marine low cloud fraction in the warmer climate, and these are in almost all cases largest in the mornings when more cloud is present in the control simulations. This results in shortwave cloud feedbacks being slightly stronger and having the largest inter-model spread at this time of day. The diurnal amplitudes of the responses of marine cloud properties to the warming climate are however small compared to the inter-model differences in their diurnally meaned responses. This indicates that the diurnal cycle of cloud feedback is not strongly relevant to understanding inter-model spread in overall cloud feedback and climate sensitivity. A number of unusual behaviours in individual models are highlighted for future investigation.

Keywords Diurnal cycle · Cloud feedback · Climate change

M. J. Webb (✉) · A. P. Lock · A. Bodas-Salcedo
Met Office Hadley Centre, FitzRoy Road, Exeter EX1 3PB, UK
e-mail: mark.webb@metoffice.gov.uk

S. Bony
Laboratoire de Météorologie Dynamique/Institute Pierre Simon Laplace (IPSL), Paris, France

J. N. S. Cole
Canadian Centre for Climate Modelling and Analysis (CCCMa), Victoria, BC, Canada

T. Koshiro · H. Kawai
Meteorological Research Institute (MRI), Tsukuba, Japan

C. Lacagnina · F. M. Selten
The Royal Netherlands Meteorological Institute, (KNMI), De Bilt, The Netherlands

R. Roehrig
Centre National de Recherches Météorologiques (CNRM), Toulouse, France

B. Stevens
Max Planck Institute for Meteorology (MPI-M), Hamburg, Germany

1 Introduction

Cloud feedbacks continue to make the largest contribution to inter-model differences in climate sensitivity (Randall et al. 2007; Dufresne and Bony 2008; Andrews et al. 2012), even when cloud adjustments (Gregory and Webb 2008; Andrews and Forster 2008) are allowed for (Webb et al. 2013; Vial et al. 2013). Understanding the underlying causes of these differences remains a priority. However, the high frequency variability of clouds means that time averaged model output gives a fairly limited picture of the physical mechanisms underlying cloud simulations. High frequency, instantaneous diagnostics are potentially able to give more insight into the physical processes operating and the interactions between them, for example convective intermittency and convective/boundary layer interactions (Zhang and Bretherton 2008). They also support the diagnosis of any unphysical behaviour related to numerical noise and vertical discretisation effects.

The US Climate Process Team (CPT) on low latitude cloud feedbacks was amongst the first to analyse high frequency output of this type from GCMs at selected points, and found for example that models could show very different high frequency variability in cloud simulations in stratocumulus regions in spite of similar values of net cloud forcing (Bretherton 2006). Mapes et al. (2009) used these data to relate cloud radiative effects to convective precipitation events, revealing substantial differences in the behaviour of the models' convection schemes. The WGNE-GCSS Pacific Cross Section Intercomparison Project (GPCI, Teixeira et al. 2011) saved high frequency data from more than twenty NWP and climate models along a section sampling the stratocumulus regime off the coast of California, the shallow cumulus to the south west and the deep convection in the ITCZ (as well as the transitions between them). They found that the systematic underestimate in cloud fraction in the stratocumulus regimes was in part due to a stratocumulus-to-cumulus transition that occurs too early along the trade wind Lagrangian trajectory, and also noted that some models exhibit a quasi-bimodal structure with cloud cover being either very large or very small, while other models show a more continuous transition.

As part of the second phase of the Cloud Feedback Model Intercomparison Project (CFMIP-2), new cloud feedback experiments were added to the CMIP5 experimental design (Taylor et al. 2011), which included additional process diagnostics designed to support investigation of the physical mechanisms underlying cloud feedbacks and adjustments (Bony et al. 2011). These included timestep frequency outputs at 120 'cfSites' locations around the globe, including those analysed by the CPT and GPCI projects, but extended to additionally include various observational sites, and locations with large inter-model differences in cloud feedback (Fig. 1; Table 1). These are included in AMIP experiments forced with observed SSTs, and two types of SST perturbation experiment, one where AMIP SSTs are increased uniformly (amip4K) and another where a more realistic patterned SST perturbation is applied (amipFuture), both being scaled to give a global SST increase of 4 K. High frequency outputs are also included in a CO_2 quadrupling experiment with SSTs specified as in the AMIP experiments (amip4xCO2). These experiments have been designed for the analysis of cloud adjustments which occur in response to CO_2 quadrupling but in the absence of SST changes. These data are now available from several models for each experiment type (Table 2).

One obvious application of the CFMIP-2/CMIP5 cfSites data is the examination of the diurnal cycle in the models. Roehrig et al. (2013) have used these data to examine the models' abilities to reproduce various features of the African monsoon, including the diurnal cycles of clouds and precipitation, by comparing with in situ observations on the AMMA transect (Bouniol et al. 2012). The availability of

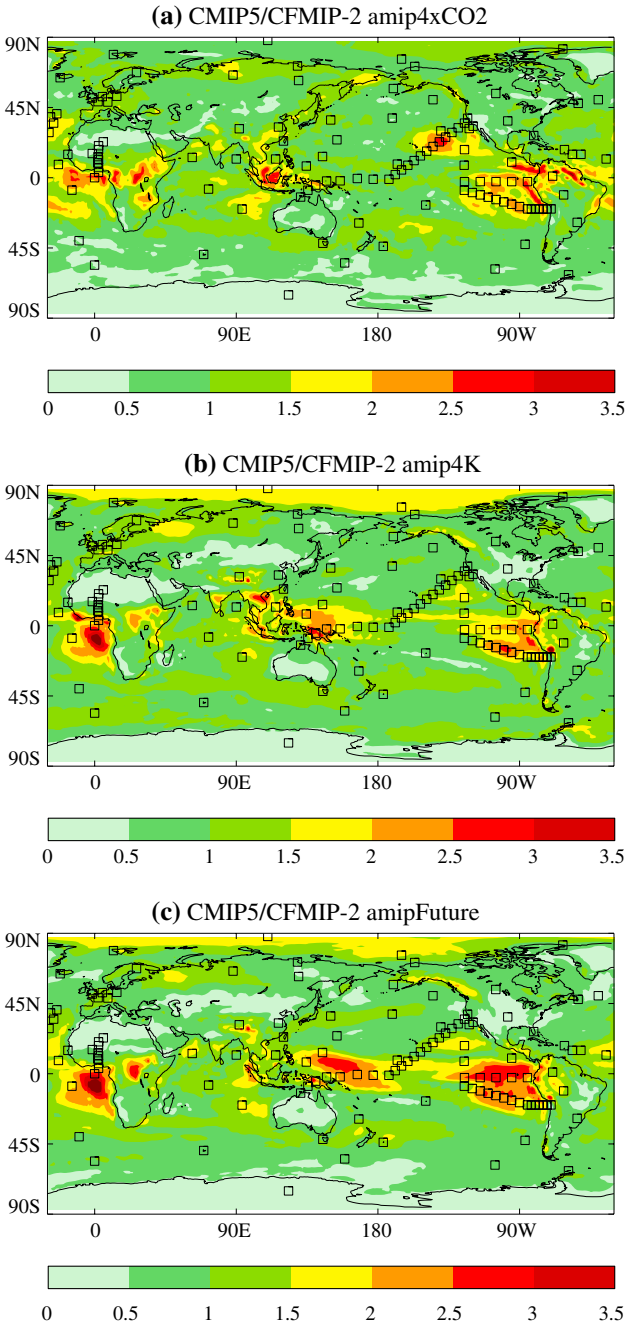

Fig. 1 CFMIP 'cfSites' high frequency output locations. The contours show ensemble standard deviations of **a** cloud adjustments and **b**, **c** cloud feedbacks in the CMIP5/CFMIP-2 experiments. The standard deviation maps are normalised by dividing by their global means, to support a dimensionless comparison highlighting regions contributing most to inter-model spread in cloud feedback and adjustment

the cfSites data in the CFMIP-2 amip4K experiments provides a new opportunity to examine the impact of changes in the diurnal cycle on cloud feedbacks. Given the huge variations in solar illumination throughout the day, a shift in the timing of the maximum cloud fraction or cloud water

Table 1 Locations of CFMIP cfSites high frequency outputs

	Lon	Lat	Description (Source)
1	**290**	**−20**	**VOCALS cross section (Rob Wood)**
2	287.5	−20	VOCALS cross section (Rob Wood)
3	285	−20	VOCALS cross section (Rob Wood)
4	282.5	−20	VOCALS cross section (Rob Wood)
5	280	−20	VOCALS cross section (Rob Wood)
6	277.5	−20	VOCALS cross section (Rob Wood)
7	275	−20	85 W 20S WHOI SE Pacific stratus buoy (http://uop.whoi.edu/stratus/) (CPT)
8	270	−18.5	South East Tropical Pacific Section (CFMIP)
9	265	−17	South East Tropical Pacific Section (CFMIP)
10	260	−15.5	South East Tropical Pacific Section (CFMIP)
11	255	−14	South East Tropical Pacific Section (CFMIP)
12	250	−12.5	South East Tropical Pacific Section (CFMIP)
13	245	−11	South East Tropical Pacific Section (CFMIP)
14	240	−9.5	South East Tropical Pacific Section (CFMIP)
15	234.9	−8	125.1 W 8S central Pacific SE trades TAO buoy (CPT)
16	**−123**	**38.1**	**Point Reyes ARM Mobile Facility N38 5.51 W122 57.33 (AMF)**
17	235	35	GCSS Pacific cross section (GPCI) (Joao Teixeira)/CGILS s12
18	231	32	GCSS Pacific cross section (GPCI) (Joao Teixeira)/CGILS s11
19	227	29	GCSS Pacific cross section (GPCI) (Joao Teixeira)/CGILS s11
20	223	26	GCSS Pacific cross section (GPCI) (Joao Teixeira)/CGILS s9
21	219	23	GCSS Pacific cross section (GPCI) (Joao Teixeira)/CGILS s8
22	215	20	GCSS Pacific cross section (GPCI) (Joao Teixeira)/CGILS s7
23	211	17	GCSS Pacific cross section (GPCI) (Joao Teixeira)/CGILS s6
24	207	14	GCSS Pacific cross section (GPCI) (Joao Teixeira)/CGILS s5
25	203	11	GCSS Pacific cross section (GPCI) (Joao Teixeira)/CGILS s4
26	199	8	GCSS Pacific cross section (GPCI) (Joao Teixeira)/CGILS s3
27	195	5	GCSS Pacific cross section (GPCI) (Joao Teixeira)/CGILS s2
28	191	2	GCSS Pacific cross section (GPCI) (Joao Teixeira)/CGILS s1
29	187	−1	GCSS Pacific cross section (GPCI) (Joao Teixeira)/CGILS s0
30	177	−1	GPCI/Tropical West Pacific link point (CFMIP)
31	166.9	−0.5	166.9E 0.5S Nauru ARM (CPT)
32	156	−2	156E 2S COARE (CPT)
33	147.4	−2.1	147.4E 2.1S Manus ARM (CPT)
34	**140.5**	**−4.75**	**Papua New Guinea (CFMIP)**
35	135.5	−8	Arafura Sea (CFMIP)
36	**130.9**	**−12.4**	**130.9E 12.4S Darwin ARM (CPT)**
37	**−97.5**	**36.4**	**97.5 W 36.4 N Oklahoma ARM (CPT)**
38	**−156.6**	**71.3**	**156.6 W 71.3 N Barrow ARM (CPT)**
39	**−62**	**−11**	**62 W 11S Amazonia (CPT)**
40	**4.9**	**52**	**4.93E 51.97 N Cabaaw Mast Netherlands (CPT)**
41	**145**	**−42**	**145E 42S Cape Grim Tasmania (CPT)**
42	−51	15	51 W 15 N WHOI Atlantic tradewind NTAS buoy (http://uop.whoi.edu/ntas/) (CPT)
43	−140	30	140 W 30 N OWS N (CPT)
44	−145	50	145 W 50 N OWS P (CPT)
45	−125.2	8	125.2 W 8 N Central Pacific ITCZ TAO buoy (CPT)
46	120	23.5	120E 23.5 N China Sea (CPT)
47	**−28**	**39**	**Graciosa in the Azores (28 W 39 N) 2009 AMF deployment (Chris Bretherton)**
48	**8.4**	**48.5**	**AMF Black forest Germany Main Site: N48 32.403 E08 23.812 (AMF)**

Table 1 continued

	Lon	Lat	Description (Source)
49	**116.8**	**32.5**	**AMF Shouxian China Location: 32 33 N 116 46E (AMF)**
50	**129.6**	**62.3**	**CEOP 2 Eastern Siberian Tiaga 62.3 N 129.6E (Martin Koehler)**
51	**91.9**	**31.4**	**CEOP 5 Tibet 31.4 N 91.9E (Martin Koehler)**
52	134.5	7.5	CEOP 10 Western Pacific Ocean 7.5 N 134.5E (Martin Koehler)
53	**14.1**	**52.2**	**CEOP 26 Lindenberg 52.2 N 14.1E (Martin Koehler)**
54	**26.6**	**67.4**	**CEOP 27 Sodankyla 67.4 N 26.6E (Martin Koehler)**
55	**−105.1**	**54**	**CEOP 33 BERMS (CliC) 54.0 N 105.1 W (Martin Koehler)**
56	**−62.5**	**82.5**	**CEOP 34 Alert Nunavut 82.5 N 62.5 W (Martin Koehler)**
57	**−53.4**	**−28.6**	**CEOP 48 Cruz Alta (LPB) 28.6S 53.4 W (Martin Koehler)**
58	−24	41	ASTEX (41 N 24 W) (Adrian Lock)
59	−26	35	ASTEX (35 N 26 W) (Adrian Lock)
60	−29	29	ASTEX (29 N 29 W) (Adrian Lock)
61	−35	12	ATEX = 12 N 35 W (Adrian Lock)
62	−56.5	15	BOMEX = 15 N 56.5 W (Adrian Lock)
63	−61.5	18	RICO = 18 N 61.5 W (Adrian Lock)
64	−119.5	33	EUROCS/FIREI = 33 N 119.5 W (Adrian Lock)
65	−122	31.5	DYCOMSII = 31.5 N 122 W (Adrian Lock)
66	−85	−2.5	East Pacific Point (CFMIP)
67	−95	−2.5	East Pacific Point (CFMIP)
68	−105	−2.5	East Pacific Point (CFMIP)
69	−115	−2.5	East Pacific Point (CFMIP)
70	−125	−2.5	East Pacific Point (CFMIP)
71	−125	18	East Pacific Point (CFMIP)
72	**−69**	**1**	**North West of Amazonia (CFMIP)**
73	62	13	MONSOON INFLOW (CFMIP)
74	**−14.4**	**−7.97**	**ASCENSION IS./WIDEAWAKE (RATPAC) (CFMIP)**
75	150	37	Kurishio region (CFMIP)
76	−21.9	64.1	64.1285 N 21.9407 W Reykjavik (CFMIP)
77	**−170.2**	**57.15**	**ST. PAUL ISLAND (RATPAC) (CFMIP)**
78	**−58.9**	**−62.2**	**BELLINGSHAUSEN (RATPAC) (CFMIP)**
79	**11.95**	**78.93**	**BSRN site Svalbard (CFMIP)**
80	**144.8**	**13.6**	**Guam (CFMIP)**
81	**69.3**	**−49.2**	**Southern Oce–n - Kerguelen Islands (CFMIP)**
82	**158.9**	**−54.6**	**Southern Oce–n - Macquarie Island (CFMIP)**
83	**−81**	**27**	**Florida (81 W 27 N) (Brian Mapes)**
84	**−167.7**	**8.7**	**Kwajalein (167.7 W 8.7 N) (Brian Mapes)**
85	90	12	JASMINE (90E 12 N) (Brian Mapes)
86	115	12	SCS (115E 12 N) (Brian Mapes)
87	−95	10	EPIC (95 W 10 N) (Brian Mapes)
88	−23	8.5	GATE (23 W 8.5 N) (Brian Mapes)
89	**−1.44**	**51.14**	**Chilbolton UK 51.1445 North 1.4370 West altitude 80 m. (Robin Hogan)**
90	**2.2**	**48.71**	**SIRTA Palaiseau (ParisFrancence 48.713 North 2.204 Est (Cloudnet)**
91	93.7	−20.1	CFMIP West of Australia
92	254.4	−58.5	CFMIP Southern Ocean
93	**−52.75**	**47.67**	**CFMIP ST. JOHNS (RATPAC)**
94	**−176.6**	**−43.95**	**CFMIP CHATHAM ISLAND (RATPAC)**
95	**72.4**	**−7.3**	**CFMIP DIEGO GARCIA (RATPAC)**
96	**−9.88**	**−40.35**	**GOUGH IS. (RATPAC) (CFMIP)**
97	189.1	38.2	CFMIP Central North Pacific

Table 1 continued

	Lon	Lat	Description (Source)
98	**−149.6**	**−17.5**	**CFMIP Tahiti 17.5S 149.6 W**
99	0	−56	CFMIP South Atlantic
100	273.5	−42.7	CFMIP off coast of Chile
101	**153.97**	**24.3**	**MARCUS IS. (RATPAC) (CFMIP)**
102	**167.9**	**−29.03**	**NORFOLK ISLAND (RATPAC) (CFMIP)**
103	−40	50	CFMIP North West Atlantic
104	**87.95**	**65.78**	**TURUKHANSK (RATPAC) (CFMIP)**
105	0	0	0. 0.N Pirata Buoy (AMMA Francoise Guichard)
106	2.5	3.5	2.5 3.5 N (AMMA Francoise Guichard)
107	**2.5**	**6.5**	**2.5 6.5 N (AMMA Francoise Guichard)**
108	**2**	**9.5**	**2. 9.5 N Oueme (AMMA Francoise Guichard)**
109	**2.5**	**11.5**	**2.5 11.5 N (AMMA Francoise Guichard)**
110	**2.2**	**13.5**	**13.5 N 2.2E Niamey ARM Mobile Facility (AMF)**
111	**−1.5**	**15.5**	**−1.5 15.5 N Gourma (AMMA Francoise Guichard)**
112	**2.5**	**18**	**2.5 18 N (AMMA Francoise Guichard)**
113	**2.5**	**20.5**	**2.5 20.5 N (AMMA Francoise Guichard)**
114	**5.5**	**23**	**5.5 23 N Tamanrasset (AMMA Francoise Guichard)**
115	**−17**	**15**	**−17. 15 N Dakar (AMMA Francoise Guichard)**
116	−165	76	165 W 76 N Location of SHEBA IceBreaker May 1998 (Stephen Klein)
117	**128.9**	**71.6**	**Tiksi Russia 71.6 128.9 - Location of NOAA SEARCH Site (Stephen Klein)**
118	110	88	Central Arctic Ocean Point midway between Svalbard & SHEBA (Stephen Klein)
119	**123.2**	**−75.1**	**Antarctica Plateau Dome C: 75 1 S 123 2 E (S. Bony/Christophe Genthon)**
120	**−59.43**	**13.16**	**Barbados 59.43 W 13.16 N (Optional extra for CFMIP2) (Louise Nuijens)**

Land points are shown in bold

path with the warming climate could in principle lead to a substantial shortwave cloud radiative feedback, even in the absence of changes in the diurnal mean cloud response. The role of the diurnal cycle in cloud feedback has not to our knowledge been investigated previously, and this motivates the present study. Cloud amounts are generally smaller over the land than the ocean, and previous studies have shown that cloud feedbacks over land regions contribute much less to inter-model spread in global cloud feedback than do those over the oceans (Webb et al. 2013; Vial et al. 2013). For this reason we focus on examining the role of the diurnal cycle in marine cloud feedbacks in the CFMIP-2 models.

This study is structured as follows. In Sect. 2 we describe our data and methods and assess the relevance of the cfSites locations to examining cloud feedback in the CMIP5 models by showing that they sample the major regimes of substantial inter-model spread in cloud feedback and cloud adjustment. In Sect. 3 we examine the diurnal cycle of cloud feedback over the oceans in the models. In Sect. 3.1 we interpret the inter-model differences in diurnal mean shortwave cloud feedback over the ocean cfSites locations in terms of the responses of different cloud properties. In Sect. 3.2 we identify the time of day which shows the largest marine shortwave cloud feedbacks and the largest inter-model spread. Section 3.3 examines the changes in the diurnal cycle of marine low cloud properties in the context of present day variations, while Sect. 3.4 discusses the diurnal cycle in longwave cloud feedback over the oceans. Unusual behaviours seen in particular models are highlighted throughout. We present our concluding remarks in Sect. 4.

2 Data and methods

We diagnose cloud feedbacks using AMIP experiments forced with 30 years of observed SSTs, and +4 K global mean SST perturbation experiments, one where AMIP SSTs are increased uniformly by 4 K (amip4K) and another where a patterned SST perturbation with a global mean of +4 K is applied, based on a composite SST response from coupled models in CMIP3 (amipFuture) (Bony et al. 2011). The composite SST pattern is shown in Fig. 1 of He et al. (2014). We diagnose the cloud feedback using the well established procedure of calculating the change in the Cloud Radiative Effect (CRE) between the AMIP and perturbed SST experiments and dividing this by the global mean change in near-surface temperature (e.g. Ringer et al.

Table 2 CMIP5/CFMIP-2 experiments and cfSites data availability

AGCM	amip	amip4xCO2	amipFuture	amip4K
BCC-CSM-1 Wu et al. (2010)	✓✓		✓	✓
CNRM-CM5 Voldoire et al. (2012)	✓✓		✓✓	✓✓
CanAM4 von Salzen et al. (2013)	✓✓		✓✓	✓✓
EC-EARTH Hazeleger et al. (2010, 2012)	✓✓		✓✓	✓✓
FGOALS-G2 Lin et al. (2013)	✓			✓
HadGEM2-A Martin et al. (2011)	✓✓	✓✓	✓✓	✓✓
IPSL-CM5A-LR Hourdin et al. (2012)	✓✓	✓✓	✓	✓✓
IPSL-CM5A-MR Hourdin et al. (2012)	✓✓		✓	✓
MIROC5 Watanabe et al. (2010)	✓		✓	✓
MPI-ESM-LR Stevens et al. (2013)	✓✓	✓✓		✓✓
MPI-ESM-MR Stevens et al. (2013)	✓	✓	✓	✓
MRI-CGCM3 Yukimoto et al. (2011)	✓✓	✓✓	✓✓	✓✓
NorESM1-M Bentsen et al. (2012)	✓	✓		
Number of models with monthly data	13	7	10	12
Number of models with cfSites data	9	5	5	7

Single ticks indicate that standard monthly outputs are available, and double ticks indicate that cfSites data are also available. Models with only monthly AMIP data are not listed

2006). This measures the impact of clouds on the overall climate feedback, including not only the contribution from cloud changes but also the impact of clouds on other feedbacks such as water vapour via climatological cloud masking (Soden et al. 2004). Vial et al. (2013) demonstrated that inter-model differences in CRE responses are a good predictor of those due to cloud changes alone, which indicates that cloud masking effects do not contribute substantially to inter-model spread in the CRE responses.

Similarly the cloud component of the effective radiative forcing due to CO_2 quadrupling is diagnosed as the change in the CRE between the AMIP and amip4xCO2 experiments. Although this quantity includes the effects of both rapid cloud adjustments and climatological cloud masking on other components of the radiative forcing, its inter-model differences are dominated by cloud adjustments (Andrews and Forster 2008).

To give an indication of the extent to which the cfSites locations sample the regions which contribute the most to inter-model spread in cloud feedbacks and cloud adjustments, Fig. 1 shows maps of ensemble standard deviations of these quantities from the CFMIP-2 experiments. These are based on all of the models for which monthly data are available (see Table 2). Ensemble standard deviations are calculated at each location and then scaled to have global means equal to unity; this is done to support a visual comparison highlighting the areas with largest differences in cloud adjustments and cloud feedbacks. They show that the cfSites points sample all of the major regimes contributing to inter-model spread in cloud feedback and cloud adjustment, in particular the subtropical marine stratocumulus and trade cumulus regions which show substantial inter-model spread in both cloud feedback and cloud adjustment. It is clear from Fig. 1b, c that marine cloud feedbacks exhibit a much larger inter-model spread than those generally found over the land, as found in previous studies (e.g. Webb et al. 2013; Vial et al. 2013). For this reason we focus on marine cloud feedbacks hereafter.

We examine the diurnal cycle in the seven models which have the CFMIP-2 'cfSites' data available in the amip and amip4K experiments (Table 2). For each of the locations, we calculate the 30 year climatological annual mean changes for each time of day (UTC). We then rotate the time coordinates for each location to align the times of the maximum solar insolation, placing these at 12 noon (mean solar time) before averaging across locations. (An alternative approach would have been to use the longitude of the sites to convert from UTC to local time; however we do not expect that this would affect our results significantly). Figure 2(a) for example shows diurnally resolved changes in the shortwave CRE between the AMIP and AMIP + 4 K experiments averaged over the CFMIP-2 marine cfSites locations (see Table 1). These are divided by the global near-surface air temperature response, and can be considered measures of the shortwave cloud feedback. (Note that the global near-surface air temperature responses of the models are quite similar because all are subject to the same SST perturbation.)

Low, mid and high level cloud fractions are diagnosed by taking the profiles of instantaneous model cloud fraction on model levels and calculating the maximum instantaneous cloud fractions below 680 hPa, between 680 and 440 hPa and above 440 hPa respectively, before applying time averaging. These levels are chosen for familiarity, mainly because they are the boundaries used to distinguish low, mid and high top clouds in ISCCP (Rossow and Schiffer 1999). However the reader should bear in mind that the low, mid and high cloud fractions diagnosed here

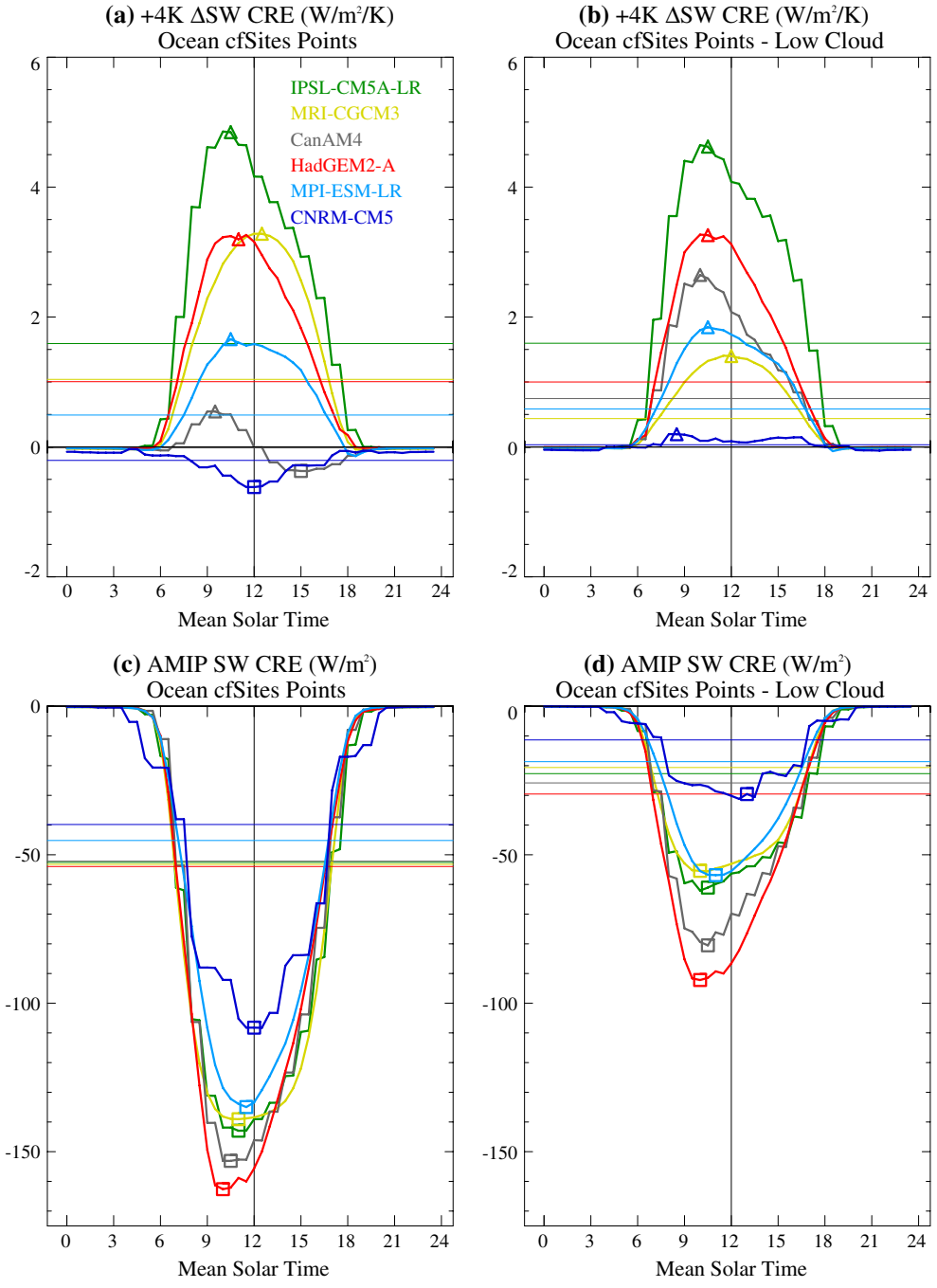

Fig. 2 Diurnal cycle of the Shortwave Cloud Radiative Effect (CRE) averaged over cfSites ocean locations in AMIP and uniform +4 K perturbation experiments. **a** shows diurnally resolved shortwave CRE responses to the uniform +4 K SST perturbation, normalised by the global mean near-surface temperature response. **b** shows the contributions to these from occasions when the low clouds are dominant. **c** shows the diurnally resolved shortwave CRE in the AMIP control experiments, and **d** the contribution from occasions when low clouds dominate. Diurnal mean values are shown as *horizontal lines*. The daytime diurnal maxima and minima are marked with *triangles* and *squares* respectively

are not diagnosed using the ISCCP simulator (Klein and Jakob 1999; Webb et al. 2001) and so are not quantitatively comparable with those from ISCCP, and not necessarily consistent with the cloud overlap assumptions used in the models' radiative transfer schemes.

We also estimate the contributions of low level clouds to the diurnally resolved shortwave CRE and its change between the AMIP and amip4K experiment using the following procedure. We recalculate the AMIP mean CRE at different times of day from the instantaneous values, but

replacing these with zero values on occasions when the instantaneous low level cloud fraction is less than twice the size of the sum of the mid and high level cloud fractions. This procedure essentially creates a conditional mean over occasions when low clouds dominate, and weights it by the frequency of occurrence of those occasions, to give an indication of the contribution those occasions to the overall mean. This same procedure is then applied to the amip4K experiments, and the difference between these two values can be considered a measure of the contribution of low clouds to the total change and hence the shortwave cloud feedback. This quantity will reflect the impact on the feedbacks of (a) changes in the frequency of occasions when low clouds dominate, (b) changes in low cloud fraction when present, and (c) changes in other low cloud properties such as cloud liquid water path. All of these factors will potentially contribute to the low cloud feedback and should therefore be included in any estimate of its magnitude.

Diurnally resolved variations in liquid and ice water paths and low, mid and high level cloud fractions are also calculated, with +4 K responses being normalised as above. The CMIP5 variable diagnostic output convention requests vertically integrated cloud ice water content (clivi) and condensed water content (clwvi). If implemented correctly, clwvi should contain the sum of the liquid and ice water paths, and clwvi should always be greater than or equal to clivi. However, we found many cases in the IPSL-CM5A-LR, MPI-ESM-LR and EC-EARTH data where clwvi was smaller than clivi, and following the correct procedure yielded a negative liquid water path. We have confirmed that the clwvi variable actually contains the cloud liquid water path in these models and we allow for this in our analysis. Confusion may well have arisen from the fact that the names for the CMIP5 cloud ice and liquid mass mixing ratios are cli and clw respectively, which means that the naming convention for mixing ratios and vertical integrals is not as consistent as it could be (Jiang et al. 2012). We also use the diurnally resolved observed cloud liquid water path climatology of O'Dell et al. (2008) to evaluate the model liquid water paths. In all cases liquid and ice water paths shown are grid-box means.

Radiative fluxes are only available every three hours from CNRM-CM5, so we replicated the three hourly values in the ± 1.5 h window spanning them. This means that the diurnal cycle is less well resolved, and the time of the maximum insolation is less accurately diagnosed than in the other models which typically provide data every 30 min. Shortwave radiative fluxes are not available at the top of the atmosphere from EC-EARTH; instead we used the net clear-sky shortwave flux at the surface to estimate the time of the maximum solar insolation.

3 The diurnal cycle of marine cloud feedback

3.1 Diurnal mean cloud feedbacks over the oceans

Before discussing the diurnal variations of the cloud feedbacks over the oceans, we examine the diurnal mean cloud feedbacks. Figure 2a shows a range of marine shortwave cloud feedbacks with diurnal mean values varying from weakly negative to positive, with a spread much larger than in the longwave (Fig. 4a), as seen in previous studies.

All of the models show a reduction in diurnal mean low cloud fraction in the warmer climate (Fig. 3a). Changes in time mean low cloud fraction can in principle be caused by changes in the frequency of occurrence of low clouds, changes in the fraction of low cloud when present, or a combination of both. The diurnal mean liquid water path increases with warming in most of the models, the exception being HadGEM2-A, which shows a small decrease (Fig. 3b). Figure 6 shows profiles of the grid-box mean cloud liquid water mixing ratio in the present-day simulations and their +4 K responses. Cloud water contents are largest at low levels where they show reductions or very small increases in the amip4K experiments. The models generally show increases in cloud liquid water contents in the free troposphere. However, HadGEM2-A shows relatively small increases at these levels which are too small to compensate for the reductions at lower levels, which explains the its reduction in LWP. This slightly unusual behaviour in HadGEM2-A may be related to the nature of its statistical cloud scheme, which uses a fixed symmetric triangular PDF. This results in a strong coupling between in-cloud water content and cloud fraction. This effect might not be present in other models which do not use PDF schemes, or which adapt the shape of their PDFs depending on environmental conditions such as the presence of convection (e.g. Bony and Emanuel 2001).

The LWP increases in the majority of models would on their own result in a negative shortwave cloud feedback, but in most cases they are not large enough to overcome the positive feedback due to reductions in the low cloud amount. For example, IPSL-CM5A-LR shows a 23 % reduction in diurnal mean low cloud fraction relative to its control value, while its liquid water path increases by just 7 % (Fig. 3a, b). These results are consistent with the findings of Zelinka et al. (2013), who show that cloud optical depth does generally increase in the warmer climate in models, but that the effect of this on the shortwave cloud feedback is more than compensated for by reductions in cloud fraction. CNRM-CM5 is an exception to this however; it has the largest increase in liquid water path and one of the smallest reductions in low cloud fraction, consistent with its weakly negative shortwave cloud feedback.

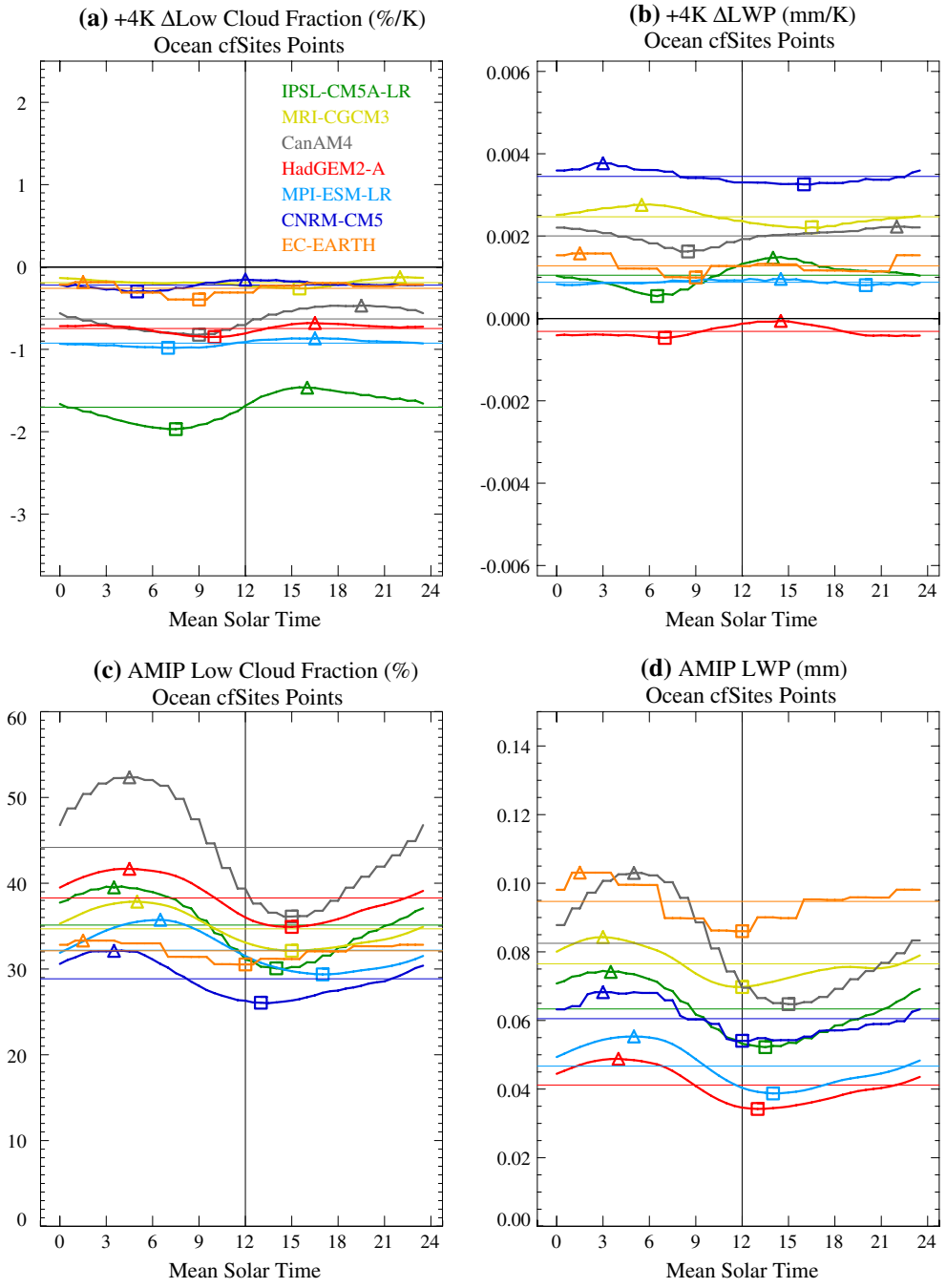

Fig. 3 As Fig. 2a, c but for low cloud fraction and liquid water path. The low cloud fraction is calculated by taking the maximum cloud fraction below 680 hPa. Note that these quantities are not conditionally averages, in contrast to those shown in Fig. 2b, d

Although inter-model differences in cloud feedbacks are known to be dominated by different responses in low cloud properties, changes in mid and high level clouds are also expected to contribute to some extent. To give an indication of the relative contribution of low cloud feedbacks compared to other types, we have recalculated the shortwave cloud feedback in the models, filtering out occasions when substantial amounts of mid and/or high level cloud are present (see Sect. 2). Comparison of Fig. 2a, b shows that most of the inter-model spread in shortwave cloud feedback can be explained by low cloud responses, although these do not explain so well the model responses at the neutral/weakly negative end of the feedback range.

Figure 2b indicates that the negative shortwave cloud feedback in CNRM-CM5 is not associated with occasions when low level clouds dominate. This, combined with the

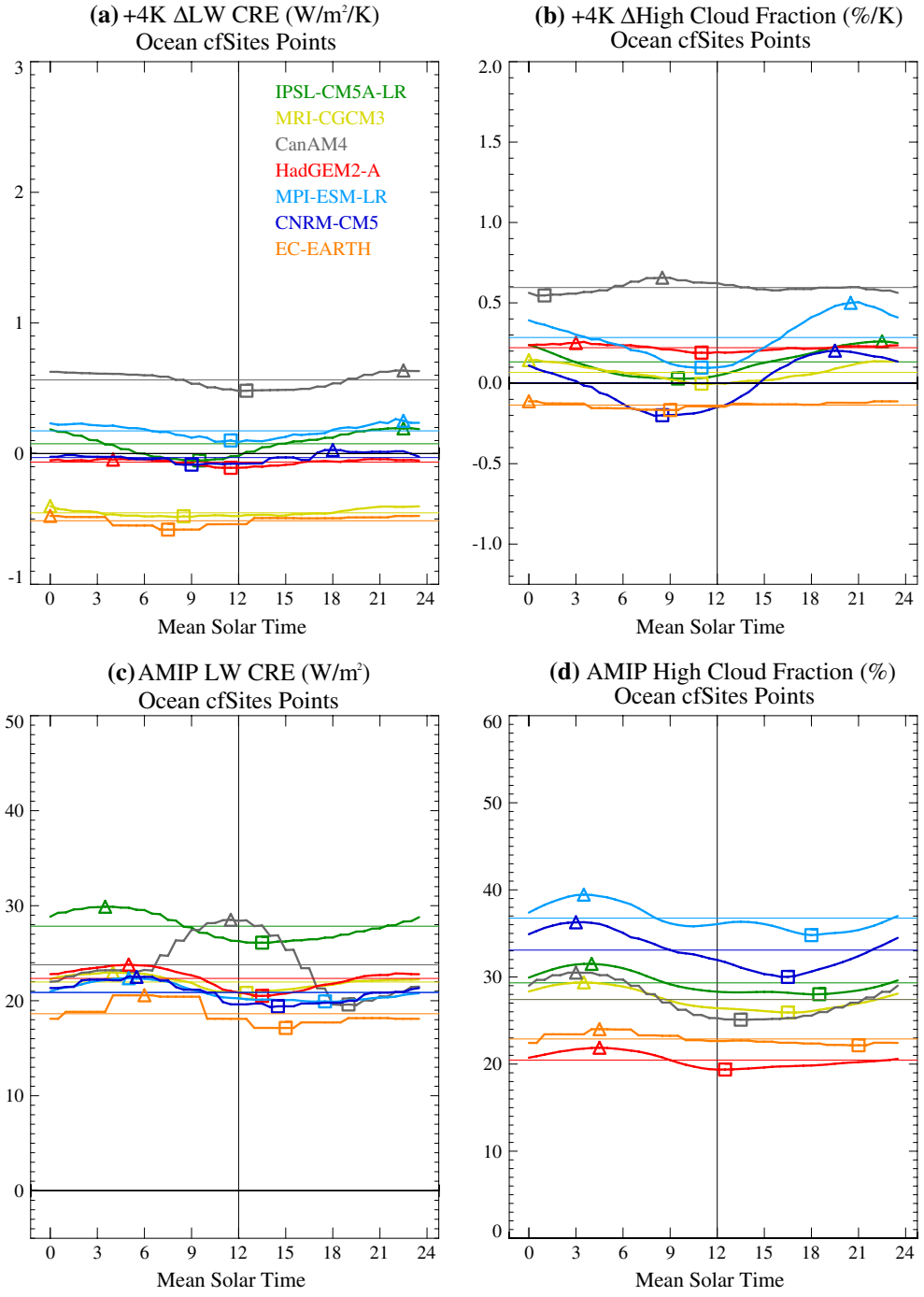

Fig. 4 As Fig. 3, but for longwave CRE and high cloud fraction. The high cloud fraction is calculated by taking the maximum cloud fraction above 440 hPa

relatively small low cloud fraction response in this model (Fig. 3a) indicates that the large increases in liquid water path cannot be due to increases in low cloud liquid water content, and so must be due to increases in liquid water at higher levels. This is confirmed by Fig. 6a, which shows that CNRM is unique in that it is the only model which shows consistent increases in cloud liquid water throughout the free troposphere, with an increasingly large response with height, peaking at 400 hPa. CNRM-CM5 has relatively large mid-level cloud fractions compared to most models (Fig. 5d), which will increase the radiative impact of any liquid water path increases at mid-levels. The relatively large increase in ice water path in CNRM-CM5 may also contribute to this negative shortwave cloud feedback (Fig. 5a).

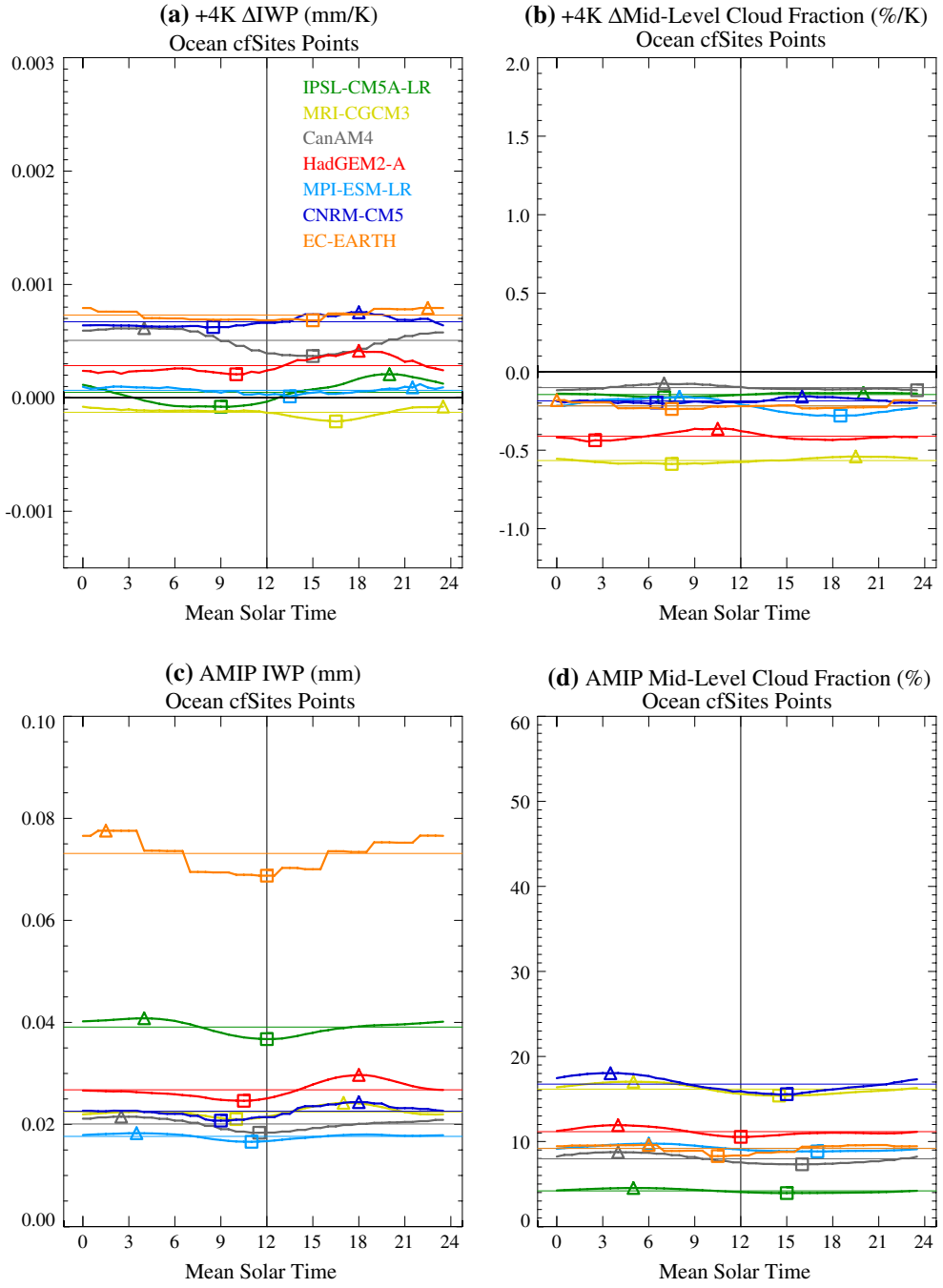

Fig. 5 As Fig. 4, but for ice water path and mid-level cloud fraction (calculated by taking the maximum cloud fraction above 680 hPa and below 440 hPa)

MRI-CGCM3 has a positive shortwave cloud feedback, and occasions when low clouds dominate explain about half of its magnitude (Fig. 2a, b). The magnitude of this positive feedback is surprising, given that this model has one of the largest increases in LWP and one of the smallest reductions in low level cloud (Fig. 3a, b). Figure 6a shows reductions in cloud water contents between 900 hPa and the surface in MRI-CGCM3, but larger increases in water contents over a greater depth at higher levels which result in an increase in LWP. Their contributions to the shortwave cloud feedback are however more than compensated for by an unusually strong reduction in mid-level cloud fraction (Fig. 5b).

Additionally we note the possibility that some of the shortwave cloud feedbacks seen here could in part be due to changes in cloud microphysical properties. For example, changes in the structure and location of clouds in the

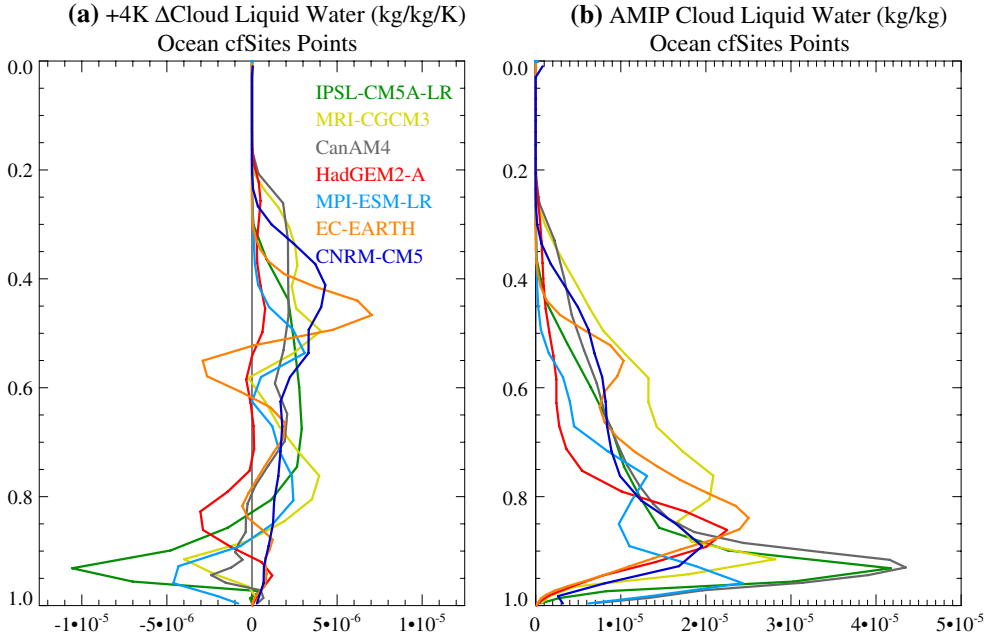

Fig. 6 **a** Profiles of +4 K responses in grid-box mean cloud liquid water mixing ratio averaged over ocean cfSites points respectively. **b** Equivalent present-day profiles. The vertical co-ordinate is sigma pressure (atmospheric pressure divided by surface pressure)

warmer climate might affect cloud droplet number concentrations. Clouds with higher tops tend to have smaller cloud droplet number concentrations, and so changes in cloud height might affect the shortwave cloud feedback via changes in cloud droplet size in the absence of any change in condensed water path. Such effects could also come about through changes in aerosol concentrations in response to changes in the hydrological cycle. We are not able to explore this possibility across the models using the cfSites data however as cloud droplet size information is not generally available. However, additional data saved from MRI-CGCM3 does indicate reductions in cloud droplet and ice crystal concentrations at low and high levels, which may also contribute to its positive cloud feedback.

CanAM4 has a very small diurnal mean shortwave cloud feedback, but a moderately positive feedback arising from occasions dominated by low clouds (Fig. 2a, b), which indicates that occasions where mid and/or high level clouds are substantial contribute a negative shortwave cloud feedback. We attribute this to the fact that CanAM4 has an unusually large increase in high-level cloud in the warmer climate (Fig. 4b), and also one of the smallest reductions in mid-level clouds (Fig. 5b). Increases in liquid water content at mid-upper levels also contribute (Fig. 6a).

3.2 Time of the largest marine shortwave cloud feedback

If there was no diurnal cycle in cloud properties, and these changed by the same amount at all times of day, then we would expect the shortwave cloud feedbacks to be symmetric about a maximum value at solar noon, with a diurnal cycle following the solar insolation but with different magnitudes depending on the size of the diurnal mean change in cloud properties. The majority of models show only modest deviations from this situation (Figs. 2a, 3a, b) show that the diurnal amplitudes of the responses in marine cloud properties such as low cloud fraction and liquid water path are generally small compared to the equivalent diurnal mean responses. CanAM4 is an exception to this however; although its shortwave cloud feedback peaks with a positive value in the morning, a negative local minimum is present in the afternoon, which is unusual compared to the other models (Fig. 2a). This is discussed further below.

Most of the models have a small asymmetry in the shortwave cloud feedback about local noon, with the maximum shifted slightly towards the late morning. Low level cloud fraction reduces in all of the models at all times of day over the oceans (Fig. 3a), and the models which have stronger shortwave cloud feedbacks in the morning (Fig. 2a) all have their largest decreases in low cloud fraction and their weakest increases in LWP before noon (Fig. 3a, b). MRI-CGCM3 is an exception however, with the largest shortwave cloud feedback occurring just after noon, which is presumably due to the relatively weak diurnal variation of its low and mid-level cloud fraction responses (Figs. 3a, 5b), combined with a maximum LWP increase in the morning and minimum in the afternoon (Fig. 3b). Any effects due to changes in cloud droplet or ice crystal concentrations

will also have a symmetric impact on the feedback if they do not have a strong diurnal cycle in their response. CNRM-CM5 is another exception, with a weakly negative shortwave cloud feedback which is largest at noon. This symmetry may be explained by the relatively small diurnal cycles in the LWP and IWP responses in CNRM-CM5.

We interpret the unusual evolution of the diurnal cycle in shortwave cloud feedback in CanAM4 as follows. The negative feedback in the afternoon is not present in the low cloud feedback (Fig. 2b), which is systematically positive, and peaks in the late morning like many of the other models. The shortwave low cloud feedback does however drop off more rapidly in the afternoon than is the case in the other models; we attribute this to the relatively strong amplitude of the diurnal cycle in the low cloud fraction response compared to its diurnal mean. There is also a very strong diurnal cycle in LWP in this model in the control simulation, with less LWP in the afternoon (Fig. 3d), which will result in +4 K cloud fraction responses in the afternoon having less of an effect on the shortwave cloud feedback than in the morning when clouds are optically thicker. As discussed above, unusually large increases in high level clouds and relatively small reductions in mid-level clouds contribute a negative component to the cloud feedback; this combined with the strongly weakening positive cloud feedback from low clouds in the early afternoon can explain the negative afternoon minimum in the total shortwave cloud feedback. The LWP also increases slightly more in the afternoon compared to the morning, which will contribute to the low or mid-level contribution depending on its vertical distribution (Fig. 3b).

Overall, the tendency for the models to show the largest shortwave cloud feedback in the morning results in the inter-model spread also being largest at that time. The shortwave cloud feedbacks sampled for low cloud events show a similar spread and behaviour in this regard, indicating that low cloud feedbacks are the main cause of the morning maxima and the timing of the maximum inter-model spread.

3.3 Relation to the present-day diurnal cycle in marine low cloud properties

Why do the models generally show the largest changes in marine low-cloud properties in the mornings? Observations and fine scale models show that oceanic stratocumulus clouds tend to form overnight and then break up through the day as the cloud layer is heated by solar absorption, resulting in 'decoupling' of the boundary layer and a reduction in the turbulent transport of moisture to the cloud layer from the sea surface (see for example Duynkerke et al. 2004). Some global models have been shown to reproduce such a diurnal cycle (e.g. Kawai and Inoue 2006). If the models examined here generally capture this behaviour, it is conceivable that smaller cloud amounts later in the day mean that there is less cloud to break up, resulting in a weaker cloud feedback. Figure 3c, d shows that the models do indeed tend to have more low cloud and higher LWP over the oceans in the mornings, when the largest reductions of low cloud are seen in the warmer climate. This potential linkage between the phase of the marine low cloud feedback and the present day diurnal cycle of marine low cloud properties motivates us to make a brief comparison with observations in this context.

The diurnal variations of the present-day values of liquid water path about the mean tend to be in phase with those of the low cloud fraction (Fig. 3c, d), which is consistent with observations (Wood et al. 2002, hereafter W02). This suggests that variations in the gridbox mean LWP in the models are mainly due to variations in cloud fraction rather than in-cloud water content. This idea is also supported by comparison of the amplitudes of the diurnal cycles in the models; CanAM4 for example has the largest diurnal amplitudes in both LWP and low cloud fraction. Diurnal variations of the low cloud and liquid water path responses also tend to be in phase in the majority of models, but MPI-ESM-LR, CNRM-CM5 and MRI-CGCM3 are exceptions to this (Fig. 3a, b). However, the exceptions tend to be models with relatively small diurnal amplitudes in their responses.

W02 showed that cloud liquid water paths retrieved from the Tropical Rainfall Measuring Mission Microwave Imager over the tropical and subtropical oceans tend to peak in the early morning. More recently, O'Dell et al. (2008) (hereafter O08) produced a climatology of diurnal cloud liquid water path variations from various satellite-based passive microwave observations, which showed LWP to peak mostly between 0400 and 0800 over the oceans. Figure 3c, d shows that the models are indeed able to broadly capture the observed phase in the diurnal cycle; all have a maximum low cloud fraction and liquid water path near dawn and a minimum at or after solar noon, and this is reflected in present-day values of the shortwave CRE which are most negative before 12 noon in general (Fig. 2c) and also when sampled only on occasions dominated by low clouds (Fig. 2d). This is consistent with expectations based on bulk arguments in the case when mixing (entrainment) efficiencies are low (Zhang et al. 2005).

To make a more quantitatively consistent comparison between the models and the observations, we averaged the values from the O08 climatology over the cfSites ocean points; this yielded a maximum LWP at 04:30 and a minimum at 15:00. The models agree remarkably well with these timings, showing if anything a slight tendency to reach peak and minimum values a little earlier than suggested by the observations and simple models (Fig. 3d).

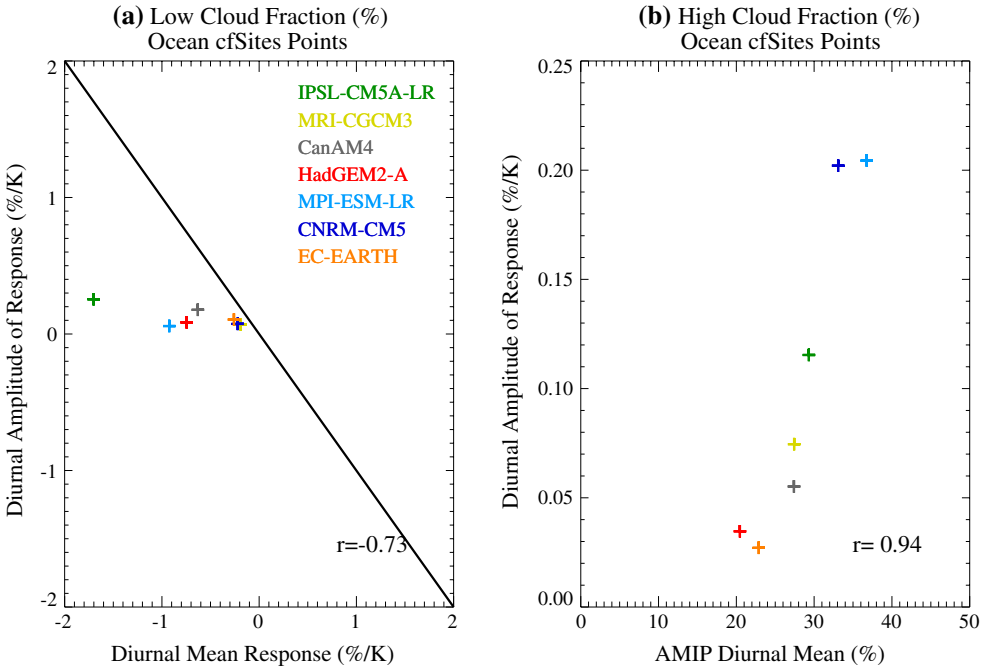

Fig. 7 **a** Scatter plot of the amplitude of the +4 K response of the low cloud fraction over ocean cfSites points versus its diurnal mean response. **b** Scatter plot of the amplitude of the +4 K response of the high cloud fraction over ocean cfSites points versus the mean values in the AMIP control experiment. r values indicate correlation coefficients; values with magnitudes greater than 0.67 and 0.75 are significant at the 90 and 95 % confidence levels respectively

The O08 climatology has a diurnal mean LWP of 0.082 mm averaged over the cfSites ocean locations. The models take values varying from 0.042 to 0.09 mm.

W02 found that diurnal amplitudes in liquid water path are observed which are considerable fractions of the mean, with relative diurnal amplitudes varying between 15 and 35 % in coastal stratocumulus regions. They define the relative amplitude of the diurnal variation in LWP as half of the difference between the maximum and minimum values, expressed as a percentage of the diurnal mean. Averaging the O08 LWP climatology over the cfSites locations only yields a relative diurnal amplitude of 14 %. The equivalent model values vary by more than a factor of two across the ensemble, with CanAM4 having the largest relative amplitude at 23 %, while MRI-CGCM3 and EC-EARTH have the smallest values, both at 9 % (Fig. 3d). Observational estimates of liquid water path have large uncertainties however, and different retrievals can vary by as much as a factor of two (e.g. Seethala and Horvath 2010; Jiang et al. 2012). The differences between the models are of a similar order, and so we do not see any basis for favouring one model over another in terms of the brief LWP evaluation performed here.

The tendency for models to have stronger feedbacks in the mornings when there is more cloud suggests that the ability of models to reproduce the present day diurnal cycle has some relevance to assessing our confidence in the diurnal cycle of their cloud feedback. However, we find no significant correlation between experiments in the timings of the morning cloud maximum the maximum cloud reduction in response to the +4 K warming. Additionally, the diurnal amplitudes of the responses of low cloud properties to the warming climate are quite small compared to the inter-model differences in the equivalent diurnal mean responses (Fig. 3a, b). This point is illustrated more clearly in Fig. 7a. This shows a scatterplot of the magnitude of the diurnal mean reduction in low cloud fraction and the amplitude of its diurnal response (both previously shown in Fig. 3a). Although there is a marginally significant relationship between these quantities, the slope of the relationship is far from unity and the amplitudes of the diurnal responses are so small compared to the range in diurnal mean responses that it is hard to imagine how the processes controlling the former could be central to understanding the latter. Such a relationship could plausibly be expected if the cloud fractions tended to reduce in similar proportions at all times of day; such behaviour could explain why the model with the largest diurnal mean response in low cloud fraction (IPSL-CM5A-LR) has a larger reduction in the morning than the afternoon, and hence the largest amplitude in its diurnal response.

3.4 Diurnal cycle in longwave cloud feedback over the oceans

A comparison of Figs. 4a, c and 2a, c show that over the oceans the diurnal cycle in the longwave CRE and its response to a +4 K perturbation is, unsurprisingly, much smaller than that in the shortwave. The diurnal cycle of the longwave CRE in the control simulations mostly tends to peak in the early morning and decrease through the day with a minimum during the afternoon (Fig. 4c). This is

consistent with and presumably explained by the diurnal cycle of the high-level cloud fraction (Fig. 4d). This peaks in the early morning and decreases throughout the day, as the free troposphere warms in response to increasing shortwave absorption, suppressing deep convection (Randall and Dazlich 1991). CanAM4 is however unusual compared to the other models in that it includes solar radiation at all wavelengths above 4 microns (mostly from the near infrared) in the longwave radiation (Li et al. 2010). This results in a peak longwave CRE around noon, much later than the high cloud maximum.

The longwave cloud feedbacks show a range of positive and negative values (Fig. 4a). Although the amplitudes of the diurnal responses are quite small, they are robust in that they tend to take minimum values around or before noon at a time when the high cloud fraction responses also tend to take their minimum values (Fig. 4b). One possible explanation for the timing of this minimum might be that higher values of free tropospheric specific humidity in the warmer climate result in a stronger diurnal cycle of atmospheric shortwave absorption. This could make the atmosphere relatively more stable during the hours of highest insolation, weakening the deep convection and suppressing high cloud production in the warmer climate.

There is no obvious relationship across the models between the changes in the diurnal cycle of these quantities and their present-day diurnal cycles. However, the models with the strongest diurnal cycles in their high-cloud responses (MPI-ESM-LR and CNRM-CM5, Fig. 4b) are also those that have the most high cloud in the present day (Fig. 4d). Figure 7b shows that there is in fact a significant correlation across the models between the amount of high cloud in the control simulation and amplitude of its diurnal response to a +4 K warming. Clearly models with more cloud in the control climate have the potential for larger responses in the warmer climate.

The diurnal mean longwave CRE responses take a range of positive and negative values, with inter-model differences which are considerably larger than their individual diurnal amplitudes (Fig. 4a), as was the case in the shortwave discussed above. As discussed in Sect. 2, the diurnal mean longwave CRE response measures the longwave impact of clouds on the overall climate feedback, including not only the contribution from cloud changes but also the impact of clouds on other feedbacks such as water vapour via climatological cloud masking. Cloud masking reduces the positive water vapour feedback and enhances the negative Planck feedback, reducing the longwave CRE response by up to 0.3 Wm^{-2}/K (Soden et al. 2004). Conversely, tropical high clouds tend to rise in such a way as to remain at nearly the same temperature as the climate warms, resulting in a more positive feedback than would be the case if cloud tops remained at the same height with warming (Zelinka and Hartmann 2010). These effects are considered to be robust across models however (Zelinka and Hartmann 2010; Vial et al. 2013), and inter-model differences in the responses of mid and high level cloud properties are expected to contribute substantially to inter-model differences in longwave cloud feedback.

MRI-CGCM3 shows an overall reduction in longwave CRE, with relatively neutral changes in high cloud fraction and ice water path (Figs. 4b, 5a). This model shows a reduction in mid-level cloud fraction however which is considerably larger than the generally quite small changes present in the other models (Fig. 5b). EC-EARTH on the other hand is the only model to show a decrease in the diurnal mean high cloud fraction, which presumably explains its reduction in longwave CRE in spite of having one of the largest increases in ice water path. CanAM4 has the largest increase in high cloud fraction and one of the larger increases in ice water path, consistent with it having the strongest longwave CRE increase. These unusually strong increases in high cloud properties could be related to the nature of the statistical cloud scheme in CanAM4, in which the variance of the cloud PDF depends on local atmospheric stability and convective mass flux, both of which would be expected to change systematically in the warmer climate (Held and Soden 2006).

The other models show diurnal mean changes in high cloud fraction and/or ice water path consistent with more neutral longwave cloud feedbacks. We also note that EC-EARTH has a very large ice water path compared to the other models; its relatively small upper level cloud fraction means that this does not result in an unusually large longwave CRE. Lacagnina and Selten (2014) argue that EC-EARTH tends to overestimate the IWP in part because it converts all liquid water to ice at temperatures below ~−21 Celsius, where super-cooled liquid water is present in reality. They also argue that deep convective mass-fluxes are too strong, resulting in an overly strong upward transport of water vapour to the upper troposphere.

4 Conclusions

Here we have examined the diurnal cycle of marine clouds and cloud feedbacks using high frequency outputs from seven CMIP5 models. Most of the inter-model spread in the diurnal mean marine shortwave cloud feedback can be explained by low cloud responses, although these do not explain the model responses at the neutral/weakly negative end of the feedback range, where changes in mid and high level cloud properties are more important. The models tend to show larger changes in marine low cloud properties in the warmer climate in the morning when more low cloud is present in the control. This results in shortwave cloud

feedbacks being strongest and having the largest inter-model spread at this time of day. This suggests that the ability of models to reproduce the present day diurnal cycle has some relevance to assessing our confidence in the diurnal cycle of their cloud feedback. The diurnal amplitudes of changes in low cloud properties in the warming climate that we see here are however quite small compared to the inter-model differences in the equivalent diurnal mean responses, and so not particularly relevant to understanding differences in cloud feedbacks overall. Hence future improvements to the representation of the diurnal cycle in climate models should not necessarily be expected to result in a reduction in the inter-model spread in climate sensitivity. This also indicates that the decision to omit the diurnal cycle in the experimental design for the first phase of CGILS (The CFMIP-GCSS Intercomparison of LES and SCMs, Zhang et al. (2013)) does not undermine its relevance to understanding the reasons for inter-model spread in cloud feedback.

The models capture the observed phase and amplitude of the diurnal cycle in present-day marine low cloud properties quite well, with maxima in low cloud fraction and liquid water paths occurring at or just before dawn, and a range of relative amplitudes in liquid water path diurnal cycle which are within observational uncertainties. The fact that the models all capture this suggests that the underlying mechanism is likely to be quite simple; one possibility is that increased solar absorption by clouds during the day heats the cloud layer, reducing relative humidity and hence cloud fraction.

A number of unusual behaviours have been noted in individual models. CanAM4 for example has an unusually strong diurnal cycle in marine liquid water path compared to the other models, although this is within current observational uncertainty. This might be related to the method of convective triggering in the CanAM4 shallow convection scheme; CanAM4 shows triggering behaviour that differs from other models in some of the CGILS experiments (Pers. comm, Knut von Salzen). Another possible contributing factor is the novel treatment of solar radiation at all wavelengths above 4 microns, which Li et al. (2010) show to increase the amount of solar radiation absorbed in the atmosphere, resulting in better agreement with line-by-line calculations. This would be expected to enhance the diurnal cycle of solar radiation absorbed in the atmosphere, and might explain the stronger diurnal cycle of marine low cloud properties. This could also potentially explain the unusual peak in the longwave CRE around noon in CanAM4. This could be tested by performing a sensitivity test with these additional solar absorption effects temporarily removed. CanAM4 also has an unusually large increase in high cloud fraction in the warmer climate, which results in an unusual competition between cloud feedbacks from low and high clouds over the oceans.

Other unusual behaviours include a reduction in liquid water path over the oceans in HadGEM2-A in the warmer climate, an unusually large ice water path in the control climate in EC-EARTH, and a strongly negative shortwave cloud feedback over ocean areas in CNRM-CM5. We would like to encourage the modelling groups to investigate the causes of such unusual behaviours by performing sensitivity tests, to establish whether such models are representing the relevant processes unusually well or unusually poorly. We consider an improved understanding of such behaviours in models a useful step towards improving the representation of cloud processes across all models.

An obvious next step would be extend this analysis to the other CFMIP-2 experiments containing cfSites data. Given that we have shown that the diurnal cycle of the cloud feedback does not contribute greatly to the overall differences in cloud feedback, there would be little to gain by repeating this particular analysis on the amipFuture and aquaplanet +4 K experiments. Investigation of the role of the diurnal cycle in cloud adjustment might be more fruitful however; a number of studies have argued that oceanic cloud adjustments are in part a response to rapid adjustments in lower tropopheric stability caused by radiative heating of the lower free troposphere by CO_2. The responses of clouds to changes in shortwave absorption through the diurnal cycle could in principle be a predictor of their sensitivity to rapid stability adjustments in response to CO_2 forcing.

Examination of the diurnal cycle is but one application of these high frequency model outputs. Many other questions remain which can be investigated using these data. They can be used to refine large scale forcings used to run LES models in cloud feedback studies such as CGILS. They can be used to separate cloud feedback into contributions from times when convection is dominant from those when turbulent boundary layer processes are dominant. More generally, relationships between clouds and other model variables such as surface fluxes, temperature and humidity profiles and their tendency terms can be investigated. One advantage of these outputs is that the order of events can potentially be used to determine causality in a way that is not possible with time mean outputs. Moreover these model outputs constitute a rich database of model behaviour against which physical cloud feedback mechanism hypotheses can be tested.

In this study we have demonstrated the value and potential of the CFMIP cfsites data for investigating high frequency responses of models to climate change. We have so far examined only seven models, and one should of course keep in mind the possibility that our conclusions might change as data from more models become available.

We hope that this work will encourage the production of cfSites outputs from more models in the future.

Acknowledgments We would like to thank Knut von Salzen and William Ingram for helpful comments on the manuscript, and Mark Ringer and Tim Andrews for useful discussions. This work was supported by the Joint DECC/Defra Met Office Hadley Centre Climate Programme (GA01101). The research leading to these results has received funding from the European Union, Seventh Framework Programme (FP7/2007–2013) under grant agreement number 244067 via the EU Cloud Intercomparison and Process Study Evaluation project (EUCLIPSE). We acknowledge the World Climate Research Programme's Working Group on Coupled Modelling, which is responsible for CMIP, and we thank the climate modelling groups for producing and making available their model output. For CMIP the U.S. Department of Energy's Program for Climate Model Diagnosis and Intercomparison provides coordinating support and led development of software infrastructure in partnership with the Global Organization for Earth System Science Portals. We would like to acknowledge in particular Philip Bentley, Alejandro Bodas-Salcedo, Sandrine Bony, Jason Cole, Herve Douville, Jean-Louis Dufresne, Hideaki Kawai, Jamie Kettleborough, Tsuyoshi Koshiro, Carlo Lacagnina, Marc Salzmann, Frank Selten, Yoko Tsushima, Sophie Tyteca, and Jonny Williams for their efforts in preparing cfSites outputs from the models.

References

Andrews T, Forster PM (2008) CO_2 forcing induces semi-direct effects with consequences for climate feedback interpretations. Geophys Res Lett 35:L04802. doi:10.1029/2007GL032273

Andrews T, Gregory JM, Webb MJ, Taylor KE (2012) Forcing, feedbacks and climate sensitivity in CMIP5 coupled atmosphere-ocean climate models. Geophys Res Lett 39:L09712. doi:10.1029/2012GL051607

Bentsen M, Bethke I, Debernard JB, Iversen T, Kirkevag A, Seland O, Drange H, Roelandt C, Seierstad IA, Hoose C, Kristjansson JE (2012) The Norwegian earth system model, NorESM1-M—Part 1: description and basic evaluation. Geosci Model Dev Discuss 5:2843–2931. doi:10.5194/gmdd-5-2843-2012

Bony S, Emanuel KS (2001) A parameterization of the cloudiness associated with cumulus convection; evaluation using TOGA COARE data. J Atmos Sci 58:3158–3183. doi:10.1175/1520-0469(2001)58<3158:APOTCA>2.0.CO;2

Bony S et al (2011) CFMIP: towards a better evaluation and understanding of clouds and cloud feedbacks in CMIP5 models. Clivar Exchanges 56(16):2

Bouniol D, Couvreux F, Kamsu-Tamo P-H, Leplay M, Guichard F, Favot F, O'Connor E (2012) Diurnal and seasonal cycles of cloud occurrences, types and radiative impact over West Africa. J Appl Meteor Climatol 51:534–553. doi:10.1175/JAMC-D-11-051.1

Bretherton CS (2006) The climate process team on low-latitude cloud feedbacks on climate sensitivity. US Clivar Variations 4:7–12

Dufresne J-L, Bony S (2008) An assessment of the primary sources of spread of global warming estimates from coupled atmosphere-ocean models. J Climate 21:5135–5144

Duynkerke PG, de Roode SR, van Zanten MC, Calvo J, Cuxart J, Cheinet S, Chlond A, Grenier H, Jonker PJ, Kohler M, Lenderink G, Lewellen D, Lappen C-L, Lock AP, Moeng C-H, Muller F, Olmeda D, Piriou J-M, Sanchez E, Sednev I (2004) Observations and numerical simulations of the diurnal cycle of the EUROCS stratocumulus case. QJR Meteorol Soc 130:3269–3296. doi:10.1256/qj.03.139

Gregory JM, Webb MJ (2008) Tropospheric adjustment induces a cloud component in CO_2 forcing. J Climate 21:58–71. doi:10.1175/2007JCLI1834.1

Hazeleger W, et al. (2012) EC-Earth V2.2: description and validation of a new seamless earth system prediction model. Clim Dyn. doi:10.1007/s00382-011-1228-5ed

Hazeleger W et al (2010) EC-Earth: a seamless earth-system prediction approach in action. Bull Am Meteorol Soc 91:1357–1363. doi:10.1175/2010BAMS2877.1

He J, Soden BJ, Kirtman B (2014) The robustness of the atmospheric circulation and precipitation response to future anthropogenic surface warming. Geophys Res Lett 41:2614–2622. doi:10.1002/2014GL059435

Held IM, Soden BJ (2006) Robust responses of the hydrological cycle to global warming. J Climate 19:5686–5699. doi:10.1175/JCLI3990.1

Hourdin F et al (2012) Impact of the LMDZ atmospheric grid configuration on the climate and sensitivity of the IPSL-CM5A coupled model. Clim Dyn. doi:10.1007/s00382-012-1411-3

Jiang JH et al (2012) Evaluation of cloud and water vapour simulations in CMIP5 climate models using NASA "A-Train" satellite observations. J Geophys Res 117:D14105. doi:10.1029/2011JD017237

Kawai H, Inoue Y (2006) A simple parameterization scheme for subtropical marine stratocumulus. SOLA 2:17–20

Klein SA, Jakob C (1999) Validation and sensitivities of frontal clouds simulated by the ECMWF model. Mon Weather Rev 127:2514–2531

Lacagnina C, Selten FM (2014) Evaluation of clouds and radiative fluxes in the EC-Earth general circulation model using the ISCCP simulator. Clin Dyn. doi:10.1007/s00382-014-2093-9

Li J, Curry CL, Sun Z, Zhang F (2010) Overlap of solar and infrared spectra and the shortwave radiative effect of methane. J Atmos Sci 67:2372–2389

Lin PF, Yu YQ, Liu HL (2013) Oceanic climatology in the coupled model FGOALS-g2: improvements and biases. Adv Atmos Sci 30(3):819–840. doi:10.1007/s00376-012-2137-1

Mapes BE, Bacmeister J, Khairoutdinov M, Hannay C, Zhao M (2009) Virtual field campaigns on deep tropical convection in climate models. J Climate 22:244–257. doi:10.1175/2008JCLI2203.1

Martin GM et al (2011) The HadGEM2 family of met office unified model climate configurations. Geosci Model Devel 4:723–757. doi:10.5194/gmd-4-723-2011

O'Dell C, Wentz FJ, Bennartz R (2008) Cloud liquid water path from satellite-based passive microwave observations: a new climatology over the global oceans. J Climate 21:1721–1739. doi:10.1175/2007JCLI1958.1

Randall DA, Dazlich DA (1991) Diurnal variability of the hydrologic cycle in a general circulation model. J Atmos Sci 48:40–62

Randall DA, Wood RA, Bony S, Colman R, Fichefet T, Fyfe J, Kattsov V, Pitman A, Shukla J, Srinivasan J, Stouffer RJ, Sumi A, Taylor KE (2007) Climate models and their evaluation. In: Solomon S, Qin D, Manning M, Chen Z, Marquis MC, Avery KB, Tignor M, Miller HL (eds) Climate change 2007: the physical science basis. Contribution of Working Group I to the fourth assessment report of the intergovernmental panel on climate change. Cambridge University Press, pp 589–662

Ringer MA, McAvaney BJ, Andronova N, Buja LE, Esch M, Ingram WJ, Li B, Quaas J, Roeckner E, Senior CA, Soden BJ, Volodin EM, Webb MJ, Williams KD (2006) Global mean cloud feedbacks in idealized climate change experiments. Geophys Res Lett 33:7

Roehrig R, Bouniol D, Guichard F, Hourdin F, Redelsperger J (2013) The present and future of the West African monsoon: a process-oriented assessment of CMIP5 simulations along the AMMA transect. J Climate 26:6471–6505. doi:10.1175/JCLI-D-12-00505.1

Rossow WB, Schiffer RA (1999) Advances in understanding clouds from ISCCP. Bull Am Meteorol Soc 80:2261–2287

Seethala C, Horvath A (2010) Global assessment of AMSR-E and MODIS cloud liquid water path retrievals in warm oceanic clouds. J Geophys Res 115:D13202. doi:10.1029/2009JD012662

Soden BJ, Broccoli AJ, Hemler RS (2004) On the use of cloud forcing to estimate cloud feedback. J Climate 17:3661–3665

Stevens B, Giorgetta M, Esch M, Mauritsen T, Crueger T, Rast S et al. (2013) Atmospheric component of the MPI-M earth system model: ECHAM6. J Adv Model Earth Syst

Taylor KE, Stouffer RJ, Meehl GA (2011) An overview of CMIP5 and the experiment design. Amer. Meteor. Soc, Bull. doi:10.1175/BAMS-D-11-00094.1

Teixeira J et al (2011) Tropical and subtropical cloud transitions in weather and climate prediction models: the GCSS/WGNE Pacific cross-section intercomparison (GPCI). J Climate 24:5223–5256. doi:10.1175/2011JCLI3672.1

Vial J, Dufresne J-L, Bony S (2013) On the interpretation of inter-model spread in CMIP5 climate sensitivity estimates. Clim Dyn Doi:10.1007/s00382-013-1725-9

Voldoire A, et al (2012) The CNRM-CM5.1 global climate model: description and basic evaluation. Clim Dyn. doi:10.1007/s00382-011-1259-y

von Salzen K, Scinocca JF, McFarlane NA, Li J, Cole JNS, Plummer D, Verseghy D, Reader MC, Ma X, Lazare M, Solheim L (2013) The Canadian fourth generation atmospheric global climate model (CanAM4) Part I: representation of physical processes. Atmos-Ocean 51:104–125

Watanabe M et al (2010) Improved climate simulation by MIROC5: mean states, variability, and climate sensitivity. J Climate 23:6312–6335. doi:10.1175/2010JCLI3679.1

Webb M, Senior C, Bony S, Morcrette JJ (2001) Combining ERBE and ISCCP data to assess clouds in the Hadley Centre, ECMWF and LMD atmospheric climate models. Clim Dyn 17:905–922

Webb MJ, Lambert FH, Gregory JM (2013) Origins of differences in climate sensitivity, forcing and feedback in climate models. Clim Dyn 40:677–707. doi:10.1007/s00382-012-1336-x

Wood R, Bretherton CS, Hartmann DL (2002) Diurnal cycle of liquid cloud water path over the subtropical and tropical oceans. Geophys Res Lett 29:2092–2095

Wu T et al (2010) The Beijing Climate Center atmospheric general circulation model: description and its performance for the present-day climate. Clim Dyn 34(1):123–147. doi:10.1007/s00382-008-0487-2

Yukimoto S, et al (2011) Meteorological research institute-earth system model version 1 (MRI-ESM1) model description. Tech. Rep. 64, Meteorological Research Institute, Japan

Zelinka MD, Hartmann DL (2010) Why is longwave cloud feedback positive? J Geophys Res Atmos 115:2156–2202. doi:10.1029/2010JD013817

Zelinka MD, Klein SA, Taylor KE, Andrews T, Webb MJ, Gregory JM, Forster PM (2013) Contributions of different cloud types to feedbacks and rapid adjustments in CMIP5. J Climate. doi:10.1175/JCLI-D-12-00555.1

Zhang M, Bretherton CS (2008) Mechanisms of low cloud climate feedback in idealized single-column simulations with the community atmospheric model (CAM3). J Climate 21:4859–4878. doi:10.1175/2008JCLI2237.1

Zhang Y, Stevens B, Ghil M (2005) On the diurnal cycle and susceptibility to aerosol concentration in a stratocumulus-topped mixed layer. Quarterly Journal of the Royal Meteorological Society 131(608):1567–1583. doi:10.1256/qj.04.103

Zhang M, Bretherton CS, Blossey PN, Bony S, Brient F, Golaz J-C (2013) The CGILS experimental design to investigate low cloud feedbacks in general circulation models by using single-column and large-eddy simulation models. J Adv Model Earth Syst. doi:10.1029/2012MS000182

PHILOSOPHICAL TRANSACTIONS A

rsta.royalsocietypublishing.org

Research

Cite this article: Webb MJ *et al*. 2015 The impact of parametrized convection on cloud feedback. *Phil. Trans. R. Soc. A* **373**: 20140414. http://dx.doi.org/10.1098/rsta.2014.0414

Accepted: 12 August 2015

One contribution of 12 to a discussion meeting issue 'Feedbacks on climate in the Earth system'.

Subject Areas:
atmospheric science, climatology

Keywords:
cloud, climate, feedback, convection, parametrization

Author for correspondence:
Mark J. Webb
e-mail: mark.webb@metoffice.gov.uk

THE ROYAL SOCIETY PUBLISHING

The impact of parametrized convection on cloud feedback

Mark J. Webb[1], Adrian P. Lock[1], Christopher S. Bretherton[2], Sandrine Bony[3], Jason N. S. Cole[4], Abderrahmane Idelkadi[3], Sarah M. Kang[5], Tsuyoshi Koshiro[6], Hideaki Kawai[6], Tomoo Ogura[7], Romain Roehrig[8], Yechul Shin[5], Thorsten Mauritsen[9], Steven C. Sherwood[10], Jessica Vial[3], Masahiro Watanabe[11], Matthew D. Woelfle[2] and Ming Zhao[12]

[1]Met Office Hadley Centre (MOHC), Exeter, UK
[2]University of Washington (UW), Seattle, WA, USA
[3]Laboratoire de Météorologie Dynamique/Institute Pierre Simon Laplace (IPSL), Paris, France
[4]Canadian Centre for Climate Modelling and Analysis (CCCma), Victoria, British Columbia, Canada
[5]Ulsan National Institute of Science and Technology (UNIST), Ulsan, Republic of Korea
[6]Meteorological Research Institute (MRI), Tsukuba, Ibaraki Prefecture, Japan
[7]National Institute for Environmental Studies (NIES), Tsukuba, Ibaraki Prefecture, Japan
[8]Centre National de Recherches Météorologiques (CNRM), Toulouse, France
[9]Max Planck Institute for Meteorology (MPI-M), Hamburg, Germany
[10]University of New South Wales (UNSW), Sydney, New South Wales, Australia
[11]Atmosphere and Ocean Research Institute (AORI), Chiba, Japan
[12]Geophysical Fluid Dynamics Laboratory (GFDL), Princeton, NJ, USA

We investigate the sensitivity of cloud feedbacks to the use of convective parametrizations by repeating the CMIP5/CFMIP-2 AMIP/AMIP + 4K uniform sea surface temperature perturbation experiments with 10 climate models which have had their convective parametrizations turned off. Previous studies have

suggested that differences between parametrized convection schemes are a leading source of inter-model spread in cloud feedbacks. We find however that 'ConvOff' models with convection switched off have a similar overall range of cloud feedbacks compared with the standard configurations. Furthermore, applying a simple bias correction method to allow for differences in present-day global cloud radiative effects substantially reduces the differences between the cloud feedbacks with and without parametrized convection in the individual models. We conclude that, while parametrized convection influences the strength of the cloud feedbacks substantially in some models, other processes must also contribute substantially to the overall inter-model spread. The positive shortwave cloud feedbacks seen in the models in subtropical regimes associated with shallow clouds are still present in the ConvOff experiments. Inter-model spread in shortwave cloud feedback increases slightly in regimes associated with trade cumulus in the ConvOff experiments but is quite similar in the most stable subtropical regimes associated with stratocumulus clouds. Inter-model spread in longwave cloud feedbacks in strongly precipitating regions of the tropics is substantially reduced in the ConvOff experiments however, indicating a considerable local contribution from differences in the details of convective parametrizations. In both standard and ConvOff experiments, models with less mid-level cloud and less moist static energy near the top of the boundary layer tend to have more positive tropical cloud feedbacks. The role of non-convective processes in contributing to inter-model spread in cloud feedback is discussed.

1. Introduction

Equilibrium climate sensitivity (ECS) is a standard measure of the sensitivity of climate models to external forcing, and is defined as the equilibrium change in global mean near-surface temperature following an instantaneous doubling of CO_2. It remains an important quantity for climate policy, because climate negotiations use the size of the increase in long-term global mean surface temperature as a metric for dangerous anthropogenic interference with the climate system [1]. The Fifth Assessment Report of the Intergovernmental Panel on Climate Change concluded that estimates of the ECS based on observed climate change, climate models and feedback analysis, as well as palaeoclimate evidence indicate a likely range of 1.5–4.5°C [2] and that the dominant source of spread among climate sensitivities from climate models is due to differences in cloud feedbacks, particularly due to low clouds [3].

The Cloud Feedback Model Intercomparison Project (CFMIP) [4] coordinates a number of idealized experiments in CMIP5, which perturb sea surface temperatures and CO_2 in atmosphere only experiments forced with observed AMIP sea surface temperatures (SSTs) and also in idealized aquaplanet configurations [5]. These experiments include satellite simulators which support quantitative evaluation of clouds using a range of satellite products [6]. Process diagnostics, such as physical temperature and humidity budget tendency terms [7] and high-frequency outputs at selected locations [8], are also included to support the generation and testing of physical hypotheses for cloud feedback mechanisms. CFMIP also coordinates a joint activity on cloud feedbacks with the global atmospheric system study (GASS). The CFMIP–GASS intercomparison of SCM and LES (CGILS) aims to evaluate the performance of global climate model (GCM) physics in single column models (SCMs) using large eddy simulations (LESs) forced consistently in idealized subtropical cloud feedback scenarios associated with well-mixed stratocumulus, stratocumulus over cumulus and shallow cumulus regimes [9,10]. Bretherton [11] provides a review of findings from CGILS and other recent high-resolution cloud feedback studies.

These experiments have led to a number of new studies investigating the physical mechanisms underlying cloud feedbacks, including [7,9,10,12–21]. A number of these studies have implicated parametrized convection (both shallow and deep) as playing a central role in the mechanisms of cloud feedback, although the relative importance of other processes remains unclear.

Additionally, a number of studies have employed the so-called 'emergent constraint' approach which exploits statistical relationships between observable and predicted quantities across climate models to constrain climate sensitivity [21–25]. These, along with other studies such as [26,27], have tended to find that models with mid-to-high climate sensitivities have more credible simulations of present-day clouds, humidity and convection than those at the lower end of the model range. Some studies have additionally combined the emergent constraint approach with physical arguments [21].

Despite such progress, further work is still required to rigorously test the robustness of the physical mechanisms proposed so far and the constraints that they imply for cloud feedback and climate sensitivity. Given the nature of most model intercomparison projects, multi-model studies can usually only demonstrate that results are consistent with a proposed physical hypothesis. Such hypotheses can be tested more rigorously if we attempt to falsify them using sensitivity experiments. For example, if a particular mechanism is proposed to contribute to positive subtropical feedback, then suppressing the processes involved should weaken that feedback. This process simplification approach has already been applied in some studies with single GCMs [7,14] but has not yet been applied consistently across multiple of climate models; hence, the findings of such studies so far remain highly model specific.

The Selected Process On/Off Klima Intercomparison Experiment (SPOOKIE) is a recent initiative associated with CFMIP which aims to establish the relative contributions of different areas of model physics to inter-model spread in cloud feedback by switching off or simplifying different model schemes or processes in turn. Here, we present results from a pilot study which assesses the impact of convective parametrizations on cloud feedbacks by switching off convective parametrizations in 10 climate models.

Convective parametrizations are generally employed in climate models to represent transports of heat, moisture and momentum associated with convective motions at subgrid scales as well as associated cloud microphysical and precipitation processes [28–30]. Convective parametrizations enable climate models to simulate various properties of atmospheric convection which cannot be accurately represented at the resolved scale, such as allowing moist convection to occur without reaching grid-scale saturation [31]. Previous studies have examined the impact and benefits of parametrized convection in individual models, both by introducing new convective parametrizations [32–35] and by running models with convective parametrizations suppressed [31,36–38]. Additionally, Gettelman *et al*. [39] and Zhao [40] have demonstrated sensitivity of cloud feedbacks to details of convective parametrizations in versions of the NCAR and GFDL models, respectively. These more recent findings (and others discussed below) motivated our choice to focus on the impact of convective parametrizations on cloud feedbacks in this initial pilot study.

Cloud feedbacks could potentially be affected in various different ways by both deep and shallow convective parametrizations. Most obviously, deep convective parametrizations would be expected to influence the formation of cirrus clouds and so could potentially affect cloud feedbacks associated with changes in the properties of high clouds. Although a near cancellation between tropical longwave and shortwave cloud radiative effects (CREs) is observed in regions of deep convective activity where clouds are optically thick [41], such a cancellation is by no means guaranteed in climate models, or in the changing climate. Deep convection schemes could potentially also affect changes in optically thinner cirrus clouds whose impact is mainly in the longwave, by influencing upper tropospheric humidities across the wider tropics. However, as noted above, the dominant source of spread in cloud feedbacks in climate models is due to low clouds. These can potentially be influenced locally by shallow convective parametrizations or by deep convective parametrizations if they trigger in regions where low clouds are prevalent. For example, results from CGILS [10] suggest that the ability of SCMs to correctly diagnose the presence of convection has a substantial impact on low cloud feedback. Zhang *et al*. [10] proposed a mechanism for positive subtropical low cloud feedback in climate models whereby increased entrainment of dry air from the free troposphere into the boundary layer by parametrized convection in the warmer climate reduces low cloud amounts. Alternatively, it is possible that

parametrized convection could exert a remote influence on shallow cloud feedbacks in climate models, for example by affecting the temperature and humidity structure of the free troposphere, as suggested by Brient & Bony [14]. Sherwood *et al.* [21] argued that a substantial fraction of the variation in the strength of low level cloud feedback across models is regulated by the strength of 'lower-tropospheric mixing' between low- and mid-levels by small-scale parametrized processes such as convection and the resolved large-scale shallow overturning circulation in the present-day climate. These were argued to control the rate at which the boundary layer dries and low cloud reduces as the climate warms. Sherwood *et al.* [21] additionally showed that indirect observable proxies for the lower-tropospheric mixing rate based on the tropical temperature, humidity and vertical velocity in ascending regions were significantly correlated with ECS and cloud feedback, statistically 'explaining' just under half of the inter-model variance in the ECS. They also showed evidence of significantly different amounts of low level drying by convective parametrizations between a subset of models in subsiding regions, and suggested that their lower tropospheric mixing mechanism could operate in shallow cloud regions as well as in regions of mean ascent.

Motivated in part by these findings, the pilot SPOOKIE experiments have repeated the CFMIP-2/CMIP5 amip/amip4K experiments with convective parametrizations turned off (convoffamip and convoffamip4K experiments). These experiments are designed to give an indication of the impact of the models' convective parametrizations on cloud feedbacks, and not of convection in the general sense; convective instability which would be removed by the convective parametrizations in the standard experiments will instead be removed by the models' turbulent mixing schemes and large-scale dynamics in the ConvOff experiments. If the details of convective parametrizations are indeed responsible for a substantial part of the inter-model spread in cloud feedback, then these experiments might be expected to exhibit a narrower range of cloud feedback. Equally, if parametrized convection is responsible for positive subtropical cloud feedbacks in the GCMs, then the ConvOff experiments would be expected to have neutral or negative cloud feedbacks.

This study is structured as follows. §2 describes the models employed and lists details of the convection schemes and the steps which were taken to switch them off. §3a discusses the impact of switching off convection on the global cloud feedbacks. §3b discusses the impact on cloud feedbacks in various cloud regimes over the low-latitude oceans. In §3c, we discuss the impact on present-day cloud variables and relationships between them and the cloud feedbacks. We discuss the potential role of other processes in contributing to inter-model spread in cloud feedback in §4, and present our overall conclusions in §5.

2. Models and experimental design

Our experimental design is based on the CFMIP2/CMIP5 amip and amip4K experiments. The amip experiment forces the atmosphere-only version of the model with observed seasonally and inter-annually varying SSTs and sea ice concentrations, and the amip4K experiment applies a uniform +4 K SST perturbation to the amip experiment [4]. This approach is derived from that of Cess *et al*. [42] which originally diagnosed cloud feedbacks in perpetual July experiments forced with an observed climatology and subject to a uniform +2 K warming. Many of the amip/amip4K experiments used here are pre-existing CMIP5 experiments, but some were run specifically for this intercomparison. These experiments were then repeated with convective parametrizations switched off. Horizontal and vertical resolutions were maintained, but in some cases, other details were changed to maintain the stability of the integrations. A brief description of each model, its convection scheme and the steps taken to switch convection off follows for the various models. Unless stated otherwise below, we use the amip/amip4K experiments from CMIP5. All of the convection off experiments were performed specifically for this study. All experiments were run for 30 years from January 1979 to December 2008, unless stated otherwise below.

CanAM4 [43] has a horizontal resolution of T63 with 35 layers in the vertical. CanAM4 uses a mass flux scheme for deep convection, including aerosol chemistry [44], a prognostic closure based on convectively available potential energy [45] and a parametrization of convective

momentum transport [43]. A separate shallow convection scheme is used which is allowed to operate at the same time and location as the deep convection [33]. For the ConvOff experiments, the model was modified, so that it completely bypassed the shallow and deep convection by setting the mass flux to zero.

CESM1-CAM5.1-FV2 [46] was run specifically for this study from UW with a resolution of 1.9° latitude × 2.5° longitude and 30 vertical levels. Deep convection within the model is parametrized using a plume ensemble approach with closure based on convective available potential energy as computed for an entraining parcel [44,47]. This parametrization includes momentum transport by convection [48]. The model uses a separate shallow convection parametrization which is formulated with a bulk plume approach and mass-flux closure [49]. The shallow convective parametrization is permitted to operate on all model levels. For the ConvOff experiments, both the deep and shallow convective parametrizations were disabled. Dynamics and physics timesteps for the simulations were shortened from their default values to avoid numerical instabilities.

CNRM-CM5 [50] has a horizontal resolution of 1.4° and 31 levels. The deep convection scheme is described by Bougeault [51] and follows a mass-flux approach. It triggers under conditions related to total (large and subgrid scale) moisture convergence at low levels and vertical conditional instability (CAPE), and the scheme is closed using the Kuo [52] hypothesis. CNRM-CM5 does not have a separate treatment of shallow convection. In the ConvOff experiments, the deep convection scheme was bypassed, and no other changes were required to make the model run.

GFDL-AM2 [53] was run specifically for this study at UNIST with a horizontal resolution of 2.5° × 2° and 24 vertical levels. GFDL-AM2 uses the relaxed Arakawa–Schubert convection scheme [54] allowing some modifications documented in [53] (i.e. precipitation efficiency and re-evaporation). There is no special treatment for shallow convection. This was completely switched off in the ConvOff experiments. No other changes were required to make the model run.

GFDL-HIRAM [55] has 50 km horizontal resolution and 30 levels in the vertical, and the amip4K experiment was run specifically for this study. The convection scheme is that of Bretherton *et al*. [56] with additional modifications documented in [55]. It is a mass flux scheme with a single bulk plume which both entrains and detrains. The entrainment/detrainment rate is computed based on buoyancy sorting, which interacts with the environment dynamically and thermodynamically. The amip/amip4K experiments were provided for the 25 year period 1981–2005. All elements of the convection were switched off in the ConvOff experiments, which were provided for the 20 year period 1981–2000.

HadGEM2-A [57] has a horizontal resolution of 1.25° latitude × 1.875° longitude and 38 vertical levels. The deep convective parametrization is a mass flux scheme based on Gregory & Rowntree [58] but modified to include a CAPE based closure, convective momentum transport and a simple radiative representation of anvils [59] and more recently an adaptive treatment of detrainment [60]. Shallow convection is treated separately and uses a closure based on [61] with entrainment/detrainment rates as in [62]. Both shallow and deep schemes were switched off in the ConvOff experiments. The timestep was shortened from 30 to 15 min to improve model stability. Additionally, we confirmed that reducing the timestep does not substantially affect the cloud feedbacks in the standard configuration with convection included.

The IPSL-CM5A-LR model has a resolution of 2.5° × 1.875° in longitude–latitude, and 39 vertical levels (including eight levels less than 2 km). The physics package of this model version is described in [63,64]. The parametrization of shallow and deep convection is based on Emanuel [65] and modified by Emanuel [66] and Grandpeix *et al*. [67]. This scheme is based on a mass flux representation of adiabatic saturated updraughts and downdraughts, unsaturated downdraughts (driven by re-evaporation of precipitation) and the induced motions of the environmental air. The mixing between cloud and environmental air is based on the 'episodic mixing and buoyancy sorting' scheme developed by Emanuel [65]. The simulations with the convection scheme switched off use the same physics, except that the time step (15 min in the original set-up)

was reduced by a factor of two (7.5 min) to avoid numerical instabilities. Previous investigations have shown that the model climatology was not significantly dependent on the time step for this range of values. The IPSL-CM5A-LR ConvOff experiments were provided for the 27 year period 1979–2005.

MIROC5 [68] has a horizontal resolution of T85 (1.4°) and 40 levels in the vertical. The convection scheme has a mass flux closure similar to Arakawa–Schubert, but the entrainment rate varies in time and space depending on the temperature and humidity [69]. Shallow convection is not treated separately, but the scheme may represent some shallow cumulus clouds. The entire convection scheme was switched off in the ConvOff experiments. No other modifications were necessary.

MPI-ESM-LR has a horizontal resolution of T63 (which translates to around 200 km grid spacing at the equator) and 47 levels in the vertical. It incorporates modified Tiedtke–Nordeng parametrizations of shallow, deep and mid-level convection [70,71], which are modelled by a unified mass flux formulation with a quasi-equilibrium closure for deep convection, and a moisture closure for shallow convection [72]. All of the above were switched off in the ConvOff experiments, and no other changes were necessary, although the model crashed a few times with high wind speeds. It could in each case however be continued by introducing a small change to the atmospheric state.

MRI-CGCM3 [73] has a resolution of (T159, L48). The Yoshimura cumulus scheme [74] is a mass flux spectral cumulus parametrization scheme that explicitly considers an ensemble of multiple convective updrafts. This cumulus scheme has the advantages that the variables in entraining and detraining convective updrafts are calculated in detail layer-by-layer as in the Tiedtke scheme, and that a spectrum of convective updrafts with different heights owing to difference in entrainment rates is explicitly represented, as in the Arakawa–Schubert scheme. No shallow convection scheme is used, and the Yoshimura cumulus scheme is designed to reproduce all depths of convection. For the ConvOff experiments, all elements related to convection scheme were switched off. No additional changes were required to make the model run stably without convection.

3. Results

(a) Global mean cloud feedbacks

Figure 1*a* shows a scatterplot of the global mean cloud feedbacks in the 10 models examined with and without convective parametrization. These cloud feedbacks are diagnosed using the commonly employed method of taking the change in the long-term annually averaged global mean net CRE between the amip and amip4K experiments for all available years (as documented in §2) and dividing by the corresponding change in the long-term annually averaged global mean near-surface temperature [75]. This method tends to yield less positive/more negative values of cloud feedback than alternative approaches based on the alternative 'partial radiative perturbation' method because it includes the masking effect of climatological cloudiness on non-cloud feedbacks [76]. It is however a good predictor of inter-model spread in cloud feedback [77].

By comparing the models' global cloud feedbacks with and without convective parametrization, we can directly test the hypothesis that a substantial fraction of the inter-model spread is due to differences in the details of the convective parametrizations. If this were the case, then we would expect to see a considerable reduction in the inter-model spread in the ConvOff experiments. The standard models have a range of 1.07 (−0.34 to 0.73) $\mathrm{W\,m^{-2}\,K^{-1}}$. This range is not reduced however in the ConvOff experiments; in fact it increases by 23% to 1.32 (−0.52 to 0.80) $\mathrm{Wm^{-2}\,K^{-1}}$. Similarly, the standard deviation increases by 25%. At face value, this would seem to indicate that differences in the details of convective parametrizations are not the dominant cause of inter-model spread in global mean cloud feedbacks in this particular selection of climate models.

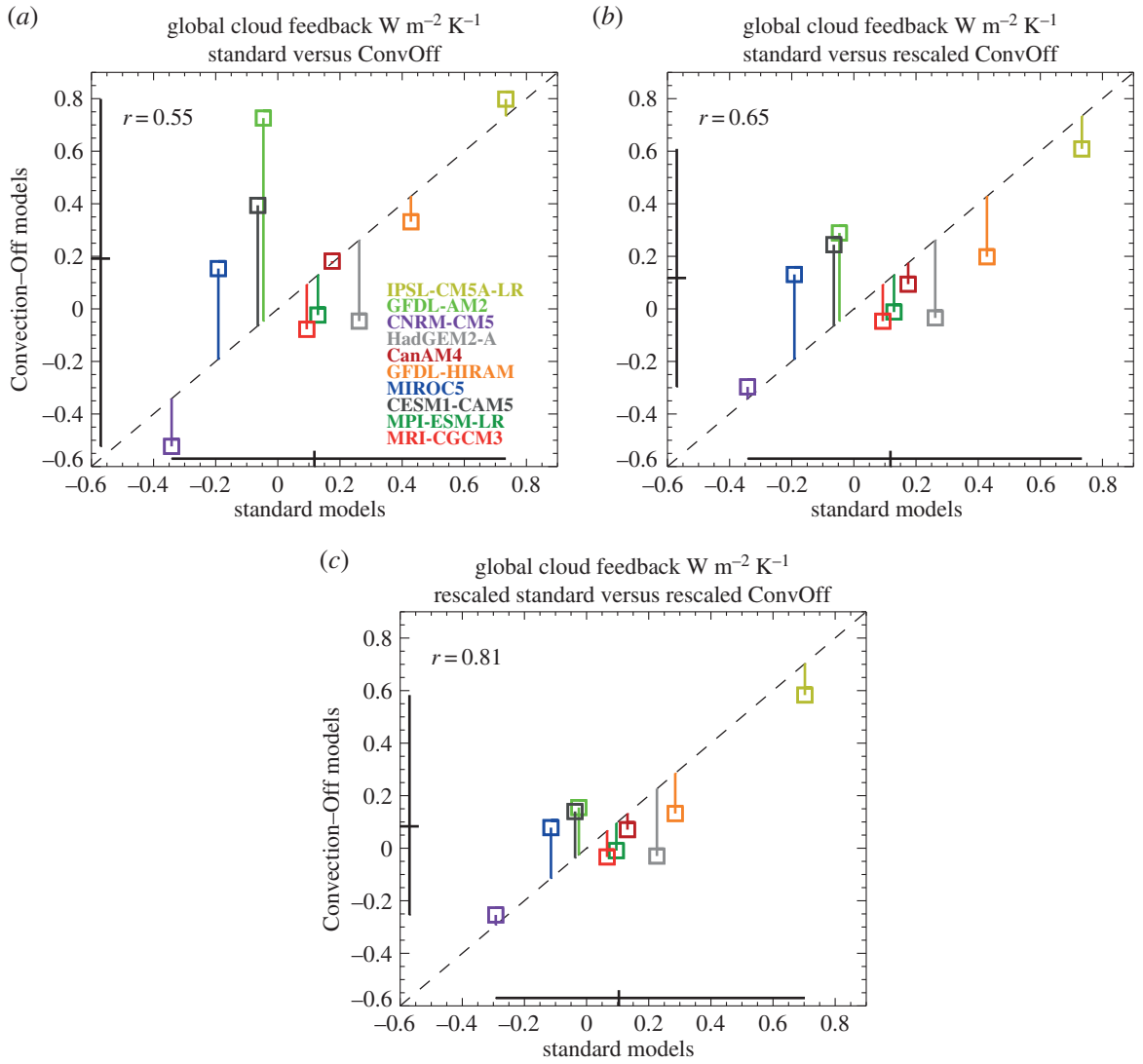

Figure 1. (*a*) Global mean net cloud feedbacks in CFMIP amip/amip4K experiments and convoffamip/convoffamip4K experiments without parametrized convection. This is diagnosed as the change in the global mean net cloud radiative effect (CRE) between the amip and amip4K experiments, normalized by the global mean near-surface temperature response and includes the effects of climatological cloud masking on the non-cloud feedbacks. Black lines denote the ranges in the values and the diagonal line indicates the one-to-one line. The lengths of the vertical coloured lines indicate the differences between standard and ConvOff values for the individual models. The linear correlation coefficient r is also shown. Panel (*b*) shows the same but with the ConvOff feedbacks rescaled by the factor required to bring the global mean net CRE in the convoffamip experiment into agreement with the standard amip experiment. Panel (*c*) shows the result of scaling all feedbacks by the factors required to bring their control experiments into agreement with an observed value of the net CRE (−17.1 W m^{-2}).

Before drawing firm conclusions on this point however, we consider an alternative potential explanation for this result. Previous studies which have examined the impact of shallow cumulus parametrizations in models have shown that the introduction of shallow convection schemes tends to reduce cloud in the boundary layer [32–35]. It is, in principle, possible that enhanced cloudiness in the ConvOff experiments could in itself have an impact on the cloud feedbacks which would not be present if all of the models were retuned to have similar amounts of cloud as the standard configurations. If this effect was to vary between the models, it could, in principle, inflate the inter-model spread in the feedbacks and offset a reduction in spread associated with the removal of differences between the convection schemes. For example, if switching off convection in a model were to say double the amount of cloud in the amip and the amip4K experiment, then that would imply a doubling of the difference between them—i.e. a doubling of the cloud response. Such a scenario would imply a relationship between the amount of cloud in the control

simulation and the strength of the cloud response to climate change, as has been proposed by Brient & Bony [13]. They found a relationship between the amount of subtropical low level cloud and the magnitude of its change in the warmer climate across different versions if the IPSL GCM. This behaviour was interpreted in terms of a 'beta feedback' between low level cloud fraction, the low clouds' longwave radiative cooling and the relative humidity of the boundary layer. Stronger coupling between these quantities was argued to result in a larger low level cloud fraction and an amplification of any change in low cloud fraction in the warmer climate. If such relationships are present in the models more generally, then it might be possible to estimate what the low level cloud response would be in the ConvOff models if they were tuned to agree with the standard versions. This could for example be achieved by scaling the convoffamip and convoffamip4K low level cloud fractions by the factor required to bring the convoffamip low cloud fraction into agreement with the amip value—i.e. dividing them both by the low cloud fraction from convoffamip and multiplying by that from the standard amip experiment. This would effectively scale the ConvOff cloud response by the same factor. Equivalently, we can estimate approximately what the global mean cloud feedback would be following a retuning by taking the global mean net cloud feedback in the ConvOff experiments and scaling that by the ratio of the global mean net CRE from the amip experiment to that from convoffamip. Figure 1*b* shows the relationship between the cloud feedbacks in the standard experiments as in figure 1*a* versus rescaled ConvOff feedbacks calculated in the manner described above, to give an estimate of the spread in the ConvOff feedback making an allowance for the effect of changes in the present-day net CRE. This results in a range of 0.91 (−0.30 to 0.61) $\mathrm{W\,m^{-2}\,K^{-1}}$ for the scaled ConvOff feedbacks, a reduction of 31% compared with their original range of 1.32 (−0.52 to 0.80) $\mathrm{W\,m^{-2}\,K^{-1}}$. Similarly, the standard deviation is reduced by 38%. This constitutes a modest reduction of 15% compared with the range of the standard models (1.07), but not a substantial one. Similarly, the standard deviation reduces by 22%. This suggests that even if the ConvOff experiments were re-tuned to bring their control simulations into closer agreement with the standard model versions, the overall range in their cloud feedbacks would not be greatly reduced, supporting our initial conclusions above.

We should of course bear in mind the fact that this estimate of the impact of retuning is very simplistic and could be inaccurate. However, there are reasons to be optimistic. First, most of the ConvOff feedback estimates are closer to the standard ones after they are rescaled. The points in figure 1*b* are mostly closer to the diagonal line than those in figure 1*a*, and the correlation coefficient between standard and ConvOff cloud feedbacks increases from 0.55 to 0.65 with the rescaling, becoming significantly different from zero at the 5% confidence level. This is what we would expect to see if (i) the scaling method was correctly adjusting for the effects of increased low level cloudiness on the cloud feedbacks in the ConvOff experiments and (ii) such impacts were contributing substantially to the differences between the cloud feedbacks in the standard and ConvOff experiments. Additionally, we find that if all of the feedbacks (standard and ConvOff) are rescaled to values consistent with the observed net CRE value of $-17.1\,\mathrm{W\,m^{-2}}$ from the CERES EBAF (Clouds and Earth's Radiant Energy Systems Energy Balanced and Filled) dataset [78], then the correlation increases even further to 0.81 (figure 1*c*). This suggests that the rescaling is generally bringing the standard and ConvOff feedbacks into closer agreement, which would only be expected if the rescaling approach was working effectively. Here again the rescaled ConvOff experiments have only a slightly smaller spread than the standard experiments (a reduction again of 15% in the range and 22% in the standard deviation). It is also interesting to note that rescaling the standard experiments to have the same global mean net CRE reduces the range in their global cloud feedbacks slightly by 8% and the standard deviation by 13%, which suggests that a small part of the spread in the standard experiments might be attributable to differences in present-day cloud biases.

Although the impact of parametrized convection on the overall range is relatively small (a reduction of 15% allowing for changes in present-day CRE), we note that larger impacts are present in some models which do not affect the overall range in this particular ensemble. The largest impact of turning off convection is seen in GFDL AM2, in which the net cloud feedback

increases from −0.05 to 0.75 W m^{-2} K^{-1}, an increase of 0.8 W m^{-2} K^{-1}. This is substantial compared with the overall range in the standard experiments of 1.07 W m^{-2} K^{-1}. However, this model has the largest increase in global mean net CRE in the control (−31.9 in amip compared with −80.1 W m^{-2} in convoffamip). Once the GFDL AM2 ConvOff feedback is rescaled by the factor 31.9/80.1, it becomes 0.3 W m^{-2} K^{-1}, just 0.35 W m^{-2} K^{-1} larger than the standard GFDL AM2 feedback. This change is now considerably smaller than the overall cloud feedback range of 1.07 W m^{-2} K^{-1}. Turning off parametrized convection can have substantial impacts on the global cloud feedback if the net CRE in the control simulation is allowed to change substantially, but in the models examined here, this effect is considerably smaller in models where the net CRE in the control does not change substantially, or where the effects of changing the present-day CRE are taken into account. It is also, in principle, possible that making different changes to the details of convective parametrizations which are not included in our current ensemble could have larger impacts on global cloud feedbacks than those seen here. Suppressing the convection schemes in a particular set of models tells us about the impact of the structure and parameter settings of the convection schemes in those models, and not the impact of all possible convection schemes or parameter settings, which might have more extreme impacts. Previous studies with individual models have in some cases indicated that changing parameter values in convection schemes can have a substantial impact on ECS. For example, Rougier *et al*. [79] show that weakening lateral entrainment in the convection scheme in HadSM3 increases the climate sensitivity substantially. However, Joshi *et al*. [80] found that that the high sensitivity in HadSM3 on reducing entrainment is attributable to a strong stratospheric water vapour feedback, and that the impact on the cloud feedback is small. It is also important to note that our current standard and ConvOff ensembles already span the range in cloud feedbacks typically seen in climate models [75]. Hence, adding new models or different convection schemes to our current ensembles would not affect our finding that the models can explore the full range of contemporary cloud feedbacks without parametrized convection.

In summary, our conclusion is that while parametrized convection influences the strength of the cloud feedbacks substantially in some models, differences in convection schemes between the models do not have a substantial impact on the overall range in global cloud feedbacks in the models examined here. The models are capable of exploring much of the overall range in feedbacks without convective parametrizations active, indicating that other aspects of model formulation are equally important in determining the overall range of cloud feedback.

(b) Cloud feedbacks over the low-latitude oceans

Many studies have highlighted the dominant role of the low-latitude oceans in contributing to inter-model spread in cloud feedback [77,81,82]. Such studies have also identified a dominant role for shallow cloud feedbacks over the tropical oceans by sorting the model responses into shallow versus deep cloud regimes using quantities such as 500 hPa vertical velocity or lower-tropospheric stability (LTS), the latter quantity being defined as the difference in potential temperature of the air at 700 hPa and at the surface [83]. Medeiros & Stevens [84] classified tropical clouds using joint distributions of these two variables, finding that vertical velocity separates regimes dominated by boundary layer clouds from those associated with higher and/or deeper clouds, whereas LTS is more effective at separating shallow cumulus and stratocumulus within shallow cloud regimes. They also noted that precipitation and 500 hPa vertical velocity are similarly effective in identifying regions of tropical convection. We have experimented with various compositing approaches for this study, and have developed a single hybrid index based on precipitation and LTS which aims to combine the benefits of these two indices. We chose precipitation, because we consider this to be a more robust indicator of the strength of tropical moist convection than, say, the vertical velocity at 500 hPa, which will be more sensitive to the profile of the resolved vertical motion.

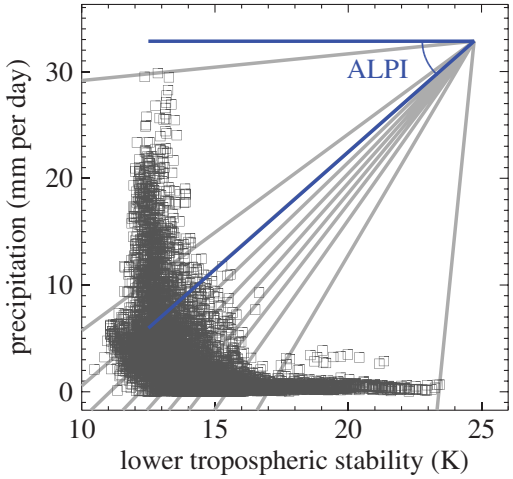

Figure 2. Scatterplot of LTS and precipitation from the HadGEM2-A amip experiment for February 1979 over the low-latitude oceans (30°N/S). The angular LTS/precipitation index (ALPI) is diagnosed as the angle of declination of a line connecting each point in LTS/precipitation space with an 'anchor point' on the top right. Locations with the strongest precipitation rates give values of ALPI of around 5°, whereas locations with the largest values of LTS result in an ALPI value of around 85°. Grey lines indicate the boundaries of ALPI percentile bins each covering 10% of the low-latitude ocean area.

Figure 2 shows a scatterplot of precipitation against LTS for a single monthly mean which serves to illustrate the difficulties of using either variable alone to characterize the joint distribution. Much of the variation in LTS occurs in a narrow range of weakly precipitating regimes and so cannot be captured by a precipitation based index, whereas much of the variation in precipitation occurs in a narrow range of weak LTS values. The angular LTS/precipitation index (ALPI) is designed to sample the joint distribution of both variables and is calculated using the following procedure. An 'anchor point' is formed near the location [$\mathrm{LTS}_{\max}$, $P_{\max}$] which appears on the top right of the scatterplot in figure 2. The normalized distances of each LTS and precipitation value from this anchor point are then calculated thus:

$$\mathrm{LTS}_{\mathrm{distance}} = \frac{\mathrm{LTS}_{\max} - \mathrm{LTS}}{\mathrm{LTS}_{\max} - \mathrm{LTS}_{\min}} + 0.1 \tag{3.1}$$

and

$$P_{\mathrm{distance}} = \frac{P_{\max} - P}{P_{\max} - P_{\min}} + 0.1. \tag{3.2}$$

ALPI is then diagnosed as the angle of declination in degrees of the line taken between the data point and the anchor point in normalized LTS/precipitation space:

$$\mathrm{ALPI} = \tan^{-1}\left(\frac{P_{\mathrm{distance}}}{\mathrm{LTS}_{\mathrm{distance}}}\right). \tag{3.3}$$

The values of 0.1 are added to move the anchor point slightly, thus avoiding division by zero for the largest values of LTS while treating LTS and precipitation symmetrically. This reduces the range of ALPI values taken from 0–90° to 5–85°.

Figure 3 shows composites of present-day CRE over the low-latitude oceans in the standard and ConvOff experiments, sorted into area-weighted percentiles of ALPI. These are calculated using monthly means for all years available in each experiment (see §2), by sorting each month by ALPI percentiles and averaging the results in each bin in time. Percentiles are used to ensure that the individual bins each cover one tenth of the total area, following the approach of Wyant *et al*. [85]. The areas contributing to each of the bins will thus be the same in the present and future climate, removing any need to take account of changing bin populations as necessary when using fixed intervals. The 0–10% percentile range of ALPI includes the tenth of the tropical ocean area with the strongest precipitation, and captures the strongest values of the longwave CRE in each

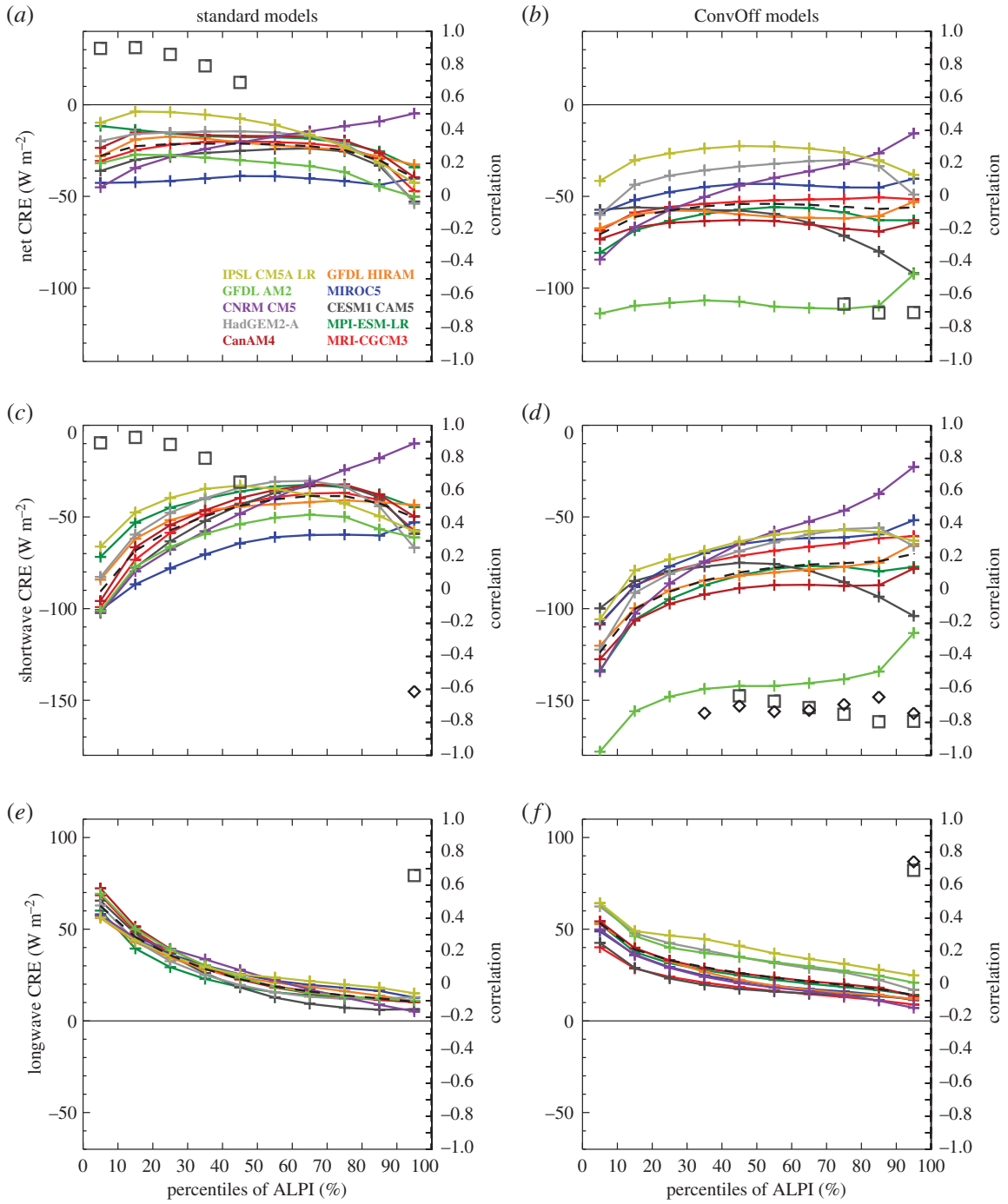

Figure 3. Composites of net, shortwave and longwave cloud radiative effect (CRE) over low-latitude oceans (30°N/S) in the amip control experiments (*a*,*c*,*e*) and convoffamip (*b*,*d*,*f*), sorted by percentiles of the angular LTS/precipitation index (ALPI). Black diamonds denote correlations with the net cloud feedback in the same ALPI bin which are significant at the 95% level. Squares indicate a significant correlation with the values in the bin and the average of the net cloud feedback over the entire low-latitude ocean domain. Ensemble mean values are shown with a black dashed line.

of the models (figure 3*e*,*f*) as well as the largest upper-level cloud fractions (figure 4*a*,*b*) and ice water paths (figure 5*c*,*d*). Meanwhile, the 80–100% ALPI range covering the strongest regimes of LTS includes the local maxima in low-level cloud fractions (figure 4*e*,*f*) and minima in the net CRE (figure 3*a*,*b*) present in many of the models and in the ensemble mean.

Figure 6 shows equivalent composites of the cloud feedbacks. These are diagnosed by sorting the net CRE in the amip and amip4K experiments into percentiles of ALPI, taking the difference in each bin and then dividing by the global mean change in near-surface temperature. This diagnosis

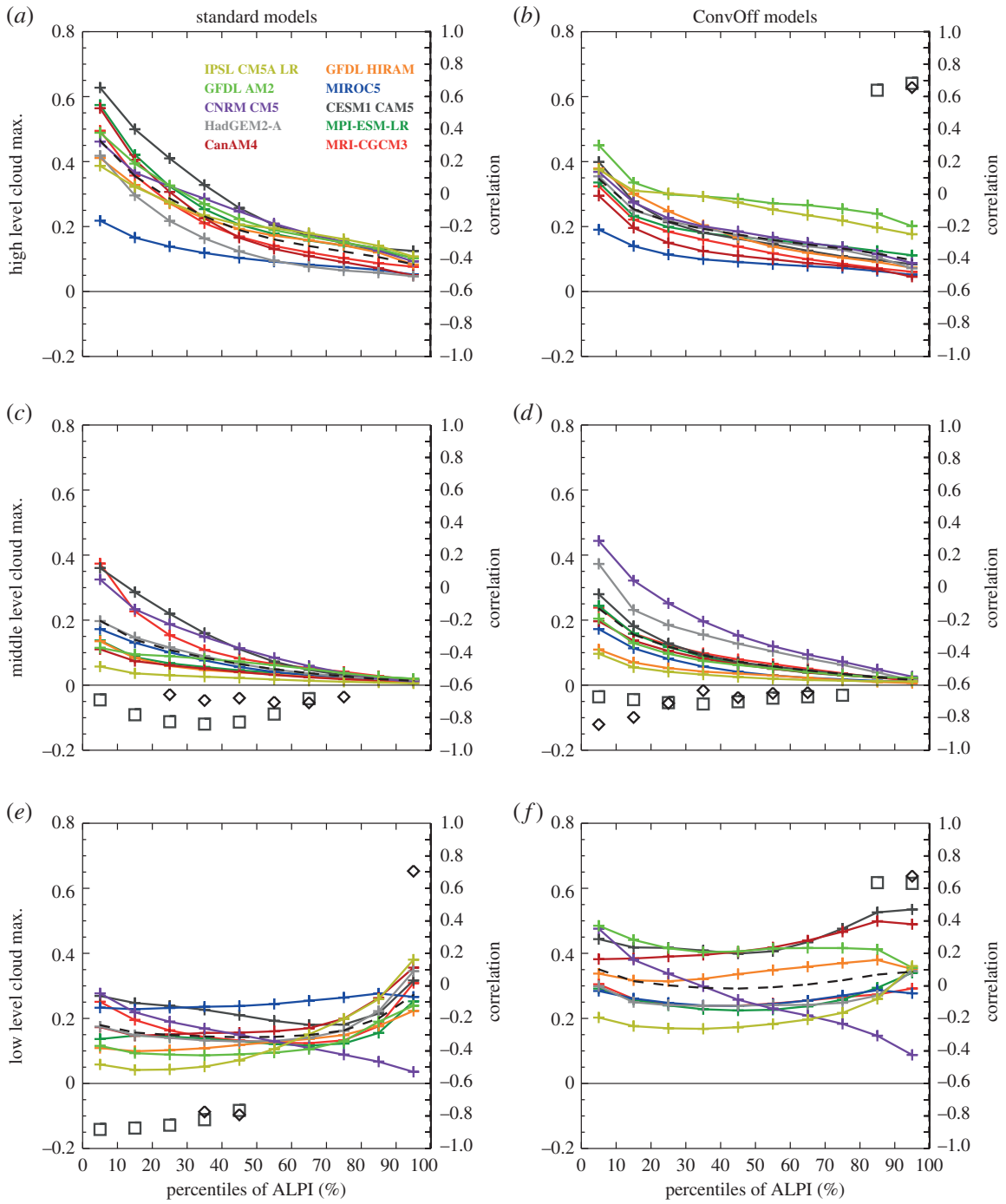

Figure 4. As figure 3 but for maximum low, mid and high cloud fractions. These are dimensionless, taking values between 0 and 1, and are diagnosed from profiles of monthly mean cloud fraction on model levels by taking the maximum values in the pressure ranges 0–440, 440–680 and 680 hPa–surface.

of the cloud feedback will include the effects of cloud masking as discussed above. Shortwave cloud masking is negligible over the tropical oceans, but the longwave component is expected to contribute up to $-1\,\mathrm{W\,m^{-2}\,K^{-1}}$ to the longwave and net CRE responses in the subsiding regions of the tropics and up to $-2\,\mathrm{W\,m^{-2}\,K^{-1}}$ in deep convective regions (see [86] and its fig. 10). In the warmer climate, both LTS and precipitation increase on average across the tropics; the position of the anchor point is tied to the maximum LTS and precipitation values, and the equally sized ALPI bins continue to sample comparable sections of the tropical cloud regime distribution; for example, the 0–10% percentile bin continues to include the 10% of the tropical ocean area with the strongest precipitation.

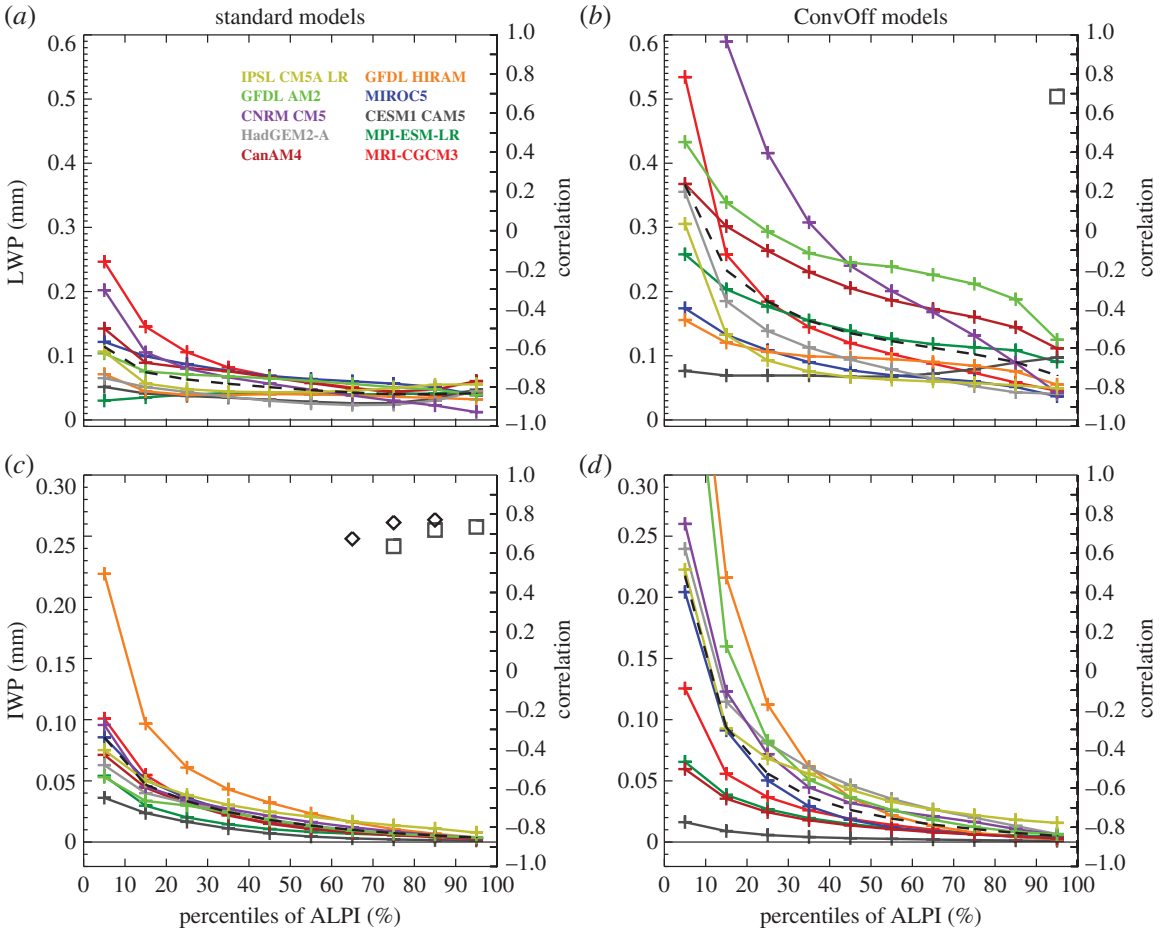

Figure 5. As figure 3 but for liquid water path (LWP) and ice water path (IWP). The compressed ranges of the LWP and IWP scales are chosen to support comparison of the smaller values, but by necessity exclude the 0–10th percentile values of LWP for the CNRM-CM5 convoffamip experiment (1.0 mm) and the 0–10th percentile values of IWP for GFDL AM2 and HIRAM convoffamip experiments (0.47 and 0.51 mm, respectively).

Figure 6*c* shows that the standard models have largely positive shortwave cloud feedbacks in the 40–100th percentile range of ALPI, where shallow clouds are expected to dominate the cloud feedbacks. Based on analysis of cloud feedbacks in single column versions of several GCMs, Zhang *et al*. [10] proposed a mechanism for positive subtropical feedback in climate models whereby increased entrainment of dry air from the free troposphere into the boundary layer by parametrized convection in the warmer climate reduces cloud. Additionally, Sherwood *et al*. [21] argued that enhanced small-scale lower-tropospheric mixing of moisture by parametrized processes such as convection in the warmer climate contributes (along with other factors) to positive low cloud feedbacks in models. The ConvOff experiments should provide an indication of the relative importance of these processes in the full models; if, for example, the dominant cause of the positive cloud feedback in the models was due to the action of the parametrized convection schemes, then we would expect to see substantial reductions in this feedback's magnitude in the ConvOff experiments. Comparison of the standard and ConvOff feedbacks in figure 6 indicates that this is not generally the case. The ensemble mean net and shortwave cloud feedbacks are if anything slightly more positive in the 40–100th percentile ranges. The magnitude of the positive subtropical cloud feedback is reduced slightly in some cases (e.g. in IPSL-CM5A-LR, HadGEM2-A and CNRM-CM5) but still remains positive in the 80–100th percentile range where stratocumulus clouds are expected to dominate the cloud feedback. These results indicate that processes other than parametrized convection are largely responsible for positive subtropical cloud feedback in the climate models examined here. For example, Zhang *et al*. [10] also suggest that enhanced cloud top entrainment by the models' boundary layer schemes might contribute to positive

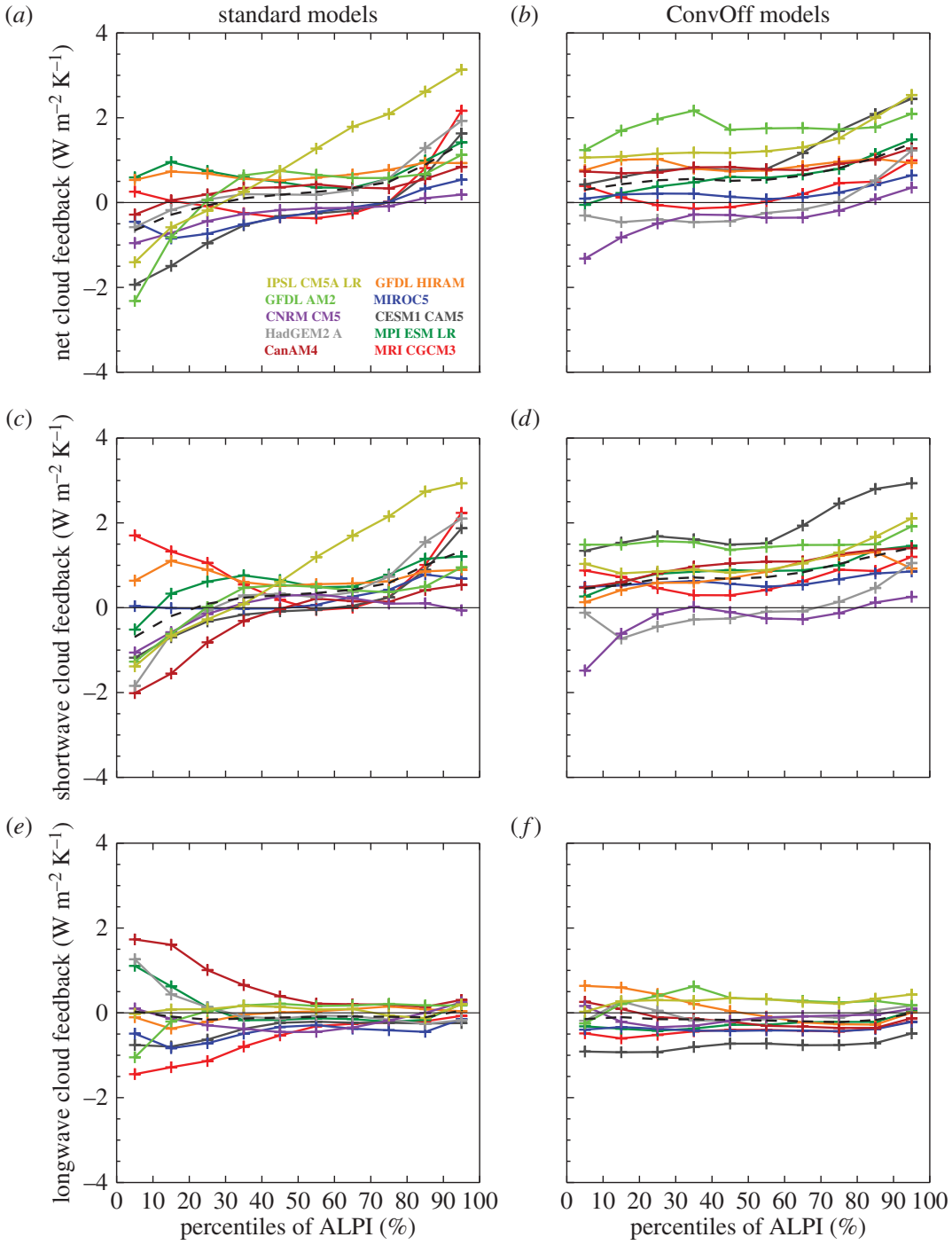

Figure 6. Composites of net, shortwave and longwave cloud feedback over low-latitude oceans (30°N/S) in the amip/amip4K experiments (*a*,*c*,*e*) and convoffamip/convoffamip4K experiments (*b*,*d*,*f*), sorted by percentiles of the angular LTS/precipitation index (ALPI). Regions of strongest precipitation associated with deep convection fall in the lower percentiles while regions of strong static stability where shallow clouds predominate fall into the higher percentiles. The black dashed line shows the ensemble mean values in each bin.

cloud feedback, whereas Sherwood *et al*. [21] argue that enhanced lower-tropospheric mixing by resolved shallow circulations will also contribute.

Sherwood *et al*. [21] also argue that inter-model differences in the strength of small-scale lower-tropospheric mixing by parametrized convection contribute to the spread in the low-level cloud feedback in models. If this was a substantial effect in our ensemble, then we might expect to see a reduction in the range in net and shortwave cloud feedback in the mid–upper ALPI range. However, our results show that the inter-model range in net and shortwave cloud feedback is not

greatly changed in the upper ALPI range (where stratocumulus clouds are expected to dominate the feedbacks), whereas it actually increases slightly in the mid ALPI range where we expect shallow cumulus clouds to dominate.

Figure 6*e,f* does however show evidence for convective parametrizations making a substantial contribution to inter-model spread in one aspect of cloud feedback; namely that of the longwave cloud feedback in strongly precipitating regions of the tropics in the 0–30th percentile range. The range of this feedback is substantially reduced in the ConvOff experiments, indicating a considerable local contribution from inter-model differences in the details of convective parametrizations. We also considered the possibility that the reduction in spread was caused by changes in water vapour and/or lapse rate feedbacks via their cloud masking contributions to the change in longwave CRE; we ruled this out, however, as the reduction in spread is also clearly seen in the outgoing longwave radiation response but not the clear-sky equivalents (not shown). In contrast to the strongly precipitating regimes, the inter-model range in longwave cloud feedback increases slightly in the 50–100th percentile ALPI range in the ConvOff experiments, which could be a consequence of increased diversity in properties of the models' cirrus clouds in the absence of retuning.

(c) Impact of convective parametrization on present-day cloud variables and relationships with cloud feedbacks

Here, we discuss the impact of convective parametrizations on various cloud variables in the present-day simulations, and their relevance to the cloud feedbacks. Many studies have identified statistically significant relationships between climate model predictions of climate sensitivity or cloud feedback and aspects of their present-day simulations which are, in principle, observable [21–25]. The use of such relationships to place observational constraints on climate predictions from models has recently come to be known as the 'emergent constraint' approach [87]. Caldwell *et al*. [88] identify a number of potential pitfalls with this approach, and argue that such 'data mining' approaches are best used to identify potential relationships which are then validated or discarded using physically based hypothesis testing. Sherwood *et al*. [21] is one of the relatively few studies of this type which develops and interprets such constraints in conjunction with testable physical arguments. In this section, we identify a number of statistically significant relationships between present-day cloud properties within ALPI regimes and the net cloud feedbacks within those regimes and also averaged over the entire low-latitude ocean area. Our results are used to motivate the following discussion of potential physical processes or mechanisms other than those associated with convective parametrization which might be contributing to inter-model spread in cloud feedback, and how such ideas could be tested via further sensitivity experiments in the future. Note that in this study we mainly focus on relationships between cloud properties and cloud feedbacks within regimes, and do not attempt to find relationships with overall climate sensitivity, the spread of which depends on other factors as well as cloud feedback [77,82]. The discussion below focuses on relationships which appear in both ensembles; we consider correlations which are present in one ensemble or the other but not both unlikely to be robust or relevant to the processes explaining the overall spread in cloud feedback.

We return to figure 3 which shows composites of the present-day CRE from the models. The near cancellation between tropical longwave and shortwave CRE observed in regions of deep convective activity where clouds are optically thick [41] is not reproduced by a number of the standard models (for example in the 0–30th percentile ALPI range), and this is exacerbated in the ConvOff experiments. These generally have more negative shortwave and net CRE values across the tropics, in line with our expectation of increased low-level cloudiness. Figure 4 confirms that low-level cloud fraction is larger as expected, although figure 5 additionally indicates considerably larger grid-box mean liquid water paths (LWPs) in the ConvOff models compared with the standard configurations, which may additionally contribute to the larger magnitude of

the net and shortwave CRE. This is particularly notable in GFDL AM2, which has relatively large values of both low cloud fraction and LWP in its ConvOff experiment.

The ConvOff models also have a tendency for increased values of longwave CRE in the 40–100th percentile range (figure 3*e*,*f*) which we attribute to a combination of increased high-level cloud fraction (figure 4*a*,*b*) and ice water path (IWP; figure 5*c*,*d*). One possible explanation for this might be that, in the absence of convective parametrization, cloud condensate is rained out less efficiently in deep convective regions, and this increases cirrus outflow into the surrounding regions in the ConvOff experiments. The ConvOff experiments show larger cloud liquid and ice water paths in strongly precipitating regions, consistent with this idea (figure 5).

The ConvOff models also show a larger spread compared with the standard models in longwave CRE (figure 3*e*,*f*), high-level cloud fraction (figure 4*a*,*b*) and IWP (figure 5*c*,*d*), which may contribute to the slightly larger spread in longwave cloud feedback in the 40–100th percentile range discussed in the previous section.

Figure 3 also shows correlations between the CRE values for the models in each ALPI bin and the net cloud feedback in that bin (diamonds) and also the net cloud feedback averaged over the entire low-latitude ocean area covered by the 10 ALPI bins (squares). These are plotted only if they are statistically significant at the 95% level, as determined by the resampling bootstrap method [89], sampling with replacement 10 000 times. In the ConvOff experiments, the shortwave CRE in the 40–100th percentile range is significantly anti-correlated with the net cloud feedback, both within the equivalent ALPI bins and across the low-latitude oceans. Because the GFDL AM2 ConvOff experiment is an outlier, we checked to see whether these correlations were mainly reflecting the unusual behaviour of this one model by repeating the calculation without it. With GFDL AM2 removed, the ConvOff experiments show similar correlations, but confined to the 80–100th percentile range only for the shortwave CRE only (not shown), much like that seen in the standard experiments in figure 3*c*. Hence, both ensembles hint at a tendency for the models with the largest magnitudes of the shortwave CRE in the most stable cloud regimes to have more positive cloud feedbacks in those regimes. This provides support for the argument of Brient & Bony [13] discussed above, in which models with more low level cloud tend to have more positive feedbacks. Additional support for this argument is provided by the fact that the low cloud fractions in the 90–100th percentile range are positively correlated with the net cloud feedbacks in the same range (figure 4*e*,*f*).

Figure 3*e*,*f* also shows that both the standard and ConvOff ensembles have positive correlations between the values of the longwave CRE in the 90–100th percentile range and the cloud feedback averaged over the low-latitude oceans, indicating that models with stronger longwave CRE tend to have more positive cloud feedbacks. Figure 4*b* and 5*c* show similar correlations between the low-latitude ocean cloud feedback and high cloud fraction in the ConvOff ensemble and IWP in the standard models, respectively.

Additionally, both ensembles have mid-level cloud fractions which are anti-correlated with the low-latitude ocean cloud feedback and also with the local net cloud feedback over much of the 0–70th percentile range (figure 4*c*,*d*). The robustness of the anti-correlation between mid-level cloud and cloud feedback across the two ensembles, combined with the large area over which such correlations are present, suggests that the processes controlling mid-level cloudiness in the tropics should be considered in any arguments put forward to explain the mechanisms of inter-model spread in cloud feedbacks over the tropical oceans.

We also examined ALPI composites of a number of other quantities including measures of vertical gradients in temperature, humidity and subsidence rate as in Sherwood *et al*. [21] (not shown). These indices did not show robust correlations with feedbacks across both of our ensembles and so we do not discuss them further here. We also examined the moist static energy (MSE), a thermodynamic quantity which measures the total energy in a parcel of air, including sensible heat owing to temperature, latent heat owing to water vapour and potential energy owing to height, which is defined as

$$\mathrm{MSE} = C_\mathrm{p} T + L_\mathrm{v} q + gz,$$

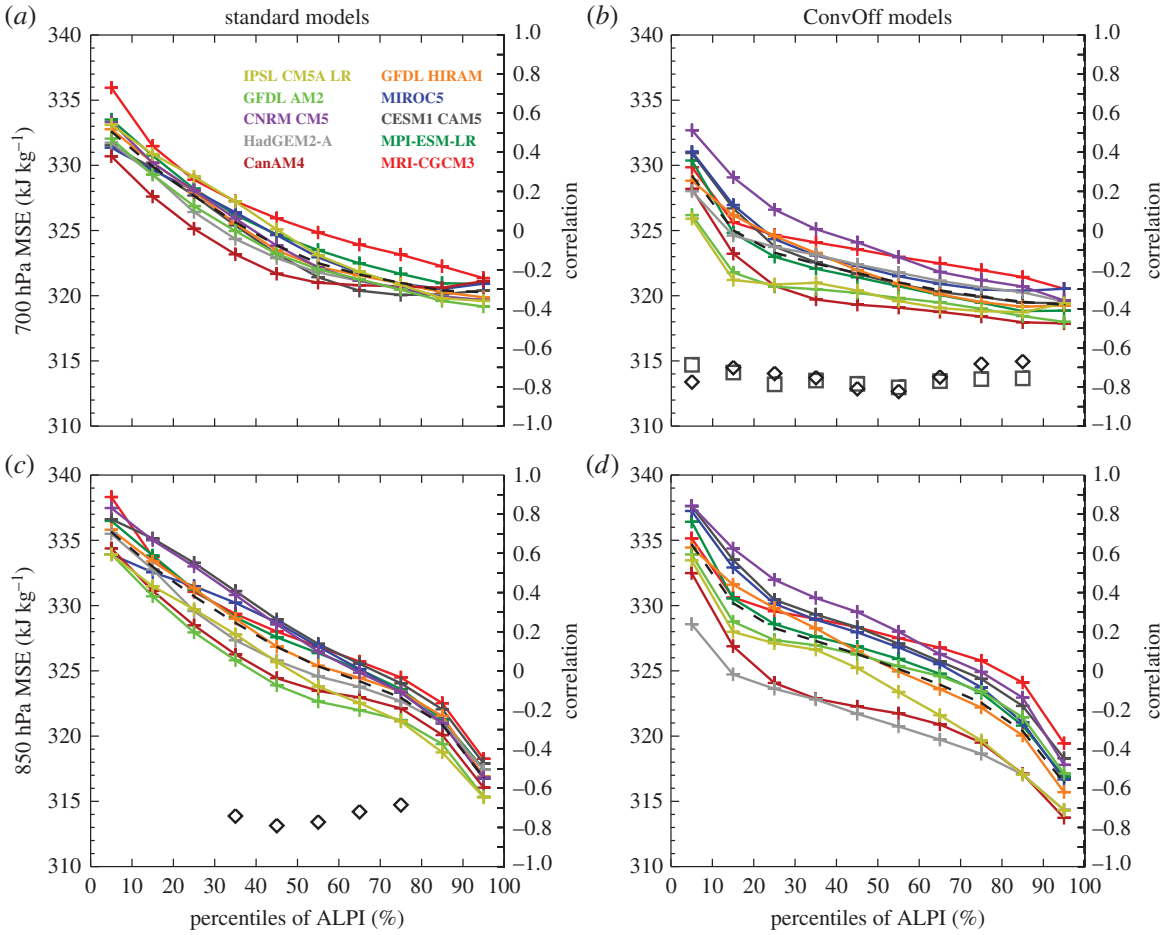

Figure 7. As figure 3 but for moist static energy (MSE) at 700 and 850 hPa.

where C_p is the specific heat of air at constant pressure, T is temperature, L_v is the latent heat of vaporization, q is the specific humidity, g is the acceleration owing to gravity and z is the height above the surface. Source terms for MSE in the atmosphere include surface sensible and latent heat fluxes and absorption of solar radiation, whereas longwave radiative cooling is the major sink term. MSE is redistributed within the atmosphere in the vertical by convective and turbulent mixing processes, and both vertically and horizontally by the large-scale atmospheric circulation. Because MSE is conserved during phase changes between water vapour and liquid water associated with cloud condensation and evaporation of clouds and precipitation it is a convenient indicator of heat transport within the atmosphere in the presence of clouds and precipitating moist convection [31,90]. MSE budgets have more recently been used in studies examining the influence of changes in large-scale advection, convective and turbulent mixing on cloud feedbacks [7,14]. Figure 7 shows that significant anti-correlations are present between the models' cloud feedbacks and their present-day values of the MSE in the lower troposphere, which is consistent with the argument that the overall spread in cloud feedback is regulated by processes associated with lower-tropospheric mixing, as proposed by Sherwood *et al*. [21]. In the standard models, the correlations are seen with the MSE at 850 hPa, a level chosen by Sherwood *et al*. [21] to represent thermodynamic properties near the top of the boundary layer. Similar correlations are present in the ConvOff models at the slightly higher level of 700 hPa, usually considered to be more representative of the lower free troposphere. It is however possible that in the absence of parametrized convection, turbulent mixing plays more of a role in transporting water vapour into the lower free troposphere and in doing so deepens the boundary layer to have a top closer to 700 hPa. The possibility of deeper boundary layers in the ConvOff experiments is supported by a tendency for slightly larger mid-level (440–680 hPa) cloud fractions in the ConvOff

experiments (figure 4). The presence of relationships between low level MSE and cloud feedback in both standard and ConvOff models again suggests that inter-model differences in parametrized convection are not the dominant cause of overall spread in the cloud feedbacks in these models, and that other processes are largely responsible. We discuss such possibilities further below.

4. Discussion

Our results indicate that inter-model differences in the details of convective parametrizations cannot explain the overall range in cloud feedbacks in the models examined here; the models exhibit comparable spread in cloud feedback when their convective parametrizations are switched off. Here, we discuss other processes which could be contributing to inter-model spread in cloud feedback, and suggest some ways in which such ideas could be tested using further process simplification experiments in future work.

Sherwood *et al.* [21] and Zhao [40] both argue that precipitation efficiency plays an important role in cloud feedback. Sherwood *et al*. [21] define precipitation efficiency in terms of the amount of precipitation for a given vertical transport of water vapour from the boundary layer to the free troposphere. These transports are associated with 'lower-tropospheric mixing' by small-scale processes such as convection or turbulence which are parametrized in GCMs, and by large-scale mixing associated with resolved motions. Sherwood *et al*. [21] argue that models with stronger lower-tropospheric mixing will have a stronger drying of the boundary layer, and that this effect will strengthen in the warming climate and will reduce low-level cloud, resulting in a positive low cloud feedback. Our finding that models with more positive cloud feedbacks tend to have less MSE near the top of the boundary layer in the present climate is consistent with this argument; stronger lower-tropospheric mixing in the present climate in higher sensitivity models could deplete boundary layer MSE more by transporting it from the boundary layer to the free troposphere at a faster rate. Our findings suggest however that processes other than parametrized convection are required to explain the overall range of cloud feedbacks in the models examined here.

Zhao [40] makes a distinction between convective precipitation efficiency associated with parametrized convection and a large-scale precipitation efficiency associated with the stratiform cloud and precipitation schemes in the models. In the absence of convective parametrization, lower-tropospheric mixing must be achieved by resolved motions or by small-scale mixing by the models' parametrized turbulence schemes. If the strength of such mixing is not regulated by inter-model differences in precipitation efficiency arising from the differences in the models' convection schemes, it might instead be regulated in a similar way, but by inter-model differences in the precipitation efficiency associated with other parts of the model formulation. The precipitation efficiency, defined as the amount of surface precipitation for a given vertical transport of water vapour from the boundary layer to the free troposphere, could depend on various aspects of model formulation, including cloud parametrizations, cloud precipitation microphysics and their interactions with turbulent mixing and entrainment. Models which form precipitating clouds easily at mid-levels in the tropics will rain out to the surface efficiently for a given upward transport of water vapour. Conversely, models that form clouds and condensate less easily at mid-levels in the tropics might instead need to produce condensation and latent heat release at higher levels in order to balance atmospheric radiative cooling in the tropical free troposphere. Precipitation falling from clouds which are higher in the atmosphere will be more likely to evaporate before reaching the surface, producing more evaporative cooling to offset the latent heat release provided by cloud condensation. Such models might thus require a larger upward transport of water vapour by lower-tropospheric mixing to maintain a given net latent heat release and surface precipitation rate, compared with models which are able to condense more easily at mid-levels and so rain out more efficiently to the surface. Hence, models with less mid-level cloud might have weaker precipitation efficiencies and need to transport more water vapour vertically by lower-tropospheric mixing, drying the boundary layer more than models with more mid-level cloud. Such an effect would be expected to strengthen proportionally with the

hydrological cycle as the climate warms and the total amount of atmospheric radiative cooling, net latent heat release and surface precipitation increase, resulting in models with less mid-level cloud having stronger positive low-level cloud feedbacks. Such arguments could potentially explain the anti-correlation between mid-level cloud fractions and cloud feedbacks seen in both ensembles examined here.

We note that these arguments rely on cloud fraction at a given level being a useful proxy for condensation rate and precipitation efficiency; although these quantities are not necessarily exactly equivalent, a relationship between them is clearly plausible in that a model with a larger cloud fraction for a given in-cloud condensation rate will have a larger grid-box mean condensation rate, and hence a stronger condensate source term to support precipitation. We also note that inter-model differences in mid-level cloud fraction and precipitation efficiency may ultimately be due to a range of model formulation differences, including model representations of turbulent mixing and entrainment, which can have effects in the free troposphere as well as the boundary layer, as demonstrated by Tsushima *et al*. [91]. The depth of the shallow circulation discussed by Sherwood *et al*. [21] could also influence the amount of mid-level cloud and the bulk precipitation efficiency; for example, a model with a shallow circulation with a maximum divergence below 700 hPa might form less mid-level cloud than a model with a shallow circulation and a peak divergence at 500 hPa.

If the overall strength of lower-tropospheric mixing is, in fact, regulated by bulk precipitation efficiency arguments such as those outlined above, then this raises the intriguing possibility that the lower-tropospheric mixing and the cloud feedback in a given model might be quite similar in magnitude in the standard and ConvOff configurations, even if much of the mixing is done by the convective parametrization in the standard configuration. A large-scale constraint on lower-tropospheric mixing could mean that resolved and parametrized turbulent mixing adjust to compensate for an absence of parametrized convective mixing in the ConvOff experiments. This question could be investigated in future work by directly quantifying the lower-tropospheric mixing associated with parametrized convection, turbulent and resolved mixing, for example by using temperature and humidity budget terms as in Zhang *et al*. [10] and Webb & Lock [7].

Our results also indicate that models with more low level clouds in the most stable areas of the tropics tend to have more positive low feedbacks in those regions. This finding is consistent with the expectations from the 'beta feedback' hypotheses of Brient & Bony [13]. Our results also hint that models with larger values of longwave CRE in the most stable regimes tend to have more positive cloud feedbacks across the tropics. Studies with LES have demonstrated that an enhanced free-tropospheric greenhouse effect can reduce turbulent mixing and cloudiness in the subtropical boundary layer [15]. There is also observational support for cirrus clouds breaking up low level cloud in the current climate [92]. In the subsidence regions, the subsidence rate is related to the lapse rate and the amount of radiative cooling [93]. In the absence of substantial differences in lapse rate, models with more upper level cloud or larger IWPs in the subsidence regions will have weaker radiative cooling in the upper troposphere, reducing the subsidence rate at upper levels and making the circulation more bottom heavy (i.e. having stronger subsidence at lower levels compared with upper levels). In a similar vein, models with more low level clouds will have more radiative cooling at low levels, which will enhance subsidence at low levels, also making the circulation more bottom heavy. Given that we find higher sensitivity models to have more low clouds and more cirrus in the more stable regimes in the tropics, this could explain why Sherwood *et al*. [21] found higher sensitivity models to have more shallow circulations. Although our analysis did not find any correlations between measures of the shallow circulation and cloud feedback which were robust across both of our ensembles, it remains possible that lower-tropospheric mixing associated with such resolved circulations contributes to inter-model spread in cloud feedback in our models, if not to a detectable degree.

We consider the potential mechanisms outlined above to be plausible but they are not the only possibilities. These and other hypothesized mechanisms could be tested in a number of ways in future process simplification experiments. For example, the precipitation efficiency in models could be reduced by modifying the cloud microphysics to alter the ease of raining from mid-level

clouds over warm SSTs. Alternatively, cloud condensation at mid-levels could be suppressed by re-evaporating cloud water. If the ideas outlined above are correct, then this would be expected to force more condensation to occur at higher levels, increase vertical transports of water vapour and boundary layer drying, reduce MSE near the top of the boundary layer and strengthen positive low level cloud feedbacks. The idea that having more low-level cloud in stable regions of the tropics results in a more positive feedback could be further tested by tuning low-level cloud fractions, extending the approach of Brient & Bony [13] to a wider range of models. More specifically, the 'beta feedback' hypothesis of Brient & Bony [13] could be tested in more models by suppressing the longwave CREs of low level clouds, building on the approach of Fermepin & Bony [94]. Similarly, the longwave radiative impact of cirrus clouds on low-level cloud feedbacks could be tested by making ice clouds transparent to longwave radiation. Such experiments might be more straightforward or inexpensive to perform in more idealized model configurations; for example, the CFMIP aquaplanet configuration which is zonally symmetric has no seasonal cycle and has been shown to reproduce the inter-model spread in cloud feedbacks on more realistic configurations very effectively [5,75].

5. Summary and conclusions

In this study, we have demonstrated a new approach for investigating the processes contributing to inter-model spread in cloud feedback. We have investigated the sensitivity of cloud feedbacks to the use of convective parametrization by repeating the CMIP5/CFMIP-2 AMIP/AMIP +4K uniform sea surface temperature perturbation experiments with 10 climate models which have their convective parametrizations turned off. This is the first study to report results from a substantial ensemble of models without parametrized convection.

Integrations without parametrized convection were successfully performed without increasing model resolution, although other minor changes such as shorter timesteps were required in some cases to maintain model stability. Some aspects of present-day model performance were degraded in these 'ConvOff' experiments compared with the standard versions. The ConvOff versions generally have more negative values of the shortwave and net CRE across the tropics, associated with increased low-level fractions and LWPs. The ConvOff models also have a tendency for increased values of longwave CRE in low cloud regimes, owing to increases in high-level cloud fractions and/or IWP. Increased shortwave reflection from low-level clouds in particular results in increased biases in the top-of-atmosphere radiative balances of the ConvOff models.

The overall range in global cloud feedback in the standard model configurations is maintained in the ConvOff experiments, increasing by 22%. The models all show increases in low level cloud fraction when parametrized convection is switched off, substantially increasing the shortwave radiation reflected to space. Applying a simple bias correction method to allow for differences in present-day global mean net CRE substantially reduces the differences between the global mean cloud feedbacks with and without parametrized convection in the individual models. The cloud feedbacks in the two ensembles become strongly correlated, with the Convoff experiments exploring 85% of the overall range from the standard models. This correlation, and the fact that the models are capable of exploring much of the overall range in cloud feedbacks without convective parametrizations active, strongly suggests that although parametrized convection influences the strength of the cloud feedbacks substantially in some models, aspects of model formulation other than convective parametrization ultimately determine the overall range in the cloud feedbacks in the models examined here.

It is in principle possible that changes to the details of convective parametrizations which are not included in our current ensemble could have larger impacts on global cloud feedbacks than those seen here. However, our current standard and ConvOff ensembles already span the range in cloud feedbacks typically seen in climate models. Hence, adding new models or different convection schemes to our current ensembles would not affect our finding that the models can explore much of the range of contemporary cloud feedbacks without parametrized convection.

We have introduced a new approach for diagnosing cloud regimes over the low-latitude oceans. The ALPI is a hybrid index which combines the benefits of LTS for isolating stable low cloud regimes and surface precipitation rate for identifying strongly precipitating regimes of deep convection, making a continuous transition between them in LTS/precipitation space. ALPI composites of cloud feedbacks over the tropical oceans show that the largely positive shortwave cloud feedbacks in shallow cloud regimes in the models are still present in the ConvOff experiments, indicating that processes other than parametrized convection must be responsible. Our results also indicate that in the absence of convective parametrization the inter-model spread in net and shortwave cloud feedback is not greatly changed in stable regimes where stratocumulus clouds are expected to dominate the feedbacks. Meanwhile, it increases slightly in the regimes where we expect shallow trade cumulus clouds to dominate.

Convective parametrizations do however make a substantial contribution to inter-model spread in the longwave cloud feedbacks in strongly precipitating regions of the tropics; the spread of this feedback is substantially reduced in the ConvOff experiments. This local effect is however clearly not large enough to have a substantial effect on the overall range of the global net cloud feedback.

We have also assessed the impact of convective parametrizations on the present-day simulation of various cloud variables and looked for relationships between them and the cloud feedbacks. We have identified a number of statistically significant relationships between present-day cloud properties within ALPI regimes and the net cloud feedbacks within those regimes and also those averaged over the entire low-latitude ocean area, which are robust across models with and without parametrized convection. Models with more low cloud and stronger values of the shortwave CRE in the most stable regimes in the tropics tend to have more positive cloud feedbacks within that regime, consistent with the findings of Brient & Bony [13], who found that subtropical feedbacks in parameter-perturbed versions of the single column version of IPSL-CM5A-LR were stronger in cases where more low level cloud and stronger values of shortwave CRE were present in the control case. Additionally, models with larger values of the longwave CRE (and more high level cloud or larger IWPs) in the most stable areas of the tropics tend to have stronger cloud feedbacks averaged across the low-latitude oceans. We also found that models with the least mid-level cloud in the deep convection and trade cumulus regimes tend to have the most positive feedbacks both within the trade cumulus regimes and averaged over the low-latitude oceans. Additionally, models with less MSE near the top of the boundary layer in the trade cumulus regimes tend to have more positive cloud feedbacks there.

We have discussed a number of possible physical mechanisms which could explain our results, and how these and other ideas could be tested in the future by performing further process simplification experiments. If a robust interpretation of such results can be confirmed by such sensitivity experiments in the future, then the relationships that we have identified between feedbacks and present-day cloud variables could form the basis for a new set of emergent constraints on tropical cloud feedback. Although mid-level clouds in strongly precipitating regions are somewhat difficult to observe, the inclusion of cloud simulators in a wider range of models based on active instruments such as CloudSat and CALIPSO (e.g. [6]) would support a quantitative evaluation of this aspect of model performance.

More generally speaking, the roles of processes other than parametrized convection in contributing to inter-model spread in cloud feedback could be explored further by modifying other aspects of model physics, either by switching them off as we have done here, or by replacing particular schemes with the same simplified version in different models. The present-day simulation of shallow clouds is known to be highly sensitive to the details of turbulent mixing and entrainment parametrizations in models. A recent LES study by Bretherton & Blossey [17] demonstrated a positive cloud feedback associated with an entrainment liquid-flux mechanism, where an increased cloud layer humidity flux in a warmer climate induces an entrainment liquid-flux adjustment that dries the stratocumulus cloud layer. Turbulent entrainment parametrizations could be switched off to assess their contributions to inter-model spread in cloud feedback. Alternatively, the turbulent mixing schemes in the models could be replaced with a simple

and consistent alternative, for example one based on a Richardson number-dependent vertical diffusivity term which would confine mixing within the boundary layer (as opposed to a constant diffusivity which would have undesirable effects near the tropopause). Additionally, the role of the large-scale circulation in contributing to inter-model spread in cloud feedback could be explored. For example, the importance of the large-scale component of the lower-tropospheric mixing mechanism proposed by Sherwood *et al*. [21] (which is argued to vary according to the depth of the subtropical circulation) could be explored by applying artificial diabatic heating terms to the models designed to change the depth of the circulation. As pointed out above, this might be more straightforward to do in aquaplanet configurations. We plan to develop the SPOOKIE approach further in the future by designing sensitivity tests for GCMs which target such questions directly.

We hope that the data used in this study will be useful to investigate the impact of convective parametrizations on many other aspects of climate model simulations. For example, we plan to write a follow-up paper that assesses the impact of parametrized convection on various aspects of present-day climate. We also plan to make the data from the ConvOff simulations available to the wider scientific community in the near future. For more details, please contact the corresponding author or refer to the CFMIP website (http://www.cfmip.net).

Data accessibility. The CMIP5 climate model output data used in this study are available via the Earth System Grid Federation portal—see http://cmip-pcmdi.llnl.gov/cmip5/data_getting_started.html. Data from other experiments performed specifically for this study are owned by the relevant modelling groups but are available on request by contacting the corresponding author.

Authors' contributions. The study was conceived and designed by M.J.W., A.P.L., C.S.B., T.M., S.C.S. and M.W. Data were provided by M.J.W., A.P.L., J.N.S.C, A.I., T.K., R.R., Y.S., T.M., J.V., M.W., M.D.W. and M.Z. M.J.W. coordinated the study and performed the data analysis. The manuscript was written by M.J.W. with contributions from A.P.L., C.S.B., S.B., J.N.S.C., S.M.K., H.K., T.O., R.R., T.M., S.C.S., J.V., M.W., M.D.W. and M.Z. All authors gave final approval for publication.

Competing interests. The authors declare no competing interests.

Funding. M.J.W. was supported by the Joint DECC/Defra Met Office Hadley Centre Climate Programme (GA01101) and by the European Union Seventh Framework Programme (FP7/2007-2013) under grant agreement number 244067 via the EU Cloud Intercomparison and Process Study Evaluation project (EUCLIPSE). M.W. and T.O. were supported by the Programme for Risk Information on Climate Change (SOUSEI programme) from the Ministry of Education, Culture, Sports, Science and Technology (MEXT), Japan. T.M. was supported by the Max Planck Gesellschaft (MPG). S.M.K. was supported by Basic Science Research Programme through the National Research Foundation of Korea (NRF) supported by the Ministry of Science, ICT and Future Planning (2013R1A1A3004589). Y.S. was supported by a UNIST president fellowship. S.C.S. was supported by ARC DP140101104.

Acknowledgements. Thanks are due to Tim Andrews, Alejandro Bodas-Salcedo, Robin Chadwick, Olivier Geoffroy, Gill Martin, Mark Ringer, Knut von Salzen, Yoko Tsushima and Minghua Zhang for useful comments and discussions. We acknowledge the World Climate Research Programme's Working Group on Coupled Modelling, which is responsible for CMIP, and we thank the climate modelling groups for producing and making available their model output. For CMIP, the US Department of Energy's Programme for Climate Model Diagnosis and Intercomparison provides coordinating support and led development of software infrastructure in partnership with the Global Organization for Earth System Science Portals.

References

1. Field CB *et al.* 2014 IPCC summary for policymakers. In *Climate change 2014: impacts, adaptation, and vulnerability. Part A: global and sectoral aspects. Contribution of Working Group II to the Fifth Assessment Report of the Intergovernmental Panel on Climate Change*, pp. 1–32. Cambridge, UK: Cambridge University Press.
2. Collins M *et al.* 2013 Long-term climate change: projections, commitments and irreversibility. In *Climate change 2013: the physical science basis. Contribution of Working Group I to the Fifth Assessment Report of the Intergovernmental Panel on Climate Change*. Cambridge, UK: Cambridge University Press.

3. Boucher O *et al.* 2013 Clouds and aerosols. In *Climate change 2013: the physical science basis. Contribution of Working Group I to the Fifth Assessment Report of the Intergovernmental Panel on Climate Change*. Cambridge, UK: Cambridge University Press.
4. Bony S, Webb M, Bretherton CS, Klein SA, Siebesma P, Tselioudis G, Zhang M. 2011 CFMIP: towards a better evaluation and understanding of clouds and cloud feedbacks in CMIP5 models. *Clivar Exchanges* **56**, 20–22.
5. Medeiros B, Stevens B, Bony S. 2014 Using aquaplanets to understand the robust responses of comprehensive climate models to forcing. *Clim. Dyn.* **44**, 1957–1977. (doi:10.1007/s00382-014-2138-0)
6. Bodas-Salcedo A *et al.* 2011 COSP: satellite simulation software for model assessment. *Bull. Am. Meteorol. Soc.* **92**, 1023–1043. (doi:10.1175/2011BAMS2856.1)
7. Webb MJ, Lock AP. 2013 Coupling between subtropical cloud feedback and the local hydrological cycle in a climate model. *Clim. Dyn.* **41**, 1923–1939. (doi:10.1007/s00382-012-1608-5)
8. Webb MJ *et al.* 2015 The diurnal cycle of marine cloud feedback in climate models. *Clim. Dyn.* **44**, 1419–1436. (doi:10.1007/s00382-014-2234-1)
9. Blossey PN *et al.* 2013 Marine low cloud sensitivity to an idealized climate change: the CGILS LES intercomparison. *J. Adv. Model. Earth Syst.* **5**, 234–258. (doi:10.1002/jame.20025)
10. Zhang M *et al.* 2013 CGILS: results from the first phase of an international project to understand the physical mechanisms of low cloud feedbacks in single column models. *J. Adv. Model. Earth Syst.* **5**, 826–842. (doi:10.1002/2013MS000246)
11. Bretherton CS. 2015 Insights into low-latitude cloud feedbacks from high-resolution models. *Phil. Trans. R. Soc. A* **373**, 20140415. (doi:10.1098/rsta.2014.0415)
12. Rieck M, Nuijens L, Stevens B. 2012 Marine boundary layer cloud feedbacks in a constant relative humidity atmosphere. *J. Atmos. Sci.* **69**, 2538–2550. (doi:10.1175/JAS-D-11-0203.1)
13. Brient F, Bony S. 2012 How may low-cloud radiative properties simulated in the current climate influence low-cloud feedbacks under global warming? *Geophys. Res. Lett.* **39**, L20807. (doi:10.1029/2012GL053265)
14. Brient F, Bony S. 2013 Interpretation of the positive low-cloud feedback predicted by a climate model under global warming. *Clim. Dyn.* **40**, 2415–2431. (doi:10.1007/s00382-011-1279-7)
15. Bretherton CS, Blossey PN, Jones CR. 2013 Mechanisms of marine low cloud sensitivity to idealized climate perturbations: a single-LES exploration extending the CGILS cases. *J. Adv. Model. Earth Syst.* **5**, 316–337. (doi:10.1002/jame.20019)
16. Demoto S, Watanabe M, Kamae Y. 2013 Mechanism of tropical low-cloud response to surface warming using weather and climate simulations. *Geophys. Res. Lett.* **40**, 2427–2432. (doi:10.1002/grl.50474)
17. Bretherton CS, Blossey PN. 2014 Low cloud reduction in a greenhouse-warmed climate: results from Lagrangian LES of a subtropical marine cloudiness transition. *J. Adv. Model. Earth Syst.* **6**, 91–114. (doi:10.1002/2013MS000250)
18. Dal Gesso SD, Siebesma AP, de Roode SR, van Wessem JM. 2014 A mixed-layer model perspective on stratocumulus steady states in a perturbed climate. *Q. J. R. Meteorol. Soc.* **140**, 2119–2131. (doi:10.1002/qj.2282)
19. Dal Gesso S, Siebesma AP, de Roode SR 2014 Evaluation of low-cloud climate feedback through single-column model equilibrium states. *Q. J. R. Meteorol. Soc.* **141**, 819–832. (doi:10.1002/qj.2398)
20. de Roode SR, Siebesma AP, Dal Gesso S, Jonker HJJ, Schalkwijk J, Sival J. 2014 A mixed-layer model study of the stratocumulus response to changes in large-scale conditions. *J. Adv. Model. Earth Syst.* **6**, 1256–1270. (doi:10.1002/2014MS000347)
21. Sherwood SC, Bony S, Dufresne JL. 2014 Spread in model climate sensitivity traced to atmospheric convective mixing. *Nature* **505**, 37–42. (doi:10.1038/nature12829)
22. Volodin EM. 2008 Relation between temperature sensitivity to doubled carbon dioxide and the distribution of clouds in current climate models. *Izv. Atmos. Ocean Phys.* **44**, 288–299. (doi:10.1134/S0001433808030043)
23. Trenberth KE, Fasullo JT. 2010 Simulation of present-day and twenty-first-century energy budgets of the southern oceans. *J. Clim.* **23**, 440–454. (doi:10.1175/2009JCLI3152.1)
24. Fasullo JT, Trenberth KE. 2012 A less cloudy future: the role of subtropical subsidence in climate sensitivity. *Science* **338**, 792–794. (doi:10.1126/science.1227465)

25. Tsushima Y, Ringer MA, Webb MJ, Williams KD. 2013 Quantitative evaluation of the seasonal variations in climate model cloud regimes. *Clim. Dyn.* **41**, 2679–2696. (doi:10.1007/s00382-012-1609-4)
26. Clement AC, Burgman R, Norris JR. 2009 Observational and model evidence for positive low-level cloud feedback. *Science* **325**, 460–464. (doi:10.1126/science.1171255)
27. Lauer A, Hamilton K, Wang Y, Phillips VT, Bennartz R. 2010 The impact of global warming on marine boundary layer clouds over the eastern Pacific—a regional model study. *J. Clim.* **23**, 5844–5863. (doi:10.1175/2010JCLI3666.1)
28. Emanuel KA. 1994. *Atmospheric convection*. New York, NY: Oxford University Press.
29. Arakawa A. 2004 The cumulus parameterization problem: past, present, and future. *J. Clim.* **17**, 2493–2525. (doi:10.1175/1520-0442(2004)017<2493:RATCPP>2.0.CO;2)
30. McFarlane N. 2011 Parameterizations: representing key processes in climate models without resolving them. *Wiley Interdisciplinary Rev. Clim. Change* **2**, 482–497. (doi/10.1002/wcc.122/full)
31. Frierson DMW. 2007 The dynamics of idealized convection schemes and their effect on the zonally averaged tropical circulation. *J. Atmos. Sci.* **64**, 1959–1976. (doi:10.1175/JAS3935.1)
32. McCaa JR, Bretherton CS. 2004 A new parameterization for shallow cumulus convection and its application to marine subtropical cloud-topped boundary layers. II. Regional simulations of marine boundary layer clouds. *Mon. Weather Rev.* **132**, 883–896. (doi:10.1175/1520-0493(2004)132<0883:ANPFSC>2.0.CO;2)
33. von Salzen K, McFarlane NA, Lazare M. 2005 The role of shallow convection in the water and energy cycles of the atmosphere. *Clim. Dyn.* **25**, 671–688. (doi:10.1007/s00382-005-0051-2)
34. de Szoeke SP, Wang Y, Xie S-P, Miyama T. 2006 Effect of shallow cumulus convection on the eastern Pacific climate in a coupled model. *Geophys. Res. Lett.* **33**, L17713. (doi:10.1029/2006GL026715)
35. Tiedtke M, Heckley WA, Slingo J. 1988 Tropical forecasting at ECMWF: the influence of physical parametrization on the mean structure of forecasts and analyses. *Q. J. R. Meteorol. Soc.* **114**, 639–664. (doi:10.1002/qj.49711448106)
36. Manabe S, Wetherald R. 1967 Thermal equilibrium of the atmosphere with a given distribution of relative humidity. *J. Atmos. Sci.* **24**, 241–259. (doi:10.1175/1520-0469(1967)024<0241:TEOTAW>2.0.CO;2)
37. Lin JL, Lee MI, Kim D, Kang IS, Frierson DM. 2008 The impacts of convective parameterization and moisture triggering on AGCM-simulated convectively coupled equatorial waves. *J. Clim.* **21**, 883–909. (doi:10.1175/2007JCLI1790.1)
38. Zhao M, Held IM, Lin SJ. 2012 Some counterintuitive dependencies of tropical cyclone frequency on parameters in a GCM. *J. Atmos. Sci.* **69**, 2272–2283. (doi:10.1175/JAS-D-11-0238.1)
39. Gettelman A, Kay JE, Shell KM. 2012 The evolution of climate sensitivity and climate feedbacks in the community atmosphere model. *J. Clim.* **25**, 1453–1469. (doi:10.1175/JCLI-D-11-00197.1)
40. Zhao M. 2014 An investigation of the connections among convection, clouds, and climate sensitivity in a global climate model. *J. Clim.* **27**, 1845–1862. (doi:10.1175/JCLI-D-13-00145.1)
41. Kiehl JT. 1994 On the observed near cancellation between longwave and shortwave cloud forcing in tropical regions. *J. Clim.* **7**, 559–565. (doi:10.1175/1520-0442(1994)007<0559:OTONCB>2.0.CO;2)
42. Cess RD *et al*. 1989 Interpretation of cloud-climate feedback as produced by 14 atmospheric general circulation models. *Science* **245**, 513–516. (doi:10.1126/science.245.4917.513)
43. von Salzen K *et al*. 2013 The Canadian fourth generation atmospheric global climate model (CanAM4). Part I: representation of physical processes. *Atmosphere-Ocean* **51**, 104–125. (doi:10.1080/07055900.2012.755610)
44. Zhang GJ, McFarlane NA. 1995 Sensitivity of climate simulations to the parameterization of cumulus convection in the Canadian Climate Centre general circulation model. *Atmosphere-Ocean* **33**, 407–446. (doi:10.1080/07055900.1995.9649539)
45. Scinocca JF, McFarlane NA. 2004 The variability of modeled tropical precipitation. *J. Atmos. Sci.* **61**, 1993–2015. (doi:10.1175/1520-0469(2004)061<1993:TVOMTP>2.0.CO;2)
46. Neale RB *et al*. 2012 Description of the NCAR community atmosphere model (CAM5). Technical report no. NCAR/TN-486+STR. Boulder, CO: NCAR.

47. Neale RB, Richter JH, Jochum M. 2008 The impact of convection on ENSO: from a delayed oscillator to a series of events. *J. Clim.* **21**, 5904–5924. (doi:10.1175/2008JCLI2244.1)
48. Richter JH, Rasch PJ. 2008 Effects of convective momentum transport on the atmospheric circulation in the community atmosphere model, v. 3. *J. Clim.* **21**, 1487–1499. (doi:10.1175/2007JCLI1789.1)
49. Park S, Bretherton CS. 2009 The University of Washington shallow convection and moist turbulence schemes and their impact on climate simulations with the community atmosphere model. *J. Clim.* **22**, 3449–3469. (doi:10.1175/2008JCLI2557.1)
50. Voldoire A *et al*. 2013 The CNRM-CM5.1 global climate model: description and basic evaluation. *Clim. Dyn.* **40**, 2091–2121. (doi:10.1007/s00382-011-1259-y)
51. Bougeault P. 1985 A simple parameterization of the large-scale effects of cumulus convection. *Mon. Weather Rev.* **113**, 2108–2121. (doi:10.1175/1520-0493(1985)113<2108:ASPOTL>2.0.CO;2)
52. Kuo HL. 1965 On formation and intensification of tropical cyclones through latent heat release by cumulus convection. *J. Atmos. Sci.* **22**, 40–63. (doi:10.1175/1520-0469(1965)022<0040:OFAIOT>2.0.CO;2)
53. Freidenreich SM, Garner ST, Gudgel RG. 2004 The new GFDL global atmosphere and land model AM2-LM2: evaluation with prescribed SST simulations. *J. Clim.* **17**, 4641–4673. (doi:10.1175/JCLI-3223.1)
54. Moorthi S, Suarez MJ. 1992 Relaxed Arakawa–Schubert: a parameterization of moist convection for general circulation models. *Mon. Weather Rev.* **120**, 978–1002. (doi:10.1175/1520-0493(1992)120<0978:RASAPO>2.0.CO;2)
55. Zhao M, Held IM, Lin S-J, Vecchi GA. 2009 Simulations of global hurricane climatology, interannual variability, and response to global warming using a 50 km resolution GCM. *J. Clim.* **33**, 6653–6678. (doi:10.1175/2009JCLI3049.1)
56. Bretherton CS, McCaa JR, Grenier H. 2004 A new parameterization for shallow cumulus convection and its application to marine subtropical cloud-topped boundary layers. Part I: description and 1D results. *Mon. Weather Rev.* **132**, 864–882. (doi:10.1175/1520-0493(2004)132<0864:ANPFSC>2.0.CO;2)
57. Martin GM *et al*. 2011 The HadGEM2 family of Met Office unified model climate configurations. *Geosci. Model. Dev.* **4**, 723–757. (doi:10.5194/gmd-4-723-2011)
58. Gregory D, Rowntree PR. 1990 A mass flux convection scheme with representation of cloud ensemble characteristics and stability dependent closure. *Mon. Weather Rev.* **118**, 1483–1506. (doi:10.1175/1520-0493(1990)118<1483:AMFCSW>2.0.CO;2)
59. Martin G, Ringer MA, Pope VD, Jones A, Dearden C, Hinton TJ. 2006 The physical properties of the atmosphere in the new Hadley Centre global environmental model (HadGEM1). I. Model description and global climatology. *J. Clim.* **19**, 1274–1301. (doi:10.1175/JCLI3636.1)
60. Derbyshire SH, Maidens AV, Milton SF, Stratton RA, Willett MR. 2011 Adaptive detrainment in a convective parametrization. *Q. J. R. Meteorol. Soc.* **137**, 1856–1871. (doi:10.1002/qj.875)
61. Grant ALM. 2001 Cloud-base fluxes in the cumulus-capped boundary layer. *Q. J. R. Meteorol. Soc.* **127**, 407–421. (doi:10.1002/qj.49712757209)
62. Grant ALM, Brown AR. 1999 A similarity hypothesis for shallow-cumulus transports. *Q. J. R. Meteorol. Soc.* **125**, 1913–1936. (doi:10.1002/qj.49712555802)
63. Hourdin F *et al*. 2006 The LMDZ4 general circulation model: climate performance and sensitivity to parametrized physics with emphasis on tropical convection. *Clim. Dyn.* **27**, 787–813. (doi:10.1007/s00382-006-0158-0)
64. Dufresne J-L *et al*. 2013 Climate change projections using the IPSL-CM5 earth system model: from CMIP3 to CMIP5. *Clim. Dyn.* **40**, 2123–2165. (doi:10.1007/s00382-012-1636-1)
65. Emanuel KA. 1991 A scheme for representing cumulus convection in large-scale models. *J. Atmos. Sci.* **48**, 2313–2335. (doi:10.1175/1520-0469(1991)048<2313:ASFRCC>2.0.CO;2)
66. Emanuel KA. 1993 A cumulus representation based on the episodic mixing model: the importance of mixing and microphysics in predicting humidity. *AMS Meteorol. Monogr.* **24**, 185–192.
67. Grandpeix JY, Phillips V, Tailleux R. 2004 Improved mixing representation in Emanuel's convection scheme. *Q. J. R. Meteorol. Soc.* **130**, 3207–3222. (doi:10.1256/qj.03.144)
68. Watanabe M *et al*. 2010 Improved climate simulation by MIROC5: mean states, variability, and climate sensitivity. *J. Clim* **23**, 6312–6335. (doi:10.1175/2010JCLI3679.1)

69. Chikira M, Sugiyama M. 2010 A cumulus parameterization with state-dependent entrainment rate. Part I: description and sensitivity to temperature and humidity profiles. *J. Atmos. Sci.* **67**, 2171–2193. (doi:10.1175/2010JAS3316.1)
70. Tiedtke M. 1989 A comprehensive mass flux scheme for cumulus parameterization in large-scale models. *Mon. Weather Rev.* **117**, 1779–1800. (doi:10.1175/1520-0493(1989)117<1779:ACMFSF>2.0.CO;2)
71. Nordeng TE. 1994 Extended versions of the convective parameterization scheme at ECMWF and their impact on the mean and transient activity of the model in the tropics. Technical report 206. Reading, UK: ECMWF.
72. Stevens B *et al*. 2013 Atmospheric component of the MPI-M earth system model: ECHAM6. *J. Adv. Model. Earth Syst.* **5**, 146–172. (doi:10.1002/jame.20015)
73. Yukimoto S *et al.* 2012 A new global climate model of the Meteorological Research Institute: MRI-CGCM3—model description and basic performance. *J. Meteorol. Soc. Japan* **90A**, 23–64. (doi:10.2151/jmsj.2012-A02)
74. Yoshimura H, Mizuta R, Murakami H. 2015 A spectral cumulus parameterization scheme interpolating between two convective updrafts with semi-Lagrangian calculation of transport by compensatory subsidence. *Mon. Weather Rev.* **143**, 597–621. (doi:10.1175/MWR-D-14-00068.1)
75. Ringer MA, Andrews T, Webb MJ. 2014 Global-mean radiative feedbacks and forcing in atmosphere-only and coupled atmosphere-ocean climate change experiments. *Geophys. Res. Lett.* **41**, 4035–4042. (doi:10.1002/2014GL060347)
76. Soden BJ, Broccoli AJ, Hemler RS. 2004 On the use of cloud forcing to estimate cloud feedback. *J. Clim.* **17**, 3661–3665. (doi:10.1175/1520-0442(2004)017<3661:OTUOCF>2.0.CO;2)
77. Vial J, Dufresne JL, Bony S. 2013 On the interpretation of inter-model spread in CMIP5 climate sensitivity estimates. *Clim. Dyn.* **41**, 3339–3362. (doi:10.1007/s00382-013-1725-9)
78. Loeb NG, Wielicki BA, Doelling DR, Louis Smith G, Keyes DF, Kato S, Manalo-Smith N, Wong T. 2009 Toward optimal closure of the Earth's top-of-atmosphere radiation budget. *J. Clim.* **22**, 748–766. (doi:10.1175/2008JCLI2637.1)
79. Rougier J, Sexton DM, Murphy JM, Stainforth D. 2009 Analyzing the climate sensitivity of the HadSM3 climate model using ensembles from different but related experiments. *J. Clim.* **22**, 3540–3557. (doi:10.1175/2008JCLI2533.1)
80. Joshi MM, Webb MJ, Maycock AC, Collins M. 2010 Stratospheric water vapour and high climate sensitivity in a version of the HadSM3 climate model. *Atmos. Chem. Phys.* **10**, 7161–7167. (doi:10.5194/acp-10-7161-2010)
81. Bony S, Dufresne JL. 2005 Marine boundary layer clouds at the heart of tropical cloud feedback uncertainties in climate models. *Geophys. Res. Lett.* **32**, L20806. (doi:10.1029/2005GL023851)
82. Webb MJ, Lambert FH, Gregory JM. 2013 Origins of differences in climate sensitivity, forcing and feedback in climate models. *Clim. Dyn.* **40**, 677–707. (doi:10.1007/s00382-012-1336-x)
83. Klein SA, Hartmann DL. 1993 The seasonal cycle of low stratiform clouds. *J. Clim.* **6**, 1587–1606. (doi:10.1175/1520-0442(1993)006<1587:TSCOLS>2.0.CO;2)
84. Medeiros B, Stevens B. 2011 Revealing differences in GCM representations of low clouds. *Clim. Dyn.* **36**, 385–399. (doi:10.1007/s00382-009-0694-5)
85. Wyant MC, Bretherton CS, Blossey PN. 2009 Subtropical low cloud response to a warmer climate in a superparameterized climate model. Part I: regime sorting and physical mechanisms. *J. Adv. Model. Earth Syst.* **1**, 7. (doi:10.3894/JAMES.2009.1.7)
86. Soden BJ, Held IM, Colman R, Shell KM, Kiehl JT, Shields CA. 2008 Quantifying climate feedbacks using radiative kernels. *J. Clim.* **21**, 3504–3520. (doi:10.1175/2007JCLI2110.1)
87. Cox P, Pearson D, Booth BB, Friedlingstein P, Huntingford C, Jones CD, Luke CM. 2013 Sensitivity of tropical carbon to climate change constrained by carbon dioxide variability. *Nature* **494**, 341–344. (doi:10.1038/nature11882)
88. Caldwell PM, Bretherton CS, Zelinka MD, Klein SA, Santer BD, Sanderson BM. 2014 Statistical significance of climate sensitivity predictors obtained by data mining. *Geophys. Res. Lett.* **41**, 1803–1808. (doi:10.1002/2014GL059205)
89. Efron B, Tibshirani RJ. 1993 *An introduction to the bootstrap*. Monographs on Statistics and Applied Probability, vol. 57. New York, NY: Chapman and Hall.

90. Back LE, Bretherton CS. 2006 Geographic variability in the export of moist static energy and vertical motion profiles in the tropical Pacific. *Geophys. Res. Lett.* **33**, L17810. (doi:10.1029/2006GL026672)
91. Tsushima Y, Iga SI, Tomita H, Satoh M, Noda AT, Webb MJ. 2014 High cloud increase in a perturbed SST experiment with a global nonhydrostatic model including explicit convective processes. *J. Adv. Model. Earth Syst.* **6**, 571–585. (doi:10.1002/2013MS000301)
92. Carrió MW, Stephens GG, Cotton GL, Christensen WR. 2013 Radiative impacts of free-tropospheric clouds on the properties of marine stratocumulus. *J. Atmos. Sci.* **70**, 3102–3118. (doi:10.1175/JAS-D-12-0287.1)
93. Knutson TR, Manabe S. 1995 Time-mean response over the tropical Pacific to increased CO_2 in a coupled ocean–atmosphere model. *J. Clim.* **8**, 2181–2199. (doi:10.1175/1520-0442(1995)008<2181:TMROTT>2.0.CO;2)
94. Fermepin S, Bony S. 2014 Influence of low-cloud radiative effects on tropical circulation and precipitation. *J. Adv. Model. Earth Syst.* **6**, 513–526. (doi:10.1002/2013MS000288)

Interactions between Hydrological Sensitivity, Radiative Cooling, Stability, and Low-Level Cloud Amount Feedback

MARK J. WEBB

Met Office Hadley Centre, Exeter, United Kingdom

ADRIAN P. LOCK

Met Office, Exeter, United Kingdom

F. HUGO LAMBERT

College of Engineering, Mathematics and Physical Sciences, University of Exeter, Exeter, United Kingdom

(Manuscript received 16 December 2016, in final form 8 December 2017)

ABSTRACT

Low-level cloud feedbacks vary in magnitude but are positive in most climate models, due to reductions in low-level cloud fraction. This study explores the impact of surface evaporation on low-level cloud fraction feedback by performing climate change experiments with the aquaplanet configuration of the HadGEM2-A climate model, forcing surface evaporation to increase at different rates in two ways. Forcing the evaporation diagnosed in the surface scheme to increase at 7% K^{-1} with warming (more than doubling the hydrological sensitivity) results in an increase in global mean low-level cloud fraction and a negative global cloud feedback, reversing the signs of these responses compared to the standard experiments. The estimated inversion strength (EIS) increases more rapidly in these surface evaporation forced experiments, which is attributed to additional latent heat release and enhanced warming of the free troposphere. Stimulating a 7% K^{-1} increase in surface evaporation via enhanced atmospheric radiative cooling, however, results in a weaker EIS increase compared to the standard experiments and a slightly stronger low-level cloud reduction. The low-level cloud fraction response is predicted better by EIS than surface evaporation across all experiments. This suggests that surface-forced increases in evaporation increase low-level cloud fraction mainly by increasing EIS. Additionally, the results herein show that increases in surface evaporation can have a very substantial impact on the rate of increase in radiative cooling with warming, by modifying the temperature and humidity structure of the atmosphere. This has implications for understanding the factors controlling hydrological sensitivity.

1. Introduction

Intermodel differences in cloud feedbacks constitute the largest source of spread in estimates of equilibrium climate sensitivity in climate models, and this is primarily due to differences in the responses of low clouds. While low-level cloud feedbacks vary substantially in magnitude, they are positive in most models, where they are associated with reductions in low-level cloud fraction, increasing the amount of solar radiation absorbed at the surface (Boucher et al. 2013).

Many arguments have been advanced to explain the reduction in low-level cloudiness seen in climate models with the warming climate. Rieck et al. (2012) proposed a mechanism where increasing surface moisture fluxes would deepen the boundary layer, increase entrainment of dry air from above the trade inversion, and reduce relative humidity and low-cloud fraction. Webb and Lock (2013) argued that reductions in surface sensible heat and surface buoyancy fluxes with warming could reduce turbulent moistening of the cloud layer. Brient and Bony (2013) proposed a mechanism whereby increases in the vertical gradient of moist static energy in the warmer climate result in a larger influx of low moist static energy and dry air into the boundary layer through subsidence. Bretherton and Blossey (2014) proposed a

Corresponding author: Mark J. Webb, mark.webb@metoffice.gov.uk

DOI: 10.1175/JCLI-D-16-0895.1

mechanism related to that of Rieck et al. (2012), whereby increases in cloud-layer humidity flux in the warmer climate lead to an entrainment liquid-flux adjustment that dries the cloud layer. Sherwood et al. (2014) argued that vertical mixing by large- and small-scale processes would be expected to dry the boundary layer as the climate warms. Following this, Brient et al. (2016) argued that low-cloud reductions in some models are caused by stronger convective mixing, which dries the boundary layer more efficiently as the surface warms, but that the low-cloud responses of many models are dominated by low-cloud shallowing caused by weakened turbulent moistening.

It is recognized that the magnitude of any low-level cloud reduction will be determined by a number of competing factors (Rieck et al. 2012; Webb and Lock 2013; Zhang et al. 2013; Bretherton et al. 2013; Blossey et al. 2013; Jones et al. 2014; Qu et al. 2015b; Vial et al. 2016). While factors that break up clouds may be dominant, their impact will be offset by other processes that, if acting in isolation, would act to increase low-level cloud fraction. Such negative cloud feedback mechanisms may include the effects of increasing stability on low cloud fraction (e.g., Blossey et al. 2013; Qu et al. 2015b) and enhanced moisture supply to the cloud layer from increasing surface evaporation (e.g., Webb and Lock 2013; Zhang et al. 2013). If we are to understand why low-level cloud feedback is positive, it is therefore necessary to understand both positive and negative low cloud feedback mechanisms and the reasons for their differing strengths.

One way to quantify the contribution of a hypothesized cloud feedback mechanism in a climate model is to prevent it from operating in a climate change experiment, and to measure the impact on the overall cloud feedback. Similarly, a given mechanism may be strengthened to explore the extent to which it compensates for other effects. Webb and Lock (2013) tested a number of mechanisms in this way in the HadGEM2-A GCM, performing sensitivity experiments targeting positive subtropical low cloud feedback. These included experiments where surface evaporation was forced to increase at different rates, following similar sensitivity experiments with a very high-resolution process model run over a small domain representative of a trade cumulus boundary layer (Rieck et al. 2012).

The rate of increase in global mean surface evaporation and precipitation per degree warming in a climate change scenario is often referred to as the hydrological sensitivity. As pointed out by Fläschner et al. (2016), it is important to distinguish between estimates of hydrological sensitivity that include temperature-independent effects of radiative forcing agents such as carbon dioxide on the global precipitation increase and those that cleanly isolate the temperature-dependent components. Here we use the term ''hydrological sensitivity'' to refer specifically to the temperature-dependent increase in global precipitation with surface warming, excluding the effects of radiative forcing agents, consistent with the approach of Mitchell et al. (1987), Lambert and Webb (2008), Andrews et al. (2010), and Fläschner et al. (2016).

If relative humidity, surface wind speed, and air sea temperature differences were to stay fixed with future climate warming, then global mean surface evaporation and precipitation would increase at 7% K^{-1} (Mitchell et al. 1987; Richter and Xie 2008; Rieck et al. 2012). However, the radiative cooling of the atmosphere is widely thought to regulate the hydrological sensitivity, limiting the rate of increase of global mean surface evaporation and precipitation to something closer to 3% K^{-1} (e.g., Mitchell et al. 1987; Lambert and Webb 2008; Pendergrass and Hartmann 2014; Fläschner et al. 2016). This is achieved through a combination of increases in near-surface relative humidity and reductions in near-surface wind speed and air–sea temperature differences (e.g., Richter and Xie 2008).

Webb and Lock (2013) noted that the surface evaporation in a region of strong subtropical cloud feedback in the northeast Pacific between Hawaii and California increased very little in a climate change experiments with HadGEM2-A, considerably less than the 3% K^{-1} increase seen globally and much less than the 7% K^{-1} increase that would occur with warming in the absence of changes in near-surface relative humidity, wind speed, and air–sea temperature difference. By forcing the local surface evaporation to increase more strongly in the warmer climate, they were able to weaken this local cloud feedback considerably, demonstrating that much of the positive low cloud feedback at that location could be attributed to the relatively weak increase in surface evaporation. A limitation of that study was the fact that the surface evaporation was perturbed over a small region, and one that focused on the location with the strongest low cloud feedback; hence, it was not clear whether this mechanism explains the low cloud feedback more generally in this model.

More recently, highly idealized ''aquaplanet'' configurations of climate models forced with zonally symmetric sea surface temperatures (SSTs) have been shown to be remarkably successful in reproducing the global cloud feedbacks predicted by climate models in realistic atmosphere only and coupled ocean–atmosphere configurations (Ringer et al. 2014; Medeiros et al. 2015).

In this study we apply the approach of Webb and Lock (2013) globally to investigate the positive low-level cloud feedback in the aquaplanet configuration

TABLE 1. Experiment names and descriptions.

Experiment	Description
APEC	Aquaplanet experiment based on APE Control SSTs
APEC4K	As APEC with a uniform +4-K SST perturbation
APECSurfaceEvap	APEC SST/surface evaporation forced to APEC zonal climatology
APEC4KSurfaceEvap0%	APEC4K SST/surface-forced evaporation to APEC zonal climatology
APEC4KSurfaceEvap3%	APEC4K SST/surface-forced evaporation to APEC4K zonal climatology
APEC4KSurfaceEvap7%	APEC4K SST/surface-forced evaporation 7% K^{-1} increase from APEC
APEC4KRadCool7%	APEC4K SST with enhanced atmospheric radiative cooling

of HadGEM2-A. We pose the following question: Does the muted (i.e., sub-7% K^{-1}) increase in global surface evaporation contribute substantially to the low cloud amount reduction and positive low cloud feedback? We test this idea by performing climate change experiments with an SST forced aquaplanet configuration of HadGEM2-A that is subject to a uniform +4-K SST perturbation, and where surface evaporation is forced to increase at 7% K^{-1}. We stimulate surface evaporation in two ways. In the first set of experiments we add a term to the surface evaporation diagnosis that brings the zonal mean evaporation in each time step into agreement with a target climatological value. In an additional experiment we stimulate the hydrological cycle by adding an artificial radiative cooling term in the atmosphere designed to approximately double the hydrological sensitivity.

Our model and experimental approach are described in more detail in section 2. We present and discuss our results in section 3. We start by discussing the low cloud responses from the surface evaporation forced experiments in section 3a and those in the radiative cooling forced experiment in section 3b. We then go on to discuss the implications of our results for understanding the hydrological sensitivity in section 3c, and provide our concluding remarks in section 4.

2. Model experiments and methods

We explore the impact of increasing surface evaporation on low-level cloud feedbacks in the HadGEM2-A climate model (Martin et al. 2011) by specifying surface evaporation following a similar approach to that in Webb and Lock (2013), but at a global scale. Our experiments are summarized in Table 1. The basis for our experiments is an aquaplanet configuration of HadGEM2-A that is forced with time-invariant zonally and hemispherically symmetric SSTs, taken from the Aqua-Planet Experiment (APE) project "Control" experiment (Neale and Hoskins 2000; here denoted as APEC). This is accompanied by an idealized climate change experiment, in which the APEC SSTs are subject to a uniform increase of 4 K (APEC4K), following the approach of Medeiros et al. (2015). The APEC and APEC4K experiments are referred to throughout as the standard experiments. These differ slightly from the aquaplanet experiments in CMIP5, which were based on the APE "Qobs" SSTs (Medeiros et al. 2015). We chose the APE Control dataset, which has slightly more peaked SSTs in the tropics, as we found that, in spite of their hemispherically symmetric forcings, the experiments based on the Qobs SSTs were prone to having strong hemispherically asymmetric responses when we applied the surface evaporation forcing. We perform a number of sensitivity experiments based on the standard APEC and APEC4K experiments in which we force the model to have various specified values of global mean surface evaporation. We apply two approaches, which we call the surface evaporation forced and radiative cooling forced methods.

For our first surface evaporation forced experiment (APECSurfaceEvap) we repeated APEC, but forcing the zonal mean surface evaporation on each model time step to agree with the APEC climatological zonal mean. This was done by diagnosing the surface evaporation in the usual interactive manner and calculating the zonal mean at every model time step. A constant value was then added at all points in a given line of latitude to force the zonal mean to agree with the target value. This sets the zonal mean evaporation to the target value while retaining variations along a line of latitude, maintaining synoptic structure in the surface evaporation field. Similarly we repeated the APEC4K experiment, fixing the zonal mean surface evaporation to the zonal mean climatology from APEC4K (APEC4KSurfaceEvap3%). These two experiments allow us to assess whether or not the positive low cloud feedback can be reproduced with specified zonal mean surface evaporation (see section 3a). Two further experiments were then performed. In one we repeated APEC4K, fixing the zonal mean surface evaporation to the climatology from APEC, preventing the surface evaporation from increasing with warming (APEC4KSurfaceEvap0%). In the other we

forced the surface evaporation in the APEC4K experiment to increase at 7% K^{-1} relative to that in APEC specifying the zonal mean surface evaporation climatology from the APEC experiment multiplied by a factor of 1.28 (APEC4KSurfaceEvap7%). This is what we would expect to see for a warming without any changes in near-surface relative humidity, wind, or air–sea temperature difference.

For the radiative cooling forced experiments, we use the APEC experiment as the present-day control and force the global mean surface evaporation to increase more rapidly in an additional +4 K experiment (APEC4KRadCool7%) by artificially enhancing the atmospheric radiative cooling rate. First we calculated the zonal mean climatology of the response in the clear-sky longwave radiative heating rate between the APEC and APEC4K experiments as a function of height, which takes negative values due to the radiative cooling increase. We then ran the APEC4KRadCool7% experiment, adding this additional radiative cooling climatology (as a function of latitude and height) to the actual radiative heating rate calculated by the model's radiation code in each model time step. This constitutes an extra 4.4 W m^{-2} K^{-1} of atmospheric radiative cooling. We expected this to approximately double the rate of increase in longwave clear-sky radiative cooling with warming, in turn approximately doubling the increase in global mean surface evaporation (see section 3a).

All experiments were run for 72 months, and climatological means were formed over the full period. As in many studies, we diagnose cloud feedbacks using the climatological mean change in the cloud radiative effect (CRE) between the aquaplanet control and +4 K experiments, divided by the global mean near-surface temperature response. This can be considered a measure of cloud feedback, including the climatological masking effects of clouds on the noncloud feedbacks [see Webb and Lock (2013) for a discussion of the merits of this approach compared to the alternatives].

3. Results and discussion

a. *Low cloud responses in surface forced evaporation experiments*

Figure 1 shows the effects of forcing surface evaporation to increase at various different rates with a uniform +4-K warming applied to the HadGEM2-A aquaplanet configuration forced with the APEC SSTs. Figure 1a shows the responses in zonal mean surface evaporation in the standard APEC4K experiment relative to APEC, and in the various experiments where surface evaporation is specified using the surface evaporation and radiative cooling forcing methods. The global mean surface evaporation increases by 3.2 W m^{-2} K^{-1} in the standard experiments APEC and APEC4K, an increase of 3.4% K^{-1} relative to the global mean control value in APEC, which is 94.2 W m^{-2}. As expected by design, the zonal mean evaporation increase in APEC4KSurfaceEvap3% relative to APECSurfaceEvap (red line in Fig. 1a) agrees well with that in the standard experiments (black line), and APEC4KSurfaceEvap0% (orange line) shows no increase, while APEC4KSurfaceEvap7% (blue line) shows an increase of 7.0% K^{-1} in the global mean, approximately twice that in the standard experiments. The APEC4KRadCool7% (green line) experiment is also quite successful in reproducing an increase close to 7% K^{-1}, with a global mean increase of 7.5% K^{-1}, with only minor differences in the meridional structure of the response. Figure 1b shows the concomitant responses in zonal mean precipitation. We note some differences in the precipitation responses in the APEC4K and APEC4KSurfEvap3% responses, with a tendency for the precipitation to decrease at the equator and increase more on the flanks of the ITCZ in APEC4KSurfEvap3% compared to the more concentrated increases seen in APEC4K. We do not expect the responses in these experiments to be exactly the same, because the method used to force the surface evaporation in the APEC4KSurfEvap3% experiment removes any temporal variability in the zonal-mean surface evaporation. The precipitation responses between the two experiments are, however, much more consistent in the subtropical regions between 10° and 25°N/S where the positive low-level cloud feedbacks occur (see below).

Many previous studies have pointed out the association between positive subtropical cloud feedback and reductions in low-level cloud. The net cloud feedback (which we define here to include cloud masking; see section 2) in the standard experiments is positive in the global mean and between 10° and 25°N/S, with the strongest positive feedback at 17°N/S (black line, Fig. 1c). The variations in the net cloud feedback are primarily due to the shortwave component (Fig. 1d). Meanwhile, the low cloud fraction reduces in the global mean and throughout the latitudes where a positive net cloud feedback is present (black line, Fig. 1e). The difference between the surface-forced evaporation experiments APECSurfaceEvap and APEC4KSurfaceEvap3% successfully reproduces the signs of the positive global mean cloud feedback and the global reduction in low-level cloud fraction in the standard experiments, and also captures well the magnitudes of their global responses. The zonal distributions of these quantities are also well captured (cf. black and red lines in

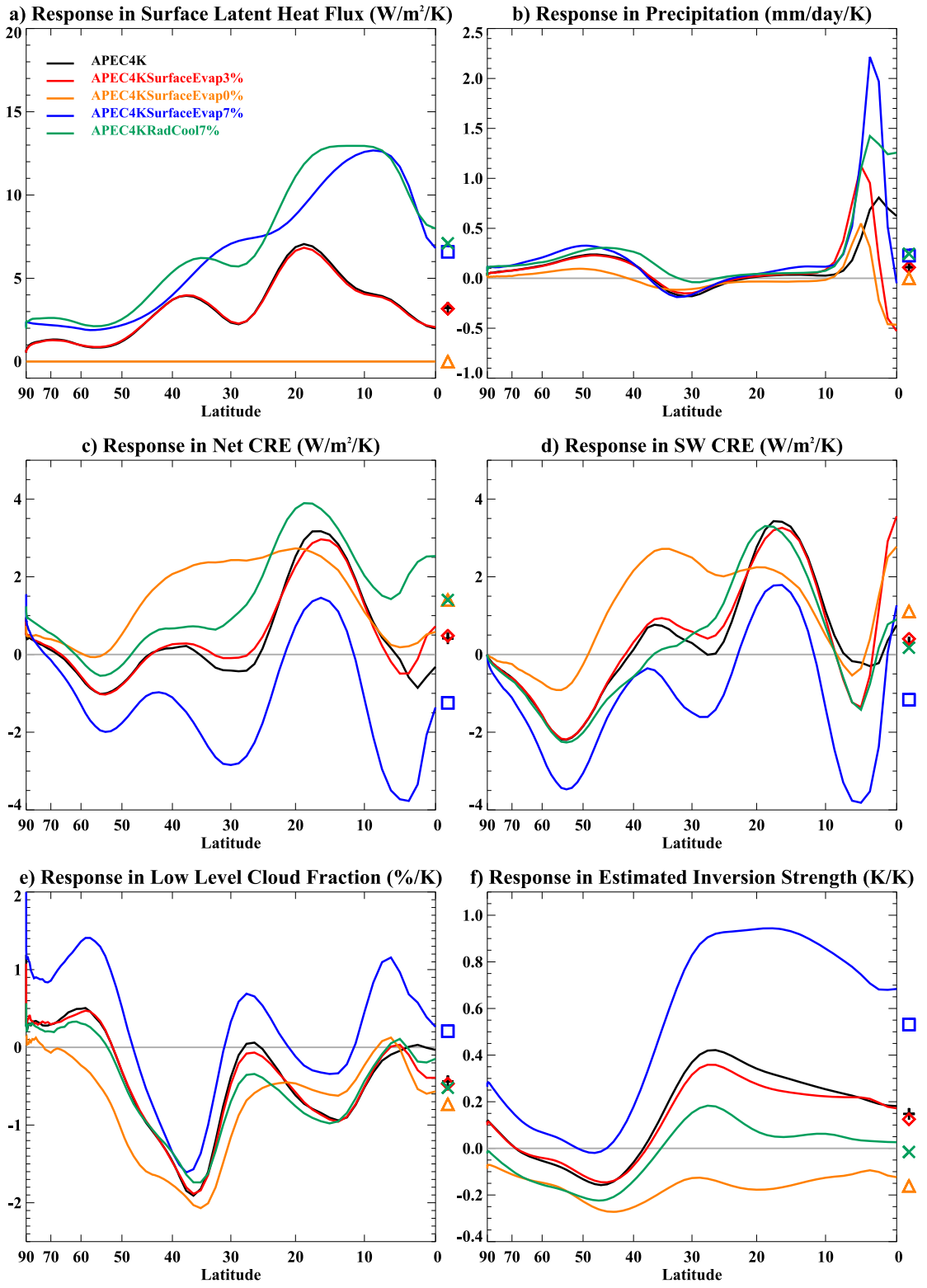

FIG. 1. Responses to a uniform +4-K SST increase in aquaplanet experiments forced with APE Control (APEC) SSTs and varying degrees of surface evaporation increase (see Table 1): (a) surface latent heat flux, (b) precipitation, (c) net (longwave plus shortwave) cloud radiative effect (CRE), (d) shortwave CRE, (e) maximum low-level cloud fraction, and (f) estimated inversion strength (EIS). Both hemispheres are averaged and results are plotted as a nonuniform function of latitude such that the area under the curve gives a good indication of the contribution to the global mean from different latitudes. The APEC4K and APEC4KRadCool7% responses are relative to APEC while the surface-forced experiment responses are relative to APECSurfaceEvap. All are divided by 4 so as to be expressed per K warming. The global mean responses are indicated by symbols on the right-hand side.

Figs. 1c–e). This demonstrates that the surface-forced evaporation method does not substantially distort the cloud feedbacks, and is therefore a suitable method for exploring the impact of differing levels of surface evaporation increase on cloud feedback.

Figures 1c and 1e also show that forcing the evaporation to increase at a rate closer to 7% K^{-1} with a +4-K warming using the surface evaporation forcing method (experiment APEC4KSurfaceEvap7%, blue line) reverses the sign of both the global mean cloud feedback and the low cloud fraction response, resulting in a negative global mean net cloud feedback and an increase in global mean low cloud fraction. Although the signs of the global mean low-level cloud fraction and cloud feedback responses reverse, the meridional structures of the responses relative to their global means are not greatly affected. The most positive cloud feedback and the associated low-level cloud fraction reduction located near to 15°N/S in the standard experiments are not completely eradicated in the APEC4KSurfaceEvap7% experiment, indicating that part of the positive cloud feedback in the APEC4K experiment cannot be explained by the muted increase in surface evaporation.

One possible explanation for this might be that while increases in surface evaporation in the climate change context generally increase low cloud fraction on occasions when there is little mixing across the inversion, in a small fraction of cases where shallow convection is able to penetrate the inversion the enhanced surface evaporation might help to break up cloud. That said, the area between the positive part of the curve and the zero line gives an indication of the contribution of this remaining positive feedback to the global mean, which is small compared to the positive contribution in the APEC/APEC4K experiments, and is dwarfed by that from the negative feedback elsewhere.

The sensitivity of the global cloud feedback and low cloud response to the strength of the surface evaporation increase is further demonstrated by the results from the APEC4KSurfaceEvap0% experiment in which the surface evaporation does not increase at all with the warming climate; in this scenario the global mean low cloud reduction is amplified compared to the standard experiment and the global cloud feedback becomes more strongly positive (cf. orange and black lines in Figs. 1c,e).

Our experiments also show substantial differences in the response of the estimated inversion strength (EIS; Wood and Bretherton 2006) to climate warming (Fig. 1f). EIS is a measure of lower tropospheric stability that is based on the potential temperature difference between the surface and 700-hPa level, and that gives an indication of the strength of low-level temperature inversions, such as those present at the top of subtropical boundary layers. EIS has been shown to be a good predictor of spatiotemporal variations in low-level cloud fraction in the present climate (Wood and Bretherton 2006). Stronger values of EIS are generally associated with a stronger capping inversions in subtropical boundary layers, which are widely thought to encourage the formation and maintenance of low-level clouds by inhibiting entrainment of dry air into the boundary layer from above and promoting shallow, well-mixed boundary layers with stratocumulus clouds that are strongly coupled to surface evaporation (Bretherton and Wyant 1997; Wyant et al. 1997; Wood and Bretherton 2006). Our results indicate that the magnitude of the EIS response to the warming climate is very sensitive to the rate of the surface evaporation increase in our surface-forced evaporation experiments, with a 7% K^{-1} increase more than doubling the magnitude of the EIS response compared to the standard case, and a modest EIS reduction in the absence of an evaporation increase (Fig. 1f). This suggests a second route whereby increasing surface evaporation can increase low-level cloud fraction beyond the local argument put forward in Webb and Lock (2013), namely that a stronger global increase in surface evaporation results in stronger increases in EIS and stronger low-level inversions in low cloud regimes, reducing drying of the boundary layer due to mixing with the free troposphere. Such an effect would mean that the muted evaporation increase acts to reduce low-level cloud fraction more relative to the 7% K^{-1} scenario than would be expected via the local argument of Webb and Lock (2013) alone.

Why should the rate of increase in surface evaporation affect changes in EIS? Many studies (e.g., Held and Soden 2006) have suggested that the tropical lapse rate (the rate of decrease of temperature with height) weakens in the warming climate because the free troposphere tends to follow a temperature profile that is close to a moist adiabat, which becomes more statically stable with surface warming. A saturated adiabat has increasing potential temperature with height, which strengthens as the lapse rate weakens with surface warming. Qu et al. (2015a) showed that a number of climate models run in a similar aquaplanet configuration to that used here show increases in potential temperature between 850 and 600 hPa that are too strong to be explained by the moist adiabatic lapse rate argument alone. Figure 2a shows the increases in potential temperature in our various experiments with warming in the tropical deep convection region centered on the equator. In the surface-forced experiments, larger increases in surface evaporation are associated with larger levels of upper tropospheric warming and larger increases at

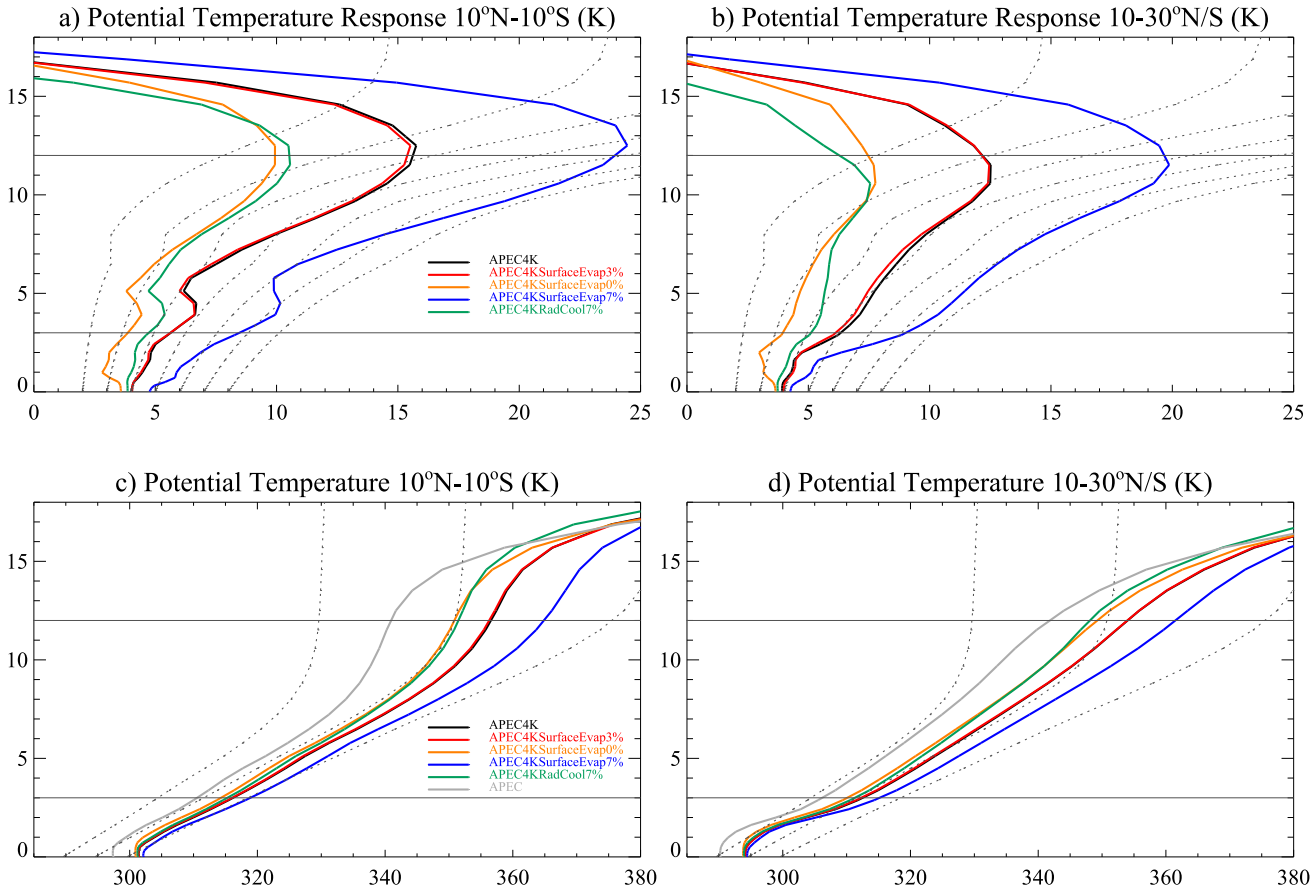

FIG. 2. Responses in profiles of potential temperature to uniform +4-K warming averaged over the areas between (a) 10°N and 10°S and (b) 10° and 30°N/S from the same experiments as shown in Fig. 1. The response in the saturated moist adiabat associated with surface temperature increases ranging from 2 to 8 K in 1-K increments over the region 10°N–10°S are shown as dashed lines in (a) and (b). (c), (d) Absolute profiles of potential temperature in the various experiments averaged over 10°N–10°S and 10°–30°N/S, respectively. The gray lines show the APEC control experiment and the colored lines show the various +4-K experiments. Saturated adiabats are plotted as dashed lines for the control SSTs over the region 10°N–10°S and for surface temperatures 5 and 10 K warmer. The horizontal lines show the heights of the 700- and 200-hPa levels.

700 hPa relative to the surface. In the APEC4KSurfaceEvap7% experiment in particular (blue line), the 700-hPa potential temperature increases considerably more than would be predicted by the change in the saturated moist adiabat. Figure 2c shows that in the APEC control experiment (gray line), the potential temperature increases with altitude throughout the lower troposphere, at a rate less than that predicted by a saturated adiabat. This is also the case for the APEC4KSurfaceEvap7% experiment, although its profile is closer to a saturated adiabat than is the case in the APEC control experiment. Thus, while the increase in potential temperature with warming between APEC and APEC4KSurfaceEvap7% at 700 hPa is more than that predicted by a change in the saturated moist adiabat, the vertical potential temperature gradient does not exceed that predicted by the moist adiabat in either of these experiments individually. This explains how the potential temperature response at 700 hPa can be more than that predicted by a change in the saturated adiabat, without violating the generally accepted principle that the absolute vertical potential temperature gradient cannot exceed that predicted by a saturated adiabat. Similar behavior is seen in the free troposphere from 700 hPa upward in the subtropics (Figs. 2b,d).

Our interpretation of these results is as follows (it is summarized by the blue arrows in the schematic in Fig. 5). In the APEC4KSurfaceEvap7% experiment, the additional moisture supply into the boundary layer from the enhanced surface evaporation with climate warming will increase near-surface humidity, generate convective instability, and increase the amount of precipitating deep convection, resulting in additional net latent heat release in regions of deep convection (allowing for the effects of evaporating clouds and precipitation). This is supported by Fig. 1b, which shows enhanced precipitation near the equator in APEC4KSurfaceEvap7% compared to APEC4K. Figure 3 shows global mean

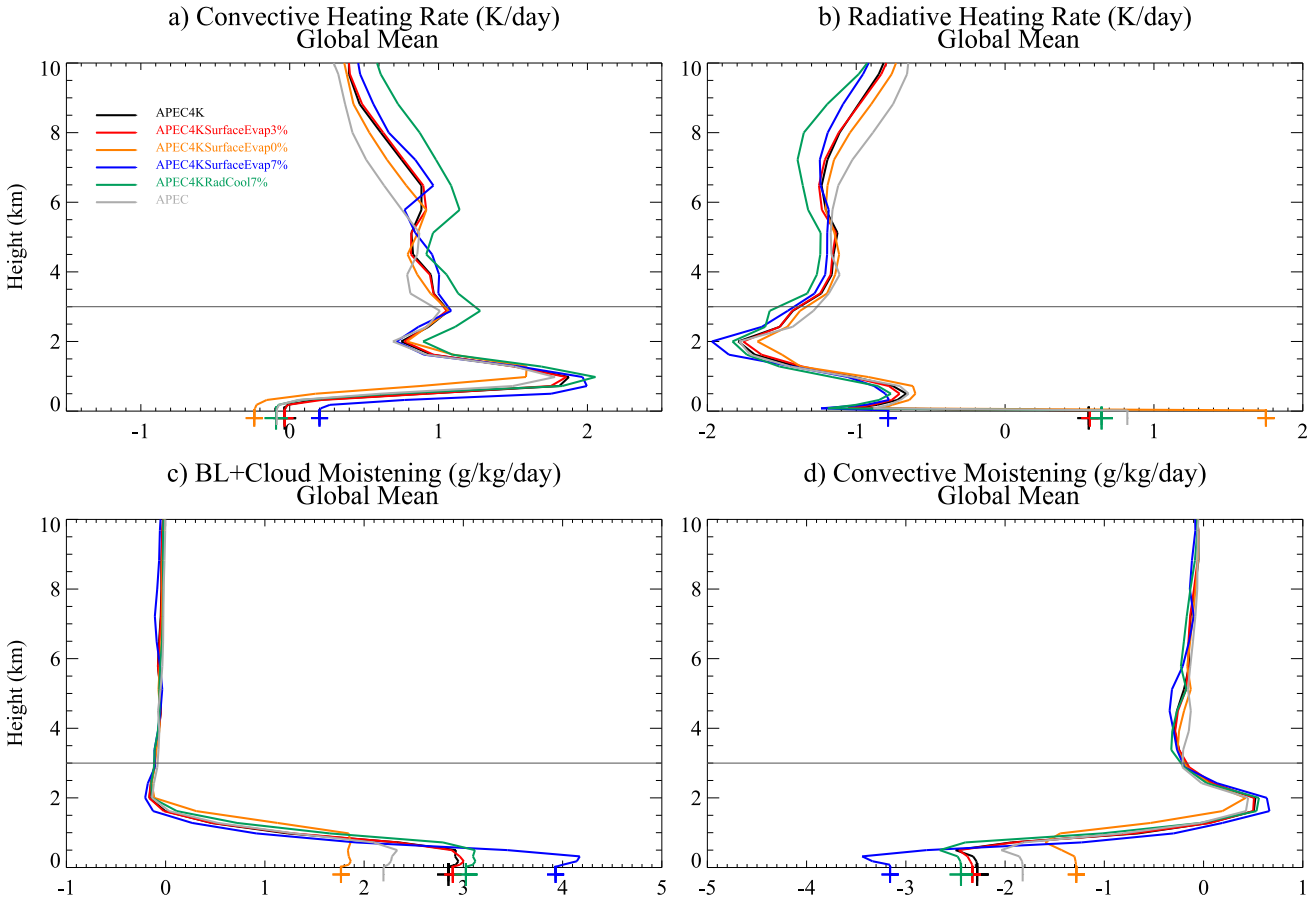

FIG. 3. Global mean atmospheric heating and moistening rates from radiation, boundary layer, convection, and cloud schemes: (a) heating rates from convection, (b) heating rates from radiation, (c) net moistening rates from surface evaporation, boundary layer, and large-scale cloud condensation, and (d) moistening rates from convection. The lines below the x axis indicate the values in the bottom model level, with the APEC experiment denoted by a vertical gray line and the various +4-K experiments denoted by + symbols. The horizontal line shows the height of the 700-hPa level.

heating and moistening rates from various components of the model physics in our experiments. Our interpretation is also supported by Fig. 3a, which shows enhanced heating by convection and cloud condensation above 700 hPa with increasing surface-forced evaporation (see the orange, red, and blue lines). Enhanced free tropospheric warming in convective regions of the tropics is then expected to propagate to the subtropics via horizontal heat transport by tropical waves and the mean overturning circulation (Sobel et al. 2001). This will result in enhanced temperature increases in the free troposphere and reductions in the lapse rate, increasing the amount by which the middle to upper free troposphere warms compared to the standard APEC4K experiment (cf. blue and black lines in Figs. 2a,b), resulting in larger increases in EIS (Fig. 1f) and a stronger subtropical inversion. This would in turn result in reduced entrainment of dry air into the boundary layer from above, and increasing (or weakening reductions in) low-level cloud fraction. This interpretation could be tested further in the future with additional sensitivity experiments—for example, by artificially enhancing the rate of latent heat release in the free troposphere with warming.

Figure 4 shows scatterplots of the responses in various global mean quantities. The differences in the global mean responses in the standard experiment (black symbols) compared to the APEC4KSurfaceEvap0% experiment (orange symbols) are qualitatively similar to the differences in the APEC4KSurfaceEvap7% experiment (blue symbols) compared to the standard experiments (black symbols). Hence the arguments outlined above may be used to interpret both sets of responses to increasing surface evaporation. For example, in both cases stronger increases in surface evaporation are associated with more positive EIS responses (Fig. 4a), and weaker decreases or stronger increases in low-level cloud fraction (Fig. 4b). The APEC4KSurfaceEvap0% experiment does not show an increase in EIS, which indicates that we can attribute the increase in EIS in the standard experiments to the increasing surface

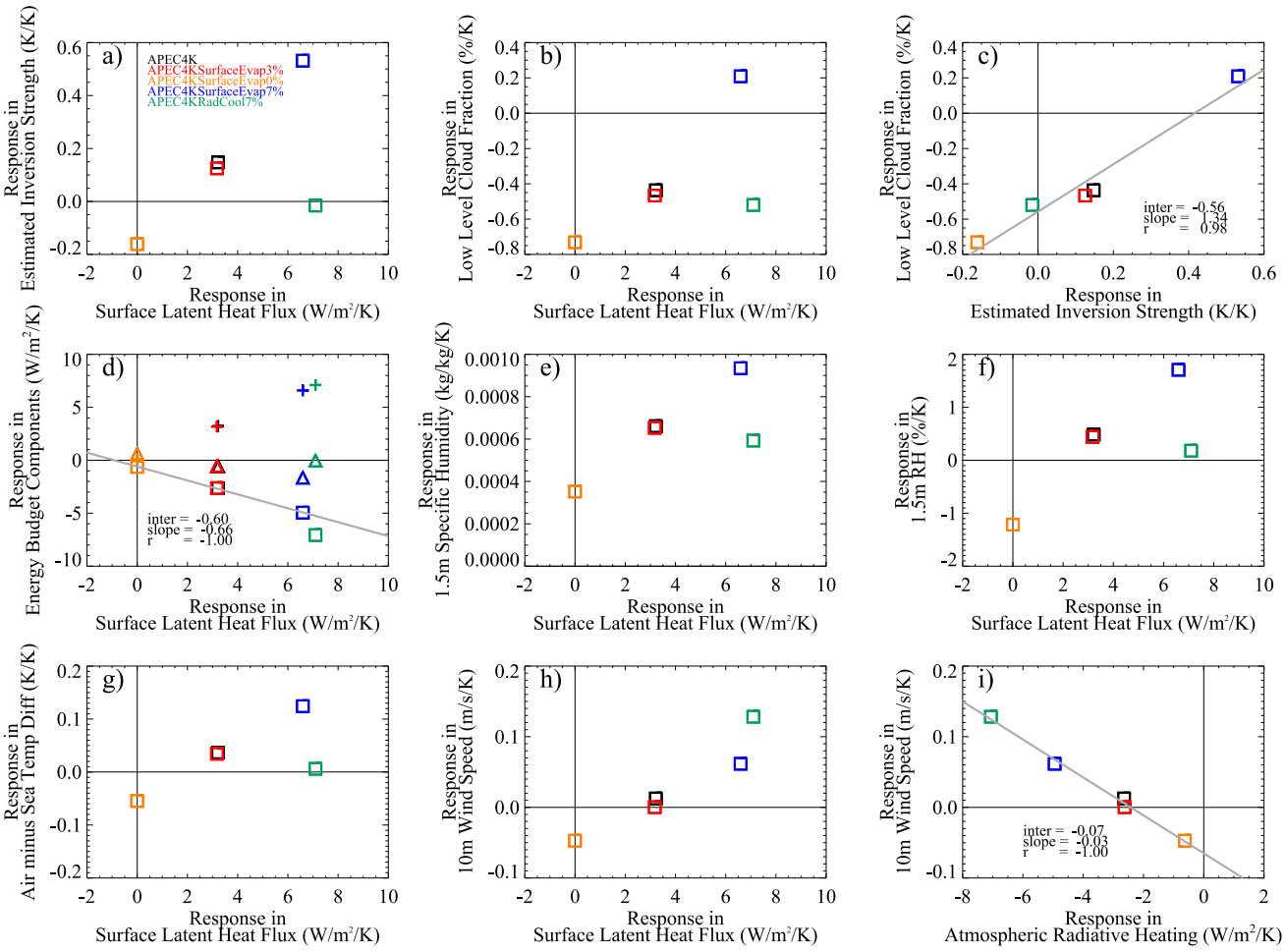

FIG. 4. Scatterplots of global mean responses, expressed per K surface warming: (a) EIS against surface evaporation, (b) low cloud fraction against surface evaporation, (c) low cloud fraction against EIS, and (d) responses in surface evaporation (plus signs), atmospheric radiative heating rate (squares), and surface sensible heat flux (triangles) against surface evaporation. (e)–(h) Near-surface specific humidity, near-surface relative humidity, air-minus-surface temperature difference, and 10-m near-surface wind speed against surface evaporation, respectively. (i) The 10-m near-surface wind speed against atmospheric radiative heating. The gray lines in (c) and (i) show fits to all five data points. The gray line in (d) is a fit to the radiative heating responses for the surface-forced experiments only.

evaporation (i.e., the fact that the hydrological sensitivity is positive).

It is interesting to note that modifying the surface-forced evaporation increase with warming in both the APEC4KSurfaceEvap7% and APEC4KSurfaceEvap0% experiments affects the EIS and low-cloud fraction responses and the net cloud feedback considerably poleward of 30°N/S (Fig. 1). This suggests that the mechanisms discussed above are also relevant to understanding extratropical cloud feedbacks. The standard experiments show a relatively weak net cloud feedback here compared to the subtropics, despite substantial reductions in low cloud fraction (Fig. 1). We attribute this partly to the fact that the annual mean insolation is less at higher latitudes, and partly to compensating effects of changes in mid- to high-level clouds, condensed water path, and cloud phase changes. The surface-forced evaporation experiments clearly change the degree to which these effects compensate for each other in contributing to the extratropical cloud feedback. This may not only be because of the effects of changing stability on low cloud. Enhanced free-tropospheric warming would also be expected to result in a stronger lifting of the freezing level. This might strengthen negative phase change feedbacks associated with increasing midlevel cloud fraction and albedo (e.g., Senior and Mitchell 1993).

b. *Low cloud responses in response to enhanced radiative cooling*

We now discuss the results from the experiment where we artificially increase the rate at which the atmospheric radiative cooling increases with warming, thus stimulating the surface evaporation indirectly. The global

mean surface evaporation increases by a comparable amount in APEC4KRadCool7% to that in the equivalent surface-forced evaporation experiment APEC4KSurfaceEvap7% and the regional distribution of the surface evaporation increase is also very similar (cf. blue and green lines in Fig. 1a). However, the cloud feedback and the cloud response are quite different; the net cloud feedback becomes more positive in APEC4KRadCool7% rather than negative, and the low cloud fraction reduces slightly more than in the standard experiments, rather than increasing strongly as it does in the APEC4KSurfaceEvap7% experiment (Figs. 1c,e). This very different cloud response with warming given a similar surface evaporation increase indicates that the surface evaporation is not the sole factor determining the different cloud feedbacks in our experiments. Figure 4b shows a scatterplot of the global mean low cloud fraction response against the global surface evaporation increase, and while this supports there being a relationship between surface evaporation and the low cloud fraction response in the surface-forced experiments, this relationship is not maintained when the APEC4KRadCool7% experiment (green square) is included. The EIS response in APEC4KRadCool7% (green) is also very different compared to that in APEC4KSurfaceEvap7% (blue), being much weaker than that in the standard APEC4K experiment (black), while APEC4KSurfaceEvap7% increases more strongly (Fig. 4a).

Our interpretation of the different responses in APEC4KSurfaceEvap7% and APEC4KRadCool7% is as follows, based loosely on the arguments of tropospheric energy balance outlined by Mitchell et al. (1987). In the APEC4KSurfaceEvap7% experiment, as argued above and as summarized by the blue lines in Fig. 5, the additional moisture supply at the surface will stimulate deep convection, resulting in additional latent heat release and free tropospheric warming compared to that seen in the standard experiments, a reduced lapse rate, a larger increase in EIS, and an increase in low cloud fraction.

In the APEC4KRadCool7% experiment, however (as indicated by the green arrows in Fig. 5), the artificially enhanced radiative cooling (Fig. 3b) will reduce the amount by which the free troposphere warms compared to the standard APEC4K experiment (Figs. 2a,b), resulting in a more enhanced lapse rate and a reduced increase in EIS (Fig. 1f). The enhanced lapse rate will also make the atmosphere more convectively unstable and enhance precipitating deep convection (Fig. 1b). The additional latent heat release in the free troposphere (Fig. 3a) will act to balance the imposed radiative cooling (Fig. 3b). Near-surface relative humidity, air–sea temperature differences, and winds will adjust accordingly, increasing the surface evaporation to balance the enhanced latent heat release. (This last aspect is explained in more detail in section 3c below.)

The relatively small change in EIS in the APEC4KRadCool7% experiment compared to that in the APEC4KSurfaceEvap7% experiment is consistent with the smaller low cloud response (Figs. 1a,b), and Fig. 4c shows that the global EIS response is in fact a better predictor of the low cloud response across all of our experiments than is surface evaporation (cf. Fig. 4b). Figure 4c shows a linear regression line that fits the data very well, with a correlation coefficient of 0.98.

It is interesting to note that the relationship illustrated here shows a substantial reduction in low cloud amount with warming in the absence of an EIS change, a reduction of $0.56\%\,K^{-1}$ as shown by the intercept. The results from the APEC4KRadCool7% experiment reproduce this very well. The slope of the regression line is $1.34\%\,K^{-1}$. Wood and Bretherton (2006) found a regression slope of $6\%\,K^{-1}$ for spatiotemporal variations in stratus cloud amount with EIS in observations. We would not expect these numbers to agree, however, for a number of reasons. One is that the global mean low-cloud fractions used in our calculation are much smaller than those in the stratus cloud regions examined by Wood and Bretherton (2006), in part because the global mean includes contributions from areas with few low-level clouds. Another is that the global mean low cloud fraction response will include contributions from changes in other low cloud regimes (e.g., trade cumulus) whose responses would not necessarily be expected to be the same as those in the stratus regions.

Although the main emphasis of this work is on understanding the role of changing surface evaporation on low cloud fraction feedback, it is interesting to note that it is in the absence of a surface evaporation response that the strongest low cloud reduction is seen (Fig. 4b). This suggests that the underlying cause of the positive low cloud feedback in this model is not explained by the surface evaporation and radiative cooling changes explored here (see the orange arrow on the left-hand side of the schematic in Fig. 5). EIS reduces slightly in the APEC4KSurfaceEvap0% experiment (Fig. 4c), suggesting that the positive feedback is partly due to a reduction in EIS in the absence of a surface evaporation increase. However, substantial low cloud reductions are also seen in the radiative cooling forced experiment in the absence of substantial changes in EIS, indicating that other factors must also contribute to the positive low cloud feedbacks seen in the absence of surface evaporation increases. For example, APEC4KSurfaceEvap0% shows a substantial drop in the in near-surface relative humidity (discussed below), which may be indicative of a

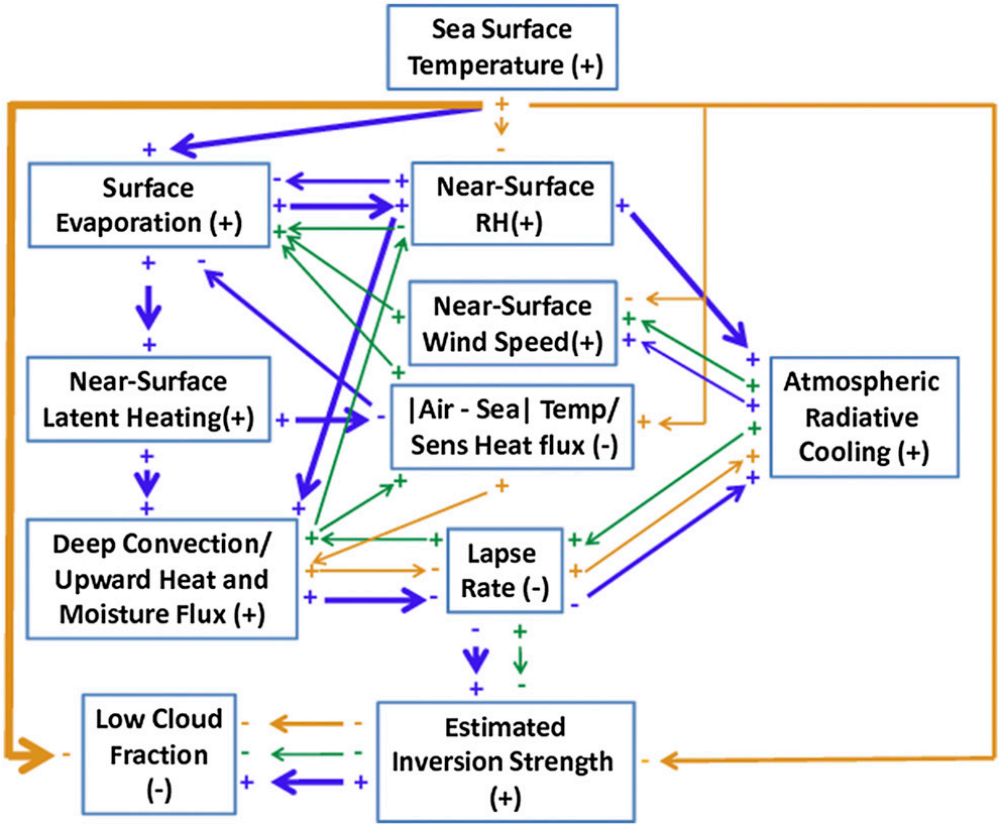

FIG. 5. Schematic summarizing interactions between global mean surface evaporation, radiative cooling, stability, and low-level cloud fraction. All quantities are positive, with plus and minus signs indicating increasing and decreasing magnitude respectively. The colors give an indication of the effects of increasing SST while holding surface evaporation fixed (orange), increasing surface evaporation (blue), and increasing radiative cooling (green). The black plus signs inside the boxes show the sign of the changes in the standard APEC4K experiment, and the thicknesses of the lines have been chosen to give an indication of the importance of the various interactions for determining the responses in APEC4K.

drop in relative humidity throughout the boundary layer, and which may in turn contribute to the strong low cloud reduction.

In summary, we argue that increasing SSTs without allowing substantial changes in surface evaporation or radiative cooling results in a reduction in low cloud fraction and a strong positive cloud feedback (see orange arrows in Fig. 5). Allowing surface evaporation to increase in response to increasing SSTs stimulates convection and free tropospheric latent heat release, warming the free troposphere, increasing EIS and opposing the reductions in low cloud fraction (blue arrows in Fig. 5). The net effect of these competing mechanisms in the standard experiment is a modest reduction in low-level cloud fraction. (The thickness of the arrows in the schematic aims to give an indication of the relative contributions of these two mechanisms in the standard experiment.) Meanwhile, artificially enhancing the radiative cooling with climate warming reduces free tropospheric warming, increases the lapse rate, and weakens increases in EIS, slightly strengthening the low cloud feedback compared to the standard experiment (green arrows in Fig. 5).

It is interesting to contrast our findings with the widely accepted understanding of the mechanism underlying the breakup of clouds observed while following air masses undergoing the subtropical stratocumulus to trade cumulus transition (Bretherton and Wyant 1997; Wyant et al. 1997; Qu et al. 2015b). Both scenarios relate to increasing surface temperatures and increasing surface evaporation, but our argument suggests an increase in boundary layer cloud while the conventional wisdom predicts the observed breakup of clouds. There are, however, important differences between the two scenarios that can explain the differing responses. The observed Lagrangian transition takes place in the context of a weakening trade inversion as SSTs increase while free tropospheric temperatures change relatively little, producing conditions more favorable to mixing or

entrainment of dry air into the boundary layer from the free troposphere. In contrast, the context of the climate change experiment is one where free tropospheric temperatures increase faster than those at the surface, increasing the strength of the inversion and inhibiting cloud-top entrainment. As we have shown, this increasing inversion strength can in itself be a consequence of a globally strengthening surface evaporation and hydrological cycle, which sets a very different context to the situation in which we observe the Lagrangian stratocumulus to trade cumulus transition. Hence while the two scenarios may seem superficially similar from the point of view of the surface evaporation increase, they are associated with opposite EIS changes. Therefore there is no inconsistency between the interpretations of these two scenarios.

We have also considered the possibility that HadGEM2-A shows an increase in low-level cloud in response to increasing surface-forced evaporation because it incorrectly captures the sign of the low cloud fraction response under the subtropical stratocumulus to trade cumulus transition. This is not the case; HadGEM2-A does show a reduction in low-level cloud fraction when forced with conditions representative of a subtropical marine low-level cloud transition from stratocumulus to fair-weather cumulus (Neggers 2015). HadGEM2-A also performs very well in reproducing observed relationships between variability in low cloud fraction, SST, and EIS (Qu et al. 2015b).

c. *Implications for understanding the hydrological sensitivity*

Our experiments also provide some new insights into the mechanisms that underlie the enhanced hydrological cycle in the warming climate. Many studies have pointed out that a change in the global mean radiative cooling of the atmosphere will result in an equivalent response in surface evaporation and precipitation, assuming that the sensible heat flux does not change substantially. For example, it has been shown that rapid precipitation adjustments in the absence of surface temperature change that occur in response to various atmospheric radiative forcings can be predicted accurately using offline radiation calculations that diagnose the effect of such radiative forcings in the atmospheric radiative heating (e.g., Andrews et al. 2010). In the case of radiative forcings (e.g., due to carbon dioxide or black carbon) we do not expect that changes in the hydrological cycle will affect the radiative forcings themselves. Hence we can say that in these cases the perturbation in the radiative heating of the atmosphere is a good predictor of the hydrological cycle response. In the somewhat different case of climate warming, however, previous studies are unclear on the degree to which changes in surface latent heat fluxes affect atmospheric radiative cooling. Here we show that increases in surface evaporation can have a very substantial impact on the rate of increase in radiative cooling itself with warming. We use our experiments to quantify the magnitude of this effect, and to explain how this dependence arises.

Figure 4d shows the changes in the main components of the global mean atmospheric energy budget, which sum to zero. If increases in surface evaporation with warming did not influence the radiative cooling, then we would expect to see the same radiative cooling response across the surface-forced experiments, and the increase in surface evaporation would have to be balanced by an equal and opposite decrease in the sensible heat flux. However, Fig. 4d indicates that the radiative cooling rate (indicated by the squares) increases by only a small amount ($0.6\,\mathrm{W\,m^{-2}\,K^{-1}}$) with warming when surface evaporation is held fixed in APEC4KSurfEvap0%, but increases progressively more with larger increases in surface evaporation in the surface-forced experiments by ($2.6\,\mathrm{W\,m^{-2}\,K^{-1}}$ in APEC4KSurfEvap3% and $4.9\,\mathrm{W\,m^{-2}\,K^{-1}}$ in APEC4KSurfEvap7%). The general agreement between the responses in the APEC4KSurfEvap3% experiment and standard APEC4K experiment suggests that the radiative cooling increases in APEC4K are to a substantial degree a consequence of the surface evaporation increases.

Our interpretation of this is as follows, and is summarized in Fig. 5 (blue arrows). As shown above, enhanced evaporation at the surface leads to enhanced free tropospheric warming (reduced lapse rate). This would be expected to contribute to the larger increase in the atmospheric longwave radiative cooling rate. This enhanced radiative cooling to space might be expected to be offset to some extent by increases in specific humidity, assuming that upper-tropospheric relative humidity does not change greatly (Ingram 2010). However, enhanced boundary layer specific humidity may also enhance atmospheric radiative cooling by increasing the longwave radiation emitted from the atmosphere to the surface (Pendergrass and Hartmann 2014). (Note the increase in near-surface specific humidity with increasing surface-forced evaporation shown in Fig. 4e). In the absence of substantial changes in surface sensible heat flux, a new tropospheric energy balance will be reached where the radiative cooling increases to a level that balances the enhanced net latent heat release in the atmosphere, and equivalently the enhanced surface latent heat flux.

The regression line for the surface-forced experiments shown in Fig. 4d indicates an increase in radiative cooling of $0.6\,\mathrm{W\,m^{-2}\,K^{-1}}$ with surface warming in the

absence of an increase in surface evaporation. The slope of the regression line indicates that the radiative cooling response increases by 0.66 $W m^{-2} K^{-1}$ per unit increase in hydrological sensitivity in the surface-forced experiments. Breaking this down into radiative heating components (not shown) indicates that the slope is mainly attributable to the clear-sky longwave component ($-0.65 W m^{-2} K^{-1}$), with $-0.1 W m^{-2} K^{-1}$ coming from changes at the top of the atmosphere and $-0.55 W m^{-2} K^{-1}$ at the surface. This suggests that the enhanced radiative cooling with increasing surface evaporation is primarily due to the impact of changes in the temperature and humidity structure of the atmosphere on the downwelling surface fluxes. This is consistent with the findings of Fläschner et al. (2016), who demonstrated that the net effect of changes in humidity and lapse rate in the lower troposphere with warming is to increase atmospheric radiative cooling.

Additionally the surface-forced evaporation experiments allow us to diagnose the dependence of near-surface humidity, air–sea temperature difference, and near-surface wind speed on changes in surface evaporation, by cutting the feedback loop that normally operates to bring them into balance as the climate warms. Similarly the APEC4KRadCool7% experiment allows us to see how these quantities respond to changes in radiative cooling while maintaining these two-way interactions near the surface. Together these experiments can inform our understanding of how changes in these near-surface properties respond to and at the same time influence changes in surface evaporation and radiative cooling.

The interactions discussed below are summarized in Fig. 5. The colors give an indication of the effects of increasing SST while holding surface evaporation fixed (orange, as in APEC4KSurfaceEvap0%), increasing surface evaporation (blue, as in APEC4KSurfaceEvap3% and APEC4KSurfaceEvap7%), and increasing radiative cooling (green, as in APEC4KRadCool7%). Figure 4f shows that near-surface relative humidity drops with climate warming when surface evaporation is held fixed but increases with increasing surface-forced evaporation. The near-surface relative humidity increases in the standard experiment, but less so in the radiative cooling experiment. The differences in these responses cannot be explained by changes in near-surface temperature; Fig. 4g shows changes in air-minus-sea temperature difference that, in the absence of changes in specific humidity, would be expected to have the opposite effect on near-surface relative humidity. (Note that surface temperatures increase by 4 K everywhere in our experiments, so differences in air–sea temperature responses between our experiments are solely due to differences in the near-surface temperature responses.) The reasons for the air–sea temperature responses will be discussed below, but for now we can conclude that the different responses in near-surface relative humidity are in the main due to differences in the responses of the near-surface specific humidity (Fig. 4e).

In general, near-surface specific humidity would be expected to be enhanced by increased surface evaporation but depleted by any enhanced vertical mixing by small-scale processes such as convection, turbulence, or resolved large-scale overturning (e.g., Sherwood et al. 2014). In the absence of increases in evaporation and assuming that other sink terms for near-surface specific humidity do not change appreciably, we might expect only small changes in near-surface specific humidity, and hence a drop in near-surface relative humidity with warming in the APEC4KSurfaceEvap0% experiment. The near-surface specific humidity actually does increase in the APEC4KSurfaceEvap0% experiment (Fig. 4e), but less than half as much as in the standard experiment, and not enough to maintain the same near-surface relative humidity with warming.

In the APEC4K, APEC4KSurfaceEvap3%, and APEC4KSurfaceEvap7% experiments, progressively larger increases in surface evaporation result in progressively stronger increases in near-surface specific and relative humidity. Increasing surface-forced evaporation results in progressively larger near-surface moistening rates from the boundary layer scheme, which distributes the surface evaporation in the vertical via turbulent mixing (Fig. 3c). The increasing near-surface relative humidity in response to increasing surface evaporation will provide a negative feedback on the surface evaporation and the hydrological sensitivity in the standard experiment.

Meanwhile, the APEC4KRadCool7% experiment shows slightly weaker increases in near-surface humidity than in APEC4K in spite of a stronger increase in surface evaporation (Figs. 4e,f) and the associated enhanced near-surface moistening rate from the boundary layer scheme (Fig. 3c). We attribute this to enhanced upward transport of near-surface humidity by convection in response to the enhanced radiative cooling. This is supported by Fig. 3d, which shows enhanced convective drying of the boundary layer in APEC4KRadCool7% compared to APEC4K. We argue that this enhanced convective drying reduces the near-surface humidity, resulting in an increase in surface evaporation, and a new balance where the surface evaporation–driven turbulent moistening rate increases to balance the enhanced convective drying rate. The weaker increase in near-surface humidity in the APEC4KRadCool7% experiment

compared to the standard APEC4K response is therefore part of the mechanism whereby the surface evaporation increases at a faster rate in the APEC4KRadCool7% experiment.

In APEC4KSurfaceEvap0% the global mean near-surface temperature increases less than the surface with warming, giving a small negative response in air-minus-sea temperature difference and an increase in the magnitude of the negative air–sea temperature difference (Fig. 4g). Our interpretation of this is as follows. Increasing the SST will initially increase the magnitude of the air–sea temperature difference, resulting in a large increase in the sensible heat flux. The near-surface air temperature will warm in response, providing a strong negative feedback on the sensible heat flux increase until a balance is reached with a smaller increase than initially. This is supported by Fig. 4d, which shows that the sensible heat flux does indeed increase slightly. This will increase the surface buoyancy flux and enhance the vertical sensible heat transport by the convection scheme. This is supported by the enhanced near-surface cooling seen in the convective heating rates in Fig. 3a in APEC4KSurfaceEvap0% (orange) compared to the APEC control (gray), and the increase in convective heating in the free troposphere. This in turn can explain the enhanced warming in the upper troposphere in APEC4KSurfaceEvap0% (orange) compared to APEC (gray) in Fig. 2c. The radiative cooling also increases slightly in the absence of an increase in surface evaporation (Fig. 4d), as would be expected given the increases in upper tropospheric temperatures. Increases in near-surface specific humidity are also present (Fig. 4e), but examination of the radiative cooling profile in Fig. 3b indicates that the radiative cooling is enhanced in the free troposphere rather than the boundary layer, suggesting that the enhanced upper tropospheric temperatures are the main cause in this case. In the case of the APEC4KSurfaceEvap0% experiment, tropospheric energy balance dictates that the changes in radiative cooling and sensible heat flux must balance each other. The interpretation above explains how the sensible heat flux and radiative cooling adjust to maintain tropospheric energy balance with warming in the case where surface evaporation cannot change.

With the surface evaporation increases in the APEC4K, APECSurfaceEvap3%, and APECSurfaceEvap7% experiments, the sign of the response of the air–sea temperature difference reverses compared to that in APEC4KSurfaceEvap0%, with the near-surface air temperature warming more than the surface, and the magnitude of the (negative) air–sea temperature difference reducing (Fig. 4g). Thus we can attribute the reduction in the magnitude of the air–sea temperature difference in the standard experiment to the effects of increasing surface evaporation. This, we argue, is a result of enhanced latent heat release in the boundary layer, which is supported by Fig. 3a, which shows reduced cooling from the convection scheme from the surface up to 1 km with increasing surface evaporation.

The air–sea temperature difference changes little with warming in the APEC4KRadCool7% experiment in contrast to the weakening in the magnitude of the air–sea temperature difference in the standard experiments. We attribute this to an enhanced near-surface cooling rate from the convection scheme in APEC4KRadCool7% compared to APEC4K (Fig. 3a), due to enhanced convection in response to the prescribed radiative cooling. The small change in the air–sea temperature difference in APEC4KRadCool7% compared to the reduction in magnitude in APEC4K will also contribute to the enhanced surface evaporation in APEC4KRadCool7%.

Additionally we note that responses in the sensible heat fluxes with warming (triangles in Fig. 4d) are broadly consistent with what would be expected from the changes in the air–sea temperature differences. The decreases of the sensible heat fluxes in response to increases in surface evaporation and radiative cooling cannot be explained by the changes in the near-surface wind speeds (Fig. 4h), which increase in both cases. Hence these responses can largely be explained in the same way as the air–sea temperature differences as outlined above. The increases in near-surface winds will offset these effects to some degree, but not by enough to change the signs of the responses. This means that the reduction in the global mean sensible heat flux with warming in the standard experiment is a direct consequence of the increasing surface evaporation.

Near-surface wind speeds increase slightly on average with warming in the standard experiments, more so in the APEC4KSurfaceEvap7% experiment, and even more so in the APEC4KRadCool7% experiment, while they reduce in the APEC4KSurfaceEvap0% experiment (Fig. 4h). The change in the global mean surface wind speed is well correlated with the change in the total radiative cooling (Fig. 4i). Our interpretation of this is that the atmospheric overturning circulation is enhanced by the progressively stronger radiatively driven subsidence in the subtropics. This effect will also contribute to the increased surface evaporation in APEC4KRadCool7%.

To quantify the impact of these changes in near-surface properties on the interactively diagnosed surface evaporation, we decompose the hydrological sensitivities in APEC4K and APEC4KRadCool7% into contributions from changes in SST, near-surface relative humidity, air-minus-sea temperature difference, and near-surface wind

TABLE 2. Decomposition of surface evaporation responses in APEC4K and APEC4KRadCool7% experiments.

$W m^{-2} K^{-1}$	APEC4K	APEC4KRadCool7%	APEC4KRadCool7%–APEC4K
Surface evaporation response	3.2	7.1	3.9
Predicted surface evaporation response	3.8	7.8	4.0
SST component	6.8	6.8	0.0
Near-surface relative humidity component	−2.0	−0.6	1.4
Air–sea temperature difference component	−0.8	−0.1	0.7
Near-surface wind speed component	−0.1	1.8	1.9

speed using the bulk formula for surface evaporation [see Eq. (1) of Richter and Xie 2008]. We use linear regression to estimate a bulk turbulent transfer coefficient suitable for use with local monthly mean values from the APEC experiment, and then use the bulk formula to predict the surface evaporation responses in the APEC4K and APEC4KRadCool7% experiments using local monthly mean values of SST and near-surface properties. Long-term averages of these predicted monthly values agree with the actual changes to within 10%–20%, while the difference in responses between APEC4KRadCool7% and APEC4K is predicted to within 3% (Table 2). The changes in surface evaporation can be decomposed into contributions from changes in SST and near-surface properties by repeating the calculations, adding changes in each property to the calculation in turn. These calculations (Table 2) show that the muted evaporation increase in the standard APEC4K experiment (weaker than the $7\% K^{-1}$ increase that would occur with surface warming in the absence of changes in near-surface relative humidity, wind speed, and air sea temperature difference) is primarily due to increases in near-surface relative humidity, but with a non-negligible contribution from increases in near-surface air temperature that reduces the magnitude of the air-minus-sea temperature difference. The additional surface evaporation in the APEC4KRadCool7% compared to APEC4K is primarily due to the enhanced near-surface winds, with a secondary contribution from the smaller increase in near-surface relative humidity, and a more modest contribution from the smaller reduction in magnitude of the air–sea temperature difference.

4. Summary and conclusions

We explore the impact of surface evaporation and hydrological sensitivity on cloud feedback by performing climate change experiments with the HadGEM2-A aquaplanet configuration where surface evaporation is forced to increase at different rates, ranging from 0% to $7\% K^{-1}$. We modify the surface evaporation response and global hydrological sensitivity first by specifying the evaporation rate at the surface, and second by adding an artificial radiative cooling term in the atmosphere.

Forcing the evaporation to increase at $7\% K^{-1}$ in the surface scheme in a uniform +4-K SST perturbed experiment results in a negative global cloud feedback and an increase in global low cloud fraction, reversing the signs of these responses compared to those in the standard model configuration. Conversely, the equivalent experiment with surface evaporation held fixed strongly increases the magnitudes of the global mean low-level cloud reduction and positive cloud feedback. In these experiments, the estimated inversion strength (EIS, a measure of the lower tropospheric stability) increases proportionally with the surface evaporation, due to enhanced free tropospheric warming in response to additional latent heat release. We argue that this enhanced stabilization of the tropics results in a progressively more negative low cloud feedback with increasing surface-forced evaporation, via the well-established effect of lower tropospheric stability on low cloud fraction. Hence our results demonstrate that modifying surface evaporation and global hydrological sensitivity can have a substantial impact on the global low cloud feedback in a climate model, on a larger scale than the local dependence on surface evaporation demonstrated by Webb and Lock (2013).

Additionally we force the surface evaporation to increase at $7\% K^{-1}$ by enhancing the rate at which atmospheric radiative cooling increases with warming. In contrast to the surface-forced evaporation increase, this reduces the free tropospheric warming, which weakens the increase in EIS and slightly strengthens the low-level cloud reduction and the positive cloud feedback relative to the standard experiments. Hence very different cloud feedbacks can arise in experiments with similar hydrological sensitivities and changes in surface evaporation. This indicates that surface evaporation is not the sole control on cloud feedback. Across all of the experiments performed, EIS is a better predictor of low cloud feedback than surface evaporation. This suggests that surface-forced increases in evaporation act to increase low cloud fraction mainly by increasing EIS. As such, our results also emphasize the important role that the

free tropospheric temperature response and the lower tropospheric stability play in low cloud feedback.

Although the main emphasis of this work is on understanding the role of changing surface evaporation on low cloud fraction feedback, it is interesting to note that it is in the absence of a surface evaporation increase that the strongest low cloud reductions are seen. Substantial low cloud reductions are also seen in the radiative cooling forced experiment, in the absence of substantial changes in EIS. We do not explore the reasons for this further here, but note that experiments where surface evaporation increases are prevented or where radiative cooling is perturbed may be a useful vehicle for future investigation of the mechanisms responsible for breaking up low cloud as the climate warms. Such experiments may help to separate positive cloud feedback mechanisms from negative cloud feedback mechanisms associated with increases in surface evaporation and EIS across cloud regimes, complementing existing approaches that have been used to separate competing terms statistically in specific cloud regimes (e.g., Qu et al. 2015b). It should be noted, however, that such experiments may not perfectly separate positive and negative feedbacks.

Intermodel differences in the strength of negative low cloud feedback mechanisms may also contribute substantially to the overall spread in cloud feedback, in addition to the contribution from positive mechanisms. As such, intermodel differences in hydrological sensitivity may also contribute to intermodel spread in cloud feedback. Quantifying the extent to which positive low cloud feedback mechanisms are offset by negative cloud feedback mechanisms such as those demonstrated here may be a necessary step toward to understanding why low cloud feedbacks are positive in models generally, and the extent to which this is true in nature.

Our experiments also provide new insights into the mechanisms underlying the hydrological sensitivity. Many studies have pointed out that a change in the global mean radiative cooling of the atmosphere will result in an equivalent response in surface evaporation and precipitation, assuming that the sensible heat flux does not change substantially, for example in the case of rapid precipitation adjustments that occur following increases in carbon dioxide before substantial surface warming occurs. In the somewhat different case of climate warming, however, our results show that increases in surface evaporation can have a very substantial impact on the rate of increase in radiative cooling. Increasing surface evaporation with surface warming modifies the atmospheric temperature and humidity structure, substantially increasing the radiative cooling. Conversely, holding surface evaporation fixed with warming yields only a small increase in atmospheric radiative cooling. Hence, while models' different hydrological sensitivities can usefully be interpreted using offline radiative decomposition methods (e.g., Pendergrass and Hartmann 2014; DeAngelis et al. 2015; Fläschner et al. 2016), it should be kept in mind that the inputs to such radiative calculations (e.g., the profiles of the atmospheric temperature and humidity changes) are themselves substantially affected by the rate of surface evaporation increase, and hence the hydrological sensitivity.

We also show that near-surface relative humidity decreases with warming in the absence of increasing surface evaporation, and hence that the increasing near-surface relative humidity in our standard experiments is a direct consequence of increasing surface evaporation. This provides a negative feedback on the surface evaporation and the hydrological sensitivity. Reductions in the magnitude of the air–sea temperature difference and the surface sensible heat flux with warming are also a consequence of the increasing surface evaporation; our results suggest that this is due to enhanced near-surface warming associated with additional latent heat release in the boundary layer. This effect also provides a negative feedback on the hydrological sensitivity. Meanwhile, artificially enhancing the radiative cooling increase which accompanies surface warming reduces the magnitude of near-surface increases in relative humidity by enhancing the rate at which convection removes humidity from the boundary layer. Similarly enhanced removal of heat from the boundary layer by convection increases the air–sea temperature difference. The additional radiative cooling also increases near-surface wind speeds, presumably by enhancing radiatively forced subsidence. These effects explain how the surface evaporation increases to balance an externally imposed radiative cooling of the atmosphere.

It is widely appreciated that increases in near-surface relative humidity will act to damp increases in surface evaporation, while increases in the magnitude of air–sea temperature differences and near-surface wind speeds will act to enhance it. Our results also demonstrate, however, that the responses in the factors controlling the surface evaporation (such as near-surface relative humidity, wind speed, and air–sea temperature differences) are affected not only by radiative cooling but also by changes in surface evaporation itself. We argue that the hydrological sensitivity will ultimately be determined by the point at which various interacting responses in near-surface relative humidity and wind speed, air–sea temperature difference, surface evaporation, sensible heat fluxes, and radiative cooling come

into a new balance following a given surface warming. This means that a full understanding of the mechanisms controlling hydrological sensitivity differences in models will require a better appreciation of these various interdependent responses. These insights may help to improve our understanding of the factors controlling hydrological sensitivity in the future.

Acknowledgments. We are grateful to Tim Andrews, Chris Bretherton, Paulo Ceppi, William Ingram, Jonathan Gregory, Steve Klein, Angeline Pendergrass, Mark Ringer, Jack Scheff, Graeme Stephens, and Alison Stirling for useful discussions about this work. We would also like to acknowledge Yoko Tsushima and Rachel Stratton for help in calculating APE APEC SST forcings, and Alison Stirling for providing code to calculate saturated adiabats. We are also grateful to Karen Shell and two anonymous reviewers for comments that helped us to improve this paper. Mark Webb was supported by the Joint UK BEIS/Defra Met Office Hadley Centre Climate Programme (GA01101).

REFERENCES

Andrews, T., P. M. Forster, O. Boucher, N. Bellouin, and A. Jones, 2010: Precipitation, radiative forcing and global temperature change. *Geophys. Res. Lett.*, **37**, L14701, https://doi.org/10.1029/2010GL043991.

Blossey, P. N., and Coauthors, 2013: Marine low cloud sensitivity to an idealized climate change: The CGILS LES intercomparison. *J. Adv. Model. Earth Syst.*, **5**, 234–258, https://doi.org/10.1002/jame.20025.

Boucher, O., and Coauthors, 2013: Clouds and aerosols. *Climate Change 2013: The Physical Science Basis*, T. F. Stocker et al., Eds. Cambridge University Press, 571–657.

Bretherton, C. S., and M. C. Wyant, 1997: Moisture transport, lower-tropospheric stability, and decoupling of cloud-topped boundary layers. *J. Atmos. Sci.*, **54**, 148–167, https://doi.org/10.1175/1520-0469(1997)054<0148:MTLTSA>2.0.CO;2.

——, and P. N. Blossey, 2014: Low cloud reduction in a greenhouse-warmed climate: Results from Lagrangian LES of a subtropical marine cloudiness transition. *J. Adv. Model. Earth Syst.*, **6**, 91–114, https://doi.org/10.1002/2013MS000250.

——, ——, and C. R. Jones, 2013: Mechanisms of marine low cloud sensitivity to idealized climate perturbations: A single-LES exploration extending the CGILS cases. *J. Adv. Model. Earth Syst.*, **5**, 316–337, https://doi.org/10.1002/jame.20019.

Brient, F., and S. Bony, 2013: Interpretation of the positive low-cloud feedback predicted by a climate model under global warming. *Climate Dyn.*, **40**, 2415–2431, https://doi.org/10.1007/s00382-011-1279-7.

——, T. Schneider, Z. Tan, S. Bony, X. Qu, and A. Hall, 2016: Shallowness of tropical low clouds as a predictor of climate models' response to warming. *Climate Dyn.*, **47**, 433–449, https://doi.org/10.1007/s00382-015-2846-0.

DeAngelis, A. M., X. Qu, M. D. Zelinka, and A. Hall, 2015: An observational radiative constraint on hydrologic cycle intensification. *Nature*, **528**, 249–253, https://doi.org/10.1038/nature15770.

Fläschner, D., T. Mauritsen, and B. Stevens, 2016: Understanding the intermodel spread in global-mean hydrological sensitivity. *J. Climate*, **29**, 801–817, https://doi.org/10.1175/JCLI-D-15-0351.1.

Held, I. M., and B. J. Soden, 2006: Robust responses of the hydrological cycle to global warming. *J. Climate*, **19**, 5686–5699, https://doi.org/10.1175/JCLI3990.1; Corrigendum, **24**, 1559–1560, https://doi.org/10.1175/2010JCLI4045.1.

Ingram, W., 2010: A very simple model for the water vapour feedback on climate change. *Quart. J. Roy. Meteor. Soc.*, **136**, 30–40, https://doi.org/10.1002/qj.546.

Jones, C. R., C. S. Bretherton, and P. N. Blossey, 2014: Fast stratocumulus time scale in mixed layer model and large eddy simulation. *J. Adv. Model. Earth Syst.*, **6**, 206–222, https://doi.org/10.1002/2013MS000289.

Lambert, F. H., and M. J. Webb, 2008: Dependency of global mean precipitation on surface temperature. *Geophys. Res. Lett.*, **35**, L16706, https://doi.org/10.1029/2008GL034838.

Martin, G. M., and Coauthors, 2011: The HadGEM2 family of Met Office Unified Model climate configurations. *Geosci. Model Dev.*, **4**, 723–757, https://doi.org/10.5194/gmd-4-723-2011.

Medeiros, B., B. Stevens, and S. Bony, 2015: Using aquaplanets to understand the robust responses of comprehensive climate models to forcing. *Climate Dyn.*, **44**, 1957–1977, https://doi.org/10.1007/s00382-014-2138-0.

Mitchell, J. F. B., C. A. Wilson, and W. M. Cunnington, 1987: On CO_2 climate sensitivity and model dependence of results. *Quart. J. Roy. Meteor. Soc.*, **113**, 293–322, https://doi.org/10.1002/qj.49711347517.

Neale, R. B., and B. J. Hoskins, 2000: A standard test for AGCMs including their physical parametrizations: I: The proposal. *Atmos. Sci. Lett.*, **1**, 101–107, https://doi.org/10.1006/asle.2000.0022.

Neggers, R. A. J., 2015: Attributing the behavior of low-level clouds in large-scale models to subgrid-scale parameterizations. *J. Adv. Model. Earth Syst.*, **7**, 2029–2043, https://doi.org/10.1002/2015MS000503.

Pendergrass, A. G., and D. L. Hartmann, 2014: The atmospheric energy constraint on global-mean precipitation change. *J. Climate*, **27**, 757–768, https://doi.org/10.1175/JCLI-D-13-00163.1.

Qu, X., A. Hall, S. A. Klein, and P. M. Caldwell, 2015a: The strength of the tropical inversion and its response to climate change in 18 CMIP5 models. *Climate Dyn.*, **45**, 375–396, https://doi.org/10.1007/s00382-014-2441-9.

——, ——, ——, and A. M. DeAngelis, 2015b: Positive tropical marine low-cloud cover feedback inferred from cloud-controlling factors. *Geophys. Res. Lett.*, **42**, 7767–7775, https://doi.org/10.1002/2015GL065627.

Richter, I., and S.-P. Xie, 2008: Muted precipitation increase in global warming simulations: A surface evaporation perspective. *J. Geophys. Res.*, **113**, D24118, https://doi.org/10.1029/2008JD010561.

Rieck, M., L. Nuijens, and B. Stevens, 2012: Marine boundary layer cloud feedbacks in a constant relative humidity atmosphere. *J. Atmos. Sci.*, **69**, 2538–2550, https://doi.org/10.1175/JAS-D-11-0203.1.

Ringer, M. A., T. Andrews, and M. J. Webb, 2014: Global-mean radiative feedbacks and forcing in atmosphere-only and coupled atmosphere–ocean climate change experiments. *Geophys. Res. Lett.*, **41**, 4035–4042, https://doi.org/10.1002/2014GL060347.

Senior, C. A., and J. F. B. Mitchell, 1993: Carbon dioxide and climate. The impact of cloud parameterization. *J. Climate*, **6**, 393–418, https://doi.org/10.1175/1520-0442(1993)006<0393:CDACTI>2.0.CO;2.

Sherwood, S. C., S. Bony, and J.-L. Dufresne, 2014: Spread in model climate sensitivity traced to atmospheric convective mixing. *Nature*, **505**, 37–42, https://doi.org/10.1038/nature12829.

Sobel, A. H., J. Nilsson, and L. M. Polvani, 2001: The weak temperature gradient approximation and balanced tropical moisture waves. *J. Atmos. Sci.*, **58**, 3650–3665, https://doi.org/10.1175/1520-0469(2001)058<3650:TWTGAA>2.0.CO;2.

Vial, J., S. Bony, J.-L. Dufresne, and R. Roehrig, 2016: Coupling between lower-tropospheric convective mixing and low-level clouds: Physical mechanisms and dependence on convection scheme. *J. Adv. Model. Earth Syst.*, **8**, 1892–1911, https://doi.org/10.1002/2016MS000740.

Webb, M. J., and A. P. Lock, 2013: Coupling between subtropical cloud feedback and the local hydrological cycle in a climate model. *Climate Dyn.*, **41**, 1923–1939, https://doi.org/10.1007/s00382-012-1608-5.

Wood, R., and C. S. Bretherton, 2006: On the relationship between stratiform low cloud cover and lower-tropospheric stability. *J. Climate*, **19**, 6425–6432, https://doi.org/10.1175/JCLI3988.1.

Wyant, M. C., C. S. Bretherton, H. A. Rand, and D. E. Stevens, 1997: Numerical simulations and a conceptual model of the stratocumulus to trade cumulus transition. *J. Atmos. Sci.*, **54**, 168–192, https://doi.org/10.1175/1520-0469(1997)054<0168:NSAACM>2.0.CO;2.

Zhang, M., and Coauthors, 2013: CGILS: Results from the first phase of an international project to understand the physical mechanisms of low cloud feedbacks in single column models. *J. Adv. Model. Earth Syst.*, **5**, 826–842, https://doi.org/10.1002/2013MS000246.

JAMES | Journal of Advances in Modeling Earth Systems

RESEARCH ARTICLE
10.1029/2019MS001999

Testing a Physical Hypothesis for the Relationship Between Climate Sensitivity and Double-ITCZ Bias in Climate Models

Mark J. Webb[1] **and Adrian P. Lock**[1]

[1]Met Office Hadley Centre, Exeter, UK

Key Points:
- We propose a mechanism for the Tian (2015, https://doi.org/10.1002/2015GL064119) finding that climate models with stronger double-ITCZ biases tend to have lower climate sensitivities
- We hypothesize that deep convection encroaching into low-cloud regions disrupts low clouds and diminishes positive low-cloud feedbacks
- Our hypothesized relationships are found in experiments with a single model, but not all are statistically significant across models

Correspondence to:
M. J. Webb,
mark.webb@metoffice.gov.uk

Citation:
Webb, M. J., & Lock, A. P. (2020). Testing a physical hypothesis for the relationship between climate sensitivity and double-ITCZ bias in climate models. *Journal of Advances in Modeling Earth Systems*, *12*, e2019MS001999. https://doi.org/10.1029/2019MS001999

Received 28 DEC 2019
Accepted 2 AUG 2020
Accepted article online 10 AUG 2020

Abstract Tian (2015, https://doi.org/10.1002/2015GL064119) found that Coupled Model Intercomparison Project Phases 3 and 5 (CMIP3 and CMIP5) climate models with too much precipitation in a region of the Southeast Pacific (due to a double-Intertropical Convergence Zone [ITCZ] bias) tend to have lower climate sensitivities and suggested that this might form the basis of an "emergent constraint," which could rule out lower values of climate sensitivity. However, no physical mechanism has been proposed to explain this relationship. Here we advance the hypothesis that deep convection encroaching into regions that should be dominated by shallow clouds hampers the formation of shallow clouds in the present climate and reduces the magnitude of positive low-level cloud feedbacks, resulting in smaller values of climate sensitivity. We test this hypothesis first by performing sensitivity tests with the HadGEM2-A aquaplanet model subject to a uniform +4 K sea surface temperature (SST) perturbation, in which we vary the degree to which deep convection associated with the single/double ITCZ extends toward subtropical low-cloud regions. Experiments with more precipitation encroaching into the subtropics have weaker subtropical cloud radiative effects in the present-day simulations and less positive subtropical cloud feedbacks, consistent with our hypothesis. We test this hypothesis further by looking for the predicted relationships across multimodel ensembles of SST forced Atmospheric Model Intercomparison Project (AMIP) experiments subject to a uniform +4 K SST increase. Relationships of the expected sign are found in the CMIP5 AMIP+4K experiments, but not all are statistically significant at the 5% level. We find no statistically significant support for our hypothesis in the currently available CMIP6 AMIP+4K experiments.

Plain Language Summary A previous study found that climate models with too much heavy rainfall extending from the tropics into the Southeast Pacific tend to have smaller amounts of global warming in response to increases in carbon dioxide. It has been suggested that this might mean that climate models that are more sensitive are more realistic. However, it is unclear what physical processes in the climate system might cause such a relationship. Here we propose a potential explanation for this relationship that heavy rainfall extending into regions that should be dominated by low-level clouds is associated with conditions that make it harder to form low-level clouds, which are known to amplify climate warming. We test this idea using two approaches. Modifying a single climate model to vary the degree to which heavy rainfall spreads out into low-cloud regions reproduces the expected relationships. However, examination of a larger set of models shows that not all parts of the suggested explanation are supported at a statistically significant level. Furthermore, no elements of our proposed explanation are supported at a statistically significant level in a newer set of models.

1. Introduction

Equilibrium climate sensitivity (ECS) is a basic measure of the sensitivity of the climate system to increases in carbon dioxide concentrations, defined as the equilibrium change in the annual global mean near-surface temperature following a doubling of atmospheric CO_2 concentration (Collins et al., 2013). Modern climate models with dynamical oceans are rarely run to equilibrium, and so climate sensitivity is often estimated using effective climate sensitivity, hereafter S (e.g., Andrews et al., 2012). Models from the last phase of the Coupled Model Intercomparison Project Phase 5 (CMIP5, Taylor et al., 2012) took a range of values for S from 2.1–4.7 K (Collins et al., 2013). The AR5 assessment report concluded that ECS was *likely* (>66% probability) in the range 1.5–4.5 K, *very unlikely* (<10% probability) >6 K, *and extremely unlikely* (<5% probability) <1 K. Cloud feedbacks remain the largest source of uncertainty for ECS, and uncertainty in the sign and magnitude

of the cloud feedback is due primarily to continuing uncertainty in the impact of warming on low clouds. Although a highly idealized quantity, S is a strong predictor of the diverse model responses in global and regional temperature in transient and equilibrium climate change scenarios (Grose et al., 2018).

Since AR5, an increasing number of studies have attempted to constrain S using so-called "emergent constraints." An emergent constraint can be defined as a relationship between something we can observe and something we want to predict which emerges from a model ensemble. Since correlations between unrelated variables may arise by chance, it is considered desirable for emergent constraints to be associated with credible physical mechanisms (Klein & Hall, 2015). Caldwell et al. (2018) assessed a number of emergent constraints against this criterion amongst others. One such emergent constraint study Tian (2015) found a robust statistical relationship between S and an index measuring the extent of double-Intertropical Convergence Zone (ITCZ) biases in CMIP3 and CMIP5 models. This indicated that models that have too much precipitation in a region of the Southeast Pacific (which is indicative of a double-ITCZ error) tend to have lower climate sensitivities, while models with smaller biases tend to have higher sensitivities. A weaker relationship was also found between subtropical free-tropospheric specific humidity and S. Taken at face value, these relationships suggest that S is greater than 3 K, which rules out models in the lower half of the AR5 1.5–4.5 likely range. However no physical hypothesis has yet been put forward to explain why such a relationship should exist between such measures of the double-ITCZ and S. The aim of this study is to develop and test a physical hypothesis that has the potential to explain this relationship seen in the CMIP3 and CMIP5 models.

Given the substantial contribution of low-level cloud feedbacks to the intermodel spread in cloud feedback and climate sensitivity, an obvious possibility is that low-cloud feedbacks are in some way dependent on the strength of the double-ITCZ bias in models. The extent to which deep convection encroaches into the subtropics will affect the free-tropospheric humidity, with a more double-ITCZ having a moister subtropical free troposphere as shown by Tian (2015). This could in principle affect subtropical low-cloud feedbacks. For example, Christensen et al. (2013) argued that increases in water vapor expected with global warming would cause a reduction in low-cloud-top cooling rates that could cause stratocumulus to thin and breakup, as suggested by their results and the Large Eddy Simulation (LES) results of Bretherton et al. (2013). However, while Tian (2015) showed that an index of midtropospheric humidity was strongly correlated with their Southeast Pacific precipitation index, the midtropospheric humidity index was less strongly correlated with S than the precipitation index. This suggests that the relationship between Southeast Pacific precipitation and S is not mediated by free tropospheric humidity.

A stronger double-ITCZ may also increase the amount of free-tropospheric cloud overlying subtropical low clouds. A number of studies have suggested that upper-level clouds can affect low-level clouds directly below them. Christensen et al. (2013) showed using satellite observations and LES models that the effects of free tropospheric clouds on downwelling longwave radiation can affect the vertical development and thickness of stratocumulus clouds by reducing their cloud-top cooling, although competing effects were present due to the shortwave effects of overlying clouds during the daytime. Bony et al. (2016) made a thermodynamic argument to explain reductions in upper-level cloud amount with warming in climate models and suggested that associated reductions in the downward longwave radiation at the top of low-level clouds could increase low-cloud cover. Additionally, they suggested that a reduction in anvil clouds could expose more of the climate system to the effects of positive feedbacks from low clouds. Coppin and Bony (2015) also argued that increased convective aggregation will expand the area covered by large-scale subsidence; this could have a similar effect. Also Coppin and Bony (2017) showed that increasing subsidence with convective aggregation increased low-level cloudiness in a climate model.

We advance the following hypothesis to explain the link between double-ITCZ and climate sensitivity, which has three components. First, models with double-ITCZs will have more deep convection encroaching into subtropical low-cloud regions. Second, because of this, it will be harder for models to form low-level clouds in subtropical subsidence cloud regions. Third, models with fewer low-level clouds will have weaker/less positive low-cloud feedbacks and higher climate sensitivities. Tian (2015) already provides evidence to support the first component of this argument. The second component is motivated by the observation that low clouds are prevalent in subtropical regions associated primarily with strong subsidence, a dry free troposphere and strong low-level temperature inversions, conditions that are incompatible with the primarily unstable conditions associated with deep convection and heavy precipitation seen in the ITCZ and South

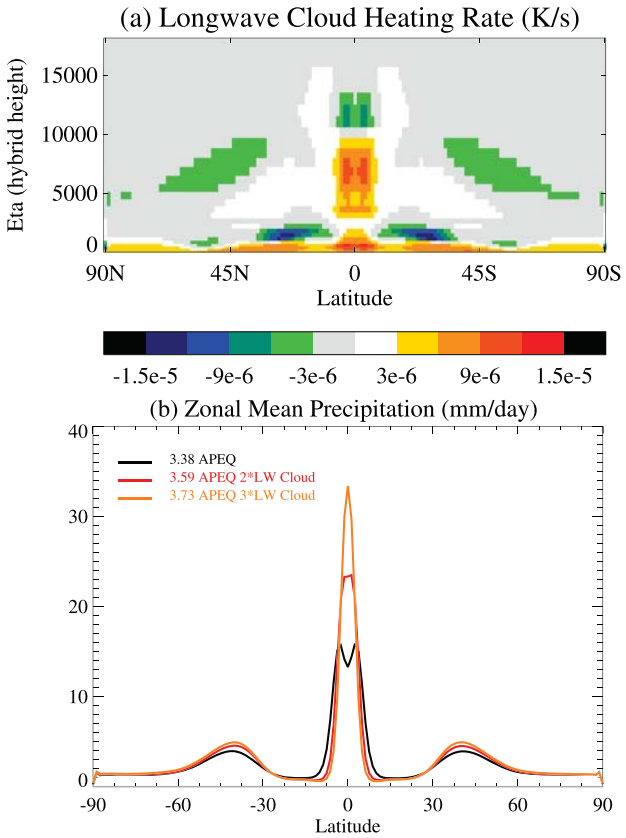

Figure 1. Zonal mean longwave cloud heating rate (a) and precipitation (b) from the aquacontrol simulation of HadGEM2-A APEQ and sensitivity tests where the longwave cloud heating rate is approximately doubled and tripled. Global mean values are shown in the legend.

Pacific Convergence Zone (SPCZ). The third component is supported by existing studies with models such as Williams and Webb (2009), Brient and Bony (2012), and Webb et al. (2015).

We test this hypothesis in two ways. First, we perform sensitivity tests in the aquaplanet configuration of the HadGEM2-A climate model, where we vary the degree to which deep convection encroaches toward subtropical low-cloud regions to see if this has the effect predicted by our hypothesis on subtropical low clouds and cloud feedbacks in perturbed sea surface temperature (SST) experiments. Second, we perform a regional correlation analysis to see if the predicted relationships are present in two multimodel ensembles of SST forced climate change experiments.

This paper is organized as follows. Section 2 describes the HadGEM2-A aquaplanet experiments and the method we employ to perturb the degree of the double-ITCZ and gauge the impact on the cloud feedbacks. Section 2 also describes the multimodel ensembles that we analyze. Section 3 presents and discusses the results from these experiments and our investigation of statistical relationships across CMIP5 and CMIP6 era atmosphere-only experiments subject to a uniform SST increase. Section 4 presents a summary and concluding remarks.

2. Model Experiments and Methods

We test our hypothesis first by perturbing the ITCZ in the Cloud Feedback Model Intercomparison Project (CFMIP)-2/CMIP5 aquaplanet configuration of HadGEM2-A (Martin et al., 2011). The CFMIP +4 K aquaplanet configuration has been shown to reproduce global cloud feedbacks in fully coupled model configurations to a remarkable degree (Medeiros et al., 2015; Ringer et al., 2014). Aquaplanet simulations such as these produce a zonally symmetric idealized representation of the ITCZ and subtropical shallow cloud regions, where the degree to which the ITCZ splits and deep convection encroaches into the subtropics

Table 1
Models Used in This Study

Model	Project	Reference
BCC-CSM1.1	CFMIP-2/CMIP5	Wu et al. (2014)
CanAM4	CFMIP-2/CMIP5	Von Salzen et al. (2013)
CESM1-CAM5-FV2	SPOOKIE	Neale et al. (2010) and Webb et al. (2015)
CNRM-CM5	CFMIP-2/CMIP5	Martin et al. (2011)
GFDL-HIRAM	SPOOKIE	Zhao et al. (2009) and Webb et al. (2015)
GFDL-AM2	SPOOKIE	GFDL GAMDT (2004) and Webb et al. (2015)
HadGEM2-A	CFMIP-2/CMIP5	Martin et al. (2011)
IPSL-CM5A-LR	CFMIP-2/CMIP5	Dufresne et al. (2013)
IPSL-CM5B-LR	CFMIP-2/CMIP5	Dufresne et al. (2013)
MIROC5	CFMIP-2/CMIP5	Watanabe et al. (2010)
MRI-CGCM3	CFMIP-2/CMIP5	Yukimoto et al. (2012)
MPI-ESM-LR	CFMIP-2/CMIP5	Stevens et al. (2013)
BCC-CSM2-MR	CFMIP-3/CMIP6	Wu et al. (2019)
CanESM5	CFMIP-3/CMIP6	Swart et al. (2019)
CESM2	CFMIP-3/CMIP6	Gettelman et al. (2019)
CNRM-CM6-1	CFMIP-3/CMIP6	Voldoire et al. (2019)
GFDL-CM4	CFMIP-3/CMIP6	Held et al. (2019)
HadGEM3-GC3.1-LL	CFMIP-3/CMIP6	Kuhlbrodt et al. (2018)
IPSL-CM6A-LR	CFMIP-3/CMIP6	Boucher et al. (2020)
MIROC6	CFMIP-3/CMIP6	Tatebe et al. (2019)
MRI-ESM2.0	CFMIP-3/CMIP6	Yukimoto et al. (2019)
GISS-E2-1-G	CFMIP-3/CMIP6	Not available

may vary depending on the model formulation. While we do not consider the characteristics of the ITCZ in an aquaplanet experiment to be a perfect analog or limiting case for the extension of the SPCZ and the double-ITCZ bias in realistic model configurations, we do consider aquaplanets a useful, idealized configuration for exploring the effects of deep convection encroaching into subtropical subsidence zones. As such we consider these experiments to be a useful vehicle for testing the physical credibility of our hypothesis.

Many theories have been put forward to explain the controls on the degree of ITCZ splitting in aquaplanets (e.g., Dixit et al., 2018; Harrop & Hartmann, 2016). Harrop and Hartmann (2016) showed that aquaplanet configurations of models tend to show more of a double-ITCZ when cloud radiative effects (CREs) are suppressed. This has been shown to be due to the atmospheric longwave cloud heating effect from middle- to high-level clouds in the tropics (Dixit et al., 2018) rather than the atmospheric cooling effects of subtropical low clouds (Fermepin & Bony, 2014). We exploit this fact to manipulate the ITCZ in HadGEM2-A. Figure 1b shows the zonal mean precipitation in the HadGEM2-A CFMIP-2 standard aquaplanet configuration (APEQ), based on the "QOBS" configuration of the Aqua-Planet Experiment Project (Blackburn et al., 2013) (black line). This exhibits a moderately bimodal/double ITCZ, as evidenced by the two local maxima in the zonal mean precipitation on either side of the equator. For our first sensitivity experiment (2XLWCLOUD) we approximately double the longwave cloud heating by adding an additional heating to the longwave radiative heating in the model, based on the zonal mean climatological longwave cloud heating rate in the control experiment (Figure 1a). In a second experiment (3XLWCLOUD) we double the size of this perturbation. We then run climate change experiments with these two perturbed model configurations, by uniformly increasing SSTs by 4 K, for comparison with the standard CFMIP aquacontrol and aqua4K experiments. All experiments are run for 5 years each. We diagnose cloud feedback using the change in the net CRE per K change in global mean SST, noting that this includes the climatological effects of clouds on noncloud feedbacks (Soden et al., 2004; Yoshimori et al., 2019).

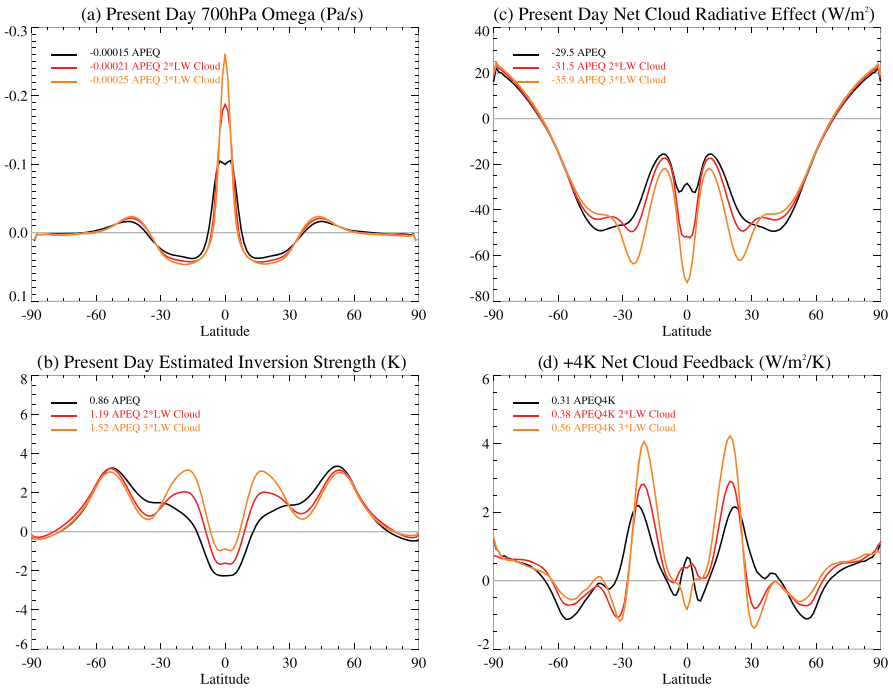

Figure 2. As Figure 1b but (a) 700 hPa pressure velocity, (b) estimated inversion strength, (c) net CRE, and (d) Net CRE feedback component. Global mean values are shown in the legend.

Second, we look for relationships predicted by our hypothesis in SST forced experiments subject to uniform +4 K warming from CFMIP-2/CMIP5 (Bony et al., 2008), SPOOKIE (Selected Process On/Off Klima Intercomparison Project, Webb et al., 2015), and CFMIP-3/CMIP6 (Webb et al., 2017) (see Table 1). One reason to use SST forced experiments is that we can diagnose regional cloud feedbacks without needing to resort to linear regression approaches and their associated uncertainties (e.g., Gregory et al., 2004).

3. Results and Discussion

3.1. ITCZ Perturbation Experiments

Here we test the physical credibility of our hypotheses by performing sensitivity experiments with the aquaplanet configuration of HadGEM2-A (see section 2). Figure 1b shows that scaling up the longwave cloud radiative heating in the aquaplanet configuration of HadGEM2-A results in a narrower/less double-ITCZ as expected, with reductions in precipitation on the subtropical flanks of the ITCZ, a transition from a bimodal to unimodal ITCZ, and an increase in the peak precipitation rate. The area encompassed by mean ascent at 700 hPa in the ITCZ also contracts, while the area of mean subsidence expands toward the equator (Figure 2a). The peak ascent rate increases in the ITCZ, as does the maximum subsidence rate in the subtropics. A more concentrated ITCZ is also associated with a stronger subtropical inversion as measured by the estimated inversion strength (EIS) index (Wood & Bretherton, 2006) (Figure 2b). Again, the largest changes are on the equatorward flank of the subtropics. Since the SSTs are the same in these experiments, the increase in EIS is caused by increases in temperatures at 700 hPa. We argue that this may in part be a response to enhanced subsidence warming in the subtropics and also to some extent to increased longwave radiative heating at 700 hPa in the subtropics (Figure 2a) and also to radiative heating in the ITCZ, which is propagated into the subtropics by gravity waves. The increase in EIS in the subtropics is associated with an increase in the net radiative cooling effect of subtropical clouds (Figure 2c), consistent with the expectation that cloud fraction and/or liquid water path will increase with EIS (Wood & Bretherton, 2006). These more reflective clouds are in turn associated with more positive subtropical cloud feedbacks, which in turn enhance the global mean cloud feedbacks (Figure 2d).

Looking across these experiments, we see that model versions with more precipitation encroaching into the subtropics have weaker subtropical CREs in the present climate, less positive subtropical cloud feedbacks,

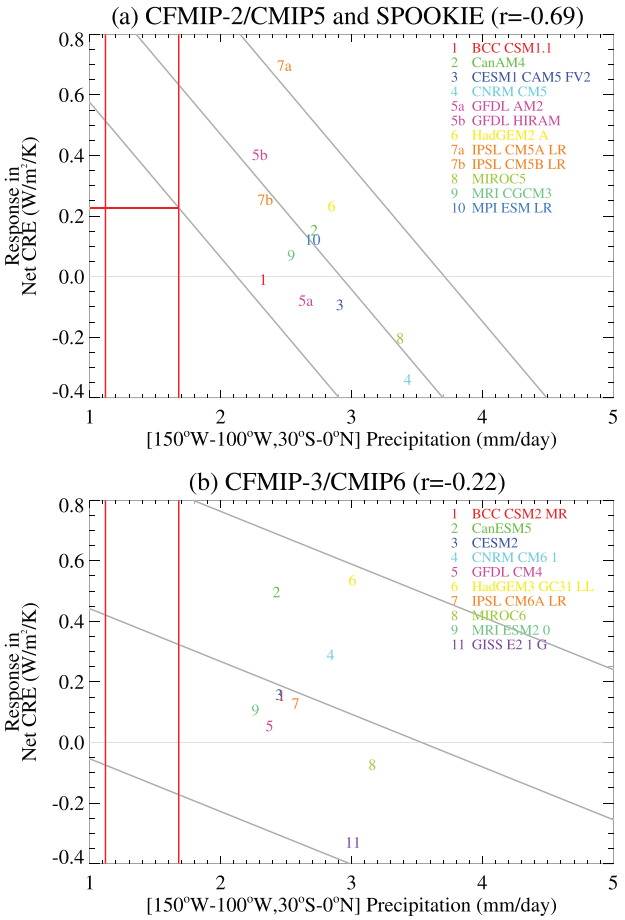

Figure 3. (a) Emergent constraint on cloud feedback in AMIP+4K experiments arising from models' Southeast Tropical Pacific precipitation versus GPCP over the region (150–100°W, 30°S to 0°N). The central gray line shows the best linear fit to the data, and the upper and lower lines are plotted at ±2 standard deviations of the residuals in the *y* direction. The vertical lines indicate the observed precipitation rate from GPCP (1.4 mm/day) ±20% (Qu et al., 2018), and the horizontal red line indicates the notional implied lower bound for the net CRE feedback.

and less positive global cloud feedbacks. These results are consistent with our hypothesis and suggest that, all other things being the same, models with more precipitation encroaching into the subtropics will have lower climate sensitivities. As such these results are consistent with our hypothesis being a plausible physical explanation for the Tian (2015) result.

3.2. CMIP5/CMIP6 AMIP+4K Analysis

Next, we perform a correlation analysis to see if the relationships predicted by our hypothesis are present in two multimodel ensembles of SST forced climate change experiments. Our argument is based on mechanisms operating in the atmosphere and does not depend on or require changes in SST patterns or ocean heat transport with climate change. Ringer et al. (2014) showed that cloud feedbacks from the CMIP5 coupled models are reproduced remarkably well in CFMIP-2/CMIP5 SST forced experiments subject to a uniform SST increase of 4 K, which suggests that intermodel spread in cloud feedback in the CMIP5 models is not strongly dependent on SST warming patterns or changes in ocean circulation. To confirm that intermodel differences in ocean responses are not important for the Tian (2015) constraint, we examine the relationship between the mean Southeast Pacific precipitation in a number of Atmospheric Model Intercomparison Project (AMIP) experiments and global cloud feedbacks diagnosed from a number of +4 K experiments. We separate the available models into two groups (Table 1). The first comprises a set of CFMIP-2/CMIP5 experiments plus some additional experiments run for the SPOOKIE project (Webb et al., 2015), including some older model versions. The second comprises some newer AMIP+4K experiments from CFMIP-3/CMIP6.

Table 2
Correlations Between Southeast Tropical Pacific Precipitation in the Region (150–100°W, 30°S to 0°N) and Present-Day CRE, EIS, and 700 hPa Subsidence Rate and CRE Cloud Feedback in the Peruvian Stratus Region (10–20°S, 80–90°W) in the CMIP5/CFMIP-2/SPOOKIE AMIP+4K Experiments

	CMIP5+SPOOKIE
SETP precipitation versus Peruvian Sc region net CRE	**0.56**
Peruvian Sc region net CRE versus Peruvian net CRE feedback	−0.44
Peruvian Sc region net CRE feedback versus global net CRE feedback	**0.58**
SETP precipitation versus Peruvian Sc region SW CRE	**0.59**
Peruvian Sc region SW CRE versus Peruvian SW CRE feedback	−0.48
Peruvian Sc region SW CRE feedback versus global net CRE feedback	**0.51**
SETP precipitation versus Peruvian Sc region EIS	−0.42
Peruvian Sc region EIS versus Peruvian Sc region SW CRE	−0.12
Peruvian Sc region EIS versus Peruvian Sc region Net CRE	−0.09
SETP precipitation versus global net CRE feedback	**−0.69**
SETP precipitation versus Peruvian Sc region net CRE feedback	−0.30

Note. Correlations with magnitude of 0.5 or more (in bold) are significant at the 5% level.

Figure 3a shows a negative correlation between precipitation in the Southeast Pacific region used by Tian (2015) and the global net CRE feedback amongst the CFMIP-2/SPOOKIE models with $r = -0.69$, which is significantly different from 0 at the 5% level based on a one-tailed t test. This supports our hypothesis that models with too much Southeast Pacific precipitation tend to have less positive global cloud feedbacks and hence, as found by Tian (2015), lower climate sensitivities. This relationship suggests a notional lower bound for the net CRE feedback of about 0.2 W m^{-2} K^{-1}, favoring models with higher sensitivities. However, while Figure 3b also shows an anticorrelation between these quantities across the CFMIP-3/CMIP6 experiments available thus far, this is weak ($r = -0.22$) and not significantly different from 0 at the 5% level. This indicates that our hypothesis does not explain the behavior of the global cloud feedback in the currently available CMIP6 AMIP+4K experiments, although it is possible that the relationship will emerge more strongly if more CMIP6 AMIP+4K experiments become available. Since the main focus of this study is to understand the relationship in the CMIP3/CMIP5 models established by Tian (2015), we do not investigate the CMIP6 models further here.

Since the Tian (2015) relationship is reproduced in the CFMIP-2/SPOOKIE experiments, we can test our hypothesis further by seeing if the other relationships predicted by our hypothesis are present across these models. First, we test the idea that models with more precipitation in the Southeast Tropical Pacific have weaker (less negative) CREs in subtropical low-cloud regions. To do this, we select a priori a region in the Southeast Tropical Pacific where we expect low cloud to be prevalent. Klein and Hartmann (1993) identified a number of regions where marine stratus clouds are prevalent in observations. One of these is their "Peruvian Subtropical Marine Stratus" region 10–20°S, 80–90°W. Our hypothesis predicts a positive correlation between the amount of precipitation in the Southeast Tropical Pacific region used in Tian (2015) and the net and SW CRE in subtropical low-cloud regions such as the Peruvian stratus region. Table 2 shows that positive correlations of more than 0.5 are present, which are significant at the 5% level based on a one-tailed t test, providing strong statistical support for this element of our hypothesis. In addition, Figure 4 shows that Southeast Tropical Pacific precipitation is significantly positively correlated with SW CRE in a number of other locations where low-level stratus clouds are prevalent, not only in the subtropics but also at middle to high latitudes. The additional correlations at middle to high latitudes are not predicted by our hypothesis, but we show them for completeness.

Next we test the hypothesis that models with more negative SW and/or net CRE in subtropical low-cloud regions tend to have more positive net and/or SW CRE feedbacks in those regions, which would predict an anticorrelation. Again Table 2 shows that the predicted anticorrelations are present, but in this case they are not strong enough to be statistically distinguishable from 0 at the 5% level. Hence, we cannot exclude the possibility that there is no underlying relationship between present-day cloud and cloud feedback averaged over the Peruvian marine stratus region and that this anticorrelation arises by chance. It is, however, possible

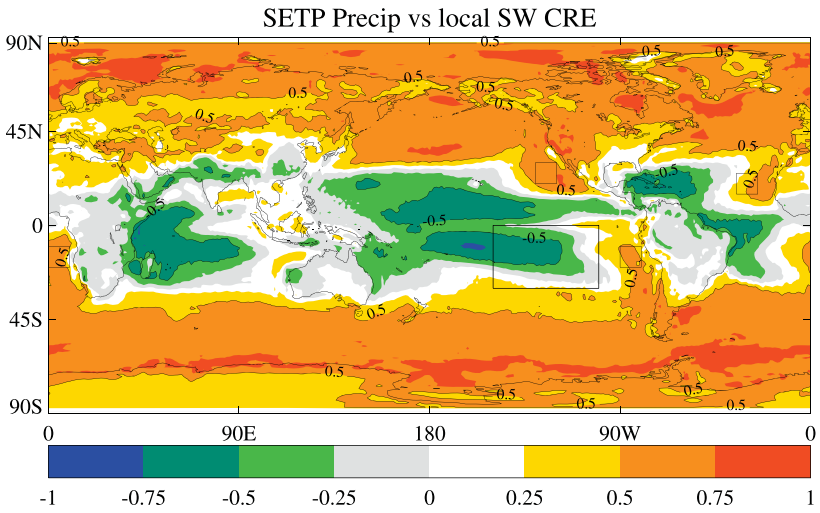

Figure 4. Correlation between Southeast Tropical Pacific Precipitation and SW CRE in CMIP5/SPOOKIE models. Positive correlations with $r > 0.5$ are significant at the 5% level. The larger box shows the region used for the Tian (2015) index, while the others show the Pacific and Atlantic subtropical marine stratus regions of Klein and Hartmann (1993).

that the relationship is not significant because the Peruvian stratus region is not representative of regimes that do contribute to an underlying relationship between present-day low clouds and low-cloud feedbacks overall. Figure 5 shows that statistically significant anticorrelations are seen between present-day SW CRE and SW CRE feedbacks in other regions associated with low clouds and even within part of the Peruvian stratus region. These are more prevalent than statistically significant positive correlations that make us think that they are unlikely to arise purely through chance. Note also that Webb et al. (2015) found a statistically significant anticorrelation between present-day SW CRE and net CRE feedback in tropical marine composite regimes with strong lower tropospheric stability in a very similar set of experiments to those analyzed here.

Another element of our hypothesis is that subtropical low-cloud feedbacks contribute substantially to inter-model spread in global cloud feedback. Hence our hypothesis predicts significant positive correlations between SW CRE feedbacks in subtropical low-cloud regions and the global mean net CRE feedback. This is supported at a statistically significant level in the Peruvian region (Table 2) and more broadly by Figure 6.

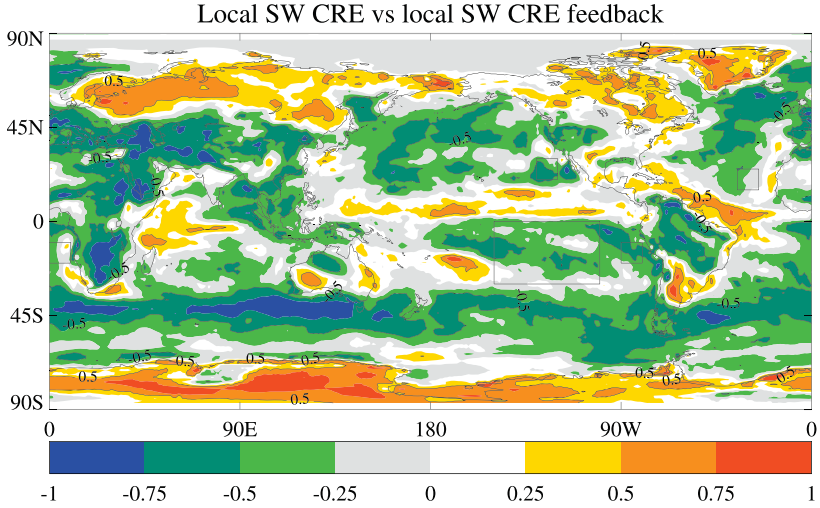

Figure 5. As figure above but correlation between local SW CRE and local SW CRE feedback in CMIP5/SPOOKIE models.

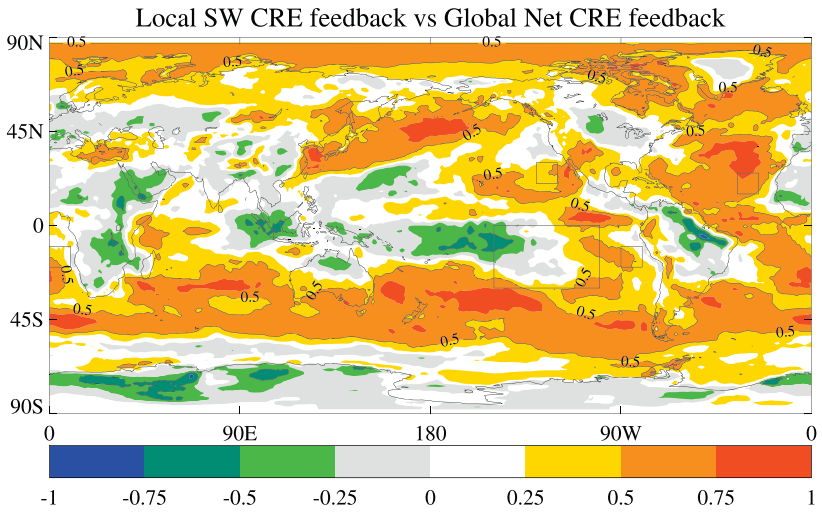

Figure 6. As figure above but correlation between local SW CRE feedback and global net CRE feedback in CMIP5/SPOOKIE models.

Our experiments with HadGEM2-A also suggest that the relationship between Southeast Pacific precipitation and CRE in the marine stratocumulus regions might be mediated by free-tropospheric warming and EIS, for example, if deep convection reduces subsidence warming and EIS. However, our examination of relationships in the CMIP5/SPOOKIE multimodel ensemble does not provide strong support for this. The correlation between precipitation in the Tian (2015) Southeast Pacific region and the EIS in the Peruvian marine stratus region is of the expected sign but is slightly too weak to be significant at the 5% level ($r = -0.42$) (see Table 2). However, the correlations of the EIS with the SW and net CRE in the Peruvian marine stratus region are much smaller (<15%), so EIS does not mediate the relationship between Southeast Pacific region precipitation and Peruvian marine stratus region CRE in the multimodel ensemble. These results indicate that some other explanation is required for this aspect of the problem.

As mentioned above, it is possible that the Peruvian marine stratus region is simply not representative of the areas in which our proposed mechanism is operating in the models. To explore this possibility, we also correlate the precipitation in the Tian (2015) region with the local net CRE feedback in all regions. Figure 7 shows that the cloud feedbacks in the subtropical stratus regions are not in general significantly anticorrelated with the Southeast Pacific precipitation in the Tian (2015) region, which suggests that the relationship

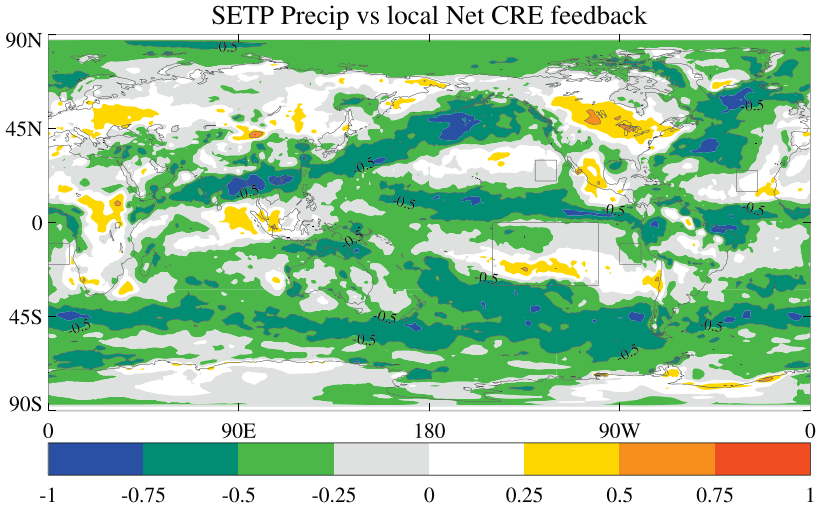

Figure 7. Correlation between Southeast Tropical Pacific Precipitation and local net CRE feedback in CMIP5/SPOOKIE models. Negative correlations with $r < -0.5$ are significant at the 5% level.

between double-ITCZ and climate sensitivity is not mediated by subtropical low clouds as we have hypothesized. Significant anticorrelations are seen in other regions. Such relationships could in principle be used to develop alternative hypotheses in the future, although the risks associated with data mining should always be kept in mind (Caldwell et al., 2014).

4. Summary and Conclusions

Tian (2015) proposed an emergent constraint on climate sensitivity where models with a more pronounced double-ITCZ bias and too much precipitation in the Southeast Pacific have lower values of the effective ECS (S) and suggested that this may rule out lower values of S. However, no clear mechanism has been provided to explain why the double-ITCZ should be related to S. We advance a physical hypothesis as a potential explanation for this relationship that deep convection encroaching into regions that should be dominated by shallow clouds hampers the formation of shallow clouds in the present climate and reduces the magnitude of positive low-level cloud feedbacks, resulting in smaller values of climate sensitivity. We tested this first by perturbing the ITCZ in a single idealized climate model and second by looking for the relationships it predicts across models.

We show in targeted experiments with the HadGEM2-A aquaplanet model that increasing the longwave radiative effects of clouds in the atmosphere makes the ITCZ more concentrated, as found by Dixit et al. (2018). This enhances midtropospheric temperatures in the subtropics, increasing low-level stability, enhancing the net radiative cooling effect of clouds in the present climate through enhanced cloud cover and/or condensed water path. This stronger radiative effect of clouds is associated with a more positive subtropical cloud feedback with climate change, resulting in a higher climate sensitivity. Looking across these experiments, we see that model versions with more precipitation encroaching into the subtropics have weaker subtropical CREs in the present climate, less positive subtropical cloud feedbacks, and less positive global cloud feedbacks. These results are consistent with our hypotheses and suggest that it is a plausible physical explanation for the Tian (2015) result.

We test this hypothesis further by looking for the predicted relationships in SST forced experiments subject to a uniform SST increase with 12 models from the CFMIP-2/CMIP5 and SPOOKIE projects. We find no statistically significant relationship between precipitation in the Southeast Tropical Pacific region of Tian (2015) and cloud feedback in the Peruvian marine stratus region of Klein and Hartmann (1993), in spite of the fact that the cloud feedback in the Peruvian region is significantly positively correlated with the global cloud feedback. Significant correlations are seen with feedbacks in other regions but not ones typically associated with subtropical low clouds. We do see a significant anticorrelation between precipitation in the Tian (2015) region and present-day CREs in the Peruvian region and other regions associated with low clouds, which supports part of our argument. The CREs in the Peruvian region are, however, not significantly correlated with local cloud feedbacks, which does not support our hypothesis. Hence, our proposed mechanism cannot explain the relationship in CMIP3/CMIP5 models identified by Tian (2015). Furthermore, we do not see a statistically significant relationship between Southeast Tropical Pacific precipitation and global cloud feedback in ten SST forced CMIP6 models subject to a uniform SST increase.

Although we have not been successful in providing a compelling explanation for Tian (2015) result, we hope that we have at least demonstrated an approach that may usefully be used to develop and test physical explanations for this and other proposed emergent constraints in the future. We conclude by noting that all emergent constraints of this type are based on climate models, and so it is difficult to rule out the possibility that they may be biased, even if they are supported by credible physical explanations. Climate models, with or without emergent constraints, are just one line of evidence on climate sensitivity. Robust assessments of climate sensitivity such as those undertaken by the Intergovernmental Panel on Climate Change (IPCC) take into account multiple lines of evidence relevant to cloud feedbacks and climate sensitivity, including climate models, process models, and observations from the current, historical, and paleoclimate eras. Physically credible emergent constraints on climate sensitivity may affect synthesis estimates of S but to a lesser degree than one might be led to believe if such emergent constraints are considered in isolation.

Data Availability Statement

The CMIP5 and CMIP6 data used in this study are available via the ESGF (https://esgf.llnl.gov), and the SPOOKIE data are available from DKRZ (https://cera-www.dkrz.de). Data from the aquaplanet experiments performed for this study are archived at https://doi.org/10.5281/zenodo.4006622.

Acknowledgments
We are grateful to Stephan de Roode, Bjorn Stevens, Angie Pendergrass, Mike Byrne, Peter Caldwell, Steve Klein, and Sandrine Bony for useful discussions about this work and to Baijun Tian and two anonymous reviewers whose comments helped to improve the manuscript. Mark Webb was supported by the Joint U.K. BEIS/Defra Met Office Hadley Centre Climate Programme (GA01101). We acknowledge the World Climate Research Programme, which, through its Working Group on Coupled Modelling, coordinated and promoted CMIP5 and CMIP6. We thank the climate modeling groups for producing and making available their model output, the Earth System Grid Federation (ESGF) for archiving the data and providing access, and the multiple funding agencies who support CMIP6 and ESGF.

References

Andrews, T., Gregory, J. M., Webb, M. J., & Taylor, K. E. (2012). Forcing, feedbacks and climate sensitivity in CMIP5 coupled atmosphere-ocean climate models. *Geophysical Research Letters*, *39*, L09712. https://doi.org/10.1029/2012GL051607

Blackburn, M., Williamson, D. L., Nakajima, K., Ohfuchi, W., Takahashi, Y. O., Hayashi, Y.-Y., et al. (2013). The Aqua-Planet Experiment (APE): Control SST simulation. *Journal of the Meteorological Society of Japan. Ser. II*, *91*, 17–56.

Bony, S., Stevens, B., Coppin, D., Becker, T., Reed, K. A., Voigt, A., & Medeiros, B. (2016). Thermodynamic control of anvil cloud amount. *Proceedings of the National Academy of Sciences*, *113*(32), 8927–8932.

Bony, S., Webb, M., Stevens, B., Bretherton, C., Klein, S., & Tselioudis, G. (2008). CFMIP-GCSS plans for advancing assessments of cloud-climate feedbacks. *GEWEX News*, *18*(4), 10–12.

Boucher, O., Servonnat, J., Albright, A. L., Aumont, O., Balkanski, Y., Bastrikov, V., et al. (2020). Presentation and evaluation of the IPSL-CM6A-LR climate model. *Journal of Advances in Modeling Earth Systems*, *12*, e2019MS002010. https://doi.org/10.1029/2019MS002010

Bretherton, C. S., Blossey, P. N., & Jones, C. R. (2013). Mechanisms of marine low cloud sensitivity to idealized climate perturbations: A single-LES exploration extending the CGILS cases. *Journal of Advances in Modeling Earth Systems*, *5*, 316–337. https://doi.org/10.1002/jame.20019

Brient, F., & Bony, S. (2012). How may low-cloud radiative properties simulated in the current climate influence low-cloud feedbacks under global warming? *Geophysical Research Letters*, *39*, L20807. https://doi.org/10.1029/2012GL053265

Caldwell, P. M., Bretherton, C. S., Zelinka, M. D., Klein, S. A., Santer, B. D., & Sanderson, B. M. (2014). Statistical significance of climate sensitivity predictors obtained by data mining. *Geophysical Research Letters*, *41*, 1803–1808. https://doi.org/10.1002/2014GL059205

Caldwell, P. M., Zelinka, M. D., & Klein, S. A. (2018). Evaluating emergent constraints on equilibrium climate sensitivity. *Journal of Climate*, *31*(10), 3921–3942.

Christensen, M. W., Carrió, G. G., Stephens, G. L., & Cotton, W. R. (2013). Radiative impacts of free-tropospheric clouds on the properties of marine stratocumulus. *Journal of the Atmospheric Sciences*, *70*(10), 3102–3118.

Collins, M., Knutti, R., Arblaster, J., Dufresne, J.-L., Fichefet, T., Friedlingstein, P., et al. (2013). Long-term climate change: Projections, commitments and irreversibility. *Climate change 2013—The physical science basis: Contribution of Working Group I to the Fifth Assessment Report of the Intergovernmental Panel on Climate Change* (pp. 1029–1136). Cambridge, United Kingdom and New York, NY, USA: Cambridge University Press.

Coppin, D., & Bony, S. (2015). Physical mechanisms controlling the initiation of convective self-aggregation in a general circulation model. *Journal of Advances in Modeling Earth Systems*, *7*, 2060–2078. https://doi.org/10.1002/2015MS000571

Coppin, D., & Bony, S. (2017). Internal variability in a coupled general circulation model in radiative-convective equilibrium. *Geophysical Research Letters*, *44*, 5142–5149. https://doi.org/10.1002/2017GL073658

Dixit, V., Geoffroy, O., & Sherwood, S. C. (2018). Control of ITCZ width by low-level radiative heating from upper-level clouds in aquaplanet simulations. *Geophysical Research Letters*, *45*, 5788–5797. https://doi.org/10.1029/2018GL078292

Dufresne, J.-L., Foujols, M.-A., Denvil, S., Caubel, A., Marti, O., Aumont, O., et al. (2013). Climate change projections using the IPSL-CM5 Earth system model: From CMIP3 to CMIP5. *Climate Dynamics*, *40*(9-10), 2123–2165.

Fermepin, S., & Bony, S. (2014). Influence of low-cloud radiative effects on tropical circulation and precipitation. *Journal of Advances in Modeling Earth Systems*, *6*, 513–526. https://doi.org/10.1002/2013MS000288

GFDL-GAMDT (2004). The new GFDL global atmosphere and land model AM2-LM2: Evaluation with prescribed SST simulations. *Journal of Climate*, *17*, 4641–4673.

Gettelman, A., Hannay, C., Bacmeister, J. T., Neale, R. B., Pendergrass, A. G., Danabasoglu, G., et al. (2019). High climate sensitivity in the Community Earth System Model Version 2 (CESM2). *Geophysical Research Letters*, *46*, 8329–8337. https://doi.org/10.1029/2019GL083978

Gregory, J. M., Ingram, W. J., Palmer, M. A., Jones, G. S., Stott, P. A., Thorpe, R. B., et al. (2004). A new method for diagnosing radiative forcing and climate sensitivity. *Geophysical Research Letters*, *31*, L03205. https://doi.org/10.1029/2003GL018747

Grose, M. R., Gregory, J., Colman, R., & Andrews, T. (2018). What climate sensitivity index is most useful for projections? *Geophysical Research Letters*, *45*, 1559–1566. https://doi.org/10.1002/2017GL075742

Harrop, B. E., & Hartmann, D. L. (2016). The role of cloud radiative heating in determining the location of the ITCZ in aquaplanet simulations. *Journal of Climate*, *29*(8), 2741–2763.

Held, I. M., Guo, H., Adcroft, A., Dunne, J. P., Horowitz, L. W., Krasting, J., et al. (2019). Structure and performance of GFDL's CM4. 0 climate model. *Journal of Advances in Modeling Earth Systems*, *11*, 3691–3727. https://doi.org/10.1029/2019MS001829

Klein, S. A., & Hall, A. (2015). Emergent constraints for cloud feedbacks. *Current Climate Change Reports*, *1*(4), 276–287.

Klein, S. A., & Hartmann, D. L. (1993). The seasonal cycle of low stratiform clouds. *Journal of Climate*, *6*(8), 1587–1606.

Kuhlbrodt, T., Jones, C. G., Sellar, A., Storkey, D., Blockley, E., Stringer, M., et al. (2018). The low-resolution version of HadGEM3 GC3. 1: Development and evaluation for global climate. *Journal of Advances in Modeling Earth Systems*, *10*, 2865–2888. https://doi.org/10.1029/2018MS001370

Martin, G. M., Bellouin, N., Collins, W. J., Culverwell, I. D., Halloran, P. R., Hardiman, S. C., et al. (2011). The HadGEM2 family of Met Office Unified Model climate configurations. *Geoscientific Model Development Discussions*, *4*, 765–841.

Medeiros, B., Stevens, B., & Bony, S. (2015). Using aquaplanets to understand the robust responses of comprehensive climate models to forcing. *Climate Dynamics*, *44*(7–8), 1957–1977.

Neale, R. B., Chen, C.-C., Gettelman, A., Lauritzen, P. H., Park, S., Williamson, D. L., et al. (2010). Description of the NCAR community atmosphere model (CAM 5.0). *NCAR Technology Note NCAR/TN-486+ STR*, *1*(1), 1–12.

Qu, X., Hall, A., DeAngelis, A. M., Zelinka, M. D., Klein, S. A., Su, H., et al. (2018). On the emergent constraints of climate sensitivity. *Journal of Climate*, *31*(2), 863–875.

Ringer, M. A., Andrews, T., & Webb, M. J. (2014). Global-mean radiative feedbacks and forcing in atmosphere-only and coupled atmosphere-ocean climate change experiments. *Geophysical Research Letters*, *41*, 4035–4042. https://doi.org/10.1002/2014GL060347

Soden, B. J., Broccoli, A. J., & Hemler, R. S. (2004). On the use of cloud forcing to estimate cloud feedback. *Journal of climate*, *17*(19), 3661–3665.

Stevens, B., Giorgetta, M., Esch, M., Mauritsen, T., Crueger, T., Rast, S., et al. (2013). Atmospheric component of the MPI-M earth system model: ECHAM6. *Journal of Advances in Modeling Earth Systems*, *5*, 146–172. https://doi.org/10.1002/jame.20015

Swart, N. C., Cole, J. N. S., Kharin, V. V., Lazare, M., Scinocca, J. F., Gillett, N. P., et al. (2019). The Canadian Earth System Model Version 5 (CanESM5. 0.3). *Geoscientific Model Development*, *12*(11), 4823–4873.

Tatebe, H., Ogura, T., Nitta, T., Komuro, Y., Ogochi, K., Takemura, T., et al. (2019). Description and basic evaluation of simulated mean state, internal variability, and climate sensitivity in MIROC6. *Geoscientific Model Development*, *12*(7), 2727–2765.

Taylor, K. E., Stouffer, R. J., & Meehl, G. A. (2012). An overview of CMIP5 and the experiment design. *Bulletin of the American Meteorological Society*, *93*(4), 485–498.

Tian, B. (2015). Spread of model climate sensitivity linked to double-Intertropical Convergence Zone bias. *Geophysical Research Letters*, *42*, 4133–4141. https://doi.org/10.1002/2015GL064119

Voldoire, A., Saint-Martin, D., Sénési, S., Decharme, B., Alias, A., Chevallier, M., et al. (2019). Evaluation of CMIP6 DECK experiments with CNRM-CM6-1. *Journal of Advances in Modeling Earth Systems*, *11*, 2177–2213. https://doi.org/10.1029/2019MS001683

Von Salzen, K., Scinocca, J. F., McFarlane, N. A., Li, J., Cole, J. N. S., Plummer, D., et al. (2013). The Canadian fourth generation atmospheric global climate model (CanAM4). Part I: Representation of physical processes. *Atmosphere-Ocean*, *51*(1), 104–125.

Watanabe, M., Suzuki, T., Oishi, R., Komuro, Y., Watanabe, S., Emori, S., et al. (2010). Improved climate simulation by MIROC5: Mean states, variability, and climate sensitivity. *Journal of Climate*, *23*(23), 6312–6335.

Webb, M. J., Andrews, T., Bodas-Salcedo, A., Bony, S., Bretherton, C. S., Chadwick, R., et al. (2017). The Cloud Feedback Model Intercomparison Project (CFMIP) contribution to CMIP6. *Geoscientific Model Development*, *2017*, 359–384.

Webb, M. J., Lock, A. P., Bretherton, C. S., Bony, S., Cole, J. N. S., Idelkadi, A., et al. (2015). The impact of parametrized convection on cloud feedback. *Philosophical Transactions of the Royal Society A: Mathematical, Physical and Engineering Sciences*, *373*(2054), 20140414.

Williams, K. D., & Webb, M. J. (2009). A quantitative performance assessment of cloud regimes in climate models. *Climate Dynamics*, *33*(1), 141–157.

Wood, R., & Bretherton, C. S. (2006). On the relationship between stratiform low cloud cover and lower-tropospheric stability. *Journal of Climate*, *19*(24), 6425–6432.

Wu, T., Lu, Y., Fang, Y., Xin, X., Li, L., Li, W., et al. (2019). The Beijing Climate Center Climate System Model (BCC-CSM): The main progress from CMIP5 to CMIP6. *Geoscientific Model Development*, *12*(4), 1573–1600.

Wu, T., Song, L., Li, W., Wang, Z., Zhang, H., Xin, X., et al. (2014). An overview of BCC climate system model development and application for climate change studies. *Journal of Meteorological Research*, *28*(1), 34–56.

Yoshimori, M., Lambert, F. H., Webb, M. J., & Andrews, T. (2019). Fixed anvil temperature feedback-positive, zero or negative? *Journal of Climate*, *33*(2019), 2719–2739.

Yukimoto, S., Adachi, Y., Hosaka, M., Sakami, T., Yoshimura, H., Hirabara, M., et al. (2012). A new global climate model of the meteorological research institute: MRI-CGCM3 model description and basic performance. *Journal of the Meteorological Society of Japan. Ser. II*, *90*, 23–64.

Yukimoto, S., Kawai, H., Koshiro, T., Oshima, N., Yoshida, K., Urakawa, S., et al. (2019). The Meteorological Research Institute Earth System Model Version 2.0, MRI-ESM2.0: Description and basic evaluation of the physical component. *Journal of the Meteorological Society of Japan. Ser. II*, *97*, 931–965.

Zhao, M., Held, I. M., Lin, S.-J., & Vecchi, G. A. (2009). Simulations of global hurricane climatology, interannual variability, and response to global warming using a 50-km resolution GCM. *Journal of Climate*, *22*(24), 6653–6678.